C-H Activation: Oxidative Addition to an Iridium(I) Center and Reactivity of the Resulting Iridium(III) Species

By

Henry Edward Selnau, Jr.

Dissertation submitted to the Faculty of the
Virginia Polytechnic Institute and State University
in partial fulfillment of the requirements for the degree of

DOCTOR OF PHILOSOPHY

in

Chemistry

APPROVED

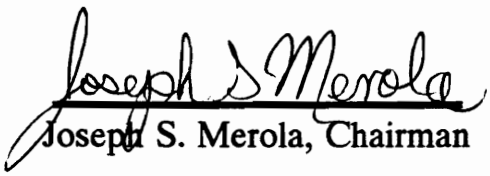

Joseph S. Merola, Chairman

Neal Castagnoli

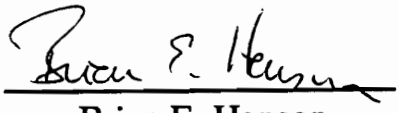

Brian E. Hanson

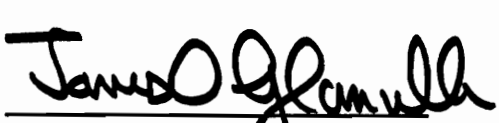

James O. Glanville

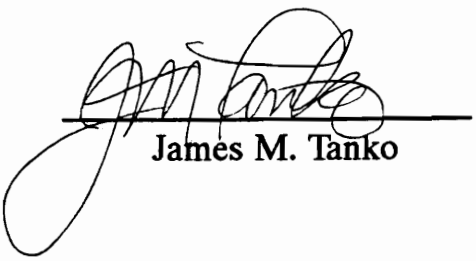

James M. Tanko

August, 1992

Blacksburg, Virginia

C-H Activation: Oxidative Addition to an Iridium(I) Center and Reactivity of the Resulting Iridium(III) Species

By

Henry Edward Selnau, Jr.

Joseph S. Merola, Committee Chairman

Department of Chemistry

(ABSTRACT)

Thermal reactions of the iridium complex, $[Ir(COD)(PMe_3)_3]Cl$ (COD=1, 5 Cyclooctadiene), with benzene, benzaldehyde, pyridine, and furan yield the C-H addition products of mer-$(Me_3P)_3Ir(Phenyl)(H)Cl$ (**I**), mer-$(Me_3P)_3Ir(COC_6H_5)(H)Cl$ (**II**), mer-$(Me_3P)_3Ir(Pyridyl)(H)Cl$ (**III**), and mer-$(Me_3P)_3Ir(furyl)Cl$ (**IV**), respectively. Each of these complexes was characterized by ^1H, ^{13}C, ^{31}P NMR spectroscopy and single crystal X-ray diffraction. Thermal reaction of the $[Ir(COD)(PMe_3)_3]Cl$ with thiophene and benzothiophene produced the C-S addition products forming thiometallacycles of $(Me_3P)_3\overline{Ir\text{-}(CH=CHCH=CHS)}Cl$ (**V**), and $(Me_3P)_3\overline{Ir(CH=CH\text{-}C_6H_4S)}Cl$ (**VI**).

The C-H addition products are unreactive and require the aid of $Tl[PF_6]$ to remove the chloride ligand to provide an open coordination site. Complex (**I**) and 3,3-dimethyl-1-butyne, produced a 1,4-di-t-butyldienyl complex (**VIII**) by a double insertion of the alkyne with one t-butyl group forming an agostic interaction with iridium. Deuterium labeling experiments revealed the mechanism to involve: initial acetylene coordination after the chloride ligand was removed by Tl^+ followed by a hydride migration forming a vinyl complex and allowing a second alkyne

to coordinate, rearrangement of the second alkyne into a vinylidene and finally a migratory-insertion of the vinyl group unto the vinylidene to form (**VIII**).

Complex (**III**) and two equivalence of 3,3-dimethyl-1-butyne produced a trans diacetylide complex (**XII**). The pyridyl ligand was able to remove acidic protons via the nitrogen lone pair, thus altering the course of the reaction. Initial investigations have led to a possible mechanism.

Complex (**IV**) and 3,3-dimethyl-1-butyne gave an interesting hydrido metallo-vinyl complex (**XIV**) with the t-butyl group forming an agostic C-H-Ir interaction. A deuterium labeling experiment revealed the alkyne to initially coordinate and rearrange into a vinylidene, followed by migratory-insertion of the furan group unto the vinylidene to give (**XIV**). The furyl group is believed to stabilize the initial intermediate by forming a five coordinate square pyramidal complex through the donation of a pair of electrons from the oxygen atom. Reductive elimination of (**XIV**) using elevated temperatures gave exclusively the trans 3,3-dimethyl-1-(2 furanyl) - 1-butyne (**XV**). The resonance structure found in (**IV**) is the most important feature of this work. While most insertions occur between the M-H bond, the resonance structure found in (**IV**) provides the necessary means for insertion of unsaturates to occur between the M-C bond, leaving the M-H bond intact.

In conclusion, it appears that the reactivity of the phenyl complex (**I**) is dependent on the alkyne used. While the reactivity of the pyridyl complex (**III**) is governed by the nitrogen lone pair; the reactivity of the furanyl complex (**IV**) follows a different pathway due to resonance stability of the furanyl ligand.

This dissertation is dedicated to my parents, who have endured the emotional burdens;

to my professors at VMI, for their inspiration and encouragement;

to my sweetheart Melisa D. Parks, for her support in typing this dissertation,

and to God, for giving me the strength throughout my endeavors.

Acknowledgements

I would like to thank my advisor, Dr. Merola, for his guidance during my studies at Virginia Tech. Special thanks go to my committee members, Dr. Castagnoli, and Dr. Tanko for their time and suggestions. I would like to thank Dr. Hanson and especially Dr. Glanville for being willing to step in.

Acknowledgement goes to the Jeffress Trust, the Petroleum Foundation, and the Chemistry Department at VPI & SU for their financial support, and to Engelhard Corporation and Johnson-Matthey for providing the iridium used for this research.

I would like to thank the following colleagues and friends: Dr. Thomas and Berit Bartik, Bill Bebout, Joe Bergmeister, Ipin Guo, Joe Knorr, Folo Ladipo, and Glen Smith for the helpful discussions. Barbra Bunn, Roger Grisle, Tom Moore and Sang Pak for the interesting conversations. Theresa Bucy, Harvey Grubbs, Laura Perry and Etsuko Usuki for their encouragement. Best wishes goes to Kelly Mathews with Kelly and to Trang Le with John. And finally, thanks goes to the members of Dr. Merola's group: Chris Roy, Gita Srinivasan, Poly Boyer and Dave Hobart.

Table of Contents

List of Illustrations

List of Tables and Graphs

Miscellaneous

Each compound is given a code which corresponds to the notebook and page of that particular experiment, and this code is also given to the corresponding characteristic ^1H, ^{13}C, or ^{31}P NMR spectrum as well as other data on that compound such as C, H elememental analysis. For example, HES II 51 represents the experiment found in book two page 51.

ORTEP- Oak Ridge Thermal Ellipsoidal Plot.

Chapter 1: Introduction and Literature Review

Introduction

The direct formation of a carbon-carbon bond between an aromatic ring and an aliphatic carbon has particular synthetic utility in the chemical industry. The most common method for this particular carbon coupling is the reaction in which an aromatic ring (the nucleophile) attacks an electrophilic carbon atom with the aid of a catalyst. A Lewis acid is the catalyst which can induce an alkyl or acyl halide to react with the aromatic ring. The first examples of electrophilic aromatic substitution were reported by Friedel and Craft in 1877[1]. The catalysts that were employed are aluminum chloride ($AlCl_3$) the most common, ferric chloride ($FeCl_3$), and boron trifluoride (BF_3). For alcohols and alkenes, strong protic acids such as phosphoric, sulfuric, or hydrofluoric acid are used. These reactions are commonly called Friedel-Crafts alkylation or acylation.

A second classical method for aryl-carbon bond formation is the Grignard Reaction[2]. In this class of reactions, arylhalides and an active metal (magnesium or lithium) would form an aryl metal complex. The aryl metal complex would then attack an electrophilic carbon atom to form the carbon-carbon bond. A third method employs a transition metal catalyst. These reactions can be best described under the class of "Oxidative additions," a term that was coined by Vaska.[3] The reaction involves a low valent metal such as palladium with aryl halides or vinyl halides and acetylenes[4, 5]. This will form a carbon bond between the sp^2-sp carbon atoms. A few examples of the above reactions are illustrated in Figure 1.1. Although the reactions in Figure 1 are brief examples of

carbon activation of arenes, they all require some functional group to activate the carbon center without direct C-H bond cleavage. The activation of C-H bonds using metal complexes may proceed through an electrophilic process, much like that of the electrophilic alkylation mechanism between aryl and alkenyl additions catalyzed by protic acids (Scheme 1.1). This will be discussed later in the Literature Review.

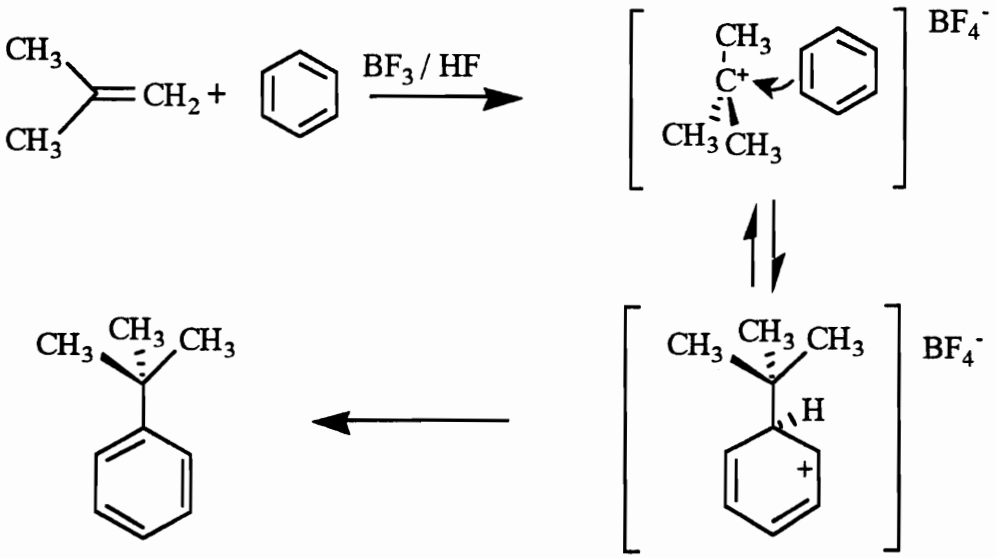

Scheme 1.1

The cleavage of C-H bonds of arenes by a transition metal was not recognized until the early 1960's. Another twenty years elapsed before enough data were obtained in order to derive a working guideline for this class of reactions. Over the past several years, only a few research groups have attempted to functionalize the C-H bond of arenes and alkanes.

A.) Alkylation:

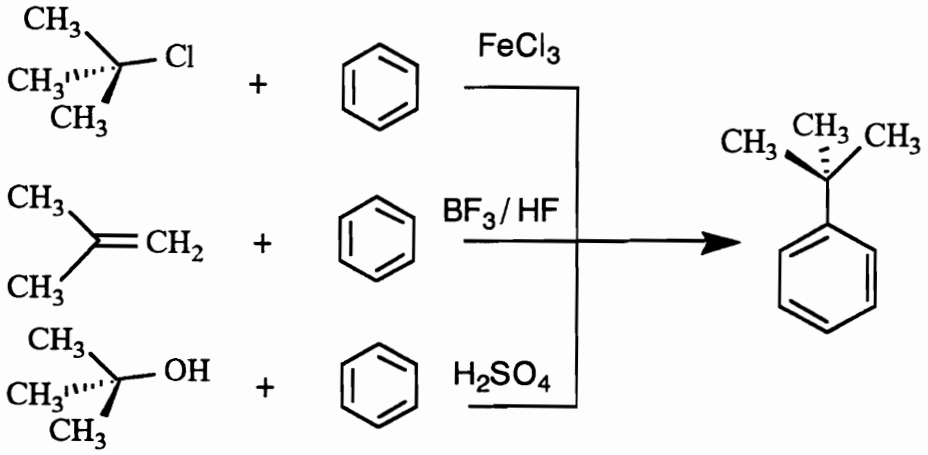

B.) Acylation:

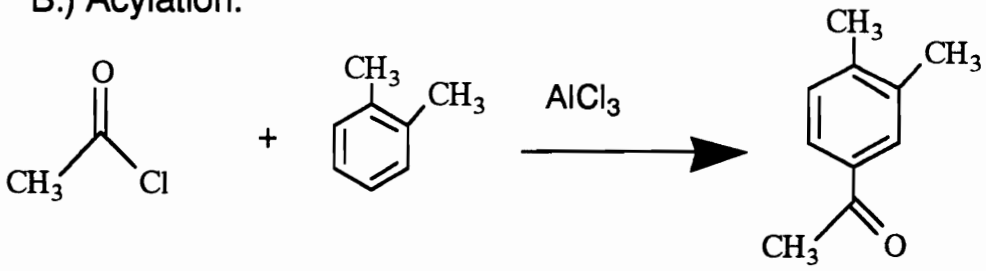

C.) Grignard reaction:

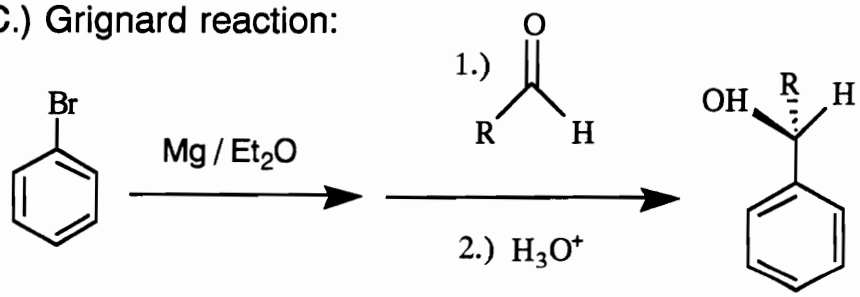

R, S

D.) "Oxidative Addition Reactions":

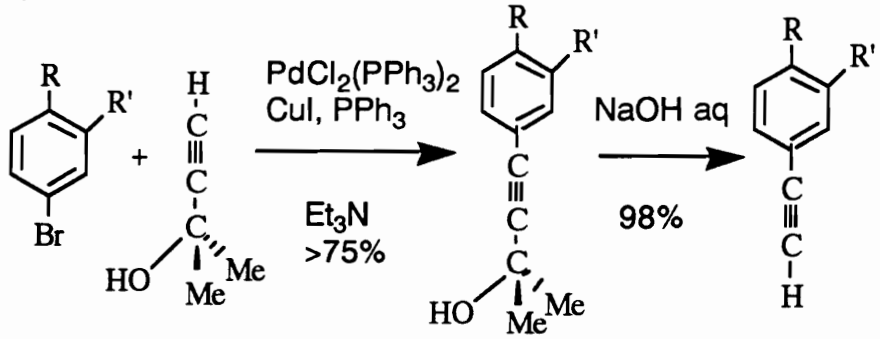

Figure 1.1 Carbon to carbon bond formations.

Therefore, the objective of this thesis was to investigate the C-H activation of several aromatic systems via the complex $[Ir(COD)(PMe_3)_3]Cl$ (COD=1,5 Cyclooctadiene) and to explore the reactivity of the resulting complexes. In this way, further steps toward the functionalization of hydrocarbons using metal complexes could be elucidated.

Literature Review: C-H Addition

The cleavage of the C-H bond in benzene had been shown to occur as early as 1937 by Farkas and Farkas[6]. They observed H/D exchange between gaseous benzene and D_2 catalyzed by a platinum film. In 1963, Kliman and Dubeck[7] observed intramolecular aryl C-H bond cleavage of azobenzene by a nickel complex (Equation 1.1)

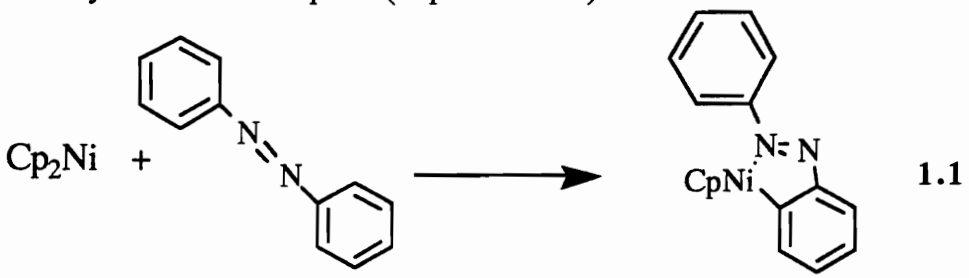

1.1

Shortly afterwards, Chatt and Davidson[8] discovered a ruthenium complex (1) that would activate the C-H bond of napthalene. This complex (2, 2a) was decomposed by heat to give the alkyl C-H addition product complex (3) via cyclometalation (see Scheme 1.2).

In a series of palladium complexes for which the intramolecular ring closure of an arene can occur, Bennett and Milner[9] found the cyclometalation product was dependent upon para-substituted functional groups. The preference for cyclometalation product for the substitiuted ring was found to be in the order of $OCH_3>CH_3>H>Cl$. Parshall[10] suggested the electron donating groups tend to cyclometalate by an

electrophilic substitution mechanism. Shaw and co-workers[11] investigated the steric effects of bulky ligands on cyclometalation reactions. Platinum and palladium complexes of <u>trans</u>-$[M]Cl_2[P(t\text{-}Bu)_2Ph]_2$ tend to cyclometalate while <u>trans</u>-$(M)Cl_2[P(Me_3)_2Ph]_2$ does not. They observed that five membered ring products were more stable than four or six membered ring products[12].

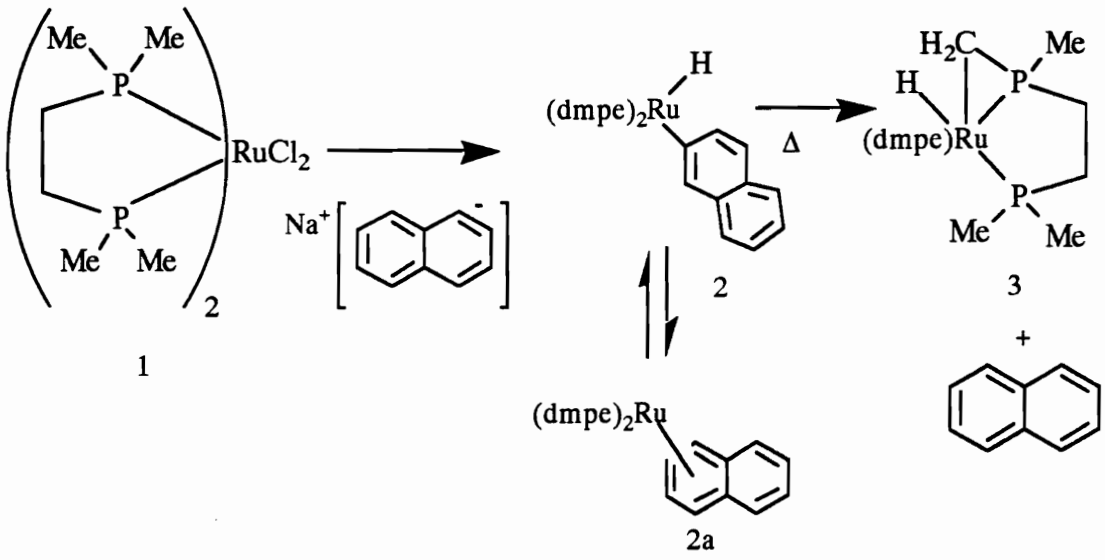

Scheme 1.2

Intramolecular reactions proceed faster than intermolecular reactions due to the proximity of the C-H bond which is a part of the attached ligand. Intermolecualr reactions must rely on a collision between the metal complex and the hydrocarbon. Work done by Page[13] and Kirby[14] investigated the rate difference and found the intramolecular reactions to be first order and the intermolecular to be second order. The ratio of the rate constants of the two reactions k_{intra}/k_{inter}, called "effective Molarity," is a measure of the effective concentration for either reaction. For example if the ratio k_{intra}/k_{inter} is infinitely small, intermolecular reaction is favored. If the ratio is large, intramolecular reaction is

favored. After a number of studies, it was concluded that many metals tend to activate the intermolecular C-H bond of arenes but not the C-H bond of alkanes. This is in contrast to the relative bond strengths of the C-H bond of arenes and alkanes. The arene C-H bond is 110 kcal/ mol and the weaker alkane C-H bond is 96-102 kcal/ mol[15].

Jones and Feher[16] performed a series of experiments to study the thermodynamics and kinetics of intermolecular arene/alkane activation. They prepared a rhodium complex with the general formula (C_5Me_5)Rh (PMe_3)(R)H R=aryl, alkyl) for several reasons. Bergman[17] discovered the intermolecular addition of cyclohexane to the (C_5Me_5)Rh(PMe_3)H_2 complex by photolysis. Thus the complex (C_5Me_5)Rh(PMe_3)(R)H where both R= aryl or alkyl can be formed. The known complex (C_5Me_5)Rh (C_2H_4)$_2$[18] was capable of H/D exchange similar to (C_5Me_5)Rh(PMe_3)(R)H and the resulting intermediate would be a 16e$^-$ low valent Rh(I) metal with good donor ligands. Lastly, the complex (C_5Me_5)Rh(PMe_3)(R)H could be formed by a second procedure (Scheme 1.3). Jones and Feher found the reductive elimination of the aryl complex occured around 60^o C and followed first order kinetics. They were able to generate an Eyring plot from which activation parameters could be derived: $\Delta H^{\ddagger}$ = 30.5(8) kcal/mol and $\Delta S^{\ddagger}$ =14.9 (2.5)eu. They suggest the positive value for entropy indicates that in the dissociation, benzene leaves as an intact molecule. The alkyl derivative showed first order kinetics of an irreversible reductive elimination at -20^o C. Aryl hydride complexes appear to be thermodynamically more stable than the alkyl hydride complexes.

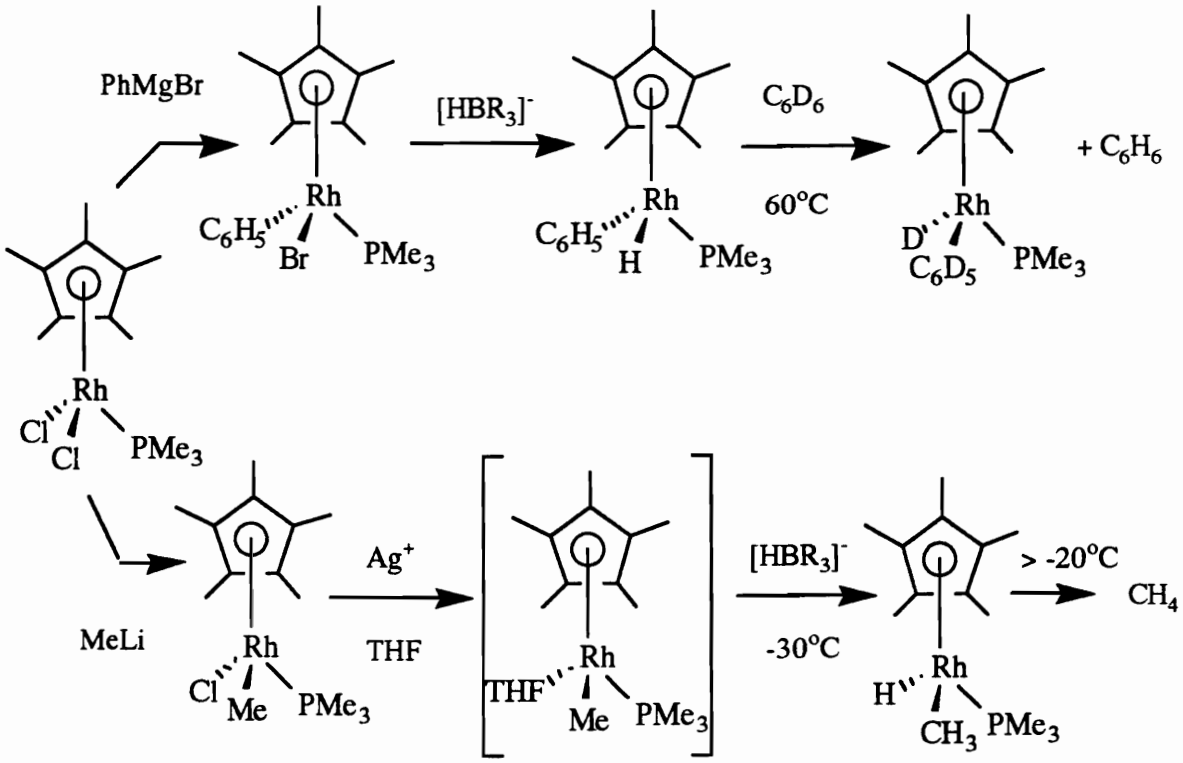

Scheme 1.3

Crabtree[19] observed this to be true since virtually all the known alkyl hyride complexes tend to eliminate the alkane and suggested a low kinetic barrier to the process. Also, Halpern[20] revealed Co-R bond strengths are dependent on the size of the axial ligand of the RCo(dmg)2L (dmg= dimethylglyoximato) complex.

In 1968, Hodges and Garnett[21] and later Parshall[22] proposed that arenes could coordinate in an η^2 fashion before the C-H addition occurred. Bennett and Milner,[9] observed small deuterium isotope effects for intramolecular substitution of ortho deuteriotriphenyl phosphine ligands. Parshall[10] suggested the transition state before the addition may proceed by a triangular three center intermediate. A precursor to this intermediate may be the observed M-H-C interactions, known as "agostic" interactions, coined by Brookhart and Green[23]. The agostic interaction occurs when a

16e- metal fragment has an available coordination site and a nearby alkyl group is able to occupy the site (Figure 1.2). The bridging C-H-M interaction is a three center two electron system that provides the metal center with two electrons and fill the last coordination site[19].

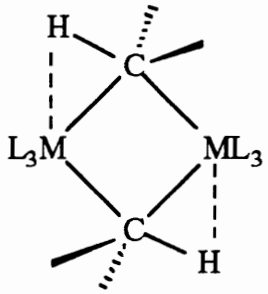

Figure 1.2 Agostic Interaction.

Muetterties[24] compiled a number of metal complexes showing the interaction to be triangular in character. Crabtree et al[25] investigated the changes of the C-H bond as it approaches the metal center by a variety of metal complexes that posses an agostic interaction (the C-H bond is not lengthened appreciably until the bond is very close to the metal). The M-H-C angle, averaging 130°, falls as the C-H bond approaches the metal center. This may shed some light on the mechanisms involved in C-H bond cleavage.

There are numerous reports in the literature of a wide variety of transition metal complexes that are able to cleave the C-H bonds in alkanes and arenes. As a matter of convenience, the most recent citations are given for each of the metals. The metals are grouped into three classes. Each class of metals are based on the type of mechanism; as, they appear to cleave the C-H bond. They are: the "four centered mechanism" such as in Ti(IV)[26], Zr(IV)[27], Ta(V)[28], and Th(IV)[29], "electrophilic substitution mechanism" in Pd(II)[30], and Co(III)[31], and the "oxidative addition mechanism" such as in Rh(I)[32], Ir(I)[33], Ru(I)[34], Os(I)[35], and Re(0)[36].

In a review by Ryabov[37], it was shown that the d^o complexes of Ti(lV), Zr(IV), Ta(V) and the lanthanide & actinides, are able to activate the C-H bond through a four center pathway. In the transition state the new M-C bond is being formed as the leaving group and the metal bond is broken (see Equation 1.2).

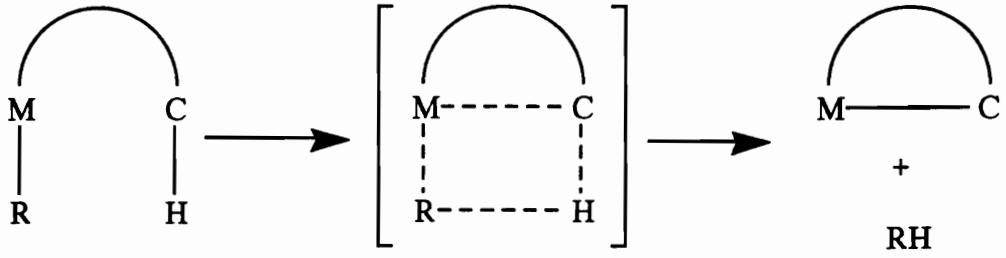

1.2

In the reactions of titanium(4) and zirconium(5) complexes that cyclometalate in toluene at 73-130° C, first order kinetics were observed which gave large and negative activation entropies $\Delta S^{\ddagger}$ (see Equation 1.3 and Table 1) consistent for multicentered pathways[38]. The tantalum (V) complexes (6), (7), (8) under similar reaction conditions, followed first order kinetics with slightly different activation parameters.

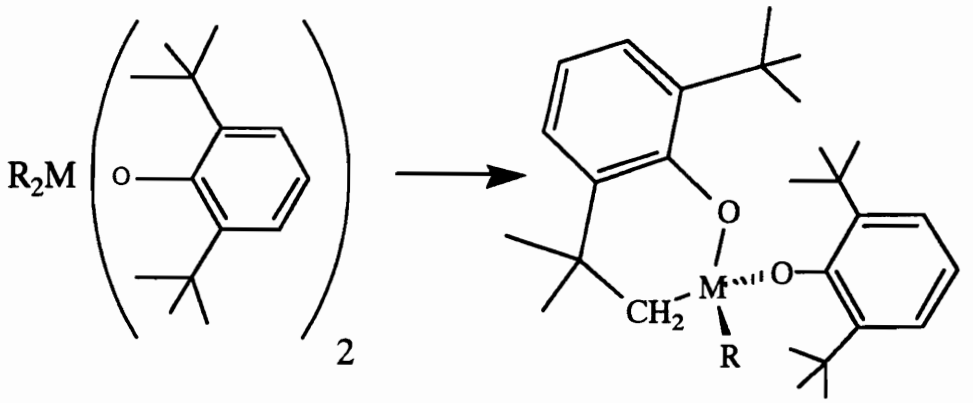

1.3

(4) M=Ti
(5) M=Zr

$R=CH_2Ph$

Complex	T, °C	10^5k, s^{-1}	$\Delta H^{\ddagger}$ kJ/mol	$\Delta S^{\ddagger}$ J/(K mol)
(4) $Ti(OAr)_2(CH_2Ph)_2$	114	126.0	97	-55
(5) $Zr(OAr)_2(CH_2Ph)_2$	114	32.3	91	-80
$Zr(OAr)_2(CH_2C_6H_4Me\text{-}4)_2$	114	39.2		
$Zr(OAr)_2(CH_2C_6H_4F\text{-}4)_2$	114	45.8		
$Zr(OAr)_2(CH_2C_6H_4F\text{-}3)_2$	114	18.4		
(6) $Ta(OAr)_2Me_3$	106	13.0	111	-29
(7) $Ta(OAr)_2(OCH2)Me_2$	106	0.42	124	-25
(8) $Zr(OAr)_2(=CH_2)Me$	27	4.3	60	-130

Table 1.1 Rate constants and activation parameters of the cyclometalation complexes of Ti, Zr, and Ta with 2,6-di-tert-butyl phenolato (OAr) ligand in toluene.

Tantalum (V) methyl complexes have higher values of $\Delta H^{\ddagger}$ and $\Delta S^{\ddagger}$ than the Ti(V) & Zr(V) counterparts. The differences in $\Delta H^{\ddagger}$ and $\Delta S^{\ddagger}$ for (6, 7) are believe to be caused by steric demands of five coordinate metal centers versus the four coordinate metal center of (8). The $(C_5Me_5)Th(CH_2SiMe_3)_2$ complexes were found to give similar values of $\Delta H^{\ddagger}$ and $\Delta S^{\ddagger}$ as well as first order kinetics in a series of reactions (Scheme 1.4 and Table 2). Watson[40] was first to observe alkane activation from the lanthanide group by $^{13}CH_4$ exchange in the following equation:

$$(C_5Me_5)_2LuCH_3 + {}^{13}CH_4 \rightarrow (C_5Me_5)_2Lu{}^{13}CH_3 + CH_4.$$

The intramolecular cyclometalation reactions for palladium(II), and cobalt(III) are believed to proceed through an electrophilic substitution mechanism as shown in Equation 1.4.

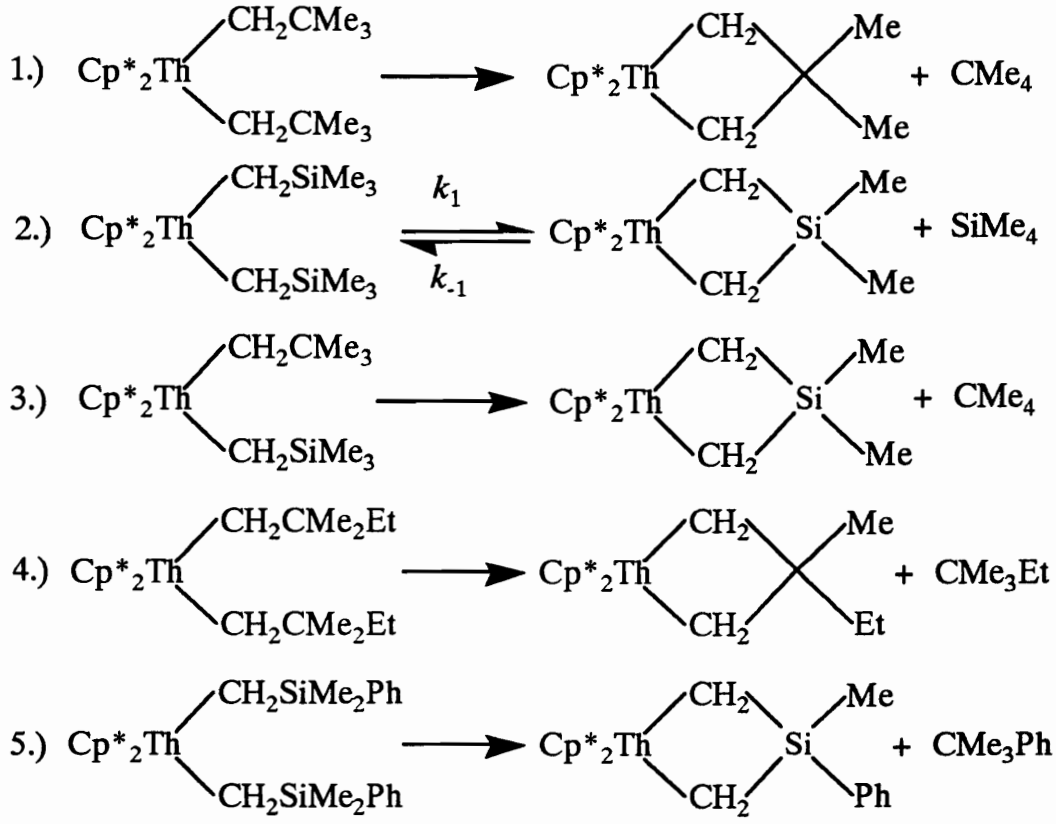

Cp* = C_5Me_5

Scheme 1.4

Reaction	10^5k, s^{-1}	$\Delta H^{\ddagger}$ kJ/mol	$\Delta S^{\ddagger}$ J/(K mol)
1	7.3	89	-67
2	0.39	105	-44
3	8.4	81.5	-87
4	8.2	78	-101
5	0.61	90	-84

Table 1.2 Rate constants and activation parameters of unimolecular reactions 1-5 in C_6D_6.

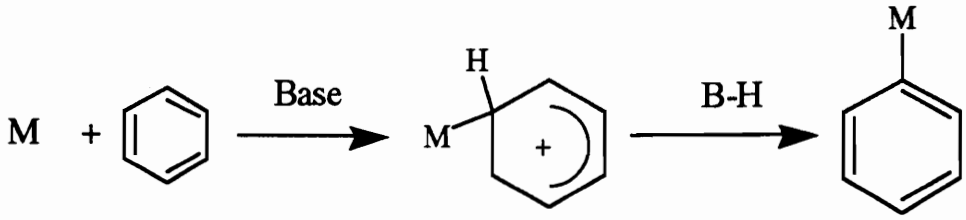

1.4

Cyclometalation of palladium(II) compounds were first studied by Cope[41] have been known to be typical electrophiles. For example, a classical reaction of azobenzene and palladium(II) chloride forms the cyclo-palladated product in shown Scheme 1.5. In aprotic solvents, palladium (II) complexes have exhibited nucleophilic character. Substituted N, N dimethylbenzlamines react with $Pd(OAc)_2$ (actually $Pd_3(OAc)_6$)[45,46] in acetic acid/NaOAc to form the cyclopalladated dimer. The rate constant *k* increased with electron withdrawing groups and the corresponding Hammett coefficient ρ is equal to $+1(\sigma p)$[47] (Equation 1.5).

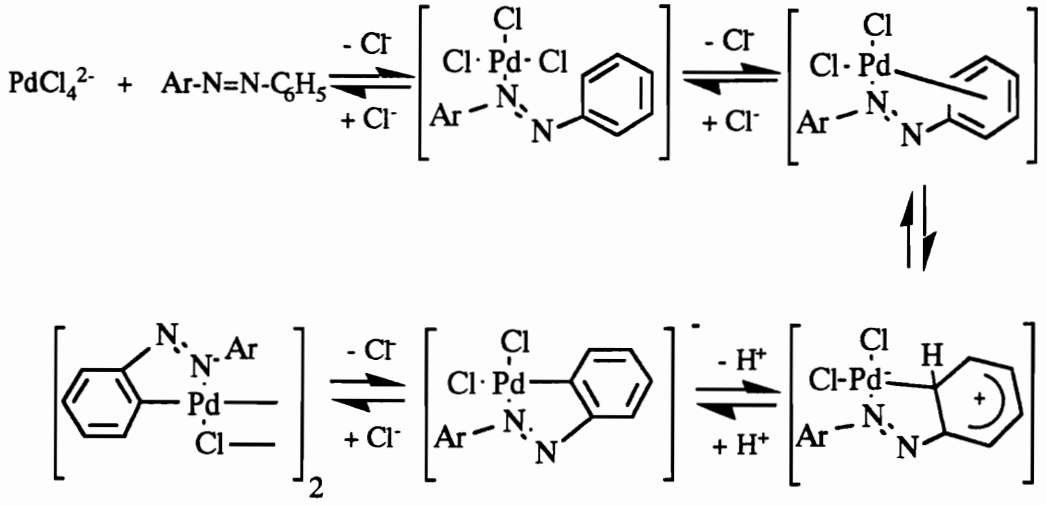

Scheme 1.5

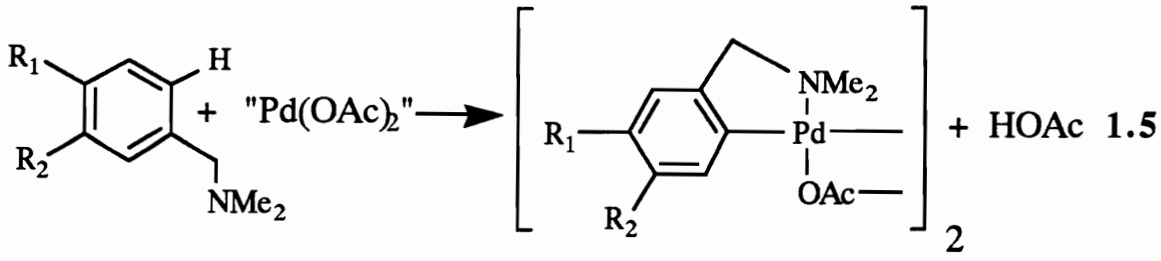

R_1, R_2 = Cl, H, Me, OMe

Fujiwara[48] and coworkers investigated the reactivity of various aromatics and the substituent effects of these aromatic compounds with olefins in the presence of palladium acetate and acetic acid. The products formed are substituted trans-stilbenes of the type $C_6H_5CH{=}CHC_6H_4X$, where X= CH_3, C_2H_5, OCH_3, Cl, and NO_2. The electron-releasing groups increase the reactivity as in the usual electrophilic aromatic substitution mechanism. Graph 1 shows the Hammett plots of the logarithm of partial rate factors k versus σ^+. This data suggests electrophilic substitution; however, the low absolute value of ρ(-1.4) was suggestive of a radical process. Radical inhibitors were then used in the reactions with no effect on the reaction rates. They argue the point that Pd(II) is a diamagnetic species and that no by-products typical of the radical process were found. Thus, they concluded the process to be an electrophilic substitution one.

As for cobalt complexes, like the known oxidizing agent $CoOAc_3/O_2$ system[49], intial electrophilic attack by Co(III) on the C-H bond was suggested to occur followed by loss of the proton[50], with a strong base usually required (Equation.1.6).

$$\text{C-H} + \text{Co(III)} \rightarrow \text{C-Co(III)} + \text{H}^+$$
$$\text{C-Co(III)} \rightarrow \text{C}\cdot + \text{Co(II)} \qquad \textbf{1.6}$$

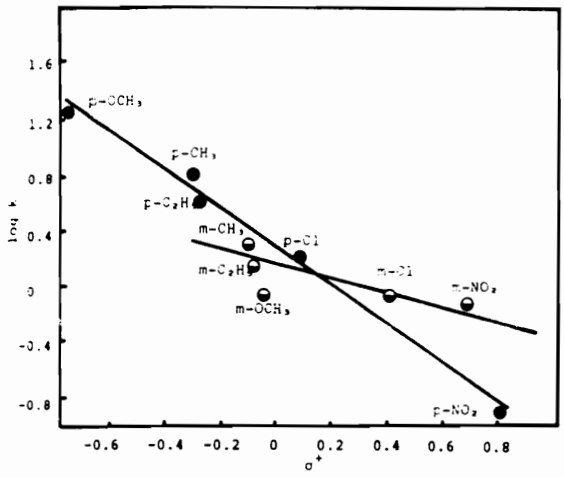

Graph 1.1 Plots of the logarithm of the partial rate factors k vs σ^+ for substitution of para-(●) and meta- (◒) substituted benzenes with styrene in the presence of palladium acetate.

In 1986, a base catalyzed intramolecular metalation of a Co(III) complex was found to occur after proton abstraction from the C-H-M interaction[51]. This gave the cobaltacycle shown in equation 1.7.

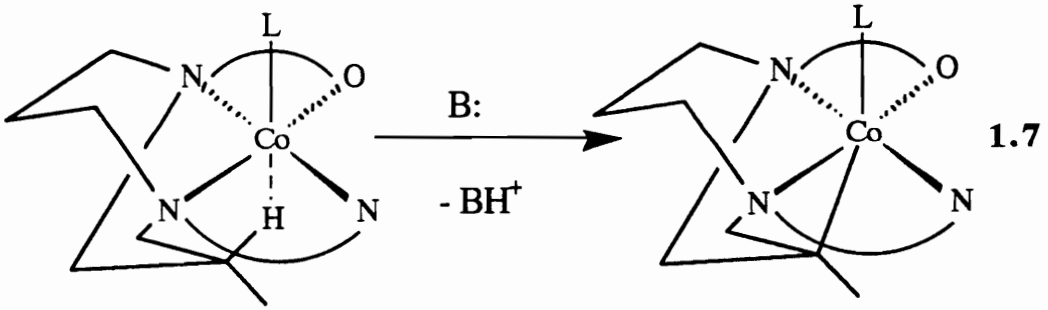

1.7

Although platinum lies below palladium in the periodic table and has shown similar chemistry, the process in which the C-H bond is cleavage by platinum compounds has been elusive for either intra or intermolecular C-H cleavage. Platinum (II) displays electrophilic substitution in cyclomelation of azabenzene[41a] and N, N dimethylbenzylamine[41b]. Whitesides and co-workers[52] proposed a mechanism in which the

phosphine ligand reversibly dissociates followed by oxidative addition of one of the neopentyl groups, reductive elimination of neopentane (rate limiting step) and finally phosphine reassociation (Scheme 1.6). A possible alternative mechanism for Scheme 1.6 would be a four centered mechanism as shown in Equation 1.8.

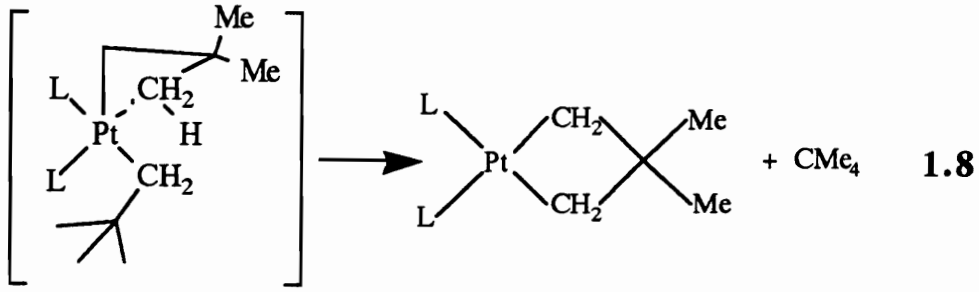

1.8

Whitesides[52] found the four-centered pathway to be inconsistent with the high positive value of $\Delta S^{\ddagger}$ because typically four centered pathways have large activation enthalpies $\Delta H^{\ddagger}$ (>80kJ/mol) and large negative entropies $\Delta S^{\ddagger}$ (ordered transition state).

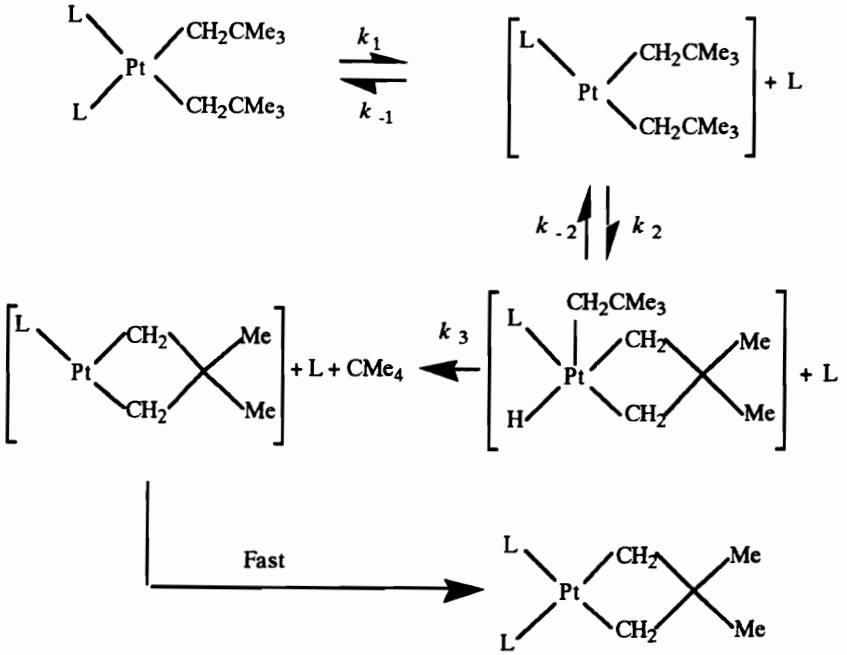

Scheme 1.6

Oxidative additions are primary reactions where an X-Y bond adds to a metal center with an increase of both the coordination number and the oxidation state of the metal by two.

$$[M]^{o} + X\text{-}Y \rightarrow Y\text{-}M^{+2}\text{-}X$$

Oxidative additions are known to occur in low valent metal complexes for a number of X-Y bonds (XY=H_2, Cl_2, HCl, MeI, R_3Si-H)[3]. Chatt and Davidson[8] observed the first C-H bond cleavage of sp^2 and sp^3 hydrocarbons, mentioned earlier. Studies have shown the additions proceed by a concerted mechanism. Bergman et al[53] have found evidence that the C-H addition may proceed by a three-centered transition state and does not involve free radicals as intermediates. The complex $C_5Me_5Ir(PMe_3)H_2$ was irradiated in a 1:1 mixture of neopentane and cyclohexane-d_{12} and the resulting products were the hydridopentyl- (**9**) and the deuterio(per-deuterocyclohexyl)- (**10**) iridium complexes, with very little cross over products (**11**) and (**12**) (equation 1.9).

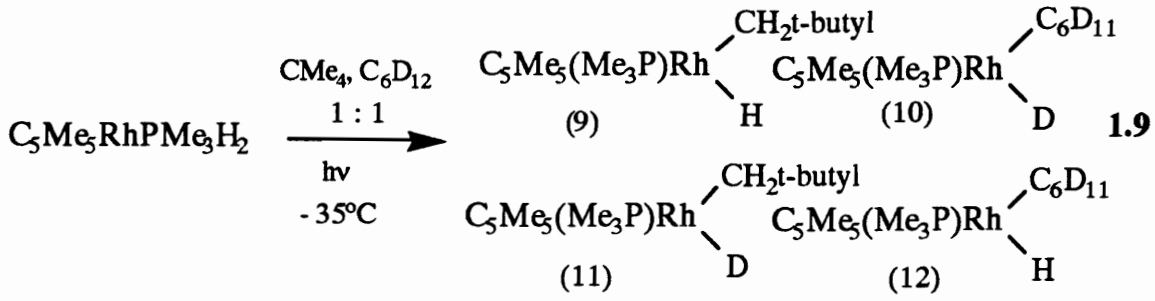

1.9

In 1989, Bergman[54] reported that benzoquinoline cyclometalates by an end on C-H addition rather than the triangular approach where 8-methyl-quinoline gave the agostic C-H-M bridged system. Another proposed

mechanism in which the phenyl ring (c), can twist allowing the carbon atom to rehybridize to an sp^3 fashion in the transition state before the C-H bond is cleaved (equation 1.10).

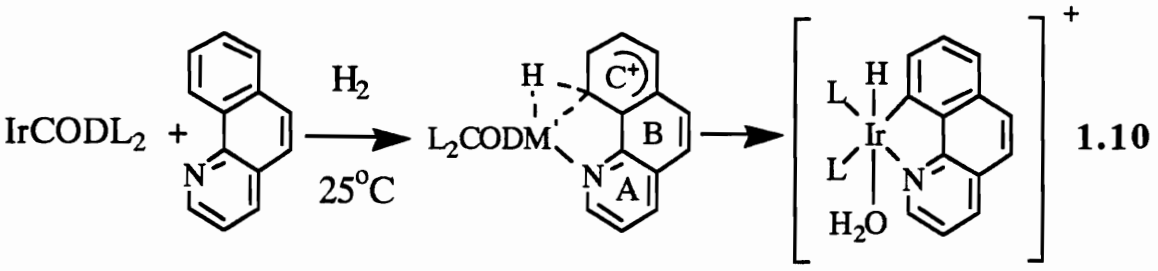

1.10

COD=1,5 cyclooctadiene, L=PPh_3

Jones and Feher[55] provided evidence of a low kinetic preference for aryl and alkyl addition by the reaction of $(C_5Me_5)Rh(PMe_3)H_2$ and a mixture of benzene and propane. Upon photolysis, a 4:1 ratio in preference for benzene was found. An interesting rearrangement of $(C_5Me_5)Rh(PMe_3)(p\text{-}C_6H_4.Me)Br$ during a reduction with $[HB(sec\text{-}Bu)_3]^-$, gave a 2:1 mixture of meta and para tolyl hydride. They believed the rhodium complex was in equilbrium with an η^2-arene species. Recently a paper by Belt et al[56] supports the η^2-arene coordination. In this report, they have controlled the preference for η^2-arene coordination versus C-H addition by the use of fused polycyclic aromatic systems. Several experiments were carried out by Jones and Feher[55a] in which the activation parameters were found with a negative entropy $\Delta S^{\ddagger} = -6.3$. This would suggest an ordered transition state shown in Scheme 1.7. The particular experiment provided evidence for a stepwise [1,2] migration of the proton from the metal to the ortho position of the phenyl group. Thus the η^2-arene coordination process rules out any mechanism where the aromatic protons are equivalent.

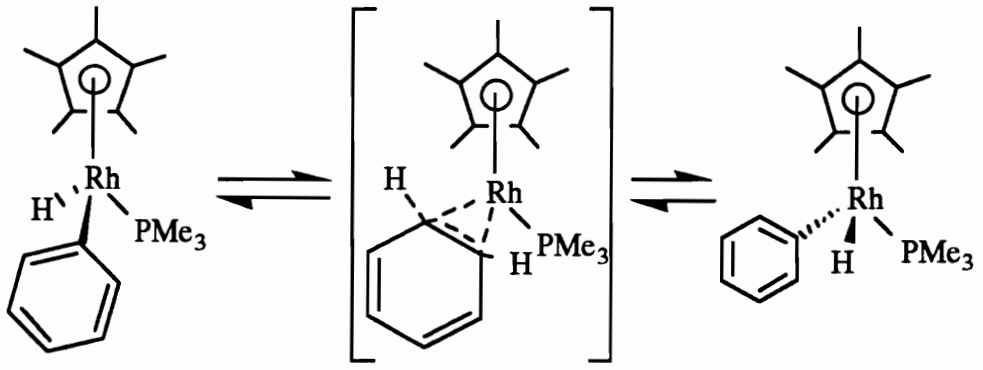

Scheme 1.7

Functionalization

Cyclopalladated aromatic complexes enjoy a number of useful reactions in organic syntheses[57]. A recent number of reports on other C-H bond activations of both aryl and alkyl hydrocarbons by various transition metal complexes have surfaced. However, functionalization of the C-H bond in these latter complexes has been limited to insertion reactions of carbon monoxide and isonitriles and only a few cases of olefin insertion. Figure 1.3 shows several typical carbon monoxide[58], and isonitrile[59] insertion reactions.

Diamond and Mares[60] found a potentially useful reaction between aniline and olefins catalyzed by a rhodium complex to give N-alkylated and heterocyclic compounds. A typical reaction consists of aniline, $RhCl_3 \cdot 3H_2O$, triphenylphosphine and ethylene at 100 atm which was heated to 200° C for 72 hrs to produce 30 turnovers of N-ethylaniline and 10 turnovers of 2-methylquinoline (relative to the metal). Lower pressures of ethylene gave mostly the N-alkylated product. In 1981, Muetterties and Sievert[61] discovered the isomerization of coordinated alkenylbenzenes.

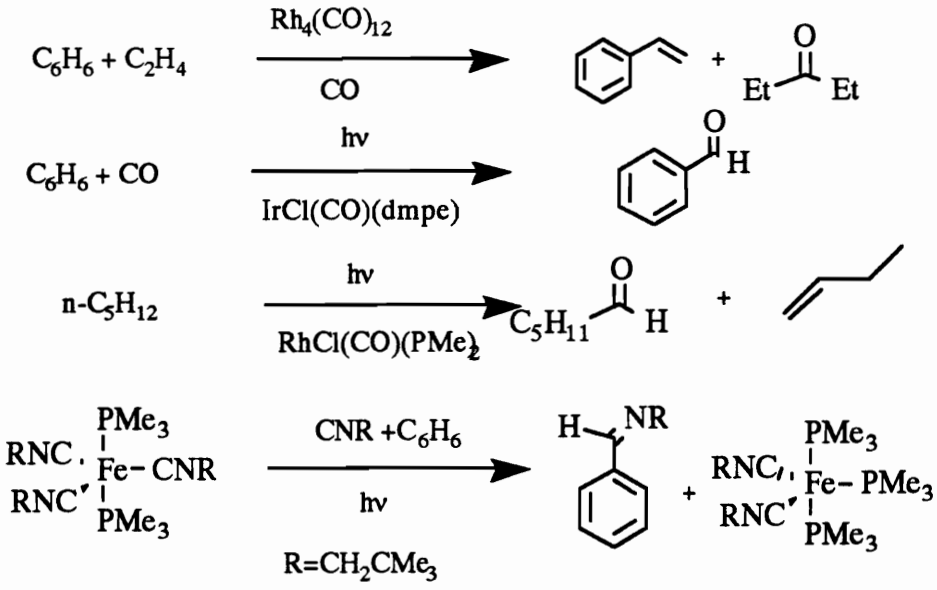

Figure 1.3 Carbon Monoxide and Isonitrile Insertion Reactions.

Acetone solutions of cis-propenyl and an allylbenzene complex were converted to the trans-propenyl benzene complex at room temperature. Further investigation of this isomerization revealed a 1, 3 hydrogen shift mechanism (Scheme 1.8).

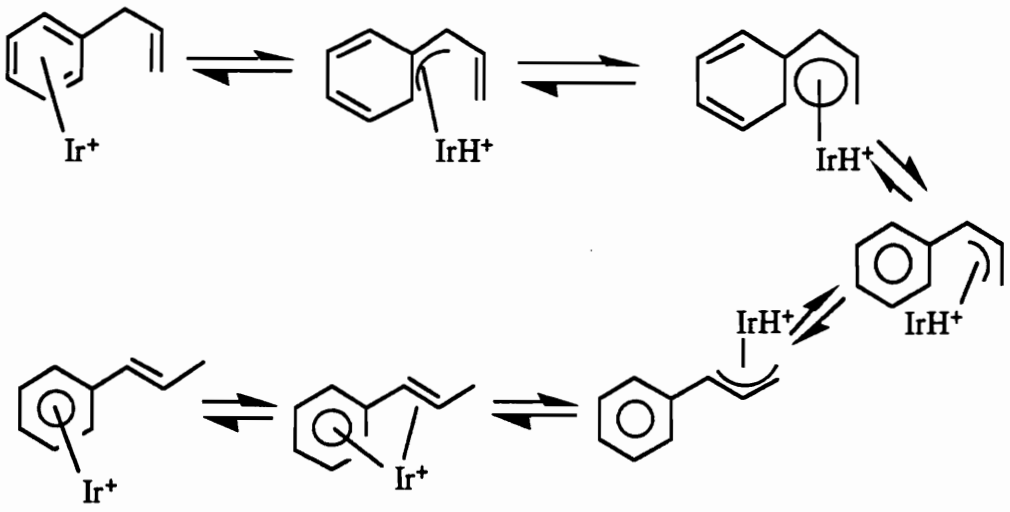

Scheme 1.8

Under rather drastic reaction conditions, rhodium carbonyl clusters have been found to activate the C-H bonds of aromatic compounds[62]. Carbon monoxide pressures of 20-30 atm and temperatures up to 220° C, are required for rhodium carbonyl clusters $Rh_4(CO)_{12}$ and $Rh_6(CO)_{16}$ to couple benzene with unsaturates like diphenylketene, isocyanates and acetylenes. The compounds formed are diphenylacetophenone, benzamides and phenylated olefins. Heterocycles such as furan, thiophene and N-methyl pyrrole were found to react as well. Monosubstituted aromatics such as toluene, anisole, and fluorobenzene react with diphenyl ketene to give aryl diphenylmethyl-ketones. The ratios for ortho, meta, para products of anisole, fluorobenzene, and toluene are 55/31/14, 60/17/13 and 6/62/32, respectively[63], see Equation 1.11.

Benzene reacts with diphenylacetylene to give triphenylethylene(**13a**) and a by product 2,3 diphenylindenone (**14a**) under similar conditions (Equation 1.12). When the reaction was allowed to proceed without the partial pressure of carbon monoxide, hexaphenylbenzene was formed.

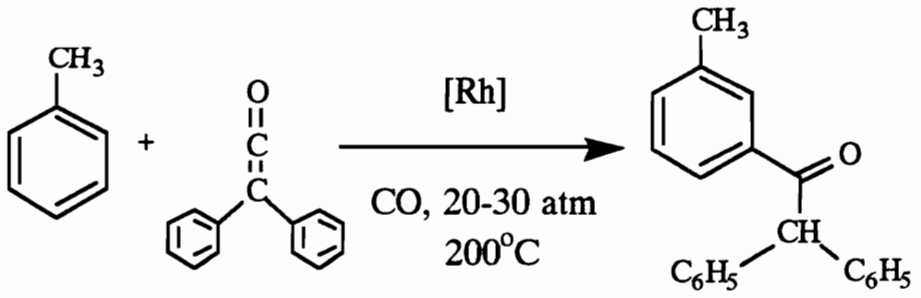

1.11

[Rh] =$Rh_4(CO)_{12}$, $Rh_6(CO)_{16}$
Yields increase as CO pressure increases from 11% to 68%

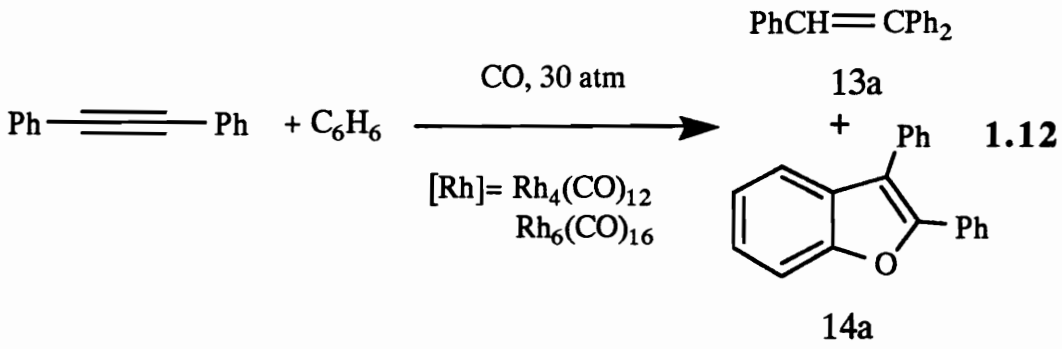

1-Phenylpropyne and benzene gave exclusively E-methylstilbene and the 3-methyl derivative of **(14a)**. Substituted aromatics and diphenylacetylene gave a mixture of isomers with ratios similar to those found in the reaction of diphenyl ketone[64]. Again under similar conditions benzene and substituted olefins produced the phenyl substituted product and acetone (Equation 1.13).

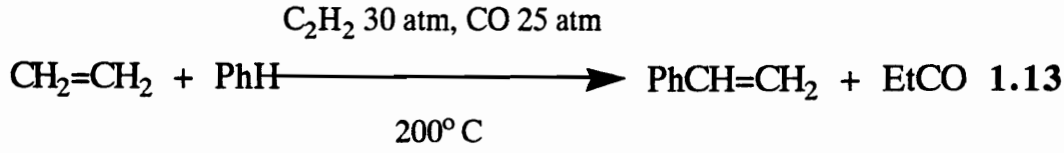

The substituted aromatics anisole, fluorobenzene, and toluene gave a mixture of ortho/meta/para isomers with ethylene in the following ratios: 67/23/10, 78/17/5, and 14/57/29 respectively[65]. The five membered heterocyclic compounds like furan, thiophene and N-methylpyrrole react with diphenyl acetylene to give a mixture of isomers. For example furan gave a combined product yield of 80% in a ratio of (78/22) for (Z) and (E)-1-(2-furyl)-1,2-diphenyl ethylene, respectively. The order of reactivity was found to be furan> thiophene> N-methylpyrrole>benzene.

The rate of conversion for furan was 200 times faster than benzene (Equation 1.14)[66].

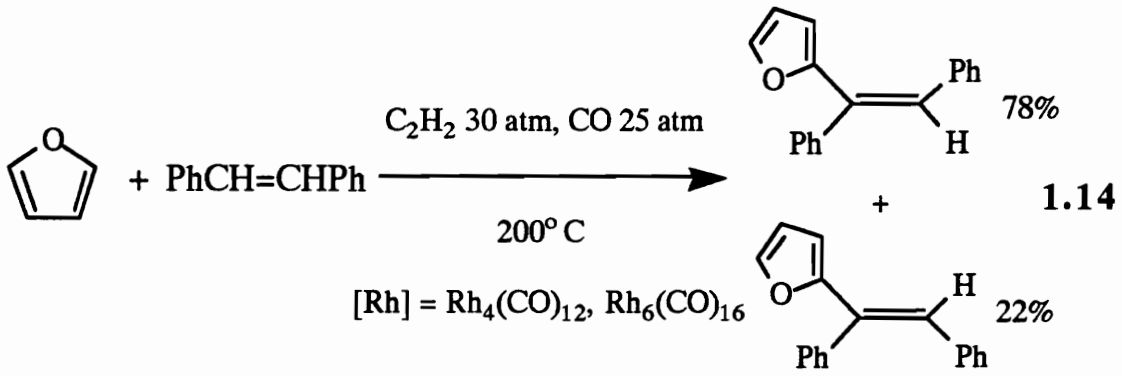

1.14

Jones and Kosar[67] catalytically converted 2,6-xylyl isocyanide into 7-methylindole by $Ru(dmpe)_2H_2$ at 140° for 24 hrs. They found that the rutherium complex remained intact and that 20 mol % of the complex was required for a yield of 98% of 7-methylindole (Scheme 1.9). Once the 7-methylindole.is formed, the N-H bond begins to react with the ruthenium complex as well.

An iridium pentahydride was found to activate alkyl C-H bonds of methyl ethers followed by olefin insertion[68] (Equation 1.15). They proposed a mechanism where upon thermolysis of $IrH_5P(i\text{-}Pr_3)$, the olefin is hydrogenated leaving a reactive metal fragment to cleave the C-H bond of methyl ethers. The olefin was inserted followed by β-hydrogen elimination to give **(19)**. **(19)** is then rapidly isomerized to the enol ethers **(17)** & **(18)**. When the reaction was heated to 150° C, the yield of **(17a)** was increased to 52%.

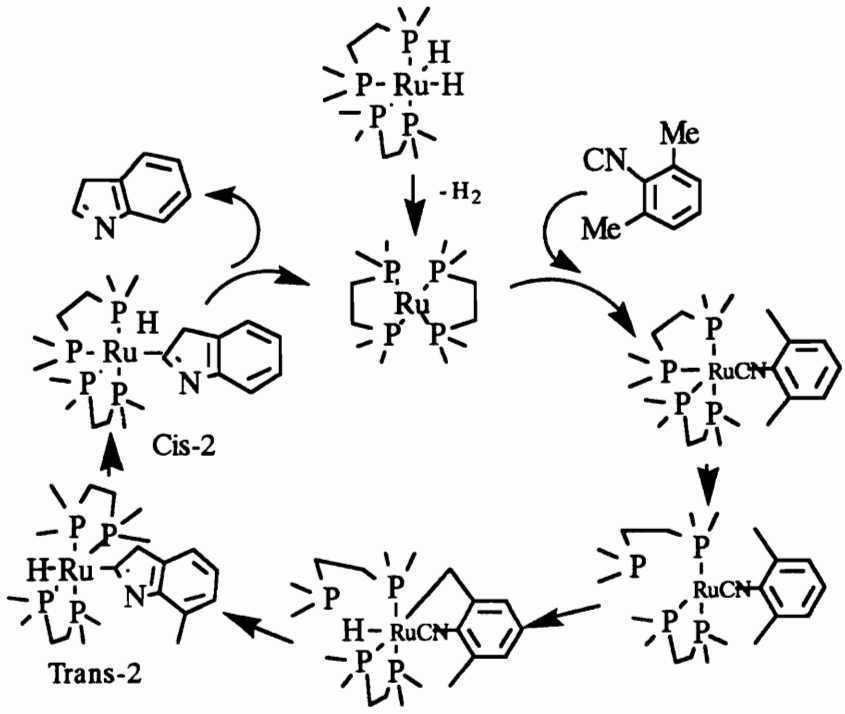

Scheme 1.9

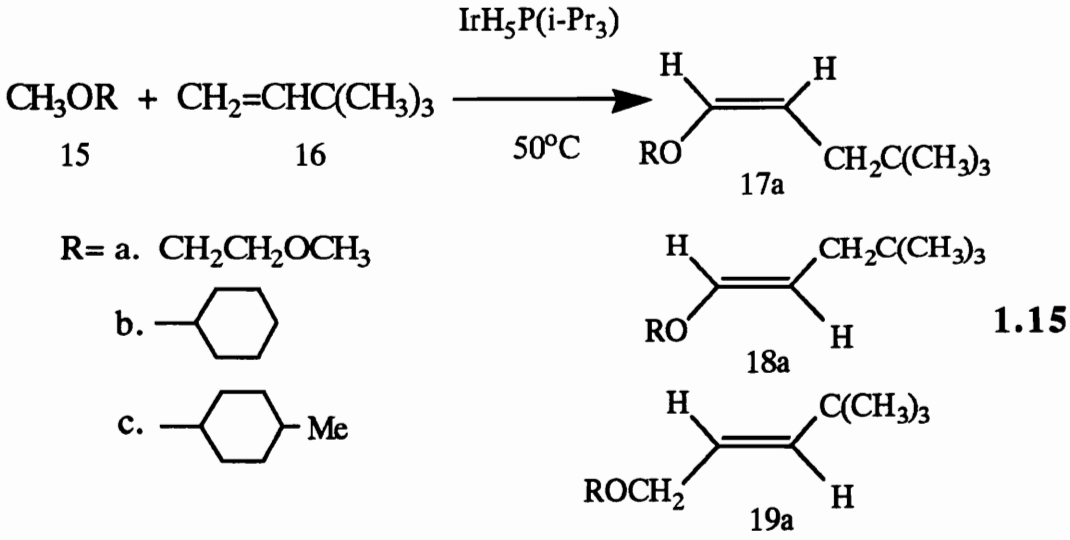

In 1989, Jordan[69] discovered a cationic zirconium complex (**20**) that would insert propene into the C-H bond of a picoline. A catalytic cycle was produced with the aid of diatomic hydrogen with a rate of 1-2

turnovers per hour at room temperature. The reaction is dependent on the partial pressures of hydrogen (1 atm), propene (1.5 atm) and the available picoline concentration (Scheme 1.10).

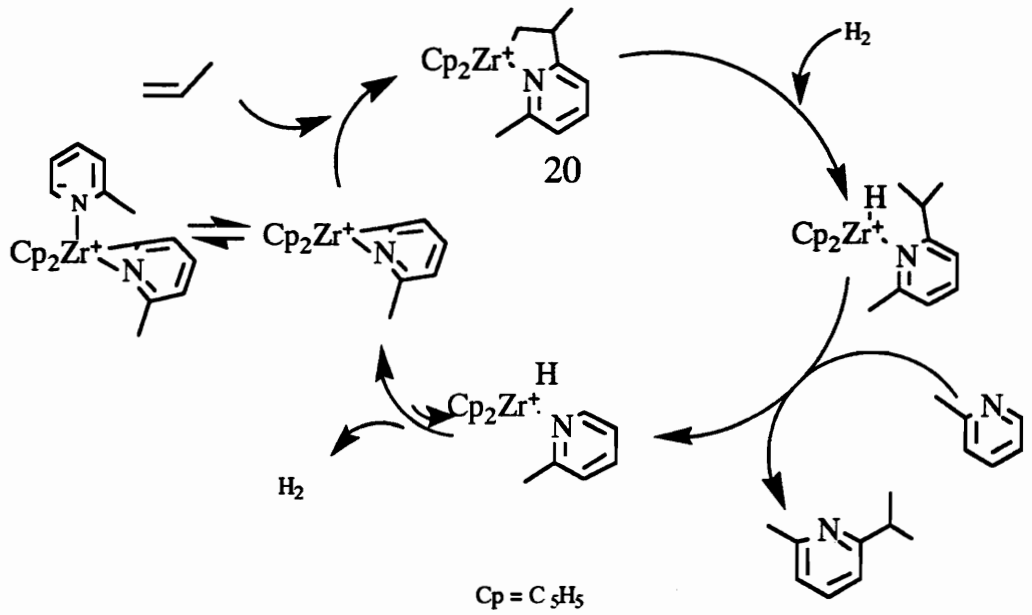

Scheme 1.10

A following paper by Jordan[70] describes regioselective control in a coupling reaction between $SiMe_3$ substituted alkenes and the η^2 (N, C^2)-6-phenyl-pyridyl) zirconium complex (**21**). The reactions gave high yields of (**22**) & (**24**) and on work-up the 1, 2 inserted product was obtained (Equation 1.16). The 1, 2 inserted products of (**23**) and (**25**) are believed to be under the influence of electronic effects (**A**) for (**23**), and steric effects (**B**) for (**25**). Figure 1.4 shows the proposed transition states for the insertion of allyltrimethyl silane (**A**) and vinyl trimethylsilane (**B**) into the Zr-C bond of pyridyl complex (**21**).

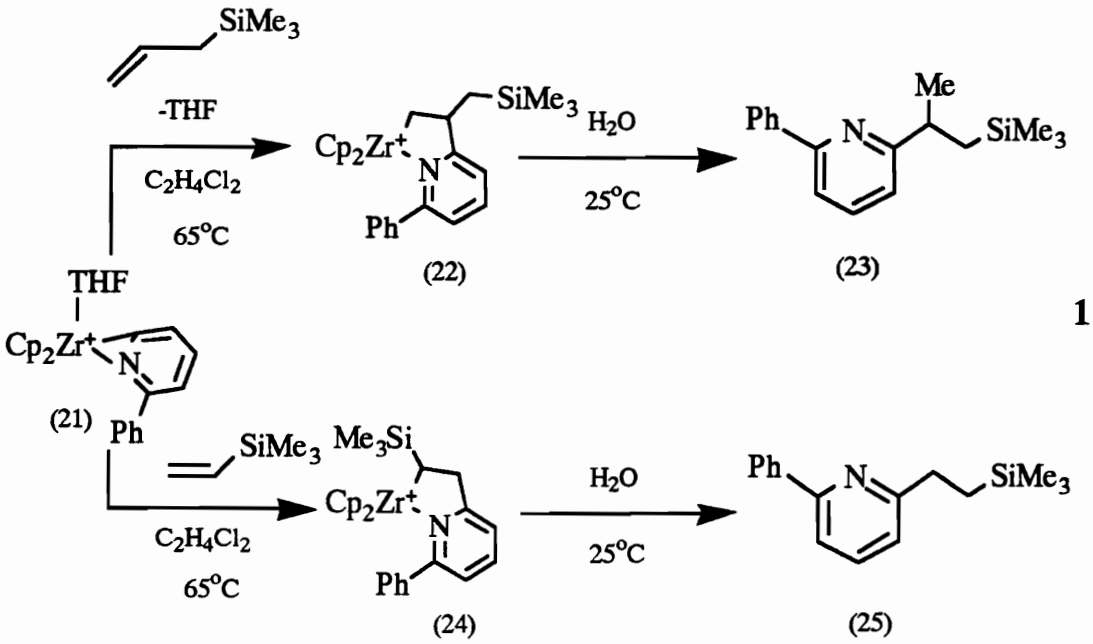

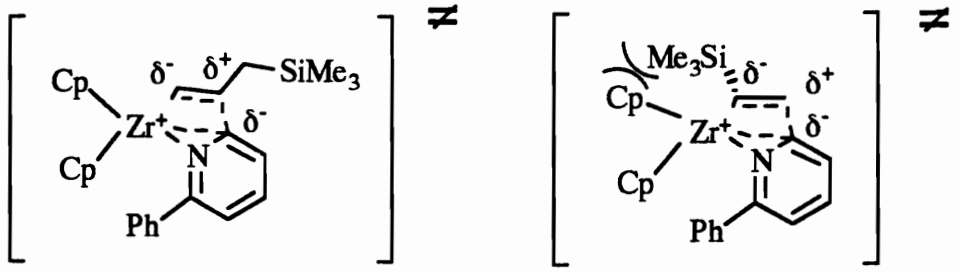

A.) B.)

Figure 1.4 Proposed Transition State for the Insertion of Allyltrimethylsilane (A) and Vinyltrimethylsilane (B).

Tanaka et al[71] were able to demonstrate alkyne insertion into aromatic and aliphatic C-H bonds with the use of a rhodium complex. The photolysis reaction of benzene, terminal alkynes and the $RhCl(CO)(PMe_3)_2$ complex gave a mixture of products (Equation 1.17). The yield of each product varies depending on the ratio of benzene and alkyne employed on a volume for volume basis. For example: a ratio of 1/29 (v/v of alkyne

(**26**) to benzene), gave a yield of 190% (per Rh) of (**27a**), 768% (per Rh) of (**30a**), and minor amounts of (**28a**), (**29**), (**32a**) and (**33a**). When the ratio was 1/300 (v/v), (**27a**) was increased to 558% (per Rh), 173% (**30a**), and minor amounts for the others. The differences were due to the competition for the catalyst by the C-H bond of either the terminal alkyne or that of benzene. Increasing the temperature has no effect on the yields of (**27**) or (**30**) but the trimer (**33a**) increases several fold. For the ratio 1/29(v/v alkyne to benzene), (**27b**) was the major product giving a yield of 176%, and (**29**) in 79% yield. On dilution to 1/300 (v/v), (**27b**) and (**29**) was produced in a yield of 159% (per Rh). Even a dilution of 1/300 (v/v (**26c**) / benzene)of the reaction, gave (**27c**) in a yield of 17%; however, the major product (**29**), was found in a 41% yield.

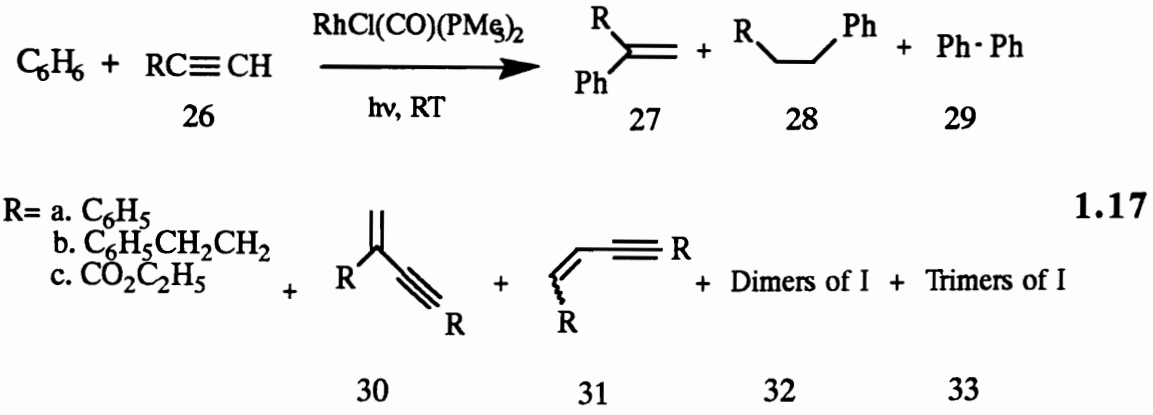

1.17

Aliphatic hydrocarbons such as cyclohexane and n-hexane, and even ethyl ether were able to insert alkynes between the alkyl C-H bond to give substituted styrenes. By-products of hydro and dehydrogenated compounds were also found (Equation 1.18).

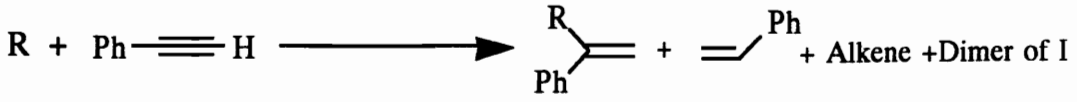

R = a - cyclohexane	a	19%	123%	420%	37%
b - n-hexane	b	77%	102%	146%	56%
c - ethyl ether	c	21%	162%	(cis & trans)	29%

1.18

R = 1/300 (v/v) RT, 4.5 hr Irradiated with a 100w high pressure Hg lamp

Shortly afterwards, Goldman[72] reported a similar reaction between benzene and terminal alkynes catalyzed by $RhCl(CO)(PMe_3)_2$ (**34**). A list of their results is shown below in Equation 1.19.

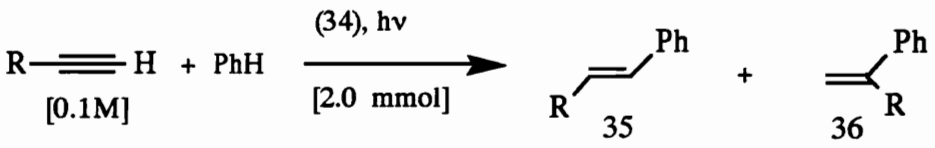

1.19

R = a n-Pr	35a (68%)	36a (14%)
b t-butyl	b (48%)	b (10%)
c Ph	c (0%)	c (90%)
d p-$MeOC_6H_4$-	d (0%)	d (95%)

The rate of turn overs per Rh was >200 when the initial concentration of p-$MeOC_6H_4C{\equiv}CH$ was at 0.5M. Crossover experiments showed the proton and the aryl ring are from the same benzene molecule when the alkyne was inserted. The proposed mechanism is shown in Scheme 1.11.

Most recently, Bergman[73] reported alkyne insertion into methyl and aryl hydride complexes of (η^5-Ind)(PMe_3)Ir(Me)H (**6a**) and (η^5-Ind)(PMe_3)Ir (Ph)H. The important aspect of this paper involves the alkyne insertion. The indenyl ligand has the ability to isomerize reversibly from η^5 to η^3 coordination and back. This is important for the alkyne coordination and insertion mechanism (scheme 1.12).

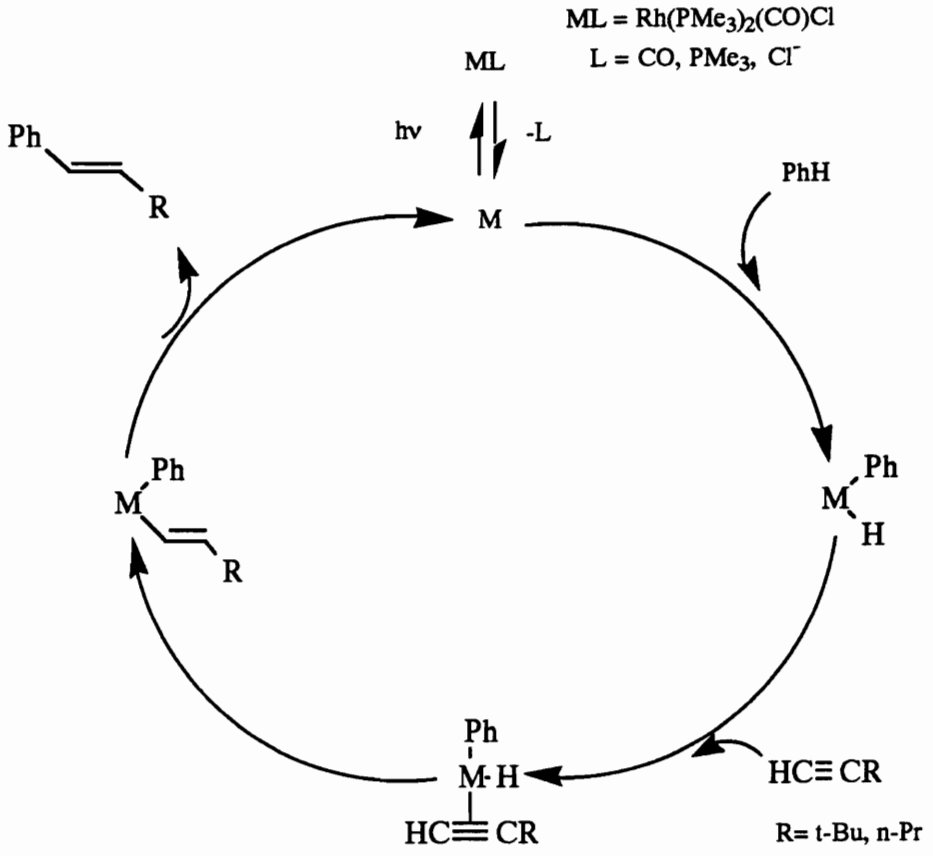

Scheme 1.11

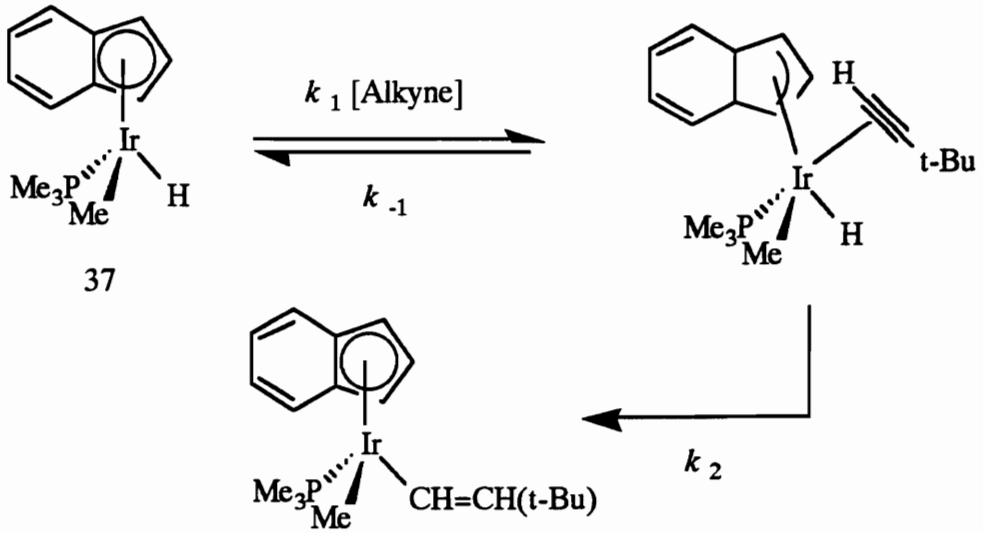

Scheme 1.12

Treatment of (**37**) with excess acetylene at room temperature gave the (η^5-Ind)(PMe_3)Ir(CH_3) ($CH{=}CH_2$) complex in 12 hours in a yield of 80%. A red solid was found as well and is believed to be a polyacetylene derivative. (**37**) and t-butylacetylene reacts at 65°C after 24hrs to give the (η^5-Ind)(PMe_3)Ir (CH_3)(CH=C(t-Bu)H) in 80% yield. However, the reductive elimination of these hydrocarbons to produce useful products has not been perfomed.

Therefore, it is the intent of this thesis to continue to explore the migratory insertion of unsaturates into several aryl hydride iridium complexes of the type (Me3P)3Ir(Aryl)(H)Cl. Chapter 2 will describe the synthesis and characterization of six interesting aromatic C-H addition complexes as well as the C-H additions of some substituted arenes. The reactivity of the phenyl complex **I**, pyridyl complex **III**, and furyl complex **IV** with acetylenes will be described in Chapters 3, 4, and 5 respectively. A discussion of the mechanism for acetylene insertion of **I**, **III**, and **IV** will be provided along with the synthesis and characterization of each resulting complex. The last chapter will cover the summary of results from which some comparisons and differences can be examined in more detail. This chapter also contains some suggestions for future work derived from knowledge of the literature and the results of this work.

Chapter 2: Oxidative Addition Of C-H and C-S Bonds By The [Ir(COD)(PMe3)3]Cl Complex

The chemistry of (tris-trimethylphosphine)iridium(I)cyclooctadiene chloride, [Ir(COD)(PMe3)3]Cl has been extensively investigated by the Merola group over the last four years. This particular complex is capable of H-H, B-H, N-H, OH, C-H and even C-S addition across the metal center. An iridium complex was chosen because of iridium's ability to cleave C-H and C-C bonds and it is used as a reforming catalyst in the petroleum industry. Previous work by Merola et al[74] revealed that under moderate reaction conditions, a carbon-hydrogen bond in benzene can be activated by [Ir(COD)(PMe3)3]Cl. This produces the mer-(Me3P)3Ir(Cl)(H)(Phenyl) complex (**I**) in a yield of 50%, as shown in equation 2.1.

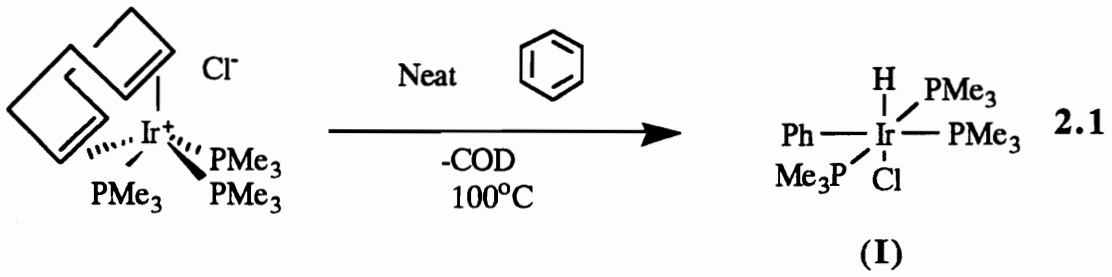

2.1

(I)

As a continuation of this work, attempts were made to increase the yield of (**I**) by the use of solvents with higher boiling points than benzene. Decalin was chosen because of its' high boiling point but made the work-up procedure rather difficult. N-octane, mesitylene and methylcyclohexane (MCH) were used as nonreactive solvents. MCH was the solvent of choice for the other aromatic additions which will be explained in some detail in the appropriate section. A yield of 60% can be reached when the solvent decalin is used. This solvent may avoid the production of unwanted by-products, hence the slight increase in yields. Upon work-up, the

undissolved solids were filtered out and the yellow solution was stripped nearly to dryness. The crude product can be easily obtained by washing a bright yellow by-product out with pentane. Analytically pure product was obtained by precipitation from a fairly concentrated solution of the product in methylene chloride by the addition of pentane. Characterization of this complex was accomplished using ^1H NMR spectroscopy. A typical ^1H NMR spectrum reveals a quartet at δ= -23.7 ppm which is due to the iridium hydride. A triplet and a doublet occur at δ= 1.35 and 1.6 ppm due to the PMe_3 ligands with the doublet/triplet pattern indicating a meridional arrangement. Finally, there are five triplets from the phenyl group between δ=6.7 and 8.2 ppm. The point worth noting about complex (**I**) is that the phenyl ligand is locked in position to give five unequivalent protons as triplets in the NMR spectrum. A variable temperature experiment was performed to determine the temperature necessary to rotate the phenyl ligand about the C-Ir bond. However, the complex decomposed before rotation was achieved indicating a high barrier for rotation.

The structure of a complex can be quickly determined by the splitting patterns of the phosphine ligands and the hydride. A meridional arrangement of the phosphine ligands would give a 2:1 ratio of a triplet and a doublet in the ^1H NMR spectrum. A facial arrangement would show three equivalent doublets. If the hydride were cis to the three the phosphine ligands a quartet would be found. If the hydride were trans to one phosphine ligand and cis to the other two, a pair of triplets would be found for the hydride resonance. The position of the organic group can then be identified through the C-H addition which must be a cis addition, and generally the last coordination site is filled by a chloride ligand.

Aromatics

Other aromatic systems are of interest for C-H activation. Benzaldehyde appeared to be a good candidate for C-H activation since aldehydes have been known to add across rhodium and iridium metal centers[75, 76]. There are two possiblities for the C-H addition : The C-H addition of one C-H bond of the aromatic ring, or the more acidic C-H bond of the benzaldehyde. Methylcyclohexane was a better solvent than decalin in the work up procedures since decalin has a boiling point of 190° C and it is rather difficult to remove, even under vacuum.

[Ir(COD)(PMe_3)$_3$]Cl, benzaldehyde and MCH were combined and placed in an oil bath in a closed tube at 100° C for 24 hours. Upon work-up, the reaction produced a 30 % yield of mer-(Me_3P)$_3$Ir(COC_6H_5)(H)Cl, (**HES II 141**), (**II**). The ^{1}H NMR spectrum of (**II**) displayed a doublet at δ=1.56 and a triplet at δ=1.51 ppm suggesting a meridional orientation of the phosphine ligands. A pair of triplets at δ= -9.2 and -9.8 ppm indicate the hydride to be in the plane of the phosphine ligands, leaving the organic group and the chloride ligand in the axis. Two multiplets at δ=7.9 and 7.3 ppm were found in the aromatic region for the phenyl group integrating for five protons (Figure 2.1). This suggests the C-H addition occurred on the aldehyde portion and this structure was confirmed by single crystal X-ray crystallography (Figure 2.2).

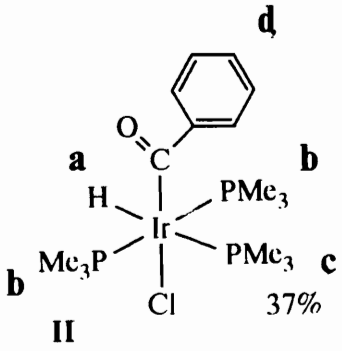

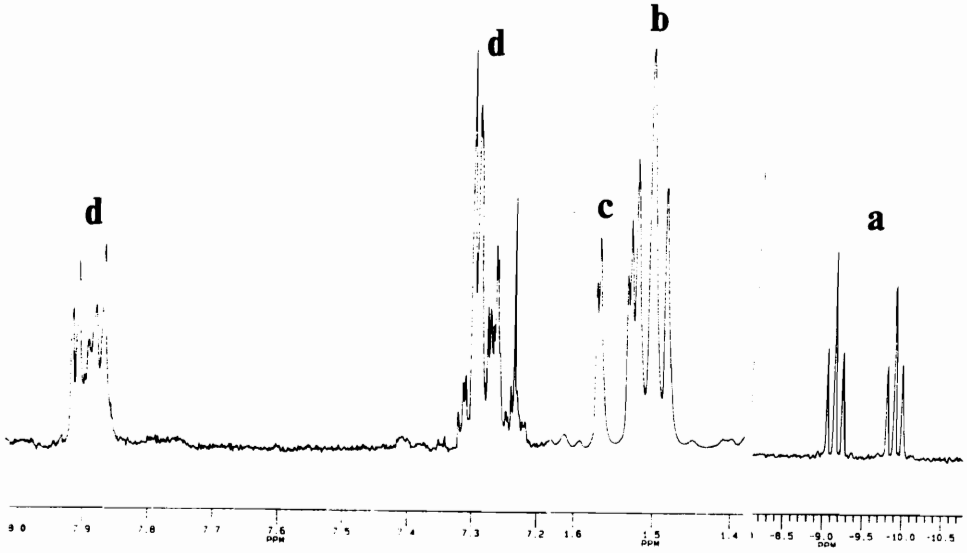

Figure 2.1 The ^{1}H NMR of *mer*-(Me3P)3Ir(COC6H5)(H)Cl (II)

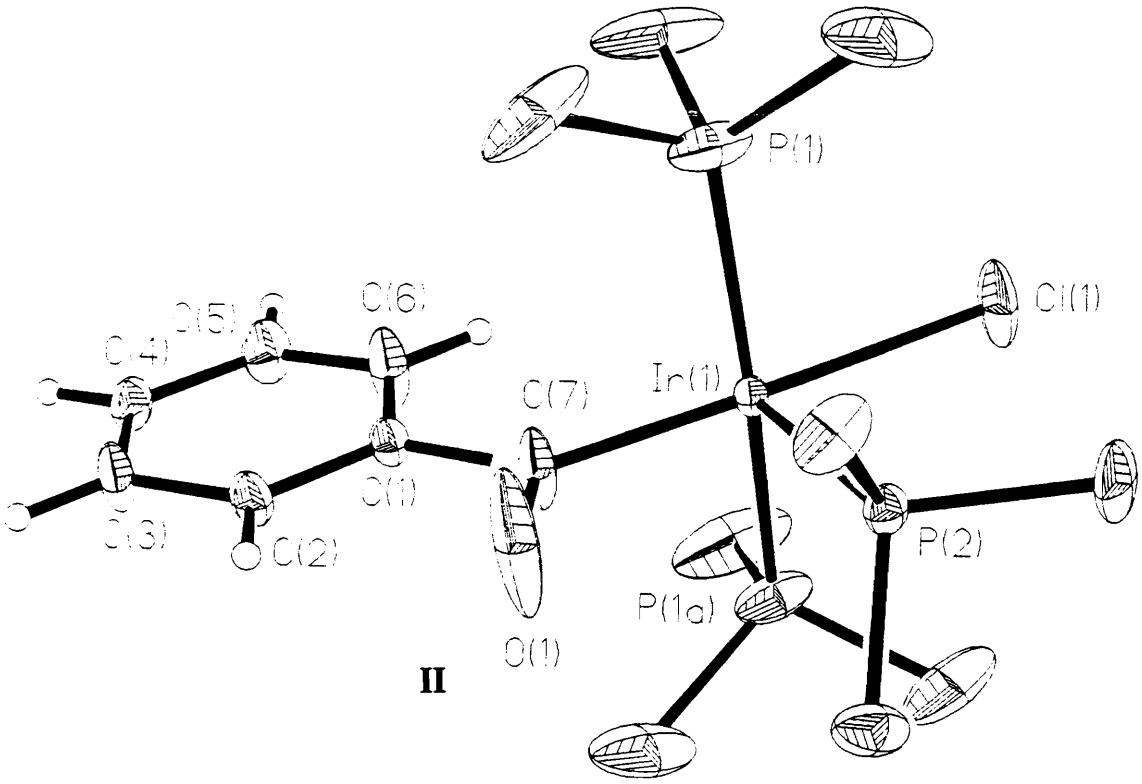

II

Figure 2.2 ORTEP of *mer*-(Me3P)3Ir(COC6H5)(H)Cl (**II**).

Since the C-H addition of the aldehyde group occured in benzaldehyde, it was of interest to see if the C-H addition of a formate ester could be carried out. Thus, $[Ir(COD)(PMe_3)_3]Cl$ reacts with neat ethyl formate at 90° C for 24 hours to form a mixture of hydrido-iridium complexes. Based on ^1H NMR, the predominant compound appears to be mer-$[(Me_3P)_3Ir(H_2)(CO)]Cl$, (**HES I 287**) (see Figure 2.3). In this case, the product from the addition of the formate group is unstable and decarbonylation can occur to give an ethoxyiridiumhydride complex. The complex continues to react via a β-hydride elimination of the ethoxy group to give the dihydrido complex (**HES I 287**) and acetylaldehyde (see Scheme 2.1). Milstein[76,77] has investigated the mechanism of aldehyde decarbonylation for homogeneous catalysis using cis-alkyl- and cis-acylmetal hydride complexes of rhodium and iridium.

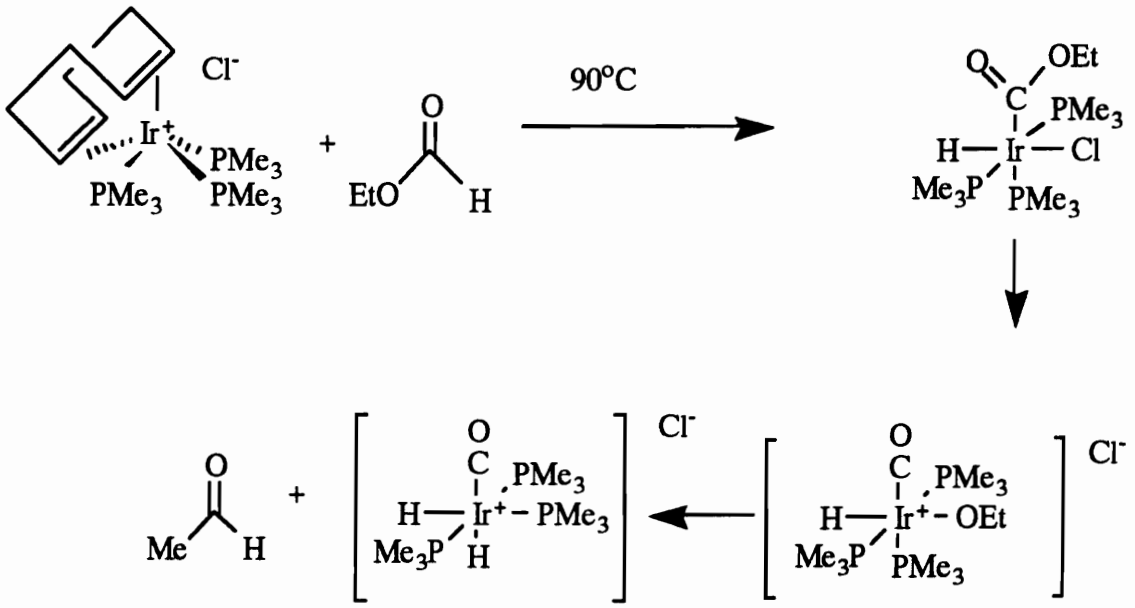

Scheme 2.1

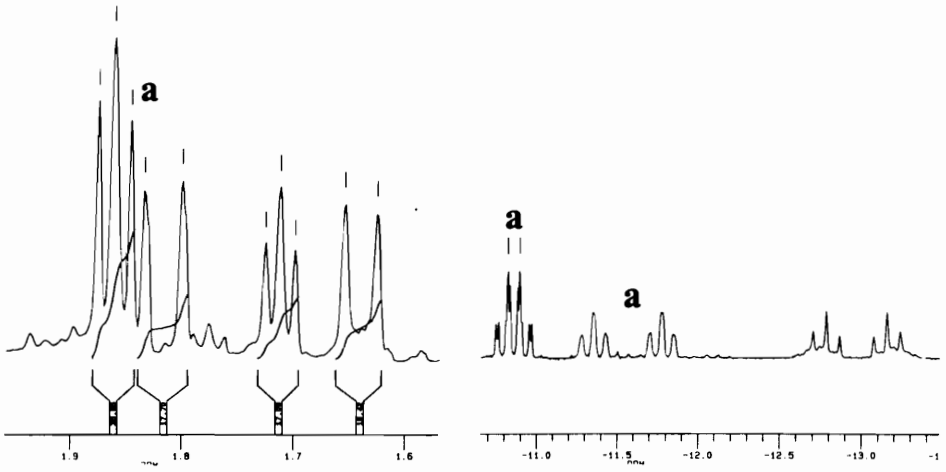

Figure 2.3 The ^1H NMR of the reaction **(HES I 287)** displaying *mer*-$(Me_3P)_3Ir(H_2)(CO)]Cl$ as the predominant product.

react with the $[Ir(COD)(PMe_3)_3]Cl$ complex to produce an identifiable product. Therefore, the means by which the C-H addition of an aromatic system adds across the iridium metal center must require certain conditions to be met before reaction can occur. This led the investigation back to benzene. Benzene being a flat, hexagonal shaped and relatively unhindered molecule, was the main focus in the search for other aromatic systems. The question boiled down to the old conflict of steric vs electronic effects. An aromatic system that was similar to benzene but electronically different was required for more information on which effect dominated. Pyridine, furan and later thiophene came to mind. They are all flat nonhindered aromatic systems that contain a heteroatom and are electronically different different from benzene. This will become evident in the reactivity of these hydrido complexes that will be discussed in the following chapters.

The $[Ir(COD)(PMe_3)_3]Cl$ complex reacts with pyridine in methylcyclohexane at 110° C for two days to give a 55% yield of mer-$(Me_3P)_3Ir(Py)(H)Cl$, (**HES II 19**)-(**III**). Characterization of (**III**) was accomplished using ^1H, ^{31}P, and ^{13}C NMR spectroscopies, single crystal X-ray diffraction and C-H analysis. The ^1H NMR spectrum displayed a doublet at δ= 1.50 ppm and a triplet at δ= 1.39 ppm consistent with a meridional arrangement of PMe_3 groups. A pair of triplets at δ=-10.7 ppm indicates the hydride is in the plane of the phosphine ligands and the pyridine group is trans to chloride ligand (Figure 2.4 and Figure 2.5).

Furan reacts with the $[Ir(COD)(PMe_3)_3]Cl$ complex in a similar fashion to give a 51% yield of mer-$(Me_3P)_3Ir(C_4H_3O)(H)Cl$, (**HES II 51**), (**IV**). This complex was characterized by ^1H, ^{31}P, ^{13}C NMR spectroscopies, single crystal X-ray diffraction and C-H analysis. The ^1H NMR spectrum of (**IV**) displayed a doublet at δ=1.55 and a triplet at δ=1.28 ppm consistent with a meridional arrangement of PMe_3 groups. The hydride was found to be a quartet at δ= -22.96 ppm and the furanyl group was found to be in the plane of the phosphine ligands. The chloride ligand was found in the axial position trans to the hydride (Figure 2.6 and 2.7). To understand the different hydride positions of the pyridyl complex versus the furanyl complex, one must take a closer look at the metal center prior to addition of the C-H bond. Benzene and furan must first displace the COD ligand which would give a reactive 16e-, square planar (trimethylphosphine)-iridium(I)chloride complex. The aromatic group must approach from the chloride side for best overlap, top or bottom to avoid the methyl groups of the phosphines. Again this may explain why bulky substituted aromatic systems fail to react in favorable yields with the $[Ir(COD)(PMe_3)_3]Cl$ complex. Although the roles are reversed,

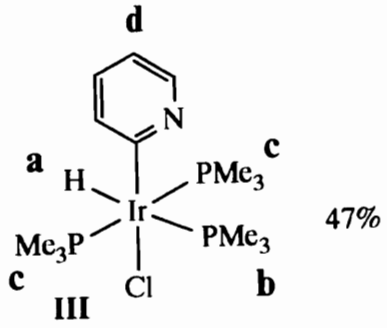

47%

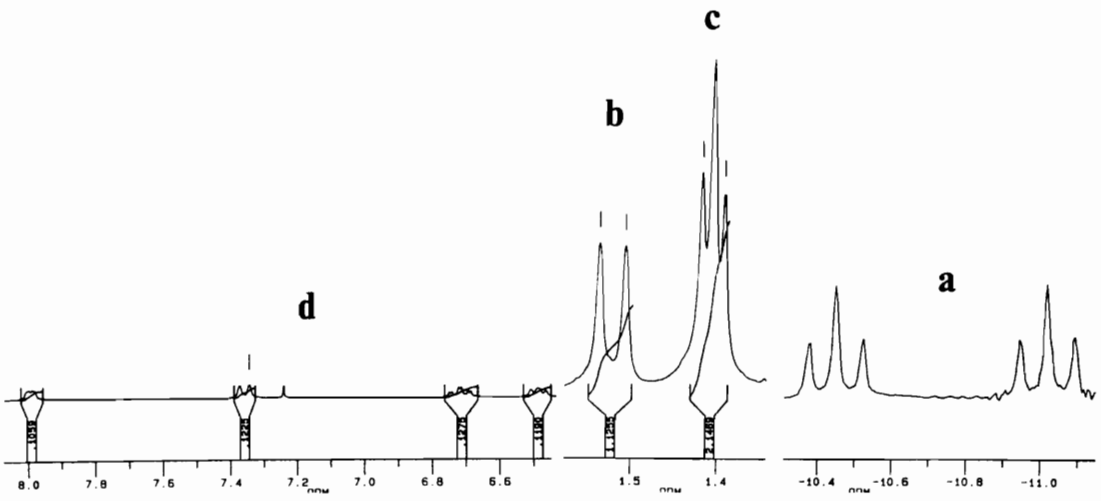

Figure 2.4 The ^{1}H NMR of *mer*-$(Me_3P)_3Ir(Py)(H)Cl$ (III).

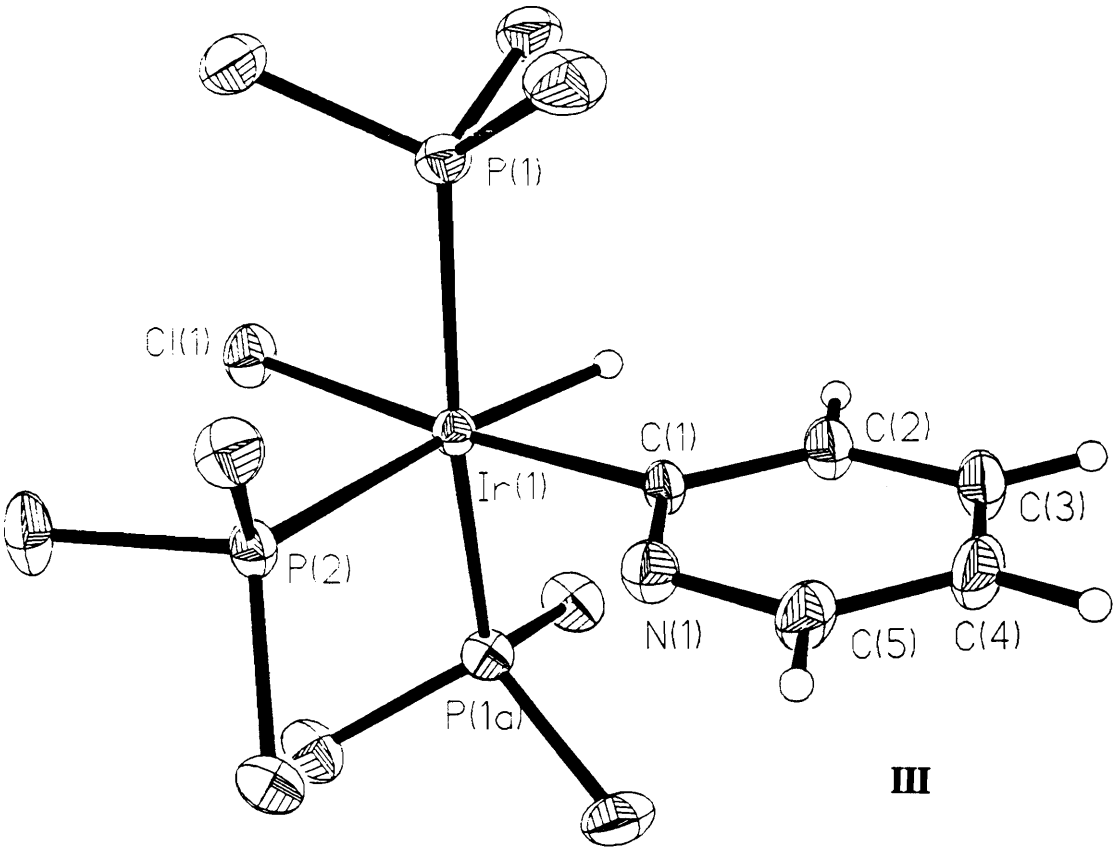

III

Figure 2.5 ORTEP of *mer*-(Me3P)3Ir(Py)(H)Cl **(III)**.

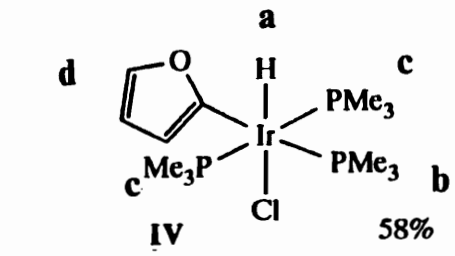

IV 58%

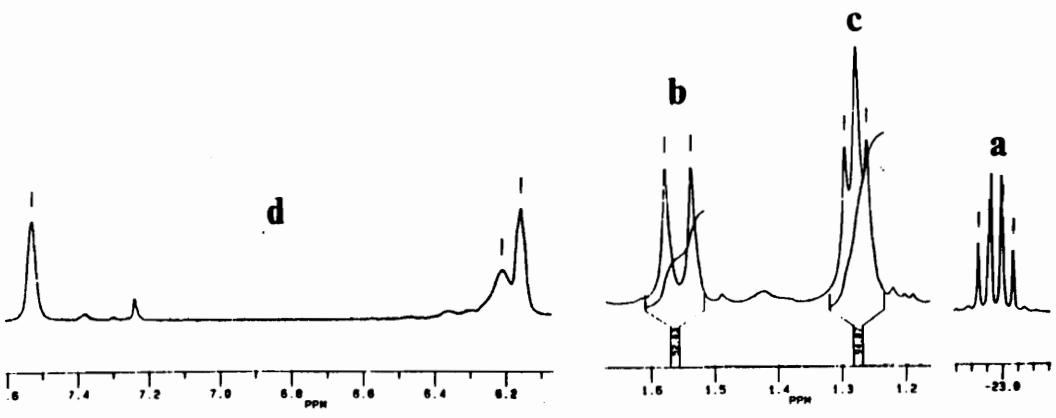

Figure 2.6 (270 MHz) ^{1}H NMR of *mer*-$(Me_3P)_3Ir(C_4H_3O)(H)Cl$ (**IV**).

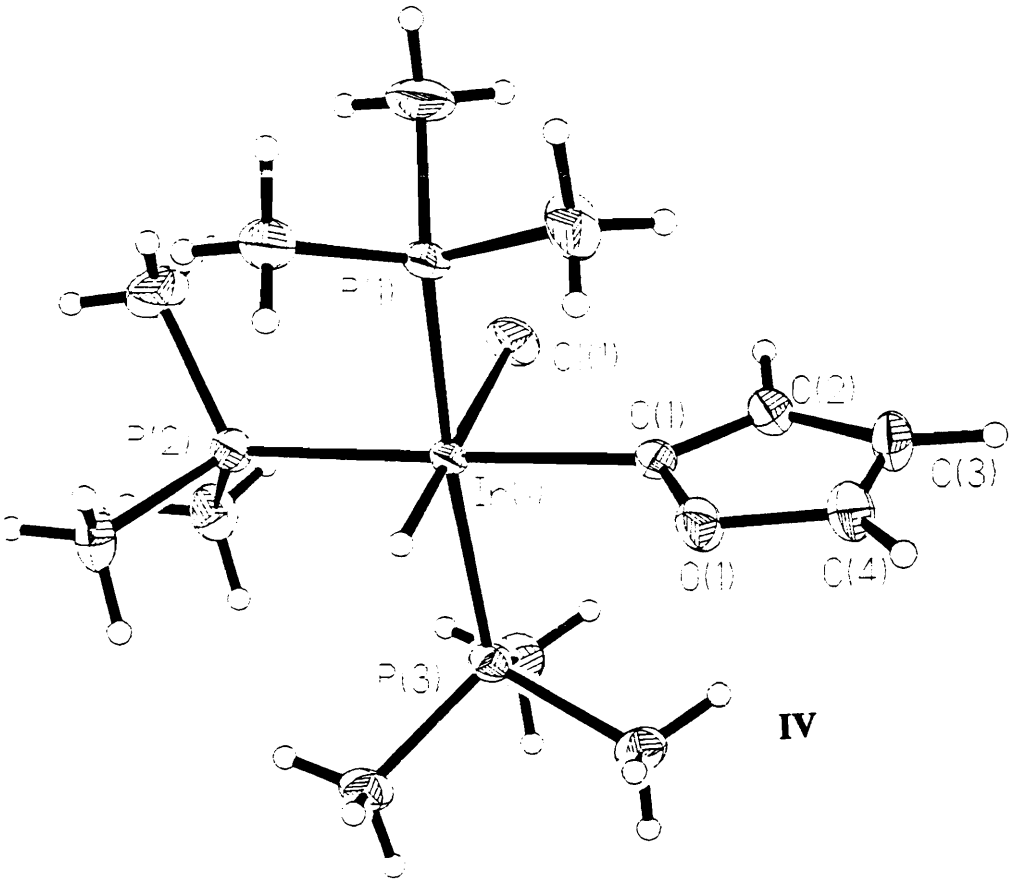

IV

Figure 2.7 ORTEP of *mer*-$(Me_3P)_3Ir(C_4H_3O)(H)Cl$ **(IV)**.

Muetterties and coworkers[78] have found that steric crowding around the metal center inhibits C-H addition even with benzene. As for the pyridyl complex, one may envision the pyridine (a good donor ligand and nucleophile) binding to the metal center through the nitrogen lone pair. In this process, pyridine may displace one of the ends of the COD ligand or a weakly held axial phosphine ligand. This will set-up the particular arrangement for the C-H addition to occur at the most convenient acidic proton. Jordan and Guram[79] have shown that the $[(C_5H_5)_2Zr(CH_3)(THF)][BPh_4]$ complex reacts with pyridine by displacing a THF ligand followed by C-H addition of the pyridine and elimination of methane. Another report by Neve and coworkers[80], suggest that the initial N-coordination is believed to procede the C-H bond cleavage. Scheme 2.2 shows the two possible pathways in which C-H addition can occur.

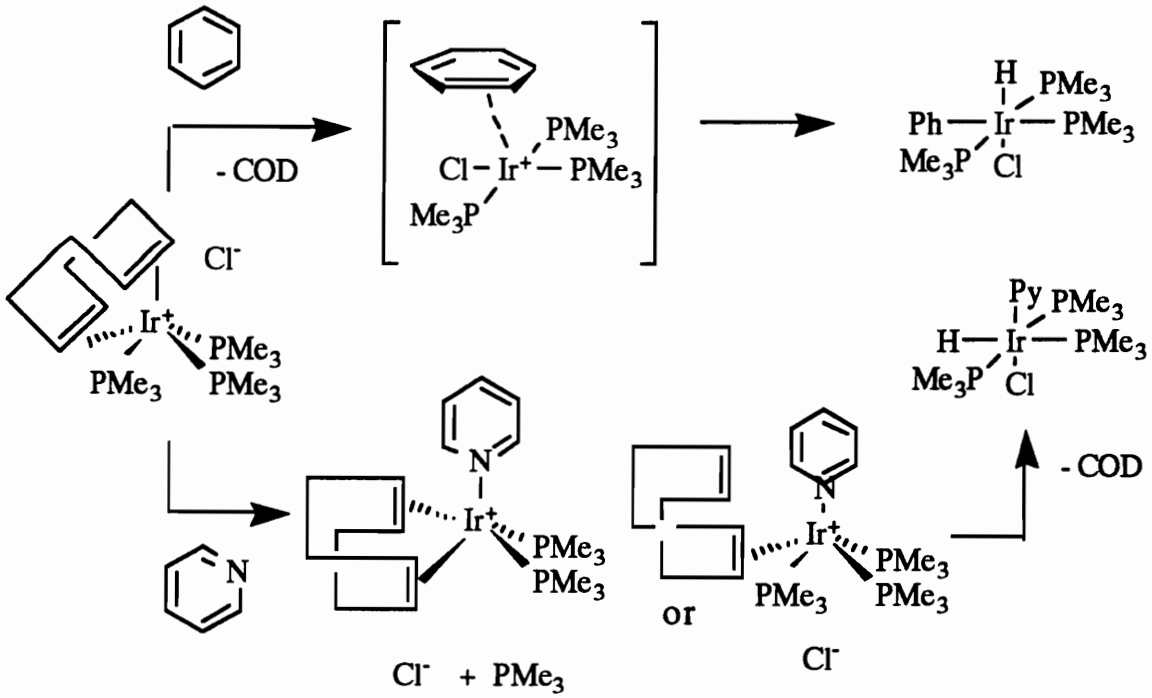

Scheme 2.2

Aromatic hydrocarbons are not the only class of compounds capable of C-H additions. Rhodium and iridium have been known to dimerize monosubstituted acetylenes via a process involving C-H addition of the alkyne's C-H bond. The $[Ir(COD)(PMe_3)_3]Cl$ complex reacts with 3,3-dimethyl-1- butyne in methylene chloride at reflux for 3 days to give a brown oil. The oil was purified by a column chromatography on silica gel to yield a pale yellow oil. The ^1H NMR and GC/MS data identified the major product to be trans 2,2,7,7-dimethyl-3-octene-5-yne, the product of alkyne dimerization.

C-S Additions

The oxidative additions of thiophene and benzothiophene deserve a separate area of discussion. Attempted C-H addition of thiophene actually produced quite a different result. The $[Ir(COD)(PMe_3)_3]Cl$ complex and thiophene react in MCH at reflux for 24 hours, and upon work up gave a mixture of products. A crude ^1H NMR spectrum did reveal a quartet at δ= -22.4 ppm, indicating a presence of the C-H addition product. However, further purification gave predominantly the thiometallacycle product, **(HES II 87)**, **(V)**. The ^1H NMR spectrum exhibited a doublet at δ=1.63 ppm (J_{P-H}= 9.20 Hz) and a triplet at δ=1.45 ppm (J_{P-H}= 3.55 Hz) again indicating a meridional arrangement of PMe_3 groups. Four proton resonances in the aromatic region were found. Two protons gave rise to a a pair of doublets at δ=5.71 (J= 9.93 & 9.07 Hz) and δ= 5.92 ppm (J=10.03 & 10.06 Hz), one broad triplet at δ= 7.27 ppm and one multiplet at δ= 6.42 ppm (Figure 2.8). The ^{13}C NMR spectrum revealed a quartet at δ= 113.0 ppm for one of the carbon atoms in thiophene. This would suggest that the

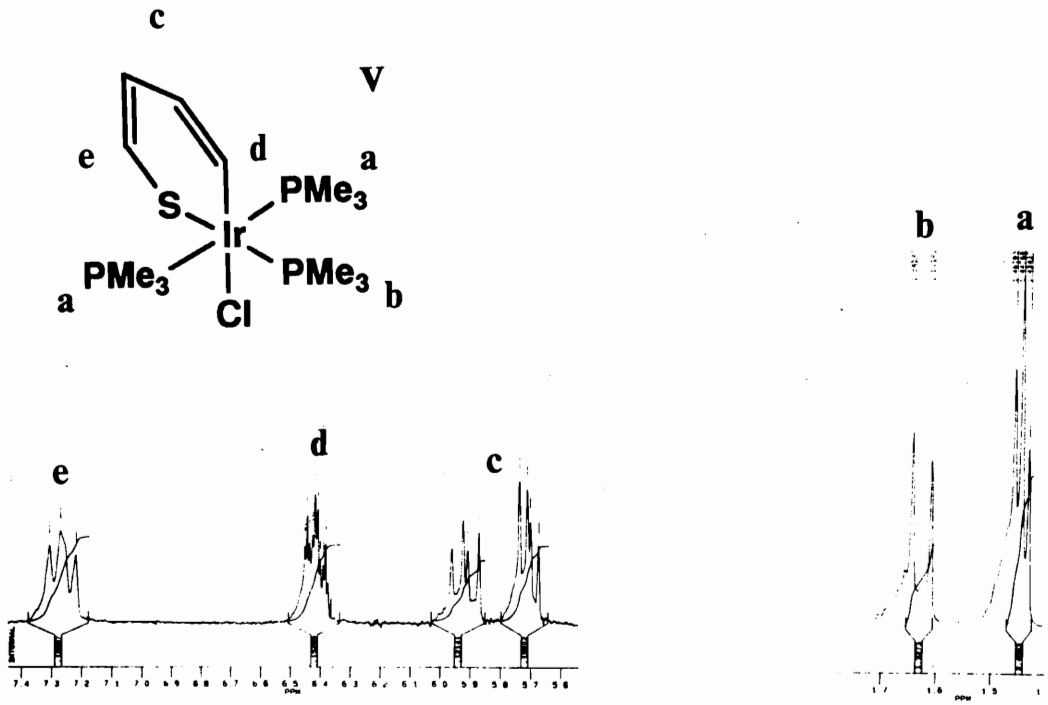

Figure 2.8 (270 MHz) ^{1}H NMR of Thiometallacycle (**V**).

carbon atom was cis to the three phosphine ligands, the sulfur atom in the plane of the phosphine ligands, and the chloride ligand trans to carbon (Figure 2.9).

Benzothiophene under similar conditions gave exclusively the carbon-sulfur addition product in a yield of 58%, (**HES II 137**), (**VI**). The X-ray crystal structure shows a meridonal arrangement of the phosphine ligands with the sulfur atom filling the fourth position in the plane and the carbon atom and chloride ligand lying trans to each other, like that of the thiophene addition (**HES II 87**), (Figure 2.10). Both thiophene and benzothiophene were also characterized by ^{31}P NMR spectrocopy and C,H analysis. However, dibenzothiophene fails to react with the $[Ir(COD)(PMe_3)_3]Cl$ complex under these conditions probably due to steric problems.

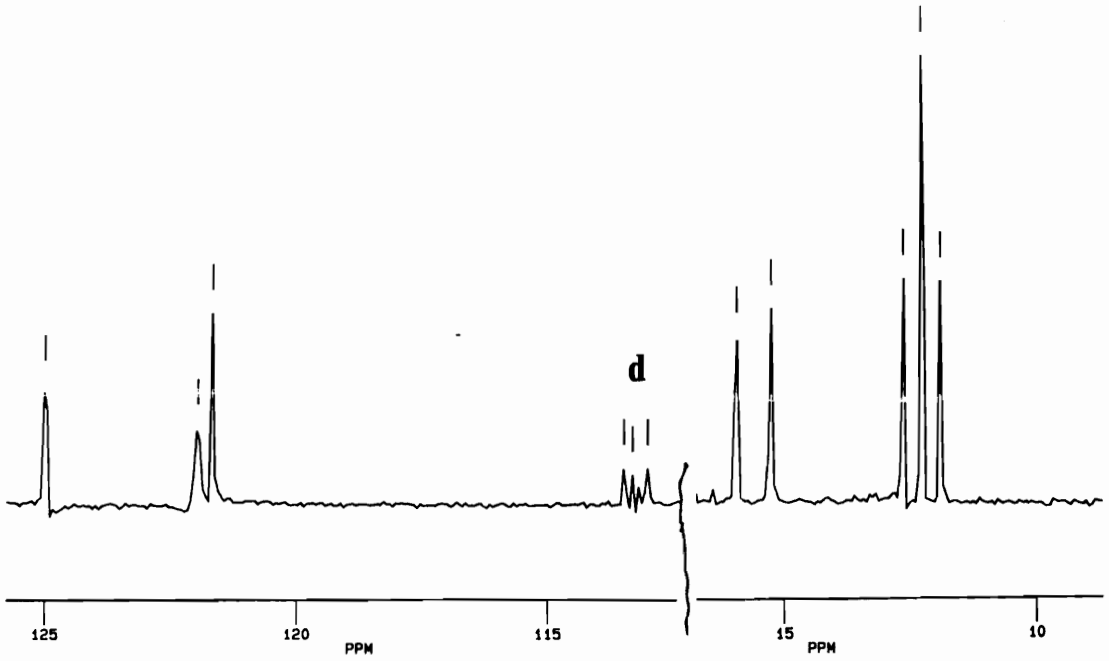

Figure 2.9 (200 MHz) ^{13}C NMR of Thiometallacycle (V).

Angelici and coworkers[81] have extensively investigated the adsorption modes of thiophene leading up to the C-S bond cleavage step. In a recent report by Angelici[83, 84], direct C-S bond addition has been observed in thiophenic compounds by a (C_5Me_5)Ir complex and in one particular case both C-H and C-S addition products were observed[85].

In this chapter, it has been shown that the [Ir(COD)(PMe_3)$_3$]Cl complex is a fairly versatile one capable of both C-H and C-S bond cleavage. The [Ir(COD)(PMe_3)$_3$]Cl complex appears to have steric demands that must be met. Relatively flat aromatic hydrocarbons such as, benzene, pyridine, furan, thiophene and benzothiophene, can all react with the [Ir(COD)(PMe_3)$_3$]Cl complex in comparable yields of 50, 53, 51, 44, and 58 % consecutively. The reactivity of the phenyl, pyridyl and furanyl adducts will be discussed in the following chapters.

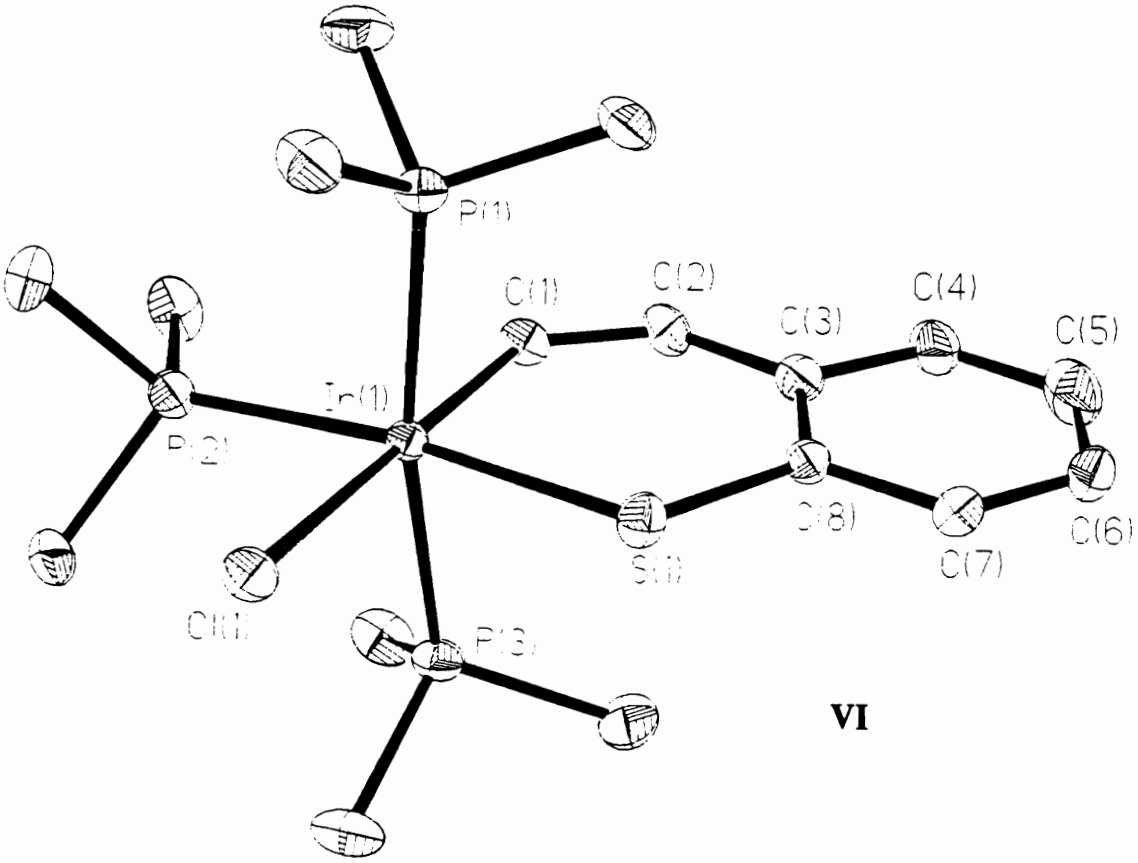

VI

Figure 2.10 ORTEP of Benzothiophene addition product (**VI**).

Experimental Section

General Comments:

All reactions were carried out on a Schlenk line under an atmosphere of pre-dried nitrogen using air sensitive procedures and techniques. All dry box manipulations were carried out in a MB-150-M glove box purchased from M. Braun, Germany. The solvents: toluene, tetrahydrofuran, ether, pentane, methylene chloride, methylcyclohexane, decalin, N-octane, and mesitylene were purchased either from Fisher Scientific or Aldrich Chemical Co. The solvents were dried using sodium or potassium with benzophenone and were distilled under nitrogen. Iridium trichloride trihydrate was either purchased or on loan from Johnson Matthey and used as received. A number of substituted acetylenes were purchased from Aldrich or Lancaster Synthesis and used without further purification. All other chemicals were reagent grade and were used as received. The synthesis of $[Ir(COD)(PMe_3)_3]Cl$ was carried out using a literature method[86]. ^1H NMR spectra were obtained using either a Bruker WP- 270 or WP-200 NMR spectrometer. ^{31}P, and ^{13}C NMR spectra were obtained using the Bruker WP-200 NMR spectrometer. The ^{13}C NMR spectra and DEPT spectra were obtained using a Varian Unity 400 spectrometer. Chemical shifts are reported in "δ" units, using the appropriate deuterated solvent peak as a reference relative to TMS.

^1H NMR : acetone-d_6, δ= 2.04 ppm; benzene-d_6, δ= 7.15 ppm; chloroform-d, δ= 7.24 ppm; dimethyl sulfoxide-d_6, δ= 2.49 ppm; dichloromethane-d_2, δ= 5.3 ppm.

^{13}C NMR : acetone-d_6, δ= 29.8 ppm; benzene-d_6, δ= 128.0 ppm; Chloroform-d, δ= 77.0 ppm; dichloromethane-d_2, δ= -53.8 ppm.

^{31}P NMR : H_3PO_4 internal reference (sealed capillary tube), δ= 0.0 ppm.

X-ray crystal structures were obtained using a Siemens R3m/v diffractometer with SHELXTL-PLUS software. C, H elemental analyses were performed by Atlantic Microlab Inc. P. O. Box 2288, Norcross, Georgia 30091. Each compound is given a code which corresponds to the Notebook and page of that particular experiment, and this code is given to the corresponding characteristic NMR spectrum as well as other data on that compound such as C, H elememental analysis. For example, HES II 51 represents the experiment found in book two page 51.

Synthesis of mer-$(Me_3P)_3Ir(Ph)(H)Cl$ (HES I 187) (I)

A thick wall reaction tube equipped with a stir bar and septum was charged with dry $[Ir(COD)(PMe_3)_3]Cl$ (5 g, 8.87 mmol) under nitrogen in a dry box. The reaction tube was then connected to a double manifold (vacuum/nitrogen) Schlenk line on the nitrogen side by a needle. Dry benzene (35 mL, 0.392 mole) was injected into the reaction tube. With an increased flow of nitrogen, the septum was quickly removed and replaced with a teflon screw cap and O-ring. This mixture was shaken and then placed in an oil bath at 100° C for 48 hours. As the reaction progressed,

the mixture turned red-orange and finally a yellow color with some solids remaining.

The solution was allowed to cool. The cap was replaced with a septum and a needle insert with flowing nitrogen along with a cannula fitted with a filter paper. The solution was filtered as it was transferred via the cannula to a 100 mL flask under nitrogen. The solvent was removed by vacuum which left a yellow solid behind. The resulting solid was washed with 20 mL of pentane to remove a small amount of a yellow impurity. The remaining solid was dissolved in 2 mL of dry CH_2Cl_2 by agitation and the product was precipitated by the slow addition of dry pentane. The off-white product was filtered out of the solution and rinsed with additional pentane (5 mL). The yield was 2.34 g (4.38 mmol,49.4% based on $[Ir(COD)(PMe_3)_3]Cl$ of mer-$(Me_3P)_3Ir(Ph)(H)Cl$). C, H elemental analysis calculated for $C_{15}H_{33}ClIrP_3$: C, 33.74%; H, 6.23%. Found : C, 33.35%; H, 6.25%.

^1H NMR (C_6D_6): δ= -23.46 ppm (q, J_{P-H}=4.6 Hz, 1H, Ir-H), δ=1.23 ppm (t, J_{P-H}=2.9 Hz, 18 Hz, trans PMe_3), δ=1.58 ppm (d, J_{P-H}=7.7 Hz, 9 H, cis PMe_3), δ=6.7-6.9 ppm (complex set of three pseudotriplet, 3 H, phenyl), δ=7.39 ppm (pseudotriplet, 1 H, phenyl), δ=8.15 ppm (pseudo-triplet, 1 H, phenyl) which is consistant with the literature values[74].

A second procedure for the synthesis of mer $(Me_3P)_3Ir(Ph)(H)Cl$ **(HES I 93)** involves the use of a nonpolar solvent, decalin. A similar procedure and work up was followed. 3g (5.3 mmol) of $[Ir(COD)(PMe_3)_3]Cl$ was added to 28.5 mL (0.319 mol) of benzene along with 140 mL of decalin in an oil bath at 100° C for 60 hrs for a twenty to one ratio of benzene to the $[Ir(COD)(PMe_3)_3]Cl$ complex. Work-up yielded 1.65g

(3.09 mmol, 58% based on $[Ir(COD)(PMe_3)_3]Cl$) of mer-$(Me_3P)_3Ir(Ph)(H)Cl$.

Synthesis of mer-$(Me_3P)_3Ir(C_6D_5)(D)Cl$ (HES I 45)

A thick wall reaction tube equipped with a stir bar and septum was charged with dry $[Ir(COD)(PMe_3)_3]Cl$ (0.5 g, 0.887 mmol) under nitrogen in a dry box. The reaction tube was then connected to a double manifold (vacuum/nitrogen) Schlenk line on the nitrogen side by a needle. Dry d_6-benzene (1.5 mL, 6.41 mmol) and dry mestylene (30 mL) were injected into the reaction tube. The septum was quickly removed and replaced with a teflon screw cap and O-ring. This mixture was shaken and then placed in an oil bath at 100° C for 24 hours. The cap was replaced with a septum and a needle insert with flowing nitrogen along with a cannula fitted with a filter paper. The solution was filtered as it was transferred via the cannula to a 100 mL flask under nitrogen. The solvent was removed by vacuum which left a yellow solid behind. The resulting solid was washed with 20 mL of pentane to remove a small amount of a yellow impurity. The remaining solid was dissolved in 2 mL dry CH_2Cl_2 by agitation and the product was precipitated by the slow addition of dry pentane. The off-white product was filtered out of the solution and rinsed with additional pentane (5 mL). The yield was 167 mg (0.313 mmol,35.3% based on $[Ir(COD)(PMe_3)_3]Cl$ of mer-$(Me_3P)_3Ir(C_6D_5)(D)Cl$). The ^1H NMR displayed: δ=1.23 ppm (t, J_{P-H}=2.9 Hz, 18 Hz, trans PMe_3), δ=1.58 ppm (d, J_{P-H}=7.7 Hz, 9 H, cis PMe_3), the aromatic and the hydride resonances were not observed.

Synthesis of mer-$(Me_3P)_3Ir(COC_6H_5)(H)Cl$ (HES I 141) (II)

A 10 mL flask equipped with a stir bar and septum was charged with $[Ir(COD)(PMe_3)_3]Cl$ (500 mg, 0.887 mmol) under nitrogen in a dry box. The flask was then connected to a double manifold (vacuum/nitrogen) Schlenk line. Dry methylcyclohexane (5 mL) was added, along with 1.0 mL (8.870 mmol) of benzaldehyde. The mixture was refluxed at 100° C for 24 hrs. The solution was allowed to cool and crystals formed which were filtered and washed with dry toluene (to dissolve the crystalline material). The solvent was removed by vacuum and the residue was recrystallized using methylene chloride and pentane. A yield of 188 mg (0.335 mmol, 37.7% based on $[Ir(COD)(PMe_3)_3]Cl$) of mer-$(Me_3P_3)Ir(COC_6H_5)(H)Cl$ was obtained. C, H elemental analysis calculated for $C_{16}H_{33}ClIrOP_3$: C, 34.19%; H, 5.93%. Found: C, 33.76%; H, 5.78%.

^1H NMR ($CDCl_3$): δ= -9.2 and -9.8 ppm (d t, trans J_{P-H}=151 Hz and cis J_{P-H}=19.3 Hz, 1H, Ir-H), δ=1.51 ppm (t, J_{P-H}=3.6 Hz, 18H, trans PMe_3), δ=1.56 ppm (d, J_{P-H}=8.0 Hz, 9H, cis PMe_3), δ=7.9 &7.3 ppm (m, 5H, phenyl).

^{13}C NMR (CD_2Cl_2): δ= -18.0 ppm (t, J_{P-C}=69.0 Hz, trans PMe_3), δ=16.5 ppm (d,J_{P-C}=108.0 Hz, cis PMe_3), δ=127.7, 129.5, 129.7, & 153.4 ppm (s, phenyl), and δ=210.0 ppm (s, carbonyl).

^{31}P NMR ($CD2Cl_2$, Internal standard): δ= -48.6 ppm (t, J=40.5 Hz, trans PMe_3), δ= -30.1 ppm (d, J=45.8 Hz, cis PMe_3).

X-Ray: Crystal color; Habit: Clear prism. Crystal size (mm): 0.2x0.2x0.3. Crystal system: Orthorhombic. Space group: Pbcm. Unit Cell Dimensions: a=12.678(4) Å, b=12.857(3) Å, c=13.832(4) Å. Volume: 2256.2(11) $Å^3$, Z=4. Formula weight=562.0. Density (Calc.):

1.654 Mg/m^3. Absorption Coefficient: 6.225 mm^{-1}. Single crystal X-ray diffraction data can be found in the appendix.

Synthesis of mer-[$(Me_3P)_3Ir(H)_2(CO)$]Cl (HES I 287)

A thickwall reaction tube equipped with a stir bar and septum was charged with [$Ir(COD)(PMe_3)_3$]Cl (552 mg, 0.979 mmol) under nitrogen in a dry box. The reaction tube was then connected to a double manifold (vacuum/nitrogen) Schlenk line. Predried ethyl formate (10 mL) was added to the [$Ir(COD)(PMe_3)_3$]Cl complex. (Ethyl formate was washed twice with 5.0% sodium carbonate then predried with magnesium sulfate. The ethyl formate was distilled twice over phosphorus pentoxide and the fraction used was collected between 52-54° C) The septum was replaced with a teflon screw cap and O-ring. The mixture was placed in an oil bath at 60° C for 36 hrs. The mixture remained cloudy and therefore, the temperature was raised to 90° C for 24 hrs. The resulting clear yellow solution was allowed to cool. The teflon screw cap was replaced with a septum, a needle with flowing nitrogen, and a cannula fitted with filter paper. The solution was filtered as it was transferred via the cannula to a 50 mL flask. The solvent was removed by vacuum which left an oil behind. The oil was redissolved in dry methylene chloride (5 mL). Ether (15 mL) was slowly added to form a layer over the solution and left overnight. A white crystalline material precipitated out of the light yellow-green solution. The crude yield was 238 mg of both the major product of the mer-[$(Me_3P)_3Ir(H)_2CO$]Cl and the minor product, mer-$(Me_3P)_3$Ir-(CO)HCl: ^1H NMR ($CDCl_3$): δ= -11.96 & -11.54 ppm (d t, trans J_{P-H}=113.53 Hz, & cis J_{P-H}=20.36 Hz, 1H, Ir-H), δ= -11.03 ppm (q,

J_{P-H}=20.12 Hz, 1H, Ir-H), δ=1.82 ppm (d, J_{P-H}=9.11 Hz, 9H, cis PMe_3), δ=1.86 ppm (t, J_{P-H}=3.89 Hz, 18H, trans PMe_3). δ= -12.97 & -13.35 ppm (d t, trans J_{P-H}=99.98 Hz, & cis J_{P-H}=21.82 Hz, 1H, Ir-H), δ=1.64 ppm (d, J_{P-H}=7.74 Hz, 9H, cis PMe_3), δ=1.71 ppm (t, J_{P-H}=3.5 Hz, 18H, trans PMe_3).

Synthesis of mer-$(Me_3P)_3Ir(C_5H_4N)(H)Cl$ (HES II 19) (III)

A thick wall reaction tube equipped with a stir bar and septum was charged with $[Ir(COD)(PMe_3)_3]Cl$ (290 mg, 0.51 mmol) under nitrogen in a dry box. The reaction tube was then connected to a double manifold (vacuum/nitrogen) Schlenk line and 5 mL of dry methylcyclohexane was added along with (0.45 mL, 0.43 moles) of dry pyridine. The septum was replaced with a teflon screw cap with an O-ring. The slurry was stirred and placed in an oil bath at 110° C for 48 hrs. The solution was allowed to cool before the teflon screw cap was replaced with a septum containing a needle with flowing nitrogen along with a cannula fitted with a filter paper. The yellow solution was filtered as it was transfered via the cannula to a 50 mL flask under nitrogen. The solution was stripped leaving a lemon yellow solid. A minimum of dry methylene chloride (2 mL) was added to dissolve the product with agitation and the product was precipitated by the slow addition of dry pentane (20 mL). A light tan product was filtered out of the solution and rinsed with additional pentane (5 mL). This yield 0.146g (0.273mmol, 53% based on $[Ir(COD)(PMe_3)_3]Cl$) of mer-$(Me_3P_3)Ir(C_5H_4N)(H)Cl$. C, H elemental analysis calculated for $C_{14}H_{32}ClIrNP_3$: C, 31.43%; H, 6.04%. Found: C, 31.94%; H, 6.10%.

^{1}H NMR ($CDCl_3$): δ= -10.45 & -11.02 ppm (d t, trans J_{P-H}=153.5 Hz, cis J_{P-H}=19.8 Hz, 1H, Ir-H), δ=1.39 ppm (t, J_{P-H}=3.38 Hz, 18H, trans PMe_3), δ=1.50 ppm (d, J_{P-H}=7.99 Hz, 9H, cis PMe_3), δ=6.48 ppm (br t, J=5.69 Hz, 1H, pyridyl), δ=6.71 ppm (t d, J=7.36 & J=2.15 Hz, 1H, pyridyl), δ=7.36 ppm (br d, J=7.89 Hz, 1H, pyridyl), δ=7.98 ppm (br d, J=2.7 Hz, 1H, pyridyl).

^{13}C NMR ($CDCl_3$): δ=16.4 ppm (d, J_{P-C}=106.3 Hz, cis PMe_3), δ=17.7 ppm (t, J_{P-C}=70.3 Hz, trans PMe_3), δ=114.7, 132.0, 141.6, & 147.0 ppm (s, pyridyl and one quarternary carbon not observed).

^{31}P NMR ($CDCl_3$, external standard): δ= -38.2 ppm (d, J=53.9 Hz, cis PMe_3), δ= -48.7ppm (t, J=55.6 Hz, trans PMe_3).

X-Ray: Crystal color; Habit: Clear rectangular plate. Crystal size (mm): 0.4x0.5x0.1. Crystal system: Orthorhombic. Space group: Cmca. Unit Cell Dimensions: a=13.340(4) Å, b=11.999(3) Å, c=26.315(9) Å. Volume: 4212.2(2) Å^3, Z=8. Formula weight=534.0. Density (Calc.): 1.684 Mg/m^3. Absorption Coefficient: 6.662 mm^{-1}. Single crystal X-ray diffraction data can be found in the appendix.

Synthesis of mer-$(Me_3P)_3Ir(C_4H_3O)(H)Cl$ (HES II 51) (IV)

A thick wall reaction tube equipped with a stir bar and septum was charged with $[Ir(COD)(PMe_3)_3]Cl$ (1.025 g, 1.82 mmol) under nitrogen in a dry box. The reaction tube was then connected to a double manifold (vacuum/nitrogen) Schlenk line. Dry methylcyclohexane (3 mL) was added along with (2.63 mL 36.2 mmol) of furan. The septum was quickly replaced with a teflon screw cap fitted with an O-ring. The mixture was shaken well and placed in an oil bath at 100° C for 24 hrs. The solution

was allowed to cool before the teflon screw cap was replaced with a septum containing a needle with flowing nitrogen, and a cannula fitted with filter paper. The brown-yellow solution was filtered as it was transferred by the cannula to a 100 mL flask under nitrogen. The solution was stripped under vacuum leaving a brown product. The material was redissolved using dry methylene chloride (4 mL). The product was precipitated out by the slow addition of dry pentane (20 mL) which gave a brown oil. The solvent was again stripped and the residue was redissolved using dry methylene chloride (4 mL). The product was precipitated out by the slow addition of dry ether (20 mL) producing an off-white solid. This yielded 482 mg (0.920 mmol, 51% based on $[Ir(COD)(PMe_3)_3]Cl$) of mer-$(Me_3P)_3Ir(C_4H_3O)(H)Cl$. C, H elemental analysis calculated for $C_{13}H_{31}ClIrOP_3$: C, 29.8%; H, 5.96%. Found: C, 29.79%; H, 5.82%.

^1H NMR ($CDCl_3$): δ= -22.96 ppm (q, J_{P-H}=21.4 Hz, 1H, Ir-H), δ=1.28 ppm (t, J_{P-H}=4.76 Hz, 18H, trans PMe_3), δ=1.55 ppm (d, J_{P-H}=11.0 Hz, 9H, cis PMe_3), δ=6.16, 6.21, & 7.53 ppm (s, 3H, furyl).

^{13}C NMR (CD_2Cl_2): δ=17.6 ppm (t, J_{P-C}=18.6 Hz, 19H, trans PMe_3), δ=19.5 ppm (d, J_{P-C}=30.6 Hz, 9H, cis PMe_3), δ=110.6, 114.6, & 142.4 ppm (s, Furyl, and one quarternary carbon not observed).

^{31}P NMR (CD_2Cl_2, external standard): δ= -36.5 ppm (d, J=57.2 Hz, cis PMe_3), δ= -50.7 ppm (t, J=54.3 Hz, trans PMe_3).

X-Ray: Crystal color; Habit: Clear colorless rectangular prism. Crystal size (mm): 0.5x0.6x0.8. Crystal system: Monoclinic. Space group: $P2_{1/n}$. Unit Cell Dimensions: a=9.723(2) Å, b=11.583(3) Å, c=17.790(5) Å, β=94.68(2)°. Volume: 1996.7(9) $Å^3$, Z=4 Formula weight=523.9. Density (Calc.): 1.743 Mg/m^3. Absorption Coefficient: 7.027 mm^{-1}. Single crystal X-ray diffraction data can be found in the appendix.

Synthesis of mer-$(Me_3P)_3Ir(C_{10}H_7)(H)Cl$ (HES II 17)

A thick wall reaction tube equipped with a stir bar and septum was charged with $[Ir(COD)(PMe_3)_3]Cl$ (280 mg, 0.497 mmol) under nitrogen in a dry box. The reaction tube was then connected to a double manifold (vacuum/nitrogen)Schlenk line. Dry methylcyclohexane (5 mL) was added along with 1 gram (7.802 mmol) of naphthalene (previously melted and placed under nitrogen). The septum was replaced with a teflon screw cap with an O-ring. The mixture was shaken well and placed in an oil bath at 110° C for 48 hrs. The yellow solution was allowed to cool. The teflon screw cap was replaced with a septum containing a needle with a cannula fitted with a filter paper. The solution was filtered as it was transferred by the cannula to a 50 mL flask under nitrogen. The solvent was removed by vacuum and dry pentane (15 mL) was added to dissolve the unreacted naphthalene. This solution was filtered and the remaining solids were dissolved using methylene chloride (3 mL). The product was precipitated by the slow addition of dry pentane (15 mL). This yielded 62 mg (0.106 mmol, 21.4% based on $[Ir(COD)(PMe_3)_3]Cl$) of mer-$(Me_3P)_3Ir(C_{10}H_7)$-(H)Cl: ^1H NMR ($CDCl_3$): δ= -23.47 ppm (q, J_{P-H}=15.39 Hz, 1H, Ir-H), δ= 1.23 ppm (t, J_{P-H}=3.52 Hz, 18H, trans PMe_3), δ=1.62 ppm (d, J_{P-H}=7.79 Hz, 9H, cis PMe_3), δ=7.2-7.9 ppm (m, 7H, aromatic).

Synthesis of mer-$(Me_3P)_3Ir(C_7H_4F_3)(H)Cl$ (HES II 93)

A thick wall reaction tube equipped with a stir bar and septum was charged with $[Ir(COD)(PMe_3)_3]Cl$ (500 mg, 0.887 mmol) under nitrogen

in dry box. The reaction tube was then connected to a double manifold (vacuum/nitrogen) Schlenk line. Anhydrous α,α,α-trifluorotoluene (10 mL) was injected into the reaction tube. The septum was replaced with a teflon screw cap with an O-ring. The mixture was shaken well and placed in an oil bath at 80° C for 48 hrs. After this time, the reaction mixture was a red-orange with remaining solids. The mixture was then heated to 100° C for 72 hrs. The yellow solution still containing some solids was allowed to cool. The teflon screw cap was replaced with a septum containing a needle with flowing nitrogen and a cannula fitted with a filter paper. The solution was filtered as it was transferred via the cannula to a 50 mL flask under nitrogen. The solvent was removed under vacuum and the crude material was examined by ^{1}H NMR spectroscopy revealing a mixture of products. The remaining solids in the reaction tube (87 mg) were examined by ^{1}H NMR spectrum displaying them as mer-$(Me_3P)_3Ir(C_7H4F_3)(H)Cl$: ^{1}H NMR ($CDCl_3$): δ= -12.87 & -13.24 ppm (d t, trans J_{P-H}=99.9 Hz & cis J_{P-H}=21.6 Hz, 1H, Ir-H), δ=1.61 ppm (d, J_{P-H}=7.73 Hz, 9H, cis PMe_3), δ=1.67 ppm (t, J_{P-H}=3.44Hz, 18H, trans PMe_3), δ=7.45 & 7.55 ppm (m, 4H, aromatic).

Synthesis of mer-$(Me_3P)_3Ir(C_7H_7O)(H)Cl$ (HES II 89)

A thick wall reaction tube equipped with a stir bar and septum was charged with $[Ir(COD)(PMe_3)_3]Cl$ (500 mg, 0.887 mmol) under nitrogen in a dry box. The reaction tube was then connected to a double manifold (vacuum/nitrogen) Schlenk line. Anhydrous anisole (5.78 mL) and dry methylcyclohexane (5 mL) was added to the reaction tube. The septum was replaced with a teflon screw cap with an O-ring. The mixture was shaken

well and placed in an oil bath at 100° C for 48 hrs. The mixture was allowed to cool before the teflon screw cap was replaced with a septum, a needle with flowing nitrogen and a cannula fitted with filter paper. The solution was filtered as it was transfered by the cannula to a 100 mL flask under nitrogen. Methylene chloride (10 mL) was used to wash and transfer the product over to the 100 mL flask which left a brown-black residue behind. Dry pentane (20 mL) was added to the yellow solution to induce precipitation of the undesired byproduct. The solvent was then removed by vacuum. The remaining solid was washed with dry pentane (10 mL) to remove a yellow byproduct. This yielded 96.0 mg (0.17 mmol, 19.2% based on $[Ir(COD)(PMe_3)_3]Cl$) of mer-$(Me_3P_3)Ir(C_7H_7O)(H)Cl$: ^1H NMR ($CDCl_3$): δ= -22.4 ppm (q, J_{P-H}=13.5 Hz, 1H, Ir-H), δ=1.72-1.80 ppm (overlapping d t, 27H, cis & trans PMe_3), δ=3.85 ppm (s, 3H, methoxy group), δ=6.9 & 7.3 ppm (m, 4H, aromatic).

Synthesis of 2,2,7,7-Tetramethyl-3-Octen-5-yne (HES I 285)

A thick wall reaction tube equipped with a stir bar and septum was charged with $[Ir(COD)(PMe_3)_3]Cl$ (50 mg, 0.0887 mmol) under nitrogen in a dry box. The reaction tube was then connected to a double manifold (vacuum/nitrogen) Schlenk line. Dry methylene chloride (10 mL) and 3, 3-dimethyl-1-butyne (3.6mL, 29.27 mmol) were added the reaction tube. The septum was replaced with a teflon screw cap and O-ring. The mixture was shaken well and placed in an oil bath at 70° C for 3 days. The mixture was allowed to cool before the teflon screw cap was replaced with a septum, a needle with flowing nitrogen and a cannula fitted with filter paper. The solution was filtered as it was transferred by the cannula to a

25 mL flask. The solvent was then removed by vacuum. Dry pentane (10 mL) was added to the material and stirred for an hour. The brown solution was then filtered off. The filtrate volume was reduced by blowing nitrogen over the solution which gave 0.505 g of a brown oil. The brown oil was placed on a silica-gel column (40 mL). The oil was eluted with an aliquot (100 mL) of the following solvents: pentane, ether, chloroform, methylene chloride, and methanol consecutively. The majority of the product was found in the ether layer and trace amounts in the methylene chloride solvent. This was combined and the solvents were allowed to evaporate leaving a pale yellow oil which was mainly the trans isomer of 2,2,7,7-tetramethy-3-octen-5-yne: ^{1}H NMR (CD_2Cl_2): δ=1.17 & 1.22 ppm (s, 9H each, t-butyl group), δ=5.33 & 5.67 ppm (d d, J=11.85 Hz, trans vinyl group)

Synthesis of mer-$(Me_3P)_3Ir(C_4H_4S)Cl$ (HES II 87) (V)

A thick wall reaction tube, equipped with a stir bar and septum, was charged with $[Ir(COD)(PMe_3)_3]Cl$ (500 mg, 0.887 mmol) under nitrogen in a dry box. The reaction tube was then connected to a double manifold (vacuum/nitrogen) Schlenk line. Dry methylcyclohexane (5 mL) and thiophene (3 mL, 38.01 mmol) were injected into the reaction tube. The septum was replaced with a teflon screw cap with an O-ring. The mixture was shaken well and placed in an oil bath at 80° C for 24 hrs. The brown solution was allowed to cool before a teflon screw cap was replaced with a septum containing a needle with flowing nitrogen and a cannula fitted with a filter paper. The brown solution was filtered as it was transferred via the cannula to a 50 mL flask under nitrogen. Dry pentane (15 mL) was slowly

added to the mixture . A peach colored product precipitated out. This was filtered and rinsed with additional pentane (5 mL). This yielded 210 mg (0.389mmol, 44% based on [Ir(COD)(PMe_3)$_3$]Cl) of mer-(Me_3P)$_3$Ir-(C_4H_3S)(H)Cl. C, H elemental analysis calculated for $C_{13}H_{31}IrClP_3S$: C, 28.90%, H, 5.80%. Found: C, 28.83%, H, 5.53%.

^1H NMR (CD_2Cl_2) δ=1.45 ppm (t, J_{P-H}=3.55 Hz, 18H, PMe_3), δ=1.63 ppm (d, J_{P-H}=9.20 Hz, 9H, PMe_3), δ=5.71 ppm (d d, J_{H-H}=9.93 & 9.07 Hz, 1H), δ=5.92 ppm (d d, J_{H-H}=10.03 & 10.06 Hz, 1H), δ=6.42 ppm (m, 1H), and δ=7.27 ppm (br t, J=11.94 Hz, 1H) from the thiometallacycle.

^{13}C NMR (CD_2Cl_2) δ=12.26 ppm (t, J_{P-C}=73.14 Hz, trans PMe_3), δ=15.55 ppm (d, J_{P-C}=135.46 Hz, cis PMe_3), δ=113.12 ppm (q, J_{P-C}=34.8 Hz), and δ=121.66, 121.94, & 124.97 ppm (s, thiophene).

^{31}P NMR (CD_2Cl_2, internal standard) δ=-44.17 ppm (t, J=53.08 Hz, trans PMe_3), and δ=-35.13 ppm (d, J=52.62 Hz, cis PMe_3).

Synthesis of mer (Me_3P)$_3$Ir(C_8H_6S)Cl (HES II 137) (VI)

A thick wall reaction tube equipped with a stir bar and septum was charged with dry [Ir(COD)(PMe_3)$_3$]Cl (250 mg, 0.444 mmol) under nitrogen in a dry box. The reaction tube was connected to a double manifold (vacuum/nitrogen)Schlenk line on the nitrogen side by a needle. A solution made-up of benzothiophene (0.298 g) in methylcyclohexane (10 mL) was injected by syringe. The septum was replaced with a teflon screw cap and O-ring and the mixture was mixed well. The tube was placed in an oil bath at 100° C for 24 hrs. Once cooled the solution was transferred to a 100 mL flask by the use of a cannula fitted with filter paper and a needle connected to the nitrogen line. The solids were dissolved using two 10 mL

portions of methylene chloride and transferred to the 100 mL flask. The solvent was removed by vacuum leaving a yellow product behind. The material was redissolved in dry methylene chloride (5 mL) and was precipitated by the slow addition of dry ethyl ether (20 mL). The solids were filter off and rinsed with ethyl ether (10 mL) leaving a light yellow product behind. The yield was 0.151 g (0.256 mmol, 57.6% based on [Ir(COD)(PMe_3)$_3$]Cl) of mer-(Me_3P)$_3$Ir(C_8H_6S)Cl. C, H elemental analysis calculated for $C_{17}H_{34}IrClP_3S$: C, 34.60%, H, 5.55%. Found: C, 34.57%, H, 5.65%.

^1H NMR ($CDCl_3$): δ=1.43 ppm (t, J_{P-H}=3.51 Hz), δ=1.67 ppm (d, J_{P-H}=9.10 Hz, 9H, cis PMe_3), δ=6.70-6.79 ppm (m, 1H, thiometallacycle), δ=6.82-6.95 ppm (m, 3H, phenyl), d=7.21 ppm-7.32 ppm(m, 1H, thiometallacycle), and δ=7.41 ppm (br d, J=7.7 Hz, 1H phenyl).

^{13}C NMR ($CDCl_3$): δ=12.60 ppm(t, J_{P-C}=73.66 Hz, trans PMe_3), δ=15.53 ppm (d, J_{P-C}=134.38 Hz, cis PMe_3), δ=114.83 ppm (q, J_{P-C}=32.2 Hz, thiometallacylce), δ=120.60, 125.21, 129.70, 129.80, 129.94, 130.73, and 138.20 ppm (s, aromatic).

^{31}P (CD_2Cl_2, internal standard): δ= -38.60 ppm (d, J=52.55 Hz, cis PMe_3), δ= -44.47 ppm (t, J=52.66 Hz, trans PMe_3).

X-Ray: Crystal color; Habit: Pale orange irregular prism. Crystal size (mm): 0.4x0.4x0.5. Crystal system: Orthorhombic. Space group: $P2_12_12_1$. Unit Cell Dimensions: a=11.550(3) Å, b=13.598(2) Å, c=14.362(4) Å. Volume: 2255.7(9) $Å^3$, Z=4. Formula weight=590.1. Density (Calc.): 1.737 Mg/m^3. Absorption Coefficient: 6.314 mm^{-1}. Single crystal X-ray diffraction data can be found in the appendix.

Chapter 3: Reactivity of the Hydrido Iridium Phenyl Complex

Mer-(Me3P)3Ir(Cl)(H)(Ph) (I) was found to be a fairly non reactive metal complex towards unsaturated organic compounds. However, complex (I) could be made to react with 2-butyne upon removal of the chloride ligand by the use of thallium hexafluorophosphate[74]. In the presence of 2-butyne, complex (I) can be transformed into the phenyl methylallyliridium complex (VII). Upon removal of the chloride by Tl^+, the open coordination site on (I) provides a place for 2-butyne to enter the coordination sphere. The hydride migrates to the alkyne to form an unstable metallo-vinyl intermediate. This intermediate was able to undergo a β-hydride elimination reaction to form a reactive allenehydridoiridium complex. The new hydride then migrates to the center carbon of the allene (carbon atom without protons) to yield complex (VII), (Figure 3.1). It was of interest to react complex (I) with a substituted alkyne which could not undergo the β-hydride elimination process. 3,3-Dimethyl-1-butyne, a monosubstituted alkyne, appeared to be a suitable candidate.

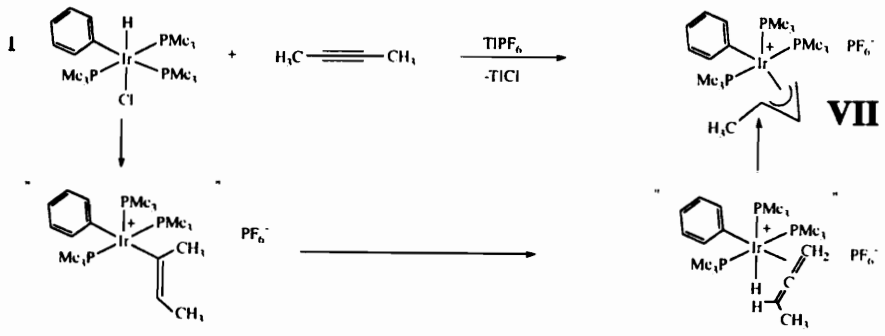

Figure 3.1 Phenyl methylallyl iridium complex (VII).

When a mixture of complex (**I**), thallium hexafluorophosphate, and an excess of 3,3-dimethyl-1-butyne in methylene chloride were allowed to react at room temperature for 24 hours, mer-[(Me_3P)$_3$(C_6H_5)Ir(C=CHt-Bu(CH=CHt-butyl))][PF_6] (**VIII**) is formed[87]. Characterization of (**VIII**) was accomplished using ^1H, ^{31}P, and ^{13}C NMR spectroscopies as well as single crystal X-ray diffraction. The ^1H NMR spectrum of (**VIII**) revealed a doublet at δ=1.68 ppm and triplet at δ=1.49 ppm showing a meridional arrangement of the phosphine ligands. A broad singlet at δ=0.53 ppm and a singlet at δ=1.06 ppm, nine protons each, suggested two different t-butyl groups. Three protons were found in the vinyl region. Two protons displayed as a doublet at δ=5.57 and a broad doublet at δ=5.88 ppm (J_{H-H}=15.5Hz) indicating a trans configuration: The third proton gave rise to a very broad doublet at δ=6.2 ppm (J_{P-H}=14.6Hz). The proton was not coupled to the other two, but coupled to a trans phosphine ligand and two cis phosphine ligands. Five protons were found in the aromatic region as a multiplet at δ=6.75-7.15 ppm for the phenyl ligand. No protons could be found in the hydride region (Figure 3.2).

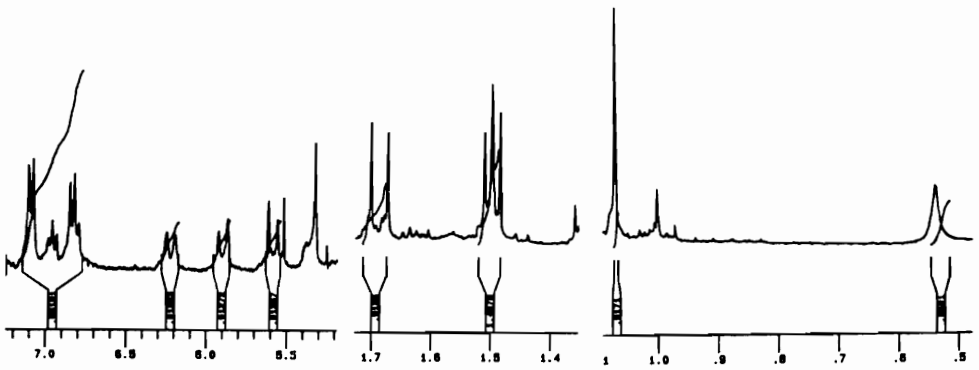

Figure 3.2 (270 MHz) ^1H NMR of (**VIII**).

An X-ray crystal determination of complex (**VIII**) confirmed the meridional position of the phosphine ligands and that two molecules of t-butylene acetylene have indeed coupled to form a 1,4-di-t-butyldienyl ligand. An interesting feature of this structure is that one methyl group from a t-butyl fragment rests over the sixth coordination site forming an "agostic" Ir-H-C interaction (Figure 3.3). Further support for the agostic interaction was obtained from low temperature ^{1}H NMR studies. These studies showed that on cooling, the broad singlet at δ=0.53 ppm broadens further into the baseline. Previous work have shown that at -90^o C, two new singlets at δ=1.1 and -0.7 ppm appear in a 2:1 ratio indicating the rotation of the three methyl groups have slowed considerably. However, the rotation of the three protons of the methyl group over the iridium center remain a fast process even at -90^o C. It was of interest to examine the mechanism by which the alkyne had coupled to each other to form the dienyl ligand. Therefore, a deuterium labeling study was performed.

Mechanism

The ^{1}H NMR spectrum of the vinylic protons of complex (**VIII**) gave three distinctive resonances: δ=6.20, δ=5.88, and δ=5.57 ppm. The proton (3) at δ=6.2 ppm is coupled to a trans phosphine and appears as a very broad doublet. The proton (2) at δ= 5.88 ppm is coupled to a trans proton (1) and is broadened by the trans phosphine ligand as well. Proton (1) is a sharp doublet coupled to proton (2) as shown previously in Figure 3.2. This distinction is important because the vinylic protons arise from three possible sources: the hydride, the first t-butylacetylene or the second t-butylacetylene molecule. Deuterium labeling experiments were

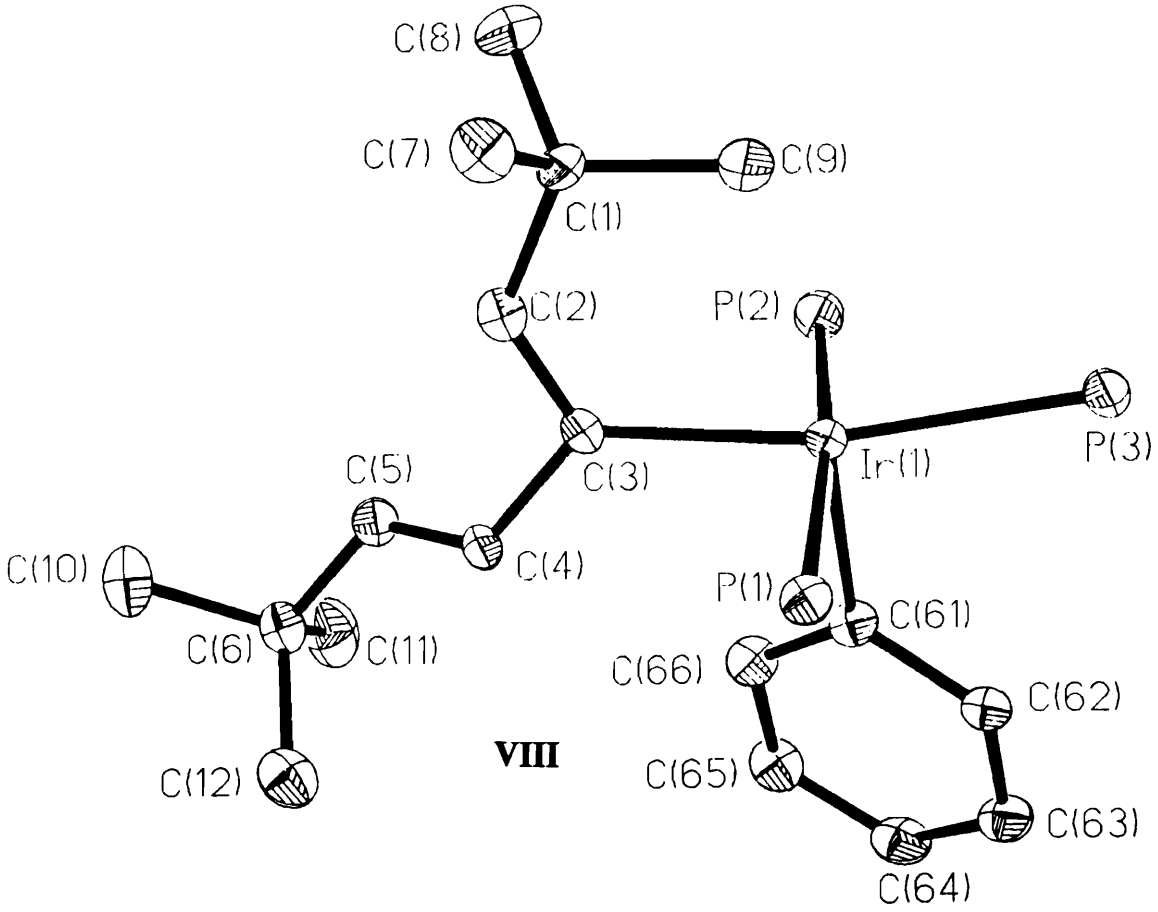

VIII

Figure 3.3 ORTEP of complex (**VIII**).

performed to first locate which proton originates as the hydride. [Ir(COD)(PMe3)3]Cl was allowed to react with d6-benzene under conditions similar to those described in Chapter 2 to afford the deuteride-iridium complex. Experiment **A** was a reaction between the labeled complex and 2 equivalence of 3,3-dimethyl-1-butyne with Tl[PF6], following the same procedures as one would in the preparation for complex (**VIII**). The ^{1}H NMR spectrum in the vinylic region revealed a broad doublet at δ= 6.2 ppm (proton 3) and a singlet at δ=5.88 ppm (proton 2). Proton 1 was not observed (Figure 3.4). This indicates that proton (1) originates from the hydride ligand.

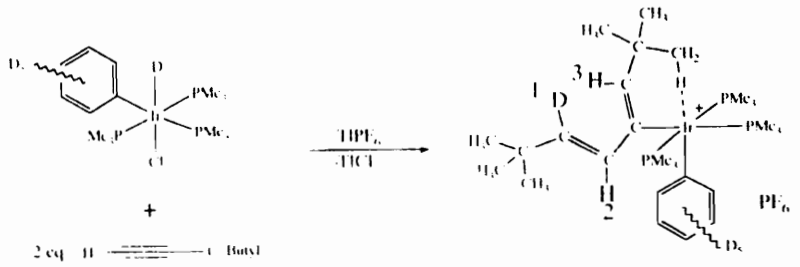

In the vinyl region, ^{1}H NMR clearly shows the loss of proton 1 at δ 5.5 ppm and gives a singlet for proton 2 at δ 5.8 ppm with a broadened doublet for proton 3 at δ 6.2 ppm.

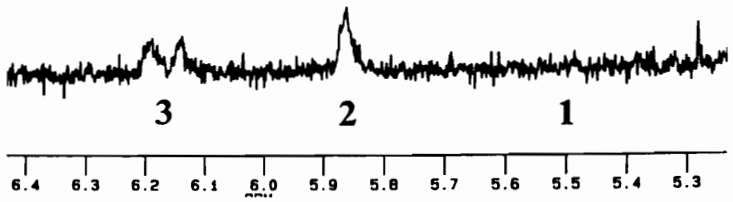

Figure 3.4 (270 MHz) ^{1}H NMR of the vinyl region of experiment (**A**).

A second parallel reaction between (**I**) and excess labeled t-butylacetylene $(CH_3)_3CC{:}C\text{-}D$ gave the complementary results in experiment **B**. The ^{1}H NMR spectrum in this case displays proton (1) as a singlet at δ=5.57 ppm where protons (2) and (3) are not observed, (Figure 3.5). However, these reactions do not fully describe how the second alkyne was incorporated. Therefore, a third labeling experiment C was performed.

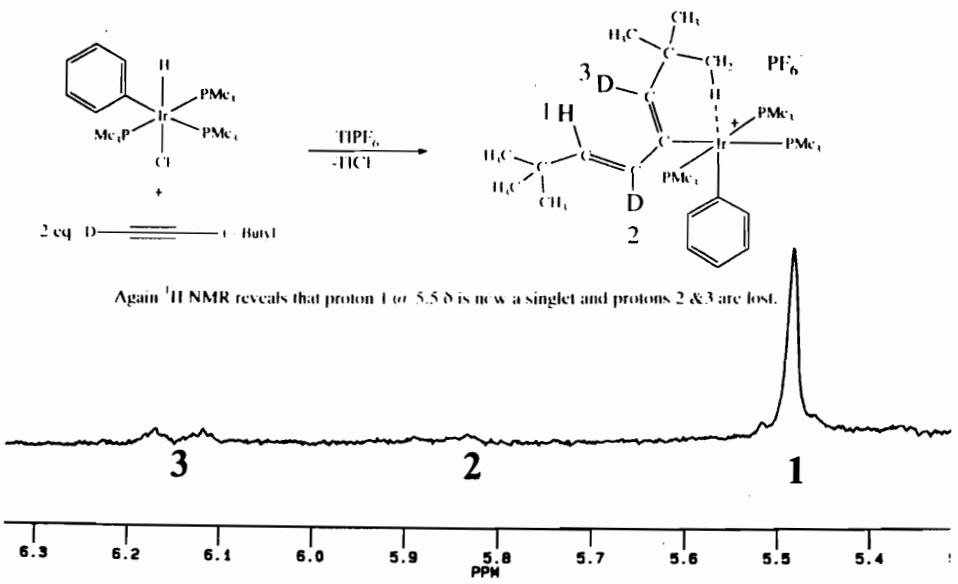

Figure 3.5 (270 MHz) ^{1}H NMR of the vinyl region of experiment **(B)**.

Complex **(I)** was allowed to react with one equivalent of normal t-butylacetylene for 30 minutes followed by an equivalent of the labeled t-butylacetylene. The ^{1}H NMR spectrum of the product from this reaction showed a mixture of two products with the predominant product incorporating deuterium in position 3 at δ=6.2 ppm. The minor product incorporated the deuterium at position 2 which collapsed position 1 to a singlet (Figure 3.6). Formation of the minor product can occur if **(I)** reacts with some of the labeled t-butylene first; since, the reaction requires at least 24 hours to undergo completion. The major product that was formed, suggests the second alkyne rearranges into a vinylidene group. A migration of the vinyl group attacks the α carbon of the vinylidene. Further support for the initial vinyl formation was performed by a reaction between **(I)**, one equivalent of 3,3-dimethyl-1-butyne and PMe_3 (Experiment **D**). Rearrangement of a coordinated alkyne to a vinylidene is not an uncommon process[88]. Once the 1,4-di-t-butyldienyl ligand was formed, one t-butyl group will eventually rest over the sixth coordination site to "stabilize" the final product, see proposed mechanism Scheme 3.1.

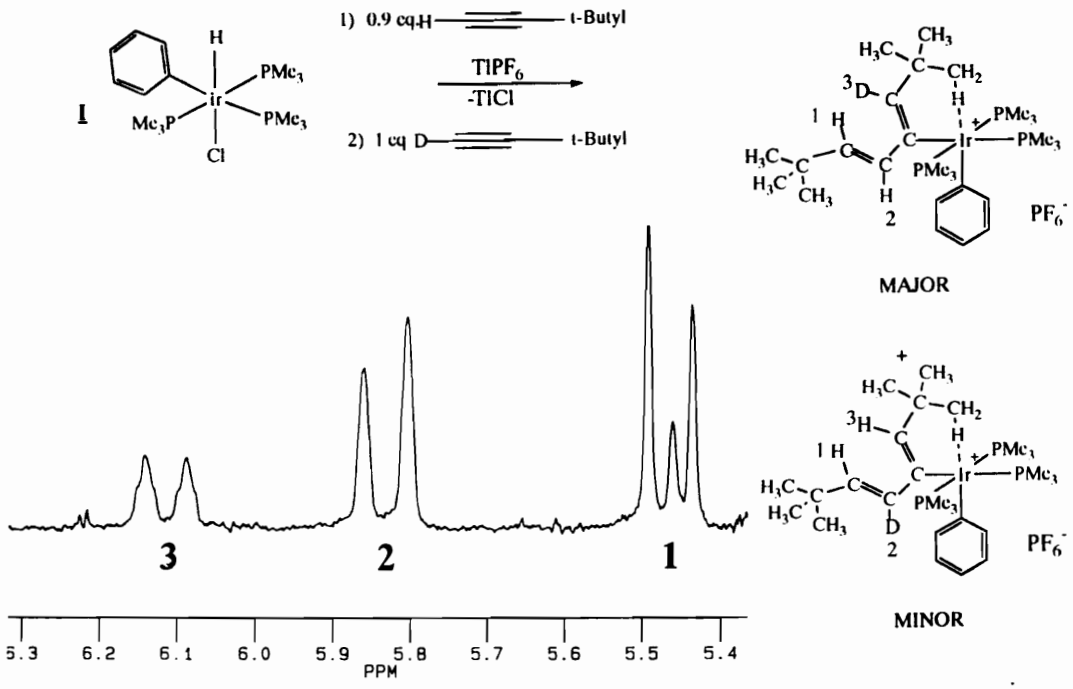

Figure 3.6 (270 MHz) ^{1}H NMR of the vinyl region of experiment (C).

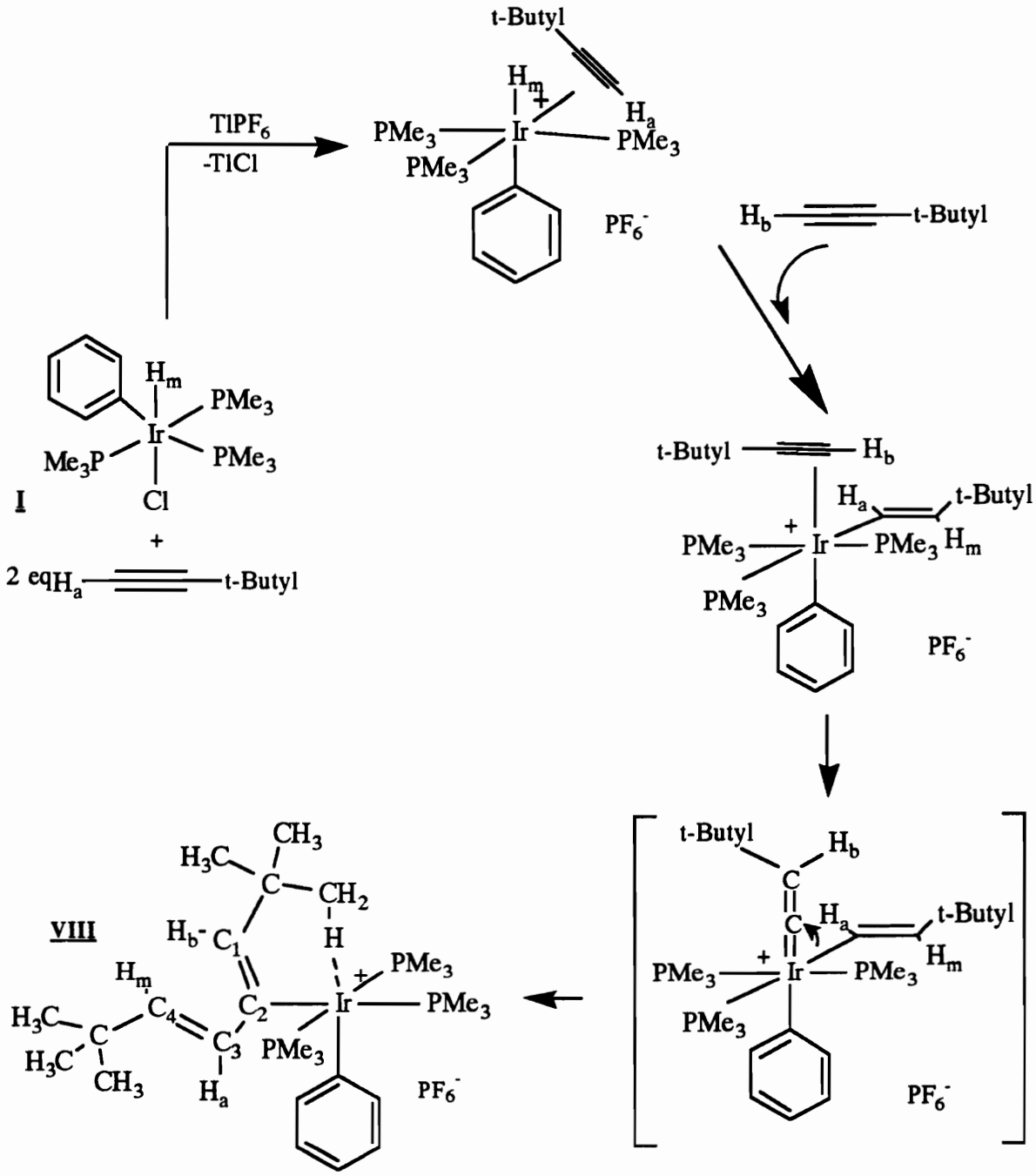
TlPF6
-TlCl
t-Butyl
Hm
Ha
PMe3
Ir
PMe3
PMe3
PF6-
Hb
t-Butyl
Hm
PMe3
Ir
PMe3
Me3P
PMe3
I
Cl
+
2 eq Ha
t-Butyl
t-Butyl
Hb
Ha
t-Butyl
+
PMe3
Ir
PMe3
Hm
PMe3
PF6-
t-Butyl
Hb
C
C
Ha
t-Butyl
+
PMe3
Ir
PMe3
Hm
PMe3
PF6-
VIII
H3C
CH3
C
CH2
Hb
C1
H
Hm
C4
C2
Ir
+
PMe3
PMe3
H3C
C
C3
PMe3
H3C
CH3
Ha
PF6-

Scheme 3.1

Since the sixth coordination site is filled by an agostic interaction which is generally weak, this site could possibly allow another alkyne to enter. The alkyne could then rearrange to a vinylidene followed by the migration of the organic group leading to oligomers, such as those depicted in Scheme 3.2.

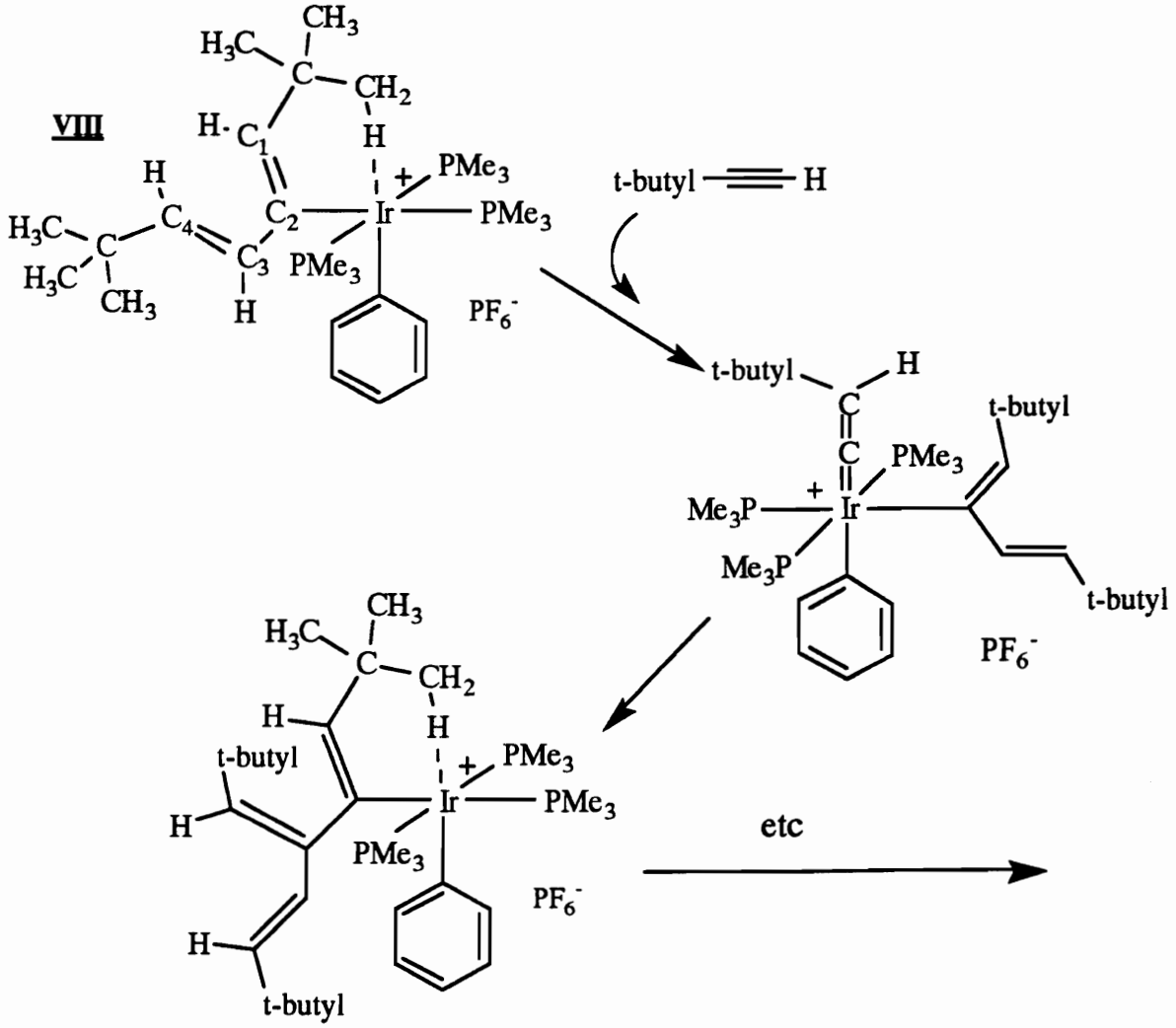

Scheme 3.2

Attempts were made to react (**VIII**) with excess 3,3-dimethyl-1-butyne by refluxing the mixture in dry methylene chloride for two days. Upon

workup, a pale yellow oil was isolated. A sample was submitted for GC/MS analysis which showed two predominant products. The major product was the E & Z isomer of 2,2,7,7-tetramethyl-3-octen-5-yne with a parent peak at 164 m/z. Minor products had long retention times on the GC with molecular weights of 246 and 306. The ^{1}H NMR spectrum of the major product was consistent for the t-butylacetylene dimer. Apparently the complex (**VIII**) generated a 16e$^-$ intermediate capable of dimerizing the alkyne. Metal centers of this kind are known to couple 1-alkynes[89], and a reaction between [Ir(COD)(PMe_3)$_3$]Cl and excess 3,3-dimethyl-1-butyne produced a light yellow oil of 2,2,7,7-tetramethyl-3-octen-5-yne was already described in Chapter 2. Since quantities were limited and of low molecular weight, this was not investigated further.

Attempts were made to react (**I**) with phenylacetylene and trimethylsilylacetylene under similar conditions. Trimethylsilylacetylene and (**I**) gave a number of products. However, the vinyl region of the ^{1}H NMR spectrum of this product showed a cis vinyl group at δ=5.56 and δ=5.78 ppm ($J_{H\text{-}H}$=3.0Hz). Several resonances were found for the trimethylsilyl groups around 0.0 ppm which made the connectivity difficult to establish (Figure 3.7).

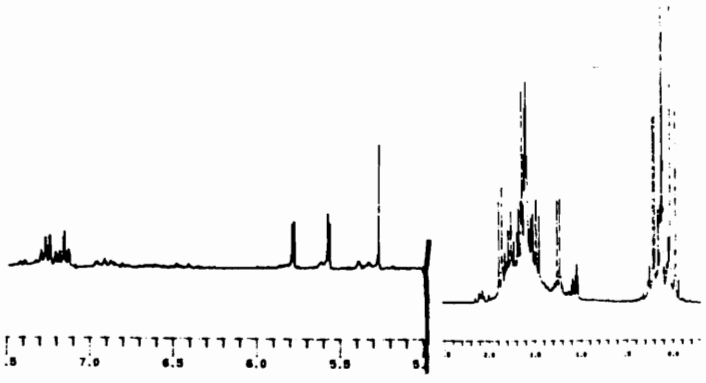

Figure 3.7 (270 MHz) ^{1}H NMR of the reaction between trimethylsilylacetylene & (**I**).

Attempts to purify this material resulted in its rapid decomposition. Complex (**I**) and phenylacetylene react in the presence of Tl[PF_6] to generate a complex mixture of products. The ^{1}H NMR spectrum of this reaction mixture showed weak vinylic proton resonances similar to (**VIII**), with broad doublets at δ=5.40, δ=5.75, and δ=6.50ppm and the usual meridional phosphine pattern was clearly visible (Figure 3.8).

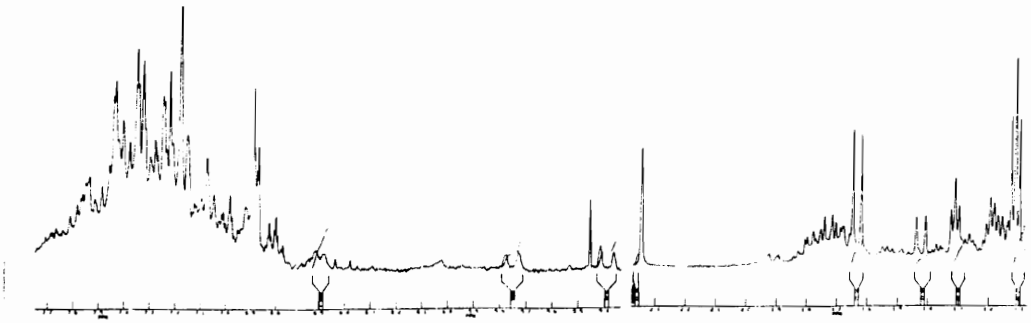

Figure 3.8 (270 MHz) ^{1}H NMR of the reaction between phenylacetylene & (**I**).

Several efforts to prepare, purify and characterize this complex failed because the product quickly decomposes. If phenylacetylene and trimethylsilyl acetylene did follow the general mechanism as t-butyl-acetylene, the stability of the complex may be dependent on the strength of the agostic interaction. For example, if one builds a molecular model of the "dienyl" complex based on (**VIII**), the sixth coordination site filled by a t-butyl gave the best overlap. The phenyl group and trimethylsilyl group gave poor overlap (Figure 3.9). This may explain why the two alkynes failed to produce a product similar to (**VIII**). With this in mind, the reaction between (**I**) and 2-ethynylpyridine was investigated. The alkyne in this case contains a nitrogen lone pair for coordination and could stabilize the product.

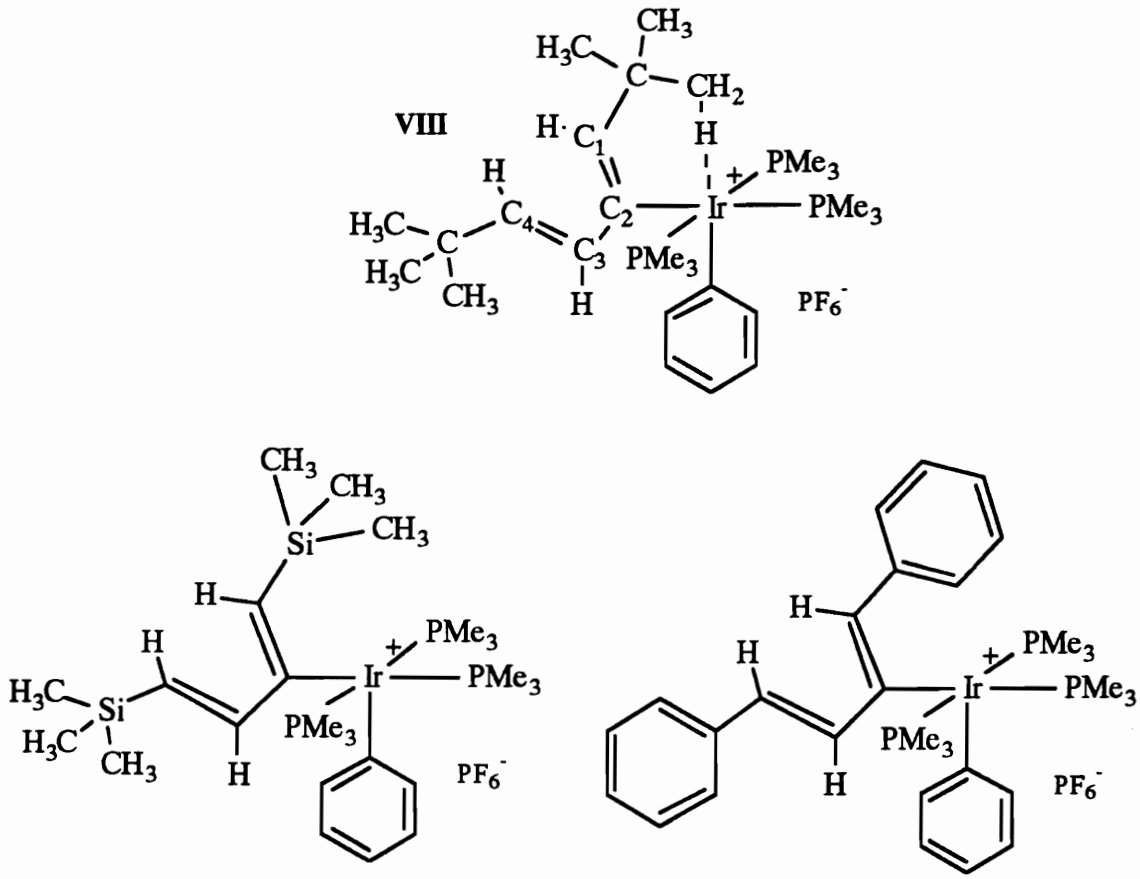

Figure 3.9 Complex (VIII) and the phenyl & trimethylsilane analogs.

2-Ethynylpyridine

Excess 2-ethynylpyridine reacts with (**I**) by the action of Tl[PF_6] to give an intense purple solution. Upon work-up, an oily purple compound was obtained. Further purification eventually gave a purple crystalline complex in high yields (81%), (**HES I 209**)-(**IX**). The ^{1}H NMR spectrum of this product revealed a number of multiplets in the aromatic region with a doublet and triplet for the meridional phosphine ligands. Since NMR spectroscopy could not provide enough information to establish the structure, a single X-ray crystal structural determination was carried

out. Figure 3.10 shows an ORTEP plot displaying the results of this study. It can be clearly seen from this figure that the phenyl group has been lost from the iridium and that three equivalence of the 2-ethynylpyridine have coupled to form an unusual tricyclic structure. One ring consists of four carbons and the iridium, while the second ring is made up of three carbons, the iridium, and a nitrogen. Although there is no direct evidence for the mechanism of this transformation, the proposed mechanism may involve the following: Once the chloride ligand is removed by Tl^+, a molecule of 2-ethynylpyridine coordinates to the open site via the nitrogen lone pair. The alkyne portion which is ortho to the heteroatom is in close proximity to the metal center possibly donating electrons to help induce reductive elimination of benzene. A second molecule of the alkyne then coordinates to the highly reactive iridium(I) center. This leads to an oxidative coupling of the alkynes forming the first metallacyclic ring. This leaves the sixth coordination site open for a third molecule to enter. A third equivalent of acetylene enters and rearranges to a vinylidene. A nearby pyridine group is then able to attack the α carbon forming the second five membered ring, (Scheme 3.3).

There are a number of monosubstituted alkynes with the general carbon back bone of $X\text{-}CR_2C{:}CH$ where X can be N, O, or a halogen atom that could possibly react in a similar fashion with complex (**I**): 3-methyl-3-hydro-1-butyne; 3-butyne-2-one; methyl propiolate; dimethyl amino 2-propyne; 1-ethynyl cyclohexanol; propargyl alcohol; and propargyl bromide (see structures in Figure 3.11). Methyl propiolate and (**I**) gave a fairly stable yellow complex (**HES I 249**), similar to the purple "trimer" (**IX**). The ^1H NMR spectrum displayed a doublet and triplet at δ=1.91 and δ=1.31 ppm for the phosphine ligands with three singlets at δ=3.79 , 3.93 ,

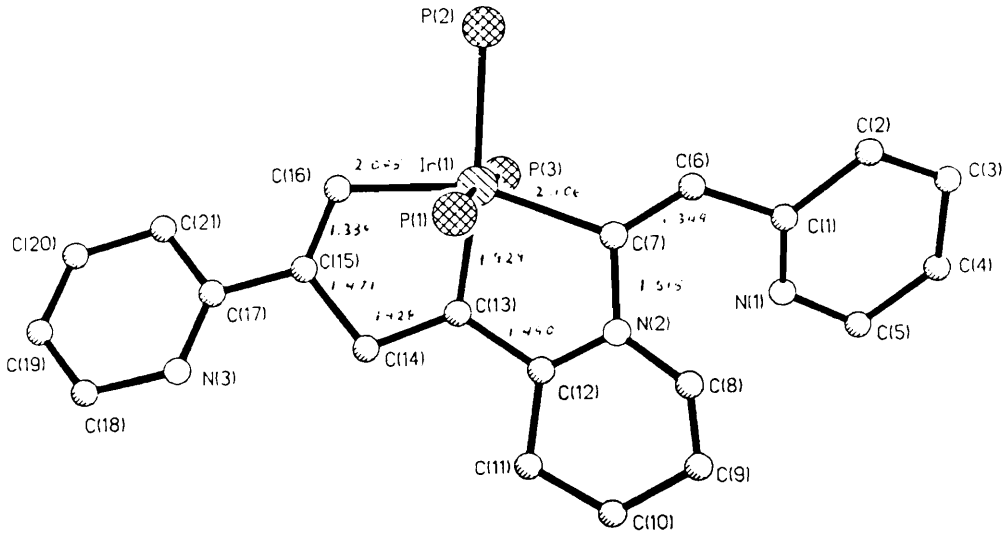

IX

Figure 3.10 ORTEP of (**IX**).

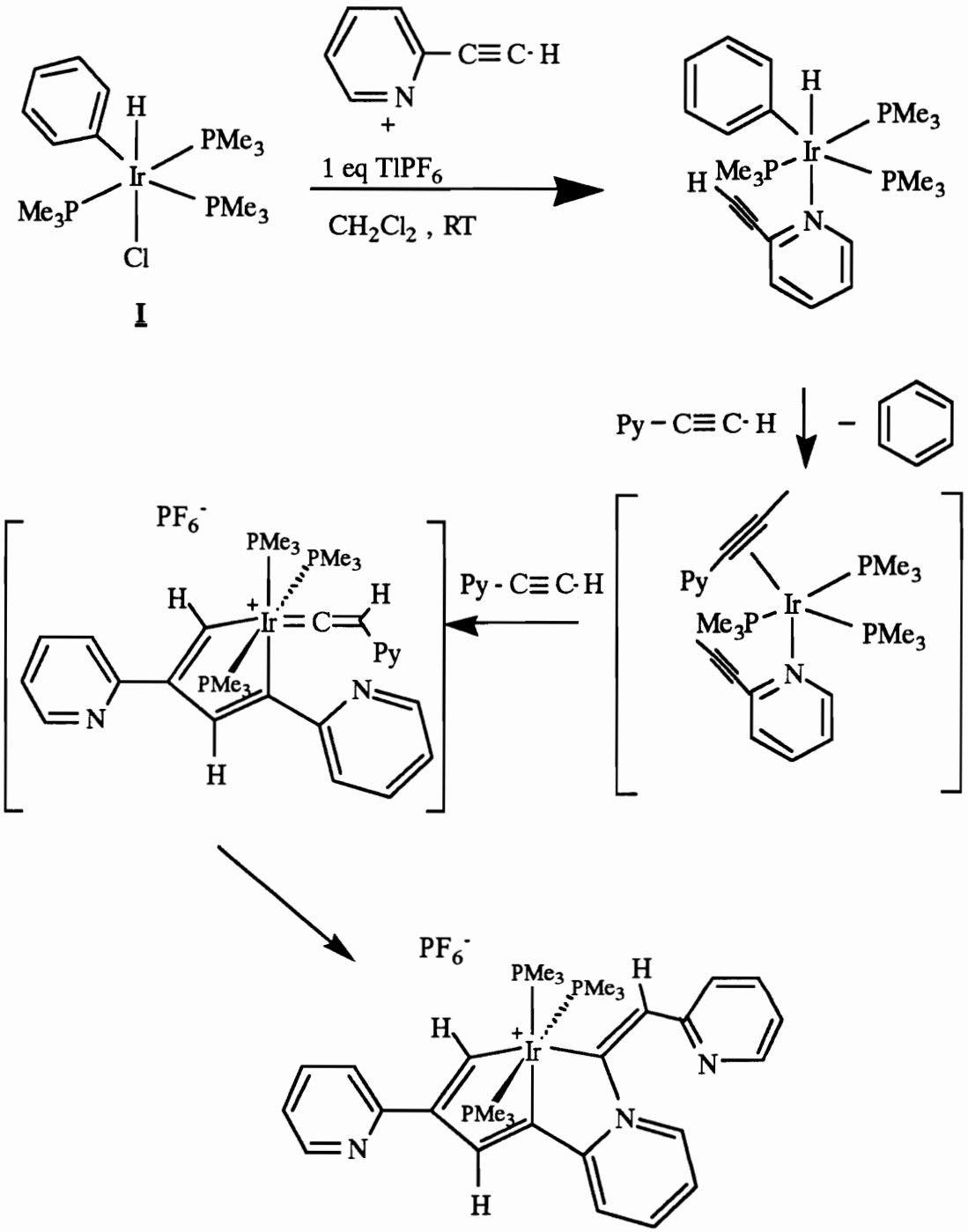

IX

Dark Purple

Scheme 3.3

and 4.29 ppm for the methyl groups on the propiolate and three resonances at δ=6.1 , 9.0 , and 10.4 ppm for the protons of the vinyl and the

metallacycle (Figure 3.12). Comparable resonances between δ= 8.0 and 6.0 ppm could be found in the crude but complicated NMR spectra of the reactions between (**I**) and the other alkynes but they failed to produce stable complexes. 3-Methyl 3-hydroxy-1-butyne and (**I**) gave a lavender colored solution and 3-butyne-2-one gave a blue colored solution;. However, they both decompose to brown-black tars.

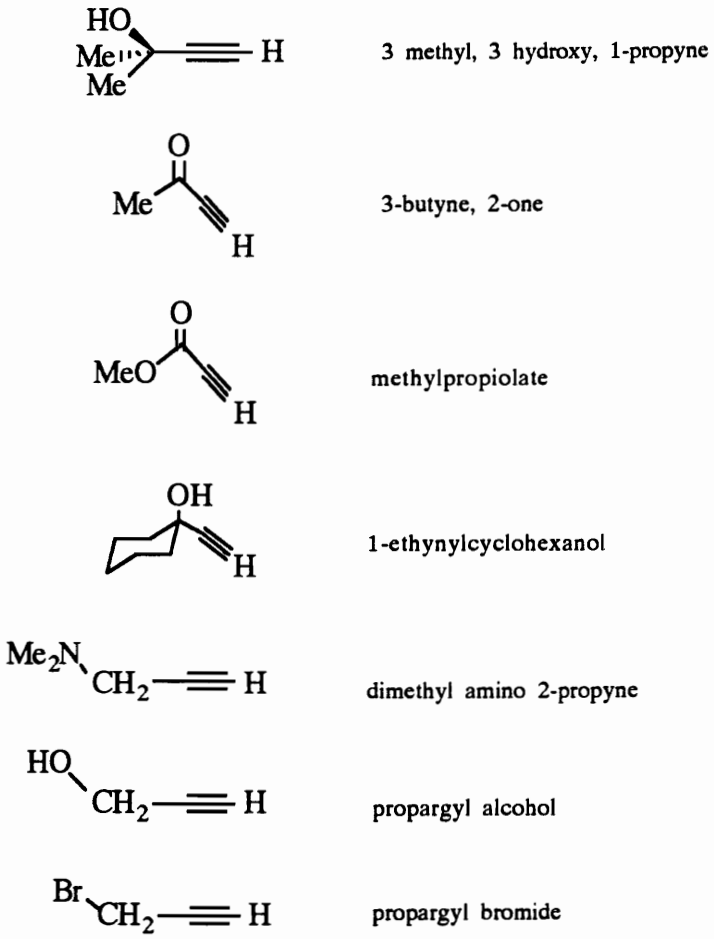

Figure 3.11 Monosubstituted alkynes.

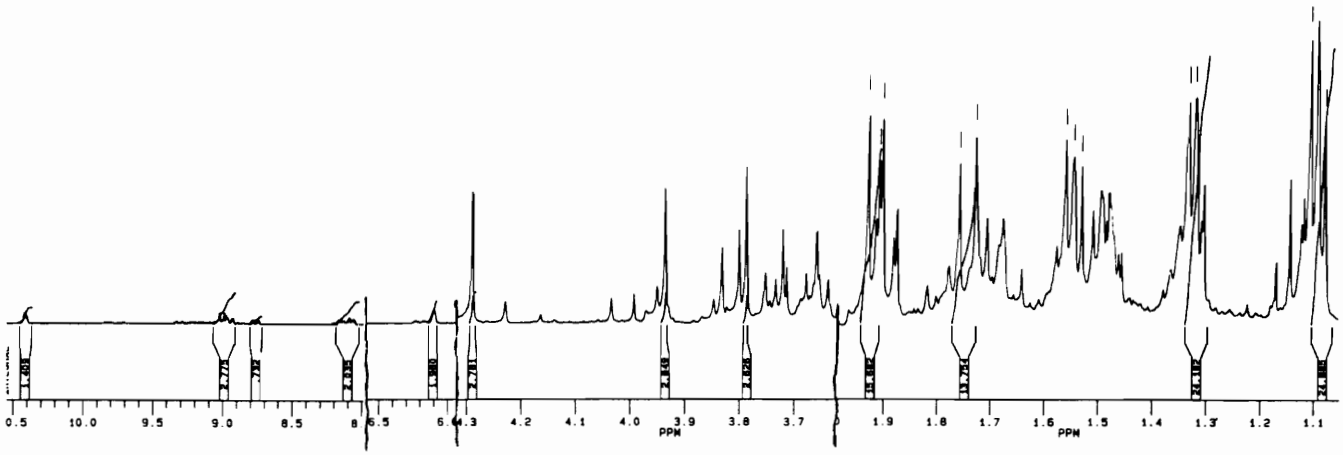

Figure 3.12 (270 MHz) ^{1}H NMR of the reaction between methyl propiolate & (I).

Even though the reactions gave beautiful colors, they were counter productive in that reductive elimination of the C-H adduct takes place in these reactions. Also, the methyl propiolate "trimer" was found to be unstable and slowly decomposes, as well. Studies by O'Connor and coworkers[90], investigated the mechanisms of metallacycle annulation reaction. They found evidence for an intramolecular methoxy group transfer which may provide a pathway for the decomposition of these complexes. An oxygen atom from an ester group was transferred to the α carbon of the vinylidene group. They found that residual water attacks the carbon atom of that ester group. After several steps, fragmentation of the oxoacyl ligand generates the carbonyl group and the organic product (see Scheme 3.4). Again this could be one possible decomposition route, but no attempts were made to isolate the by-products.

A reaction between (I) and Tl[PF_6] without the presence of unsaturates was performed in an attempt to create a reactive hydrogen bridged dimer. In this way, the complex can be used directly with unsaturates and reduce the work up procedures by avoiding the TlCl filtration step. The ^{1}H NMR spectrum did not provide the necessary data to deduce the structure

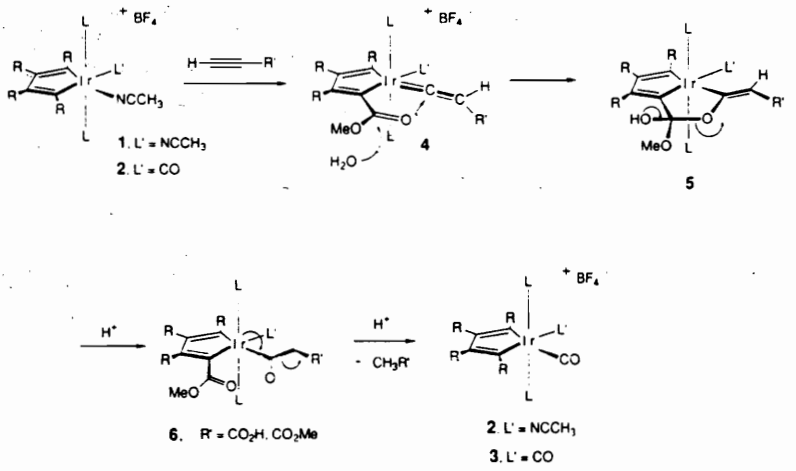

Scheme 3.4

therefore a single X-ray crystal determination was carried out. The structure contained two phenylhydrido-iridium centers but sharing one chloride atom forming a chloro-bridged dimer (**X**). The interesting bond was the bridging Ir-Cl-Ir bond with a nearly linear bond angle of 179°. The Ir(1)-Cl bond of 2.647(4)Å and Ir(2)-Cl bond of 2.665(5) Å are long Ir-Cl bonds in comparison to normal Ir-Cl bond of 2.507(3) Å, (see Figure 3.13). Addition of excess 3,3-dimethyl-1-butyne added to (**X**) produced the expected complex (**VIII**). Attemps to purify (**X**) for characterization have failed due to the instability of this species. A reaction between (**I**), Tl[PF_6], and pyridine produced the desired complex of mer-[(Me_3P)$_3$Ir-(Phenyl)(H)(Py)]PF_6, (**XI**) where the chloride ligand is replaced with pyridine. Addition of excess 3,3-dimethyl-1-butyne added to (**XI**) produced (**VIII**) as well. As for future work in this area, the phenyl ligand of (**I**) appears to have little affect on the course of the reaction and seems to be solely dependent on the available alkyne. The next chapter describes the reactivity of iridium complexes formed from C-H addition of heteroaromatic compounds.

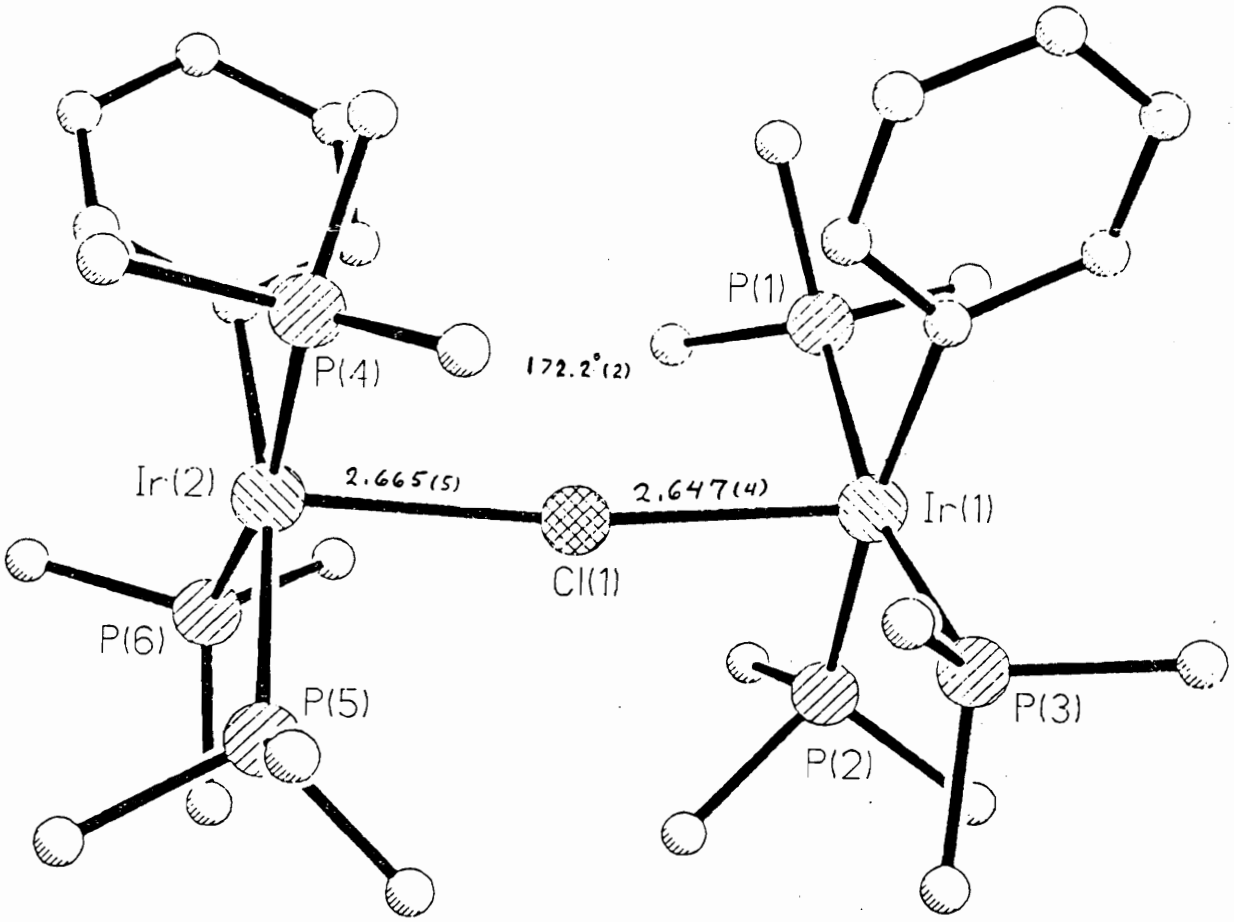

X

Figure 3.13 ORTEP of the chloro-bridged iridium dimer (**X**).

Experimental Section

General Comments:

All of the general comments in Chapter 2 apply here. Most of the alkyne additions were carried out at room temperature in dried solvents and standard inert atmosphere techniques. Reagents were obtained commercially from Aldrich Chemical Co. and Farchan Research Chemicals and were used as supplied.

Preparation of mer-(tris-Trimethylphosphine)(Phenyl) σ-1,4-(di-t-butadienyl)iridium(III) Hexafluorophosphate (VIII)

In a typical reaction, 200 mg (0.375 mmoles) of complex (I) was dissolved in 8 mL of dry methylene chloride along with 61.6 mg (92.0 μl, 0.750 mmoles) of 3,3-dimethylbutyne (2 eq). The mixture was stirred and 131.0 mg (0.375 mmoles) of thallium hexafluorophosphate was added as a solid. This was allowed to react for 24 hours at room temperature. The TlCl was filtered off and the methylene chloride was removed from the filtrate under vacuum. Fresh methylene chloride (2-3 mL)was used to redissolve the crude product and pentane (8 mL)was added to precipitate a pure off-white product, 212.0 mg (0.262 mmole, 70% based on (I)) of mer-(tris-Trimethylphosphine)(Phenyl) σ-1,4-di-t-butadienyliridium(III) Hexafluorophosphate (VIII). C, H elemental analysis calculated for $C_{27}H_{53}F_6P_4Ir$: C-40.15%, H-6.13%. Found: C-38.75%, H-6.46%.

^1H NMR (200MHz, CD_2Cl_2): δ=0.53 ppm (br s, 9H, $C(CH_3)_3$), δ=1.06 ppm (s, 9H, $C(CH_3)_3$), δ= 1.49 ppm (t, J_{P-H}=3.5 Hz, 18H, trans PMe_3), δ=1.68 ppm (d, J_{P-H}=7.6 Hz, 9H, cis PMe_3), δ=5.57 ppm (d, J_{H-H}=15.5 Hz, 1H), δ=5.88 ppm (br d, J_{H-H}=15.5 Hz, 1H), δ=6.20 ppm (br d, J_{P-H}=14.6Hz, 1H), δ=6.75-7.15 ppm (m, 5H, phenyl).
^{13}C NMR (50 MHz, CD_2Cl_2): δ=15.55 ppm (t, J_{P-C}=18.0 Hz, trans PMe_3), δ=18.8 ppm (d, J_{P-C}=27.0 Hz, cis PMe_3), δ=26.6 ppm (br s, $C(CH_3)_3$), δ=29.1 ppm (s, $C(CH_3)_3$), δ=33.0 ppm (s, $C(CH_3)_3$), δ=36.5 ppm (br s, $C(CH_3)_3$), δ=111.2 ppm (q, $J_{P(trans)-C}$=4.5 Hz, Ir-C of phenyl C),δ=123.8, and 126.7 ppm (vinylic C), δ=141.8 ppm (d of t, $J_{P(trans)-C}$=93 Hz, $J_{P(cis)-C}$=12.0 Hz, Ir-C of vinylic C), δ=136.3, 138.3, and 145.2 ppm (phenyl C).
^{31}P NMR (81 MHz, CD_2Cl_2) δ=-34.0 ppm (d, J=18.0 Hz, trans PMe_3) δ= -46.0 ppm (t, J=18 Hz, cis PMe_3).
X-Ray: Crystal color; Habit: Yellow rectangular plate. Crystal size (mm): 0.1x0.3x0.4. Crystal system: Orthorhombic. Space group: Pbac. Unit Cell Dimensions: a=11.658(4) Å, b=18.041(4) Å, c=33.731(8) Å. Volume: 7094(4) $Å^3$, Z=8 Formula weight=807.8. Density (Calc.): 1.513 Mg/m^3. Absorption Coefficient: 3.973 mm^{-1}. Single crystal X-ray diffraction data can be found in the appendix.

A.) Reaction Between mer-$(Me_3P)_3Ir(C_6D_5)(D)Cl$ and 3,3-Dimethyl-1-butyne (HES I 47)

A 50 mL flask equipped with a stir bar and septum was charged with 100 mg of mer-$(Me_3P)_3Ir(C_6D_5)(D)Cl$ (0.187 mmol) under nitrogen in a dry box. The flask was connected to a double manifold (vacuum/nitrogen)

Schlenk line. Dry methylene chloride (25 mL) was injected by syringe into the flask along with 46.1μl (2eq) of 3,3-dimethyl-1-butyne. Thallium hexafluorophosphate (65.5 mg, 0.187 mmol) was then added as a solid to the flask under a counter-stream of nitrogen. This mixture was stirred well for 24 hours. The thallium chloride was then allowed to settle. The solution was filtered as it was transferred via a cannula to another 50 mL flask. The solvent was stripped leaving a brown tar. The tar was redissolved using dry methylene chloride (2-3 mL). While stirring, dry ether (20 mL) was added to precipitate a light tan product. The brown solution was filtered and the product was rinsed twice with ether (3 mL) and vacuum dried.

^{1}H NMR ($DCCl_3$) δ=0.52 ppm (br s, 9H, agostic Ir-$(CH_3)_3C$), δ=1.05 ppm (s, 9H, $(CH_3)_3C$), δ=1.48 ppm (t, J_{P-H}=3.45Hz, 18H, trans PMe_3), δ=1.69 ppm (d, J_{P-H}=7.68Hz, 9H, cis PMe_3), δ=5.86 ppm (s, 1H, vinylic), δ=6.14 & 6.19 ppm (br d, J_{P-H}=13.51Hz, 1H, vinylic).

B.) Reaction Between (I) and $(CH_3)_3CC{:}CD$ (HES I 53)

A 50 mL flask equipped with a stir bar and septum was charged with 84.3 mg of $(Me_3P)_3Ir(C_6H_5)HCl$ (I) (0.158 mmoles) under nitrogen in a dry box. The flask was connected to double manifold (vacuum/nitrogen) Schlenk line. Dry tetrahydrofuran (10 mL) was injected into the flask to dissolve the starting material. In a separate flask the labeled 3,3-dimethyl-1-butyne was prepared by mixing 230.8 μL of 3,3-dimethyl-1-butyne with 20 mL of dry tetrahydrofuran under nitrogen and chilled in a dry ice/acetone mixture. Once cooled, n-butyllithium (760 μL, 2.5 M in hexane) was injected and the reaction was allowed to warm up on its own

to room temperature for twenty minutes. Deuterium oxide (32.2 μL, ≤1eq) was slowly injected into the mixture. The solution was distilled and the first few mL were collected. This fraction consisted mostly of the labeled 3,3-dimethyl-1-butyne (>2eq) bp. 37° C and some tetrahydrofuran which was injected into the flask containing the solution of complex (**I**). Thallium hexafluorophosphate (55.0 mg, 1eq) was added as a solid against a counter-stream of nitrogen. The mixture was allowed to stir for 24 hours. The thallium chloride was then filtered as the solution was transferred via a cannula to a 50 mL flask. The solvent was removed under vacuum leaving a tan crystalline solid behind.
^{1}H NMR ($DCCl_3$) δ=0.49 ppm (br s, 9H, agostic Ir-$(CH_3)_3C$), δ=1.03 ppm (s, 9H, $(CH_3)_3C$), δ=1.46 ppm (t, J_{P-H}=7.88Hz, 18H, trans PMe_3), δ=1.66 ppm (d, J_{P-H}=7.91Hz, 9H, cis PMe_3), δ=6.00 ppm (s, 1H, vinylic), δ=6.70-7.04 ppm (m, 5H, phenyl).

C.) Reaction Between (I), 3,3-Dimethyl-1-butyne and Deuterium Labeled 3,3-Dimethyl-1-butyne (HES I 65)

A 50 mL flask equipped with a stir bar and septum, was charged with 61.0 mg of complex (**I**) (0.114 mmol) under nitrogen in a dry box. The flask was connected to a double manifold (vacuum/nitrogen) Schlenk line. Dry tetrahydrofuran (20 mL) was injected to dissolve (**I**). Thallium hexafluorophosphate (39.93 mg, 0.114 mmol) was added as a solid against a counter-stream of nitrogen. A mixture of 3,3-dimethyl-1-butyne (13.0 μL, 0.9 eq) and tetrahydrofuran (10 mL) was injected into the solution. The mixture was allowed to react for 30 minutes. The labeled 3,3-dimethyl-1-butyne, previously made by the same procedure described in

experiment B, was then injected and the reaction mixture was stirred overnight. The thallium chloride was filtered out and the solvent was removed leaving a tan product behind.

^1H NMR reveals a mixture of products. The major product ($DCCl_3$) δ=0.49 ppm (br s, 9H, agostic Ir-$(CH_3)_3C$), δ=1.03 ppm (s, 9H, $(CH_3)_3C$), δ=1.46 ppm (t, J_{P-H}=3.17Hz, 18H, trans PMe_3), δ=1.66 ppm (d, J_{P-H}=7.67Hz, 9H, cis PMe_3), δ=5.41 ppm (d, J_{H-H}=15.31Hz, 1H, trans-vinyl), δ=5.78 ppm (d, J_{H-H}=15.32Hz, 1H, trans-vinyl), δ=6.70-7.04 ppm (m, 5H, phenyl). The minor product in the vinyl region at δ=5.40 ppm (s, 1H, vinyl), δ=6.50 ppm (br d, JP-H=8.97Hz,1H, vinyl) .....

D.) Reaction of (I), 3,3-Dimethyl-1-butyne, and Trimethylphosphine (HES I 139)

A 100 mL flask equipped with a stir bar and septum was charged with 100 mg of (**I**) (0.187 mmol) under nitrogen in a dry box. The flask was connected to a double manifold (vacuum/nitrogen) Schlenk line. Dry tetrahydrofuran (20 mL) was injected to dissolve the material. One equivalent of 3,3-dimethyl-1-butyne (23 μL, 0.187 mmol) was injected into the solution and then 65.5 mg (0.187 mmol) of thallium hexafluorophosphate was added as a solid. The solution was stirred for 30 minutes, after that time one equivalent of trimethylphosphine (19.4 μL, 0.187 mmol) was injected and stirred for 15 minutes. The thallium chloride was filtered off and the solvent was stripped. The crude product was washed with toluene to remove any remaining trimethylphosphine . Attempts to purify the product by dissolving in methylene chloride and precipitating by

using pentane had failed. A mixture of products were found including complex (**I**), $(Me_3P)_4Ir(Ph)H$, and $(Me_3P)_3Ir(t\text{-}CH{=}CH(t\text{-butyl}))(Ph)H$. ^1H NMR.($DCCl_3$).δ= -23.72 ppm (q, 1H, Ir-H of (**I**)), δ=-13.15 & -12.65.ppm (d q, 1H, Ir-H, tetrakis (PMe_3)), δ=1.12 ppm (s, 9H, t-butyl), δ=1.25, 1.32, & 1.39 ppm (t, 18H, trans PMe_3), δ=1.63, 1.69, & 1.73 ppm (d, 9H, PMe_3), δ=5.35 ppm (q, 1H, vinyl), δ=6.55 ppm (m, 1H, vinyl), δ=6.72, 6.85, 7.55, & 8.17 ppm (m, phenyl of (**I**)), δ= 6.9-7.2, & 7.4 ppm (m, phenyl).

E.) Reaction of (VIII) with excess 3,3-dimethyl-1-butyne (HES I 235)

A thick-wall reaction tube equipped with a stir bar and a septum was charged with compound (**VIII**) (50 mg, 0.062 mmol) under nitrogen in a dry box. The reaction tube was connected to a double manifold (vacuum/nitrogen) Schlenk line. Dry methylene chloride (25 mL) and 3,3-dimethyl-1-butyne (2 mL, 36.5 mmol) were added by syringe. The tube was sealed with a teflon cap, shaken, and placed in an oil bath at 70° C for 24 hours. After cooling, the solution was transferred by a cannula to a 100 mL flask. The solvent was removed under vacuum to give a dark brown oil. Dry pentane (15 mL) was used to dissolve the organic portion. This was filtered and the residue was washed with additional pentane (5 mL) leaving a tan solid behind. The pentane was removed under vacuum yielding a pale yellow oil (2 mL, 0.869 g). A sample was submitted for GC/MS analysis. The pale yellow oil was a mixture of several products. The major product consists of the E & Z isomer of 2,2,7,7-tetramethyl-3-

octen-5-yne, identified by library match. The major m/z units are: 164, 149, 134, 121, 107, 91, 77, 57, 41, 27, & 15.
The crude ^1H NMR ($DCCl_3$) displayed: δ=1.1 ppm (s, 18H, t-butyl), δ=5.67 ppm (d, J_{H-H}=15.12Hz, 1H, trans vinyl), δ=5.97 ppm (d, J_{H-H}=16.23Hz, 1H, trans vinyl).

The ^1H NMR of the solids revealed two multiplets δ=7.55 and 7.69 ppm in the aromatic region and a singlet δ=1.53 ppm in the phosphine region. Crystals were grown from the tan solid using methylene chloride and pentane. An X-ray crystal determination revealed the structure of fac-tris (trimethylphosphine)Iridium(III) trichloride.

F.) Reaction between (I) and Trimethylsilylacetylene (HES I 71)

A 25 mL flask equipped with a stir bar and a septum was charged with 77 mg (0.144 mmoles) of complex (**I**). (**I**) was dissolved in 20 mL of dry methylene chloride along with 28.3 mg (40.0 μL, 0.288 mmoles) of trimethylsilylacetylene (>2eq). The mixture was stirred and 50.4 mg (0.144 mmoles) of thallium hexafluorophosphate was added as a solid. This was allowed to react for 24 hours at room temperature. The TlCl was filtered out and the methylene chloride was removed under vacuum. Attempts to recrystallize in methylene chloride or chloroform with ether failed leaving a dark green-black oil. A crude ^1H NMR ($DCCl_3$): δ= -0.02, 0.04, 0.21, & 0.22 ppm (s, Me_3Si), δ=0.14-0.11 ppm (m, Me_3Si), δ=1.56-165 ppm (m, PMe_3), δ=5.56 ppm (d, J_{H-H}=3.02Hz, 1H, cis vinyl), δ=5.78 ppm (d, J_{H-H}=3.02Hz, 1H, cis vinyl), δ=7.1-7.3 ppm (m, phenyl).

G.) Reaction between (I) and Phenylacetylene (HES I 191)

A 10 mL flask equipped with a stir bar and septum was charged with (I) (100 mg, 0.187 mmol) under nitrogen in a dry box. The flask was connected to a double manifold (vacuum/nitrogen) Schlenk line. Dry methylene chloride (6 mL) and phenyl acetylene (42 μL, 0.374 mmol) were injected by syringe. The flask was chilled by dry ice and acetone. Thallium hexafluorophosphate (68.0 mg, 0.187 mmol) was then added as a solid against a counter-stream of nitrogen. This mixture was allowed to react overnight. The thallium chloride was quickly filtered off as the solution was transferred to a 50 mL flask. The solvent was removed under vacuum. A crude ^1H NMR ($DCCl_3$) displayed: δ=1.11 ppm (t, J_{P-H}=3.63Hz, 18H, trans PMe_3), δ=1.63 ppm (d, J_{P-H}=7.52 Hz, 9H, cis PMe_3), δ=5.40 & 5.75 ppm (br d, 1H each, vinyl), δ=6.5 ppm (m, 1H, vinyl), δ=6.85- 7.6 ppm (m, phenyl).

H.) Reaction between (I) and 2-Ethynylpyridine (HES I 209) (IX)

A 25 mL flask equipped with a stir bar and septum was charged with (I) (100 mg, 0,187 mmol) under nitrogen in a dry box. The flask was connected to a double manifold (vacuum/nitrogen Schlenk line. Dry methylene chloride (10 mL) and 2-ethynylpyridine (0.576 g, 5.59 mmol) were added by syringe. Thallium hexafluorophosphate (65.5 mg., 0.187 mmol) was added as a solid against a counter-stream of nitrogen and the mixture stirred for 24 hours. The dark purple solution was filtered to

remove the thallium chloride. The product was forced out of solution using toluene (10 mL) and then pentane (15 mL). This procedure was repeated twice. A yield of 133 mg (0.152 mmol, 81.0% based on (**I**)) of the bimetallacycle (**IX**). Analysis calculated for $C_{30}H_{42}F_6IrN_3P_4$: C-41.19, H-4.85. Found: C-39.86, H-4.76.

^1H NMR (CD_2Cl_2) displayed: δ=1.20 ppm (t, J_{P-H}=3.6 Hz, 18H, trans PMe_3), δ=1.83 ppm (d, J_{P-H}=7.4 Hz, 9H, cis PMe_3), δ=6.5 ppm (br s, 1H, vinyl), δ=8.8 ppm (m, 1H, metallacycle), δ=9.4 (m, 1H, metallacycle), δ=6.85 ppm (m, 1H, aromatic), δ=7.15 (m, 6H, aromatic), δ=7.67, 7.80, 8.18, 8.5 and 8.27 ppm (m, 5H, aromatic).

^{13}C NMR ($CDCl_3$) δ=199, 155, 149, 147, 140, 139, 137, 136, 128, 127, 123, 121, 120, 119.6, and 119.0 ppm. (s, aromatic), δ=18.3 ppm (d, J_{P-C}=114.28Hz, cis PMe_3), δ=15.3 ppm (t, J_{P-C}=78.74 Hz, trans PMe_3).

^{31}P NMR (CD_2Cl_2) δ=43.1 ppm (d, J=60.9 Hz, cis PMe_3), δ=60.5 ppm (t J=61.2 Hz, trans PMe_3).

Crystal color; Habit: Purple irregular prism. Crystal size (mm): 0.2x0.2x0.2. Crystal system: Triclinic. Space group: P-1. Unit Cell Dimensions: a=12.060(3) Å, b=12.512(3) Å, c=14.833(3) Å, α=87.25(2)°, β=73.21(2)°, γ=69.93(2)°. Volume: 2009.4(9) $Å^3$, Z=2 Formula weight=932.8. Density (Calc.): 1.542 Mg/m^3. Absorption Coefficient: 3.521 mm^{-1}. Single crystal X-ray diffraction data can be found in the appendix.

I.) Reaction between (I) and Methyl Propiolate (HES I 249)

A 10 mL flask equipped with a stir bar and septum was charged with (**I**) (100 mg, 0.187 mmol) under nitrogen in a dry box. The flask was

connected to a double manifold (vacuum/nitrogen) Schlenk line. Dry methylene chloride (8 mL) and methylpropiolate (31.5 mg, 0.375 mmol) were injected by syringe. Thallium hexafluorophosphate (65.5 mg, 0.178 mmol) was added as a solid against a counter-stream of nitrogen and the mixture was stirred overnight. The brown-yellow solution was filtered to remove thallium chloride as it was transferred via a cannula fitted with filter paper to a 50 mL flask. The solvent was removed leaving a brown oil behind. The oil was dissolved in methylene chloride (3 mL) and a brown by-product was forced out using pentane (8 mL). This yellow solution was filtered and the solvent was stripped under vacuum to give a dark yellow oil. The material was recrystallized using methylene chloride and ether.

The ^{1}H NMR (CD_2Cl_2) revealed: δ=1.31 ppm (t, J_{P-H}=3.32 Hz, 18H, trans PMe_3), δ=1.91 ppm (d, J_{P-H}=7.23 Hz, 9H, cis PMe_3), δ=3.79, 3.93, & 4.29 ppm (s, 3H each methylester), δ=6.1 ppm (br s, 1H, vinyl), δ=9.0 & 10.4 (m, 1H each, metallacycle).

^{31}P NMR (CD_2Cl_2) δ= -72.5 ppm (t,J=88.7Hz, trans PMe_3), δ= -45.18 ppm (d, J=86.1 Hz, cis PMe_3).

J.) Reaction between (I) and Tl[PF_6] (HES I 79) (X)

A 25 mL flask equipped with a stir bar and septum was charged with (I) (200 mg, 0.375 mmol) under nitrogen in a dry box. The flask was connected to a double manifold (vacuum/nitrogen) Schlenk line. Dry methylene chloride (20 mL) was injected by syringe. Thallium hexa-fluorophosphate (131.0 mg, 0.375 mmol) was added as a solid against a counter-stream of nitrogen and the mixture was stirred overnight. The

thallium chloride was removed using a cannula fitted with filter paper. The solvent was then removed under vacuum. The crude product was redissolved in methylene chloride (3 mL) and precipitated using pentane (10 mL). A yield of 165.0 mg (0.140 mmols, 74.8% based on (**I**)) of a white crystalline solid of mer-[μ-Cl-(Ir(PMe_3)$_3$(Ph)(H))$_2$]PF_6.
The ^{1}H NMR (CD_2Cl_2) displayed: δ=-28.2, and -23.8 ppm (br s, 2H, Ir-H), δ=1.26 ppm (br s, 36H, PMe_3), δ=1.62 ppm (br s, 18H, PMe_3), δ=6.6 - 8.3 ppm (m, 10H aromatic).
Crystal color; Habit: Clear rectangular prism. Crystal size (mm): 0.2x0.2x0.3. Crystal system: Monoclinic. Space group: $P2_1$. Unit Cell Dimensions: a=10.323(3) Å, b=19.337(5) Å, c=12.204(2) Å, β=110.090(10)^o. Volume: 2288.0(8) Å^3, Z=2 Formula weight=1177.5. Density (Calc.): 1.709 Mg/m^3. Absorption Coefficient: 6.133 mm^{-1}. Single crystal X-ray diffraction data can be found in the appendix.

K.) NMR tube reaction between (X) and 3,3-dimethyl-1-butyne

A screw-cap NMR tube was charged with (**X**) (10 mg, 8.5x10^{-6} mol) under nitrogen in a dry box. The NMR tube was connected to a double manifold (vacuum/nitrogen) Schlenk line via needle. CD_2Cl_2 (400 μL) and 3,3 dimethyl 1-butyne (3 μL) were injected by syringe. The mixture was allowed to react for ten minutes. The ^{1}H NMR (CD_2Cl_2) revealed resonances similar to (**VIII**): δ=0.52 ppm (br s, 9H, agostic Ir-$(CH_3)_3C$), δ=1.06 ppm (s, 9H, $(CH_3)_3C$), δ=1.50 ppm (t, J_{P-H}=3.45 Hz, 18H, trans PMe_3), δ=1.69 ppm (d, J_{P-H}=7.68 Hz, 9H, cis PMe_3), δ=5.90 ppm (d,J_{H-H}=15.19 Hz, 1H, trans vinylic), δ=6.14 ppm (d, J_{H-H}=15.72 Hz, 1H, trans

vinylic),.δ=6.22 ppm (br d, J_{P-H}=13.89 Hz, 1H, vinyl), δ=6.79-7.2 ppm (m, 5H, phenyl).

L.) Reaction between (I) and Pyridine (HES I 231) (XI)

A 25 mL flask equipped with a stir bar and septum was charged with (I) (100 mg, 0.187 mmol) under nitrogen in a dry box. The flask was connected to a double manifold (vacuum/nitrogen) Schlenk line. Dry methylene chloride (10 mL) and pyridine (14.8 mg,.187mmol) were injected by syringe. Thallium hexafluorophosphate (65.5 mg, 0.187 mmol) was added as a solid against a counter-stream of nitrogen and the mixture was stirred overnight. The thallium chloride was removed using a cannula fitted with filter paper. The solvent was then removed under vacuum. The crude product was redissolved in methylene chloride (3 mL) and precipitated using pentane (10 mL). A yield of 125.6 mg (0.174 mmols, 93% based on (I)) of a white crystalline solid of mer-[$(Me_3P)_3Ir(Ph)$-(H)(Py)]PF_6. Analysis calculated for $C_{20}H_{38}F_6IrNP_4$: C-33.24, H-5.31. Found: C-32.18, H-5.21. The ^1H NMR (CD_2Cl_2) displayed: δ=-23.8 ppm (q, J_{P-H}=15.3 Hz, 1H, Ir-H), δ=1.3ppm (t, J_{P-H}=3.52 Hz, 18H, trans PMe_3), δ=1.7 ppm (d, J_{P-H}=10.0 Hz, 9H, cis PMe_3), δ=9.8 and 8.2 ppm (br s 2H aromatic), δ=8.0, 7.5, and 7.3 ppm (br t, J=6.2 Hz, 3H, aromatic), δ=7.1 ppm (m, 4H, aromatic).

M.) NMR tube reaction between (XI) and 3,3-dimethyl-1-butyne

A screw-cap NMR tube was charged with (XI) (10 mg, 0.0187 mmol) under nitrogen in a dry box. The NMR tube was connected to a double

manifold (vacuum/nitrogen) Schlenk line via needle. CD_2Cl_2 (400 μL) and 3,3 dimethyl 1-butyne (3 μL) were injected by syringe. The mixture was allowed to react for ten minutes. The ^1H NMR (CD_2Cl_2) revealed resonances similar to (**VIII**): δ=0.52 ppm (br s, 9H, agostic Ir-$(CH_3)_3C$), δ=1.06 ppm (s, 9H, $(CH_3)_3C$), δ=1.50 ppm (t, J_{P-H}=3.45 Hz, 18H, trans PMe_3), δ=1.69 ppm (d, J_{P-H}=7.68 Hz, 9H, cis PMe_3), δ=5.90 ppm (d, J_{H-H}=15.19 Hz, 1H, trans vinylic), δ=6.14 ppm (d, J_{H-H}=15.72 Hz, 1H, trans vinylic),.δ=6.22 ppm (br d, J_{P-H}=13.89 Hz, 1H, vinyl), δ=6.79-7.2 ppm (m, 5H, phenyl).

Chapter 4: Reactivity of The Hydrido Iridium Pyridyl Complex

The mer-$(Me_3P)_3Ir(pyridyl)(H)Cl$ complex, **(III)**, contains an active nucleophilic site capable of coordination to a metal center or of attack on an acidic proton of an electrophilic species. It was of interest to compare the reactivity of **(I)** with the pyridyl complex **(III)** to determine if the nitrogen affects the reaction. At first, an attempt was made to dimerize this complex through the pyridyl ligand upon removal of the chloride ligand with $Tl[PF_6]$. A reaction between complex **(III)** and $Tl[PF_6]$ in methylene chloride was carried out at room temperture. This gave a fairly pure product in a yield of 85%, **(HES II 43)-(XII)**. The ^1H NMR spectrum of **(XII)** revealed resonances due to the common meridional phosphine arrangement as well as four multiplets between δ=7.4 and δ=8.3 ppm for the four aromatic protons. In the hydride region, the appearance of a quartet at δ=-22.4 was found to be quite odd, since the hydride of the starting material complex **(III)** was previously a pair of triplets at δ=-10.45 and δ=-11.02 ppm (Figure 4.1). A single crystal X-ray determination was carried out confirming the phosphine arrangement, (Figure 4.2). The pyridine ring and hexafluorophosphate was expected; however, a chloride ligand was not anticipated. Complex **(XII)** is an octahedral complex with an iridium(III) metal center possessing three phosphine ligands, a pyridine ring, a chloride ligand and a hydride with an electron count of 18; yet the PF_6^- anion remained (Figure 4.2). It was doubtful the metal center was an iridium(IV) complex. Although, there are known phosphine and hydride Ir(IV) complexes of $IrCl_4(PMe_2Ph)_2$[91], , and $Ir(H)_2(Cl)_2(P\textit{i}\text{-}Pr_3)_2$[92]. A protonated pyridine ring was possible.

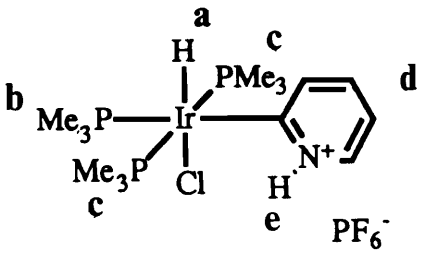

(XII)

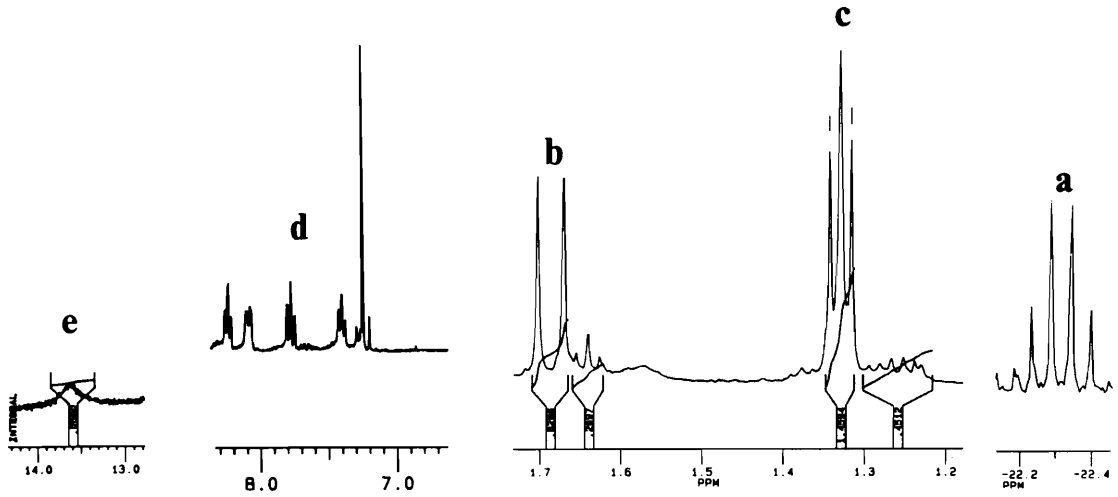

Figure 4.1 (270 MHz) ^1H NMR of mer-$[(Me_3P)_3Ir(C_6H_4NH^+)(H)]PF_6$, **(XII).**

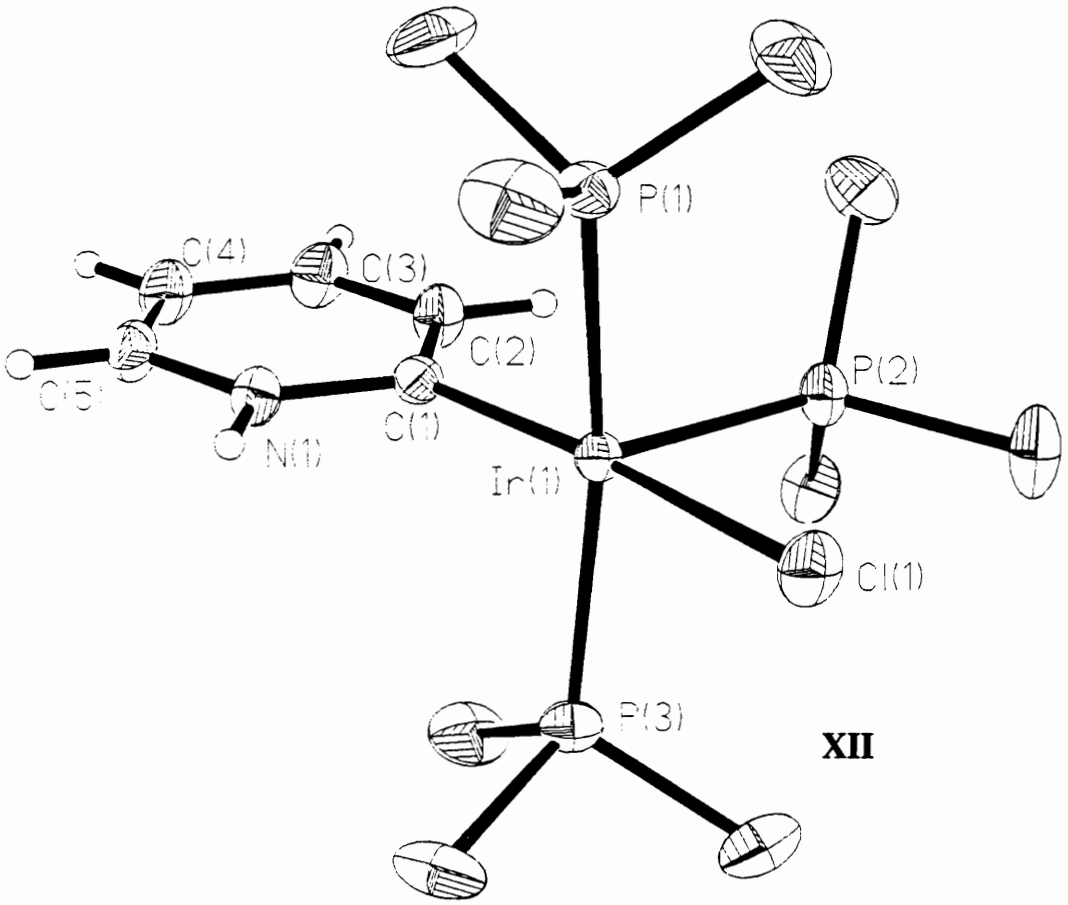

Figure 4.2 ORTEP of mer-[$(Me_3P)_3Ir(C_6H_4NH^+)(H)$]$PF_6$, (**XII**).

The protonated pyridine ring was verified by a reexamination of the ^1H NMR spectrum and it displayed a broad resonance signal at δ= 14.0 ppm for a $C_6H_4NH^+$ proton.

Since one equivalent of TlCl was obtained from the above reaction, the chloride remaining on the isolated complex must have come from the CH_2Cl_2 solvent. Van Beek[93] had observed an intact I_2 molecule attached to the PtI(Me_2-NCN) complex forming the PtI(Me_2-NCN)(η^1-I_2) complex; where, the I-I bond length has increased from 2.78 angstroms for free I_2 to 2.822(1) angstroms thus increasing the activation of the halogen. Crabtree et al[94] observed alkyl or aryl halocarbons of RX (X=Cl, Br or I) to displace the solvent ligand of Me_2CO in cis, trans-[$IrH_2(Me_2CO)_2$-$(PPh_3)_2$]BF_4 to form the corresponding complex cis, trans-[$IrH_2(L)_2$-$(PPh_3)_2$]BF_4 where L=RX. Apparently, the open coordination site was filled by a molecule of methylene chloride through the chloride atom. With the CH_2Cl_2 attached to the iridium, the pyridine ring is now in close proximity and able to remove the acidic proton from the bound CH_2Cl_2, (Scheme 4.1). The reaction process may have produced a reactive carbene molecule on a molar basis. Attempts to trap the carbene have failed. In one case, a reaction between (**III**), 2 equivalence of 1,2,3,4,5,6,7,8-octahydronaphthalene, and Tl[PF_6] in methylene chloride gave the newly rearranged complex (**XII**) in a yield of 63%. One equivalent of the thallium chloride was recovered. The product (**XII**) was forced out of solution and rinsed with pentane. (**XII**) was then dried and weighed. The desired product was believed to be soluble in the methylene chloride/ pentane solution. The solvent was removed under vacuum to produce a very light yellow oil. The ^1H NMR spectrum of the yellow oil turned out to be fairly pure 1,2,3,4,5,6,7,8-octahydronaphthalene. Two equivalence

of the 1,2,3,4,5,6,7,8-octahydronaphthalene weighing 101.45 mg was used in the reaction; but, 55.4 mg of the 1,2,3,4,5,6,7,8-octahydronaphthalene was recovered. The other equivalent of 1,2,3,4,5,6,7,8-octahydronaphthalene that was lost may have trapped the carbene.

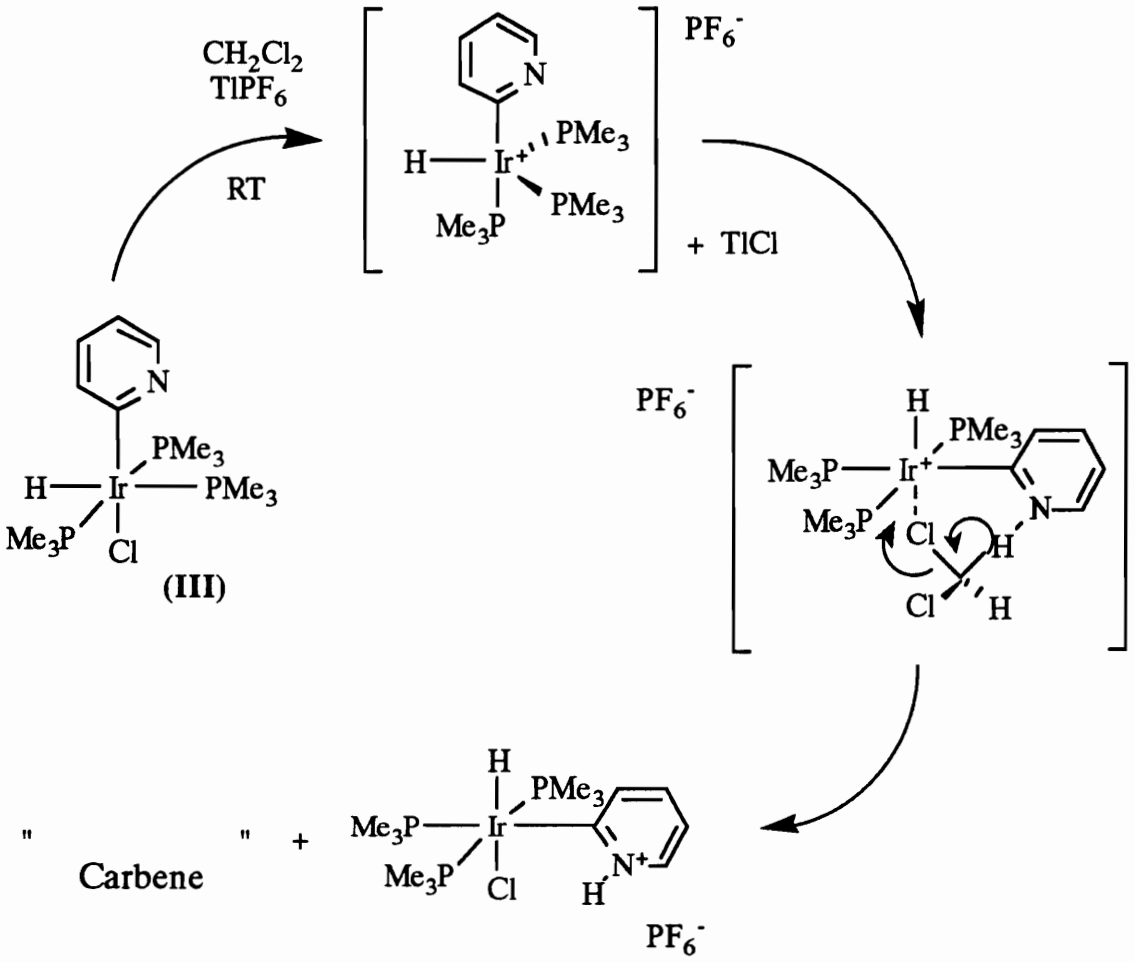

Scheme 4.1

A second experiment using benzylchloride and cyclooctene again produced the pyridinium complex (**XII**). Methylene chloride was replaced by benzylchloride with the expectation that upon attack of the pyridine in (**III**) the resulting carbene maybe stabilized via the phenyl ring. This would form a cyclopropyl group that could be easily identified by ^1H

NMR. After complex (**XII**) and TlCl was removed, the remaining solution was vacuum distilled very carefully. The first two fractions collected were benzylchloride and cyclooctene. The ^1H NMR spectrum of the remaining distillate indicated a number of products. Resonances for the expected cyclopropyl group were not visible; however, the products appear to be that of a Friedel-Crafts reaction to produce $C_6H_5CH_2C_6H_4CH_2Cl$. A triplet at δ=3.35 ppm, two doublets at δ=3.47 and 3.71 ppm, and a broad singlet at δ=3.98 ppm were found along with another broad singlet at δ=4.55 ppm, a doublet at δ=5.21 ppm, and several multiplets in the aromatic region between δ= 7.1-7.4 ppm (see possible mechanism Scheme 4.2). The electrophilic iridium complex attacks the chloride atom of a molecule of benzychloride. This will create a positive charge on the CH_2 group. A pair of electrons are donated from the aromatic ring of a second molecule of benzychloride. The pyridyl group from the iridium complex can remove the acidic proton from this ring and regain it's aromatic character to produce $C_6H_5CH_2C_6H_4CH_2Cl$. This maybe the case for benzylchloride as the solvent but it does not rule out the formation of a carbene when the solvent was strictly methylene chloride in the initial formation of (**XII**).

Another attempt was made to dimerize complex (**III**) using tetrahydrofuran as solvent instead of methylene chloride. However, the reaction failed to give the desired complex. The ^1H NMR spectrum of the product displayed resonance for a hydride at δ=-22.0 ppm, a set of multiplets for the phosphines but very weak proton resonance signals for the aromatic region. 3,3-Dimethyl-1-butyne was injected into the NMR tube containing the mixture,and a white precipitate of TlCl formed immediately. A similar reaction was seen with the chloro-bridged iridium

dimer which gave the 1,4-di-t-butyldienyl complex (**VIII**) and a precipitate of TlCl when the alkyne was added. In this case, several unidentifiable products were formed.

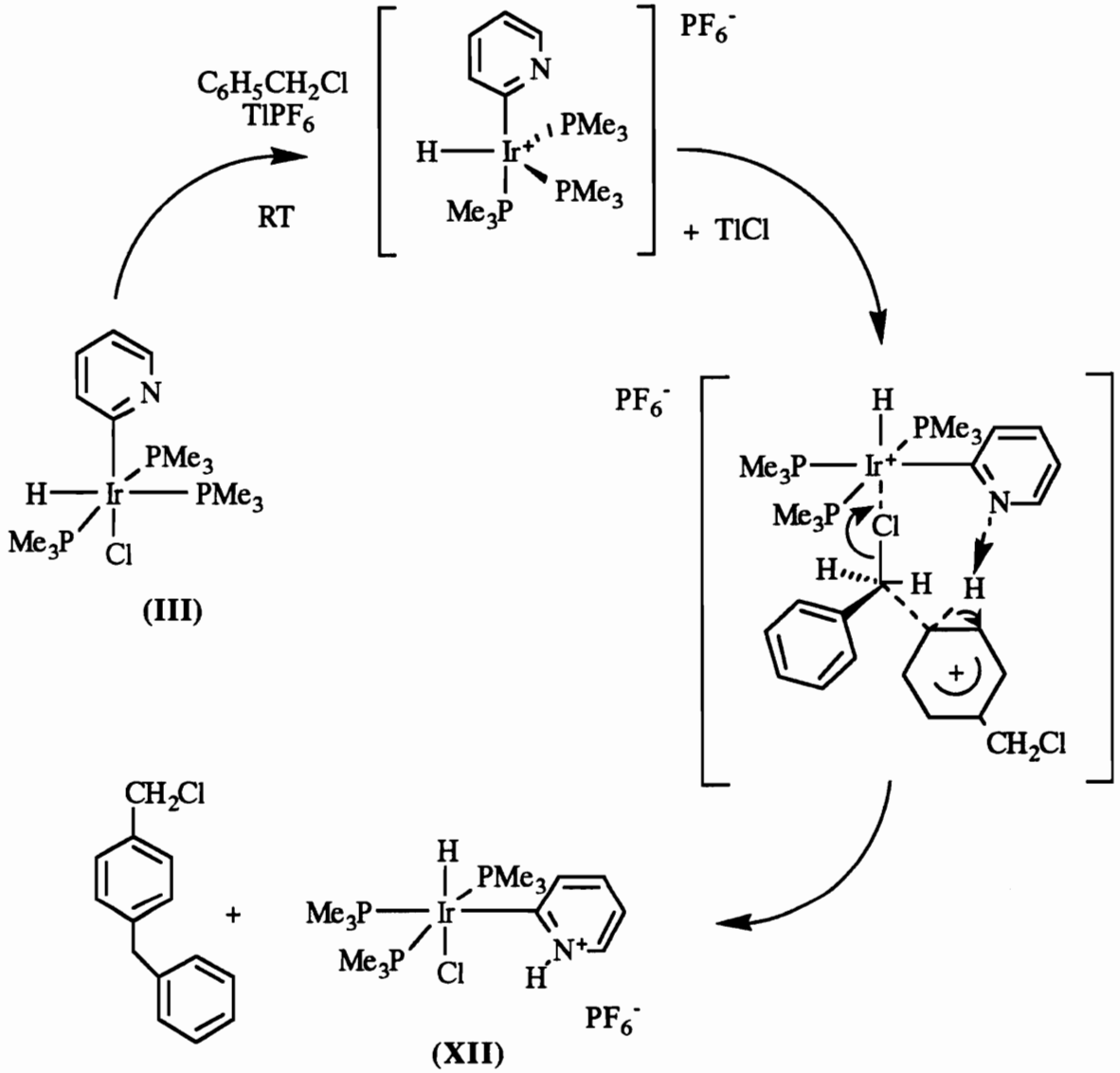

(**III**)

(**XII**)

Scheme 4.2

With this active nucleophilic site, it was of interest to examine the reaction between (**III**) and 3,3-dimethyl-1-butyne. There are two possible pathways that the reaction could follow. The hydride could migrate unto the alkyne to first form a vinyl complex as seen in the mechanism for the formation of the 1,4-di-t-butyldienyl complex (**VIII**). The second

possibility would be a nucleophilic attack on the alkyne forming a new intermediate. This intermediate can alter the course of the reaction. **(III)** reacts with excess 3,3-dimethyl-1-butyne and Tl[PF_6] in methylene chloride at room temperature to form a new product. The ^1H NMR spectrum of this product displayed a doublet and triplet for the meridional phosphine ligands with two singlets at δ=1.24 and δ=1.20 ppm for t-butyl groups. In the aromatic region, four multiplets were found for the protons of the pyridine ligand with a very broad singlet at δ= 14.0 ppm indicating a NH^+ proton (Figure 4.3). Single x-ray crystal determination provided the structure, **(HES II 33)-(XIII)** (Figure 4.4). The pyridine ligand was found in the plane of the phosphine ligands and two t-butylacetylide ligands are on an axis trans to each other. An interesting oil was obtained after the product was filtered and the solvent was removed. The ^1H NMR spectrum of the oil displayed proton resonance signals in the vinyl and in the alkyl region, similar to 2,2,7,7-tetramethyl-5-octen-3-yne, the t-butylacetylene "dimer". On standing for 24 hours, a small quantity of an oil (2-3μL) separated from the d-chloroform solution. This oil was dissolved in d_6-benzene and the observed ^1H NMR spectrum revealed a quintet at δ= 5.45 ppm and four singlets in the alkyl region at δ=0.25, 1.07, 1.18, and δ=1.23 ppm. After a period of time, the same NMR tube was observed again but the spectum had changed. The "dimer" was now visible and the resonance signals had shifted at δ=0.28, 1.08 ppm for the alkyl region and δ= 5.5 ppm in the vinyl region. The oil maybe a mixture of 2,2,7,7-tetramethyl-5-octen-3-yne and a by-product of 5,5-dimethyl-2-t-butyl-1-hexen-3-yne[89]. It is important to note that, the reaction between **(III)** and 3,3-dimethyl-1-butyne was performed about the same time the attempts were made to

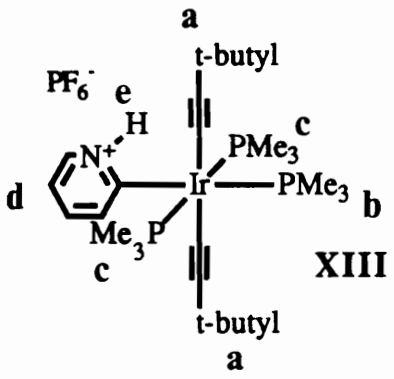

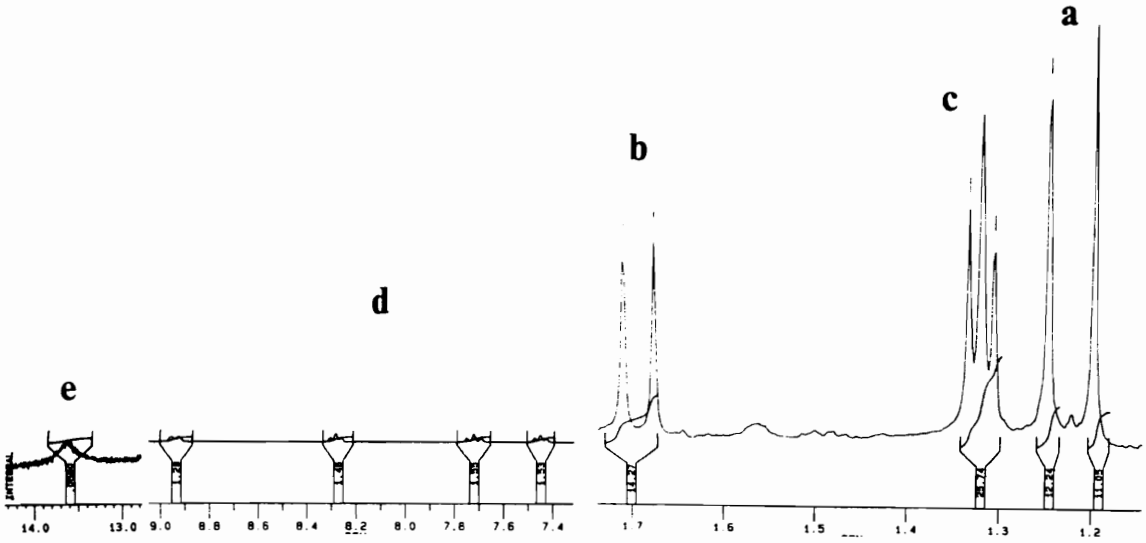

Figure 4.3 (270 MHz) ^{1}H NMR of the di-acetylide complex **(XIII)**.

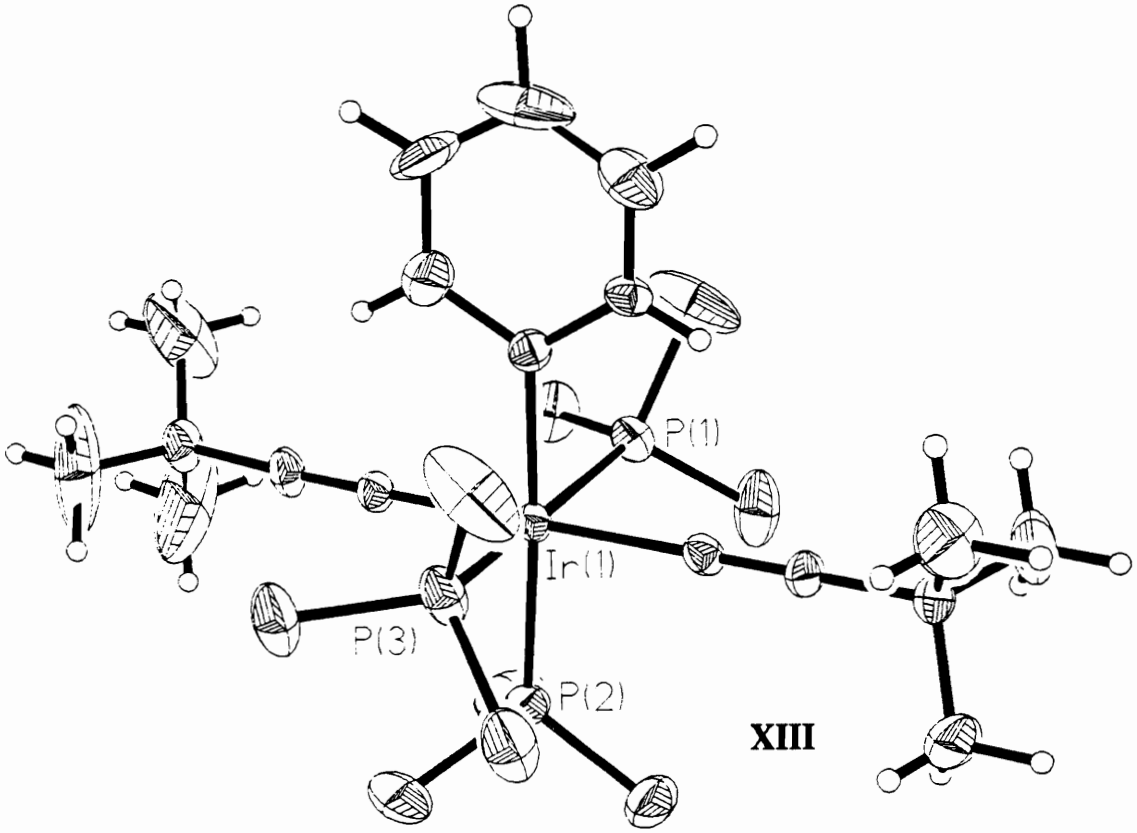

XIII

Figure 4.4 ORTEP of the di-acetylide complex (**XIII**).

dimerize (**III**); therefore, it was not known that (**III**) had reacted with methylene chloride. Thus, the reaction between (**III**) and 3,3-dimethyl-1-butyne was repeated using tetrahydrofuran to afford the same complex as (**XIII**), without residual oils.

These results suggest the pyridyl ligand with the nucleophilic site was able to influence the course of the reaction. One possible pathway may involve the initial attack of the nitrogen onto the alkyne forming (**A**). The loss of diatomic hydrogen from a hydride migration to the acidic proton would allow the nitrogen to regain the lone pair of electrons and would allow a second alkyne to enter and rearrange to a vinylidene (**B**). This proton could be removed by the pyridyl group to form (**XIII**), (Scheme 4.3).

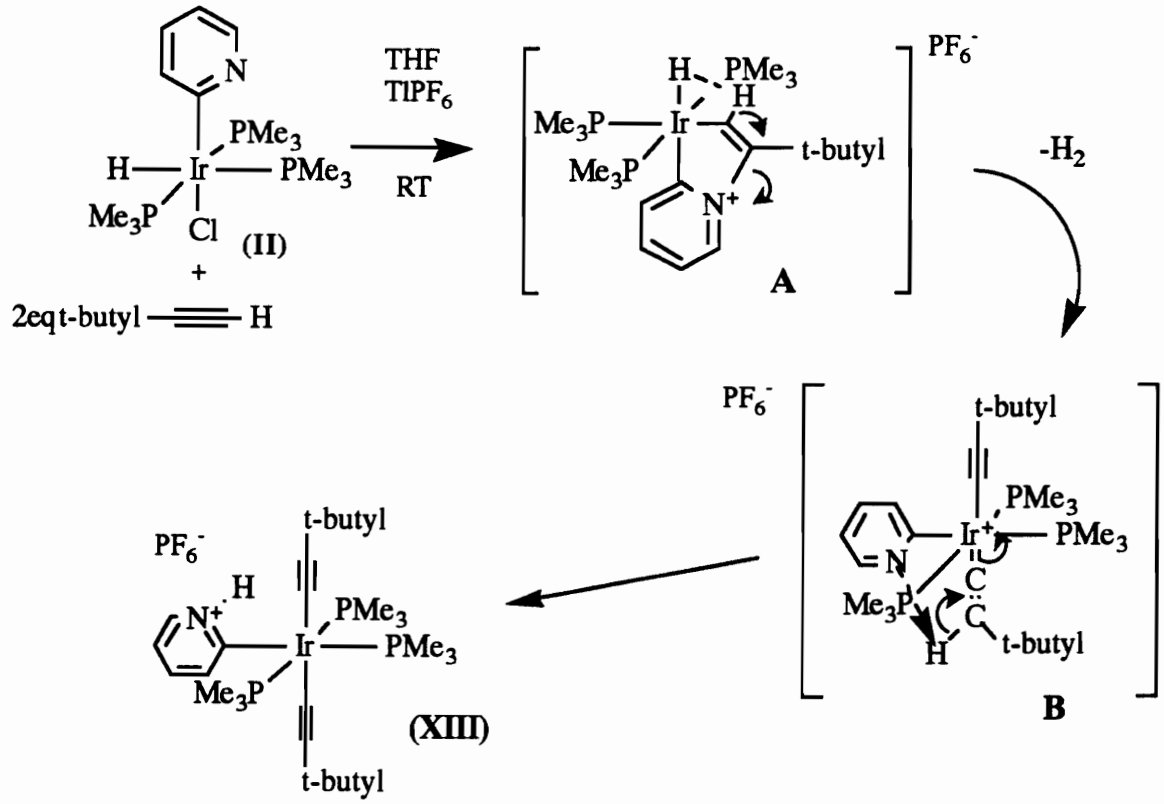

Scheme 4.3

The mechanism for this reaction is very complicated when methylene chloride was used which produced an oily byproduct since **(III)** was found to react with CH_2Cl_2. If tetrahydrofuran was used, only the product **(XIII)** was observed without residual oils.

The reaction between complex **(III)** and phenylacetylene failed to produce an identifiable product; however, a reaction between **(III)** and 2-butyne produced a methylallyl complex like that of **(VII)** (see Figure 4.5). The reactivity of **(III)** was just as interesting when compared to the phenyl complex **(I)**. Complex **(XII)** and the di-acetylide complex **(XIII)** are quite different products due to the involvement of the pyridyl ligand. As for future work in this area, a detailed study of the mechanisms may provide a better understanding of this complex **(III)**. Based on this knowledge, a number of reactions between **(III)** and certain alkynes have yet to be performed, such as internal alkynes.

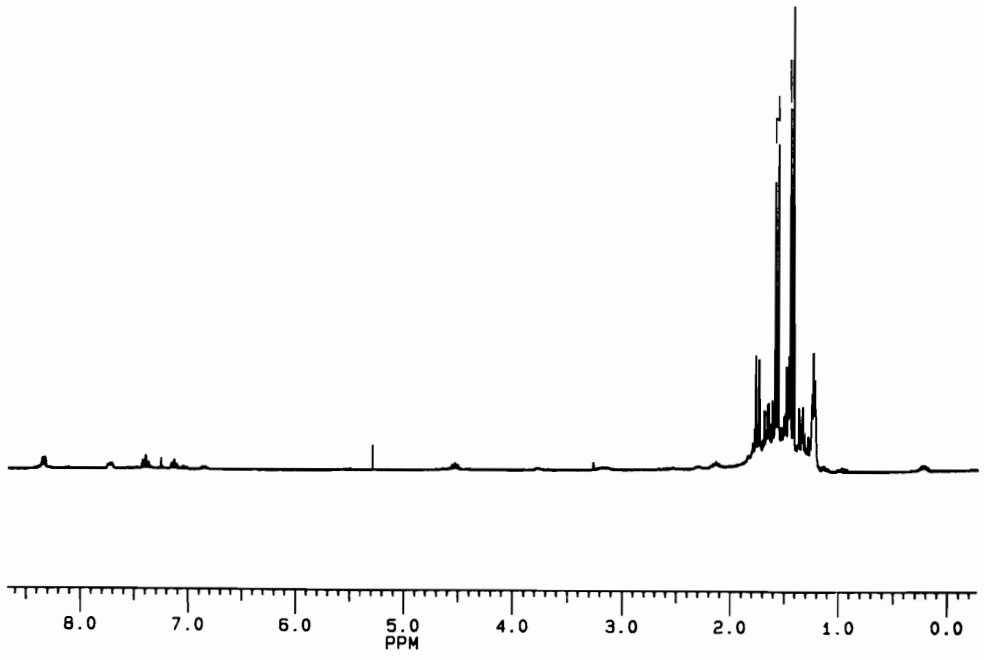

Figure 4.5 (270 MHz) ^1H NMR of the reaction between **(III)** and 2-butyne.

Experimental Section

General Comments can be found in Chapter 2:

Synthesis of mer $[(Me_3P)_3Ir(H)(C_6H_4NH)Cl]PF_6$ (HES II 43) (XII)

A 10 mL flask with a stir bar and septum was charged with **(III)** (100 mg, 0.176 mmols) under nitrogen in a dry box. The flask was connected to the nitrogen line on a double manifold (vacuum/nitrogen) Schlenk line. Dry methylene chloride (5 mL) was injected and thallium hexafluorophosphate (65.5 mg) was added. The reaction was stirred for 36 hrs. The thallium chloride was filtered off carefully and the solvent was removed from the filtrate under vacuum. The material was dissolved in methylene chloride (3 mL) and precipitated with ethyl ether (15 mL). The product was collected to yield 108 mg of an off white solid (0.159 mmol, 85% based on **(III)**) of mer $[(Me_3P)_3Ir(H)(C_6H_4NH)Cl]PF_6$. C, H elemental analysis calculated for $C_{14}H_{33}ClF_6IrNP_4$: C-24.60, H-4.80. Found: C-23.91, H-4.71.

^1H NMR (CD_2Cl_2): δ= -22.23 ppm (q, J_{P-H}=35.59 Hz, 1H, Ir-H), δ=1.34 ppm (pseudo-q, J_{P-H}=3.11 Hz, 18H, trans PMe_3), δ=1.70 ppm (d, J_{P-H}=8.8 Hz, 9H, cis PMe_3), δ=7.40, 8.23 ppm (br t, J_{P-H}=5.4 Hz, 1H each, aromatic), δ=7.78 ppm (br t, J_{P-H}=2.7 Hz, 1H , aromatic), δ=8.08 ppm (br d, J_{P-H}=10.8 Hz, 1H , aromatic), δ=13.6 ppm (br s, 1H, NH^+).

^{13}C NMR (CD_2Cl_2): δ=17.34 ppm (t, J_{P-C}=77.70 Hz,trans PMe_3), δ=19.69 ppm (d, J_{P-C}=133.36 Hz, cis PMe_3), δ=120.81, 139.96, 140.47, & 146.80 ppm (s, aromatic).

^{31}P NMR (CD_2Cl_2): δ= -50.27 ppm (t, J=64.48 Hz,trans PMe_3), δ= -40.50 ppm (d, J=64.62 Hz, cis PMe_3).

A.) Crystal color; Habit: Clear flat plate. Crystal size (mm): 0.4x0.4x0.2. Crystal system: Monoclinic. Space group: C2/c. Unit Cell Dimensions: a=22.943(6) Å, b=19.457(5) Å, c=13.292(3) Å, β=121.35(2)°. Volume: 5068(2) $Å^3$, Z=8 Formula weight=679.9. Density (Calc.): 1.782 Mg/m^3. Absorption Coefficient: 5.649 mm^{-1}. Single crystal X-ray diffraction data can be found in the appendix.

B.) Crystal color; Habit: Clear amber rectangular prism. Crystal size (mm): 0.4x0.4x0.5. Crystal system: Monoclinic. Space group: $P2_1/c$. Unit Cell Dimensions: a=9.876(2) Å, b=15.327(3) Å, c=16.427(3) Å, β=97.58(2)°. Volume: 2464.8(8) $Å^3$, Z=4 Formula weight=679.9. Density (Calc.): 1.832 Mg/m^3. Absorption Coefficient: 5.807 mm^{-1}. Single crystal X-ray diffraction data can be found in the appendix.

Synthesis of mer $[(Me_3P)_3Ir(C{:}CC(Me)_3)_2(C_6H_4NH)]PF_6$ (HES II 27 & 33) (XIII)

A 10 mL flask with a stir bar and septum was charged with **(III)** (200 mg, 0.374 mmol) under nitrogen in a dry box. The flask was connected to the nitrogen line. Dry methylene chloride (5 mL) and t-butylacetylene 578 µl (20 x's, 7.48 mmol) were injected by syringe. Thallium hexafluorophosphate (0.131 g, 0.374 mmol) was added to the solution and stirred for 48 hrs. The thallium chloride was filtered and rinsed with pentane(5 mL). The solvent was removed to leave an oily solid behind. The solid was redissolved in methylene chloride (5 mL) and a layer of pentane (15 mL) was placed over the solution and left overnight. The solution was filtered

leaving a crystalline solid behind which was collected to yield 189 mg (0.234 mmol, 63% based on (**III**)) of mer-[$(Me_3P)_3Ir(C{\equiv}CC(Me_3))_2$-$(C_6H_4NH)$]$PF_6$. The solution was slowly evaporated under vacuum which yielded an oil. The ^1H NMR of the oil was found to be 2,2,7,7,-tetramethyl-3-octen-5-yne. The crude ^1H NMR ($DCCl_3$) displayed resonances at: δ=1.1 ppm (s, 18H, t-butyl), δ=5.67 ppm (d, J_{H-H}=15.12 Hz, 1H, trans vinyl), δ=5.97 ppm (d, J_{H-H}=16.23 Hz, 1H, trans vinyl).

A second procedure involved the use of tetrahydrofuran as the solvent. A 10 mL flask with a stir bar and septum was charged with (**III**) (75.0 mg, 0.140 mmol) under nitrogen in a dry box. The flask was connected to the nitrogen line. Dry tetrahydrofuran (5 mL) and t-butylacetylene 23 μL (20 x's, 2.80 mmol) were injected by syringe. Thallium hexafluoro-phosphate (49.0 mg,0.140 mmol) was added to the solution and stirred for 48hrs. The thallium chloride was filtered and rinsed with pentane(5 mL). The solvent was removed leaving an oily solid behind. This was redis-solved in tetrahydrofuran (1-2 mL) and was reprecipitated using pentane (5 mL). Analysis calculated for $C_{26}H_{50}F_6IrNP_4$: C-38.70, H-6.30. Found: C-37.76, H-6.02.

^1H NMR (CD_2Cl_2): δ= 1.20, & 1.24 ppm (s, 9H each, t-butyl), δ=1.32 ppm (t,J_{P-H}=3.59 Hz, 18H, trans PMe_3), δ=1.69 ppm (d, J_{P-H}=9.14 Hz, 9H, cis PMe_3), δ=7.45, 7.71 ppm (br t, J_{P-H}=8.1Hz, 1H each, aromatic),δ=8.80 ppm (br t, J_{P-H}=2.7 Hz, 1H , aromatic),δ=8.92 ppm (br, d, J_{P-H}=10.8 Hz, 1H , aromatic), δ=13.8 ppm (br s, 1H, NH^+).

^{13}C NMR (CD_2Cl_2): δ=15.3 ppm (t, J_{P-C}=82.00 Hz,trans PMe_3), δ=17.45 ppm (d, J_{P-C}=140.00 Hz, cis PMe_3), δ=32.93, & 33.18 ppm (s, t-butyl), δ=122.04, 141.07, 141.77, & 141.80 ppm (s, aromatic).

^{31}P NMR (CD_2Cl_2): δ= -143.69 ppm (m, J_{P-F}=1,761.0 Hz, PF_6^-), δ= -56.00 ppm (t, J=63.1 Hz,trans PMe_3), δ= -49.70 ppm (d, J=61.9 Hz, cis PMe_3).

Crystal color; Habit: Clear irregular prism. Crystal size (mm): 0.3x0.3x0.4. Crystal system: Monoclinic. Space group: $P2_1/c$. Unit Cell Dimensions: a=9.847(3) Å, b=18.284(8) Å, c=19.849(3) Å, β=92.96(3)^0. Volume: 3569(2) $Å^3$, Z=4 Formula weight=806.8. Density (Calc.): 1.501 Mg/m^3. Absorption Coefficient: 3.949 mm^{-1}. Single crystal X-ray diffraction data can be found in the appendix.

A.) Reaction of (III), 1,2,3,4,5,6,7,8-Octahydronapthalene, and Tl[PF_6] in Methylene chloride (HES II 67)

A 10 mL flask equipped with a stir bar and septum was charged with **(III)** (200 mg, 0.374 mmol) under nitrogen in a dry box. The flask was connected to the nitrogen line. Methylene chloride (3 mL) and 1,2,3,4,5,6,7,8-octahydronaphthalene (111 μL, 0.748 mmol) were injected by syringe. Thallium hexafluorophosphate (0.156 g, 0.447mmol) was added and the reaction mixture was stirred for two days. The thallium chloride was filtered off and recovered (0.107 g, 0.446 mmol). The solvent was removed under vacuum and the material was then redissolved in methylene chloride (5 mL). Pentane (15 mL) was used to precipitate the product. The precipitate was identical to **(XII)**, yielding 0.161 g (0.236 mmol, based on **(III)**). The remaining methylene chloride pentane solution was stripped under vacuum leaving an oil behind. The ^1H NMR spectrum was identical to that of 1,2,3,4,5,6,7,8-octahydronaphthalene with a recovered weight of 0.554 g (0.407 mmol).

^{1}H NMR ($CDCl_3$): δ=1.55, & 1.82 ppm (br s, 8H each, CH_2).

B.) Reaction of (III), Cyclooctene, and Tl[PF_6] in Benzyl chloride (HES II 125)

A 10 mL flask equipped with a stir bar and septum was charged with **(III)** (100mg, 0.187 mmol) under nitrogen in a dry box. The flask was connected to the nitrogen line. Benzyl chloride (5 mL) and cyclooctene (61μL , 0.468 mmol) were injected by syringe. Thallium hexafluorophosphate (66.5 mg, 0.187 mmol) was added as a solid and the mixture was stirred for 2 days. The thallium chloride was filtered and rinsed with pentane (10 mL). Additional pentane (15 mL) was added to precipitate out the iridium complex. The complex was filtered and dried under vacuum. The ^{1}H NMR spectrum of this product was identical to that of **(XII)**. The benzyl chloride/pentane solution was distilled by distillation under vacuum. The receiving flask was placed in a dry ice/acetone solution. Most of the solvent was removed and found to be benzyl chloride and cyclooctene. The ^{1}H NMR spectrum of the remaining crude oil ($CDCl_3$) displayed multiple signals between δ=1.1 and 1.3 ppm with several singlets between δ=1.45 and 1.60 in the alkyl region. A triplet at δ=3.35 ppm, two doublets at δ=3.47 and 3.71 ppm, and a broad singlet at δ=3.98 ppm were found along with another broad singlet at δ=4.55 ppm, a doublet at δ=5.21 ppm, and several multiplets in the aromatic region between δ= 7.1-7.4 ppm. These signals are believed to be alkylation products of mostly benzyl chloride and some of cyclooctene. A singlet at δ=4.58 ppm represents unreacted benzyl chloride.

C.) Reaction between (III) and Phenylacetylene (HES II 71)

A 10 mL flask with a stir bar and septum was charged with (**III**) (200 mg, 0.374 mmol) under nitrogen in a dry box. The flask was connected to the nitrogen line on a double manifold (vacuum/nitrogen) Schlenk line. Dry tetrahydrofuran (5 mL) and phenylacetylene (823.0 μL, 0.764 g, 20 x's) were injected by syringe. Thallium hexafluorophosphate (0.131 g, 0.374 mmol) was added and the reaction mixture was stirred overnight. The thallium chloride was filtered and rinsed with additional tetra-hydrofuran (5 mL). The solvent was removed from the filterate under vacuum. The crude material was redissolved using tetrahydrofuran (3 mL) and a black solid(0.219 g) was precipitated from the solution using ethyl ether (15 mL). The black solid was rinsed with pentane (5 mL) and this solution was added to the ether filtrate. The solvent was then removed from the dfilterate under vacuum leaving 32.6 mg of an oil behind. The ^1H NMR of the solid ($CDCl_3$) displayed: δ=1.50 ppm (t, J_{P-H}=3.75 Hz, 18H, trans PMe_3) δ=1.63 ppm (d, J_{P-H}=5.61 Hz, 9H, cis PMe_3), δ=7.0-7.6 ppm (m, aromatic). The ^1H NMR of the oil ($CDCl_3$) revealed: δ=5.9, 6.4, 6.7, & 7.0 ppm (d, vinyl), and between δ=7.2 and 7.5 ppm (m, aromatic).

D.) Reaction between (III) and 2-Butyne (HES II 79)

A 10 mL flask with a stir bar and septum was charged with (**III**) (100 mg, 0.187 mmol) under nitrogen in a dry box. The flask was connected to the nitrogen line. Dry methylene chloride (6 mL) and 2-butyne (29.0 μL, 0.202 g, 20x's) were injected by syringe. Thallium hexafluorophosphate

(0.0657 g, 0.187 mmol) was added as a solid and the reaction mixture stirred for 24 hr. The thallium chloride was filtered and rinsed with methylene chloride (3 mL). Ethyl ether (15 mL) was added to this solution which produced a tarry solid; therefore, the solvent was removed by vacuum.

^{1}H NMR (CD_2Cl_2): δ= 1.43 ppm (d, J_{P-H}=8.04 Hz, 18H, PMe_3), δ= 1.57 ppm (d, J_{P-H}=7.48 Hz, 9H, PMe_3) δ= 1.47 ppm (d, J=8.1 Hz, 3H, allyl methyl), δ=0.15, & 2.1 ppm (m, 1H each, CH_2 allyl), δ=3.15 ppm (m, 1H, CH allyl), δ=4.51 ppm (m, 1H, C**H** methylallyl), δ=7.12, & 7.39 ppm (t, J_{P-H}=5.4 Hz, 1H, aromatic), δ=7.72 ppm (m, 1H, aromatic), δ=8.33 ppm (t, J_{P-H}=8.1 Hz, 1H, aromatic).

Chapter 5: Reactivity of the Hydrido Iridium Furanyl Complex

After observing the spectacular differences between the reactivity of (I) and (III) with unsaturated hydrocarbons, it was of interest to investigate the reactivity of other heteroaromatic compounds and how could they influence the reaction chemistry. In this Chapter, the unusual chemistry of the furanyl iridium hydride complex (**IV**) is described, chemistry which is quite different from that of the pyridyl complex (**III**) or of the phenyl complex (**I**). The mer-$(Me_3P)_3Ir(Furanyl)(H)Cl$ complex (**IV**) and excess 3,3-dimethyl-1-butyne react in methylene chloride at room temperature for 24 hours to produce a metallo-vinyl complex (**XIV**). A relatively clean product was formed as shown by a crude ^1H NMR spectrum. Analytically pure product (54% yield) can be obtained by recrystallization using methylene chloride and pentane. The ^1H NMR spectrum of the product displayed the common doublet and triplet at δ=1.73 and δ=1.56 ppm found for meridional phosphine ligands. A broad singlet at δ=0.64 ppm appeared to indicate a t-butyl group in an agostic interaction with iridium Three proton resonance signals were found for the furanyl group at δ=6.11 and δ=7.29 ppm (doublets), a pair of doublets at δ=6.28 ppm and a pair of triplets around δ=6.69 ppm for the vinyl proton. The most interesting resonance signal was in the hydride region where a quartet at δ= -29.42 ppm was found (Figure 5.1). At first, the structure was thought to be formed by the alkyne inserting into the Ir-furan bond with the oxygen atom from the furanyl group, filling the sixth coordination site. However, this was not consistent with the presence of an agostic interaction. A single X-ray crystal determination was carried out confirming the furan insertion and the agostic interaction (Figure 5.2).

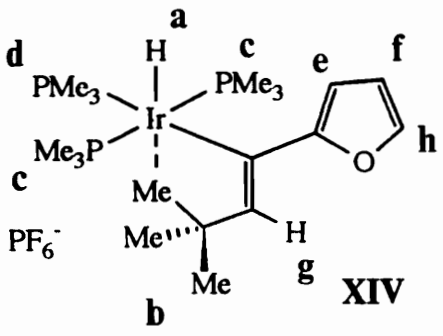

XIV

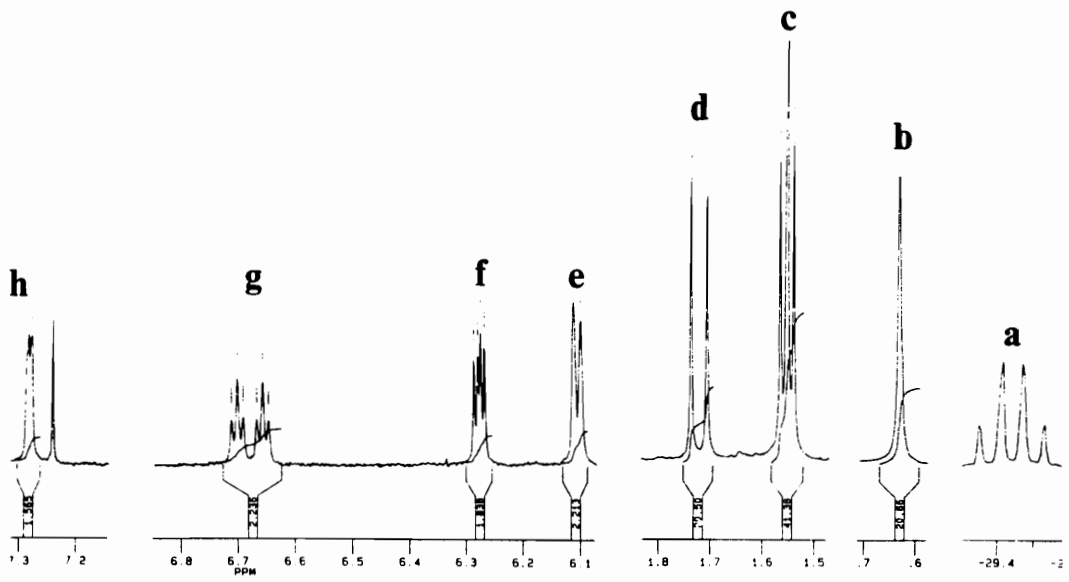

Figure 5.1 (270 MHz) ^{1}H NMR of the metallo-vinyl complex (**XIV**).

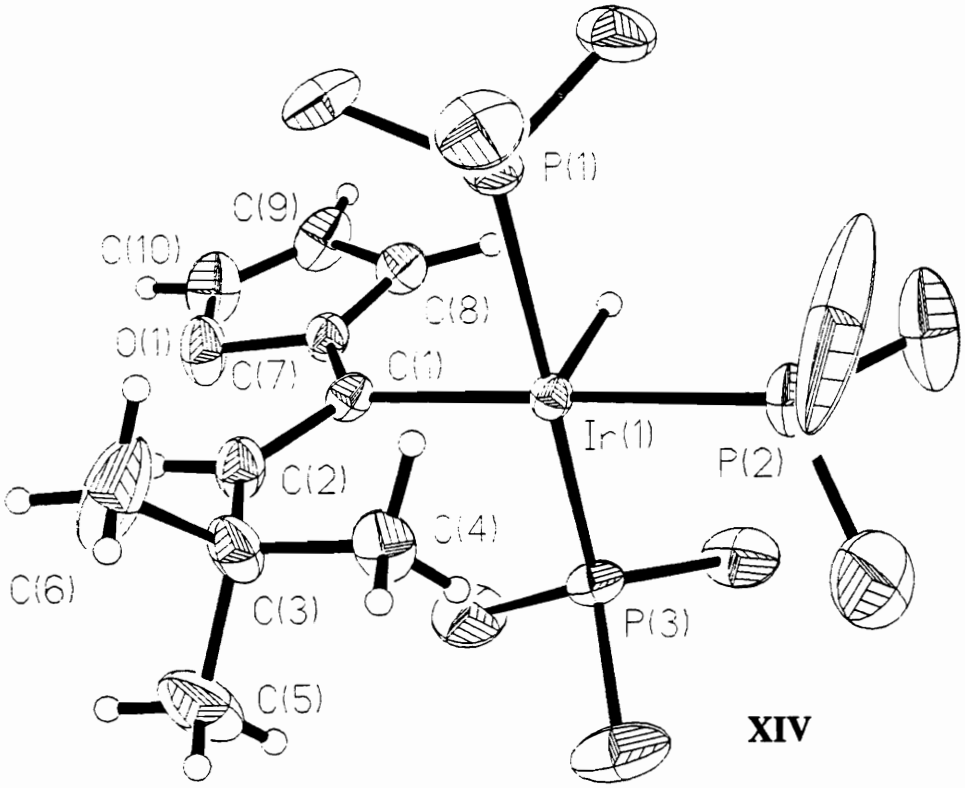

XIV

Figure 5.2 ORTEP of the metallo-vinyl complex (**XIV**)

A low temperature NMR study was carried out to find further evidence for the agostic interaction. When the complex was cooled to -90° C two peaks appeared at δ=1.03 and δ= -0.12 ppm in a 2:1 ratio. Upon warming, the two signals collapsed giving the observed broad singlet (Figure 5.3).

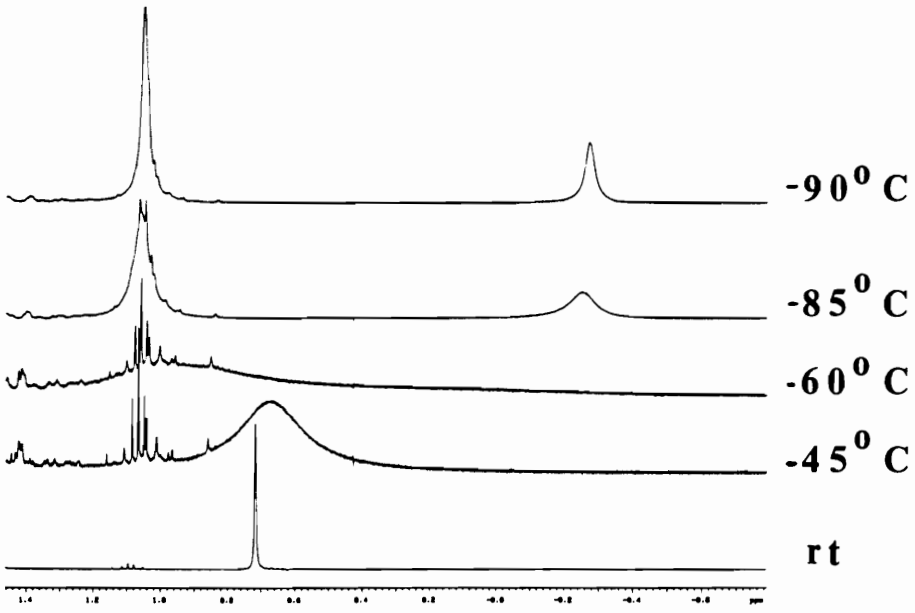

Figure 5.3 Low temperature (400 MHz) ^{1}H NMR of the agostic interaction.

It is believed that the oxygen atom in the furan ring is responsible for the difference in the reactivity between (**IV**) and t-butylacetylene when compared with that of the phenyl complex (**I**). Once the chloride ligand is removed by Tl^+, the oxygen atom can donate a pair of electrons to the iridium metal center forming a metal to carbon double bond and the postive charge located on the oxygen atom (**A**) (see Scheme 5.1). This will lock the iridium complex into a five coordinate structure which will influence how the alkyne adds: The structure (**A**) will allow the alkyne to coordinate and will allow the oxygen atom to regain the electron pair. The alkyne can rearrange into a vinylidene but in this case it is trans to the

hydride; therefore, a migratory-insertion of the cis furanyl group takes place (**B**) (see Scheme 5.1).

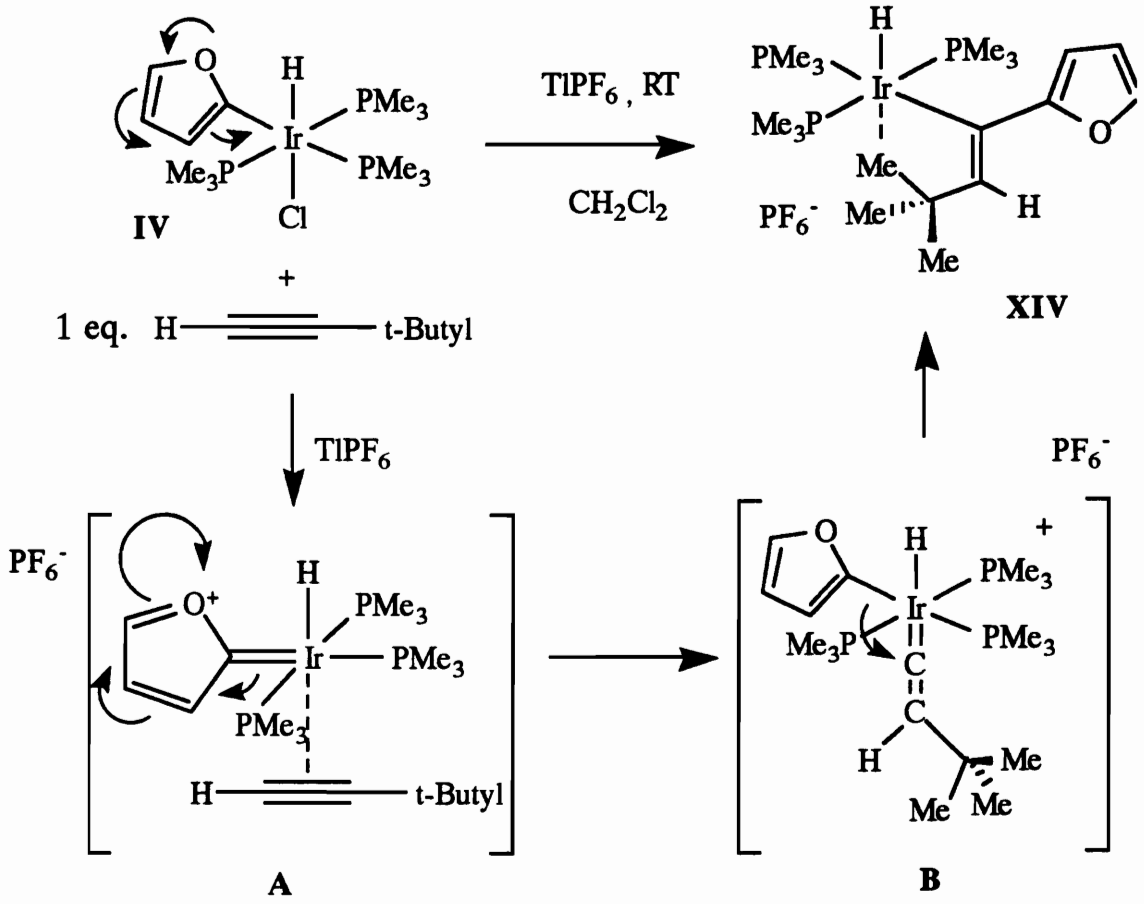

Scheme 5.1

To gather support for the proposed mechanism, a deuterium labeling experiment was performed. Complex (**IV**) was allowed to react with excess deuterium labeled 3,3-dimethyl-1-butyne (t-butylC≡CD) and Tl[PF_6] in methylene chloride. The ^1H NMR spectrum of the product displayed all the corresponding resonance signals with the exception of that for the vinylic proton. The pair of triplets at δ=6.69 ppm are no longer visible (**D**) (Figure 5.4).

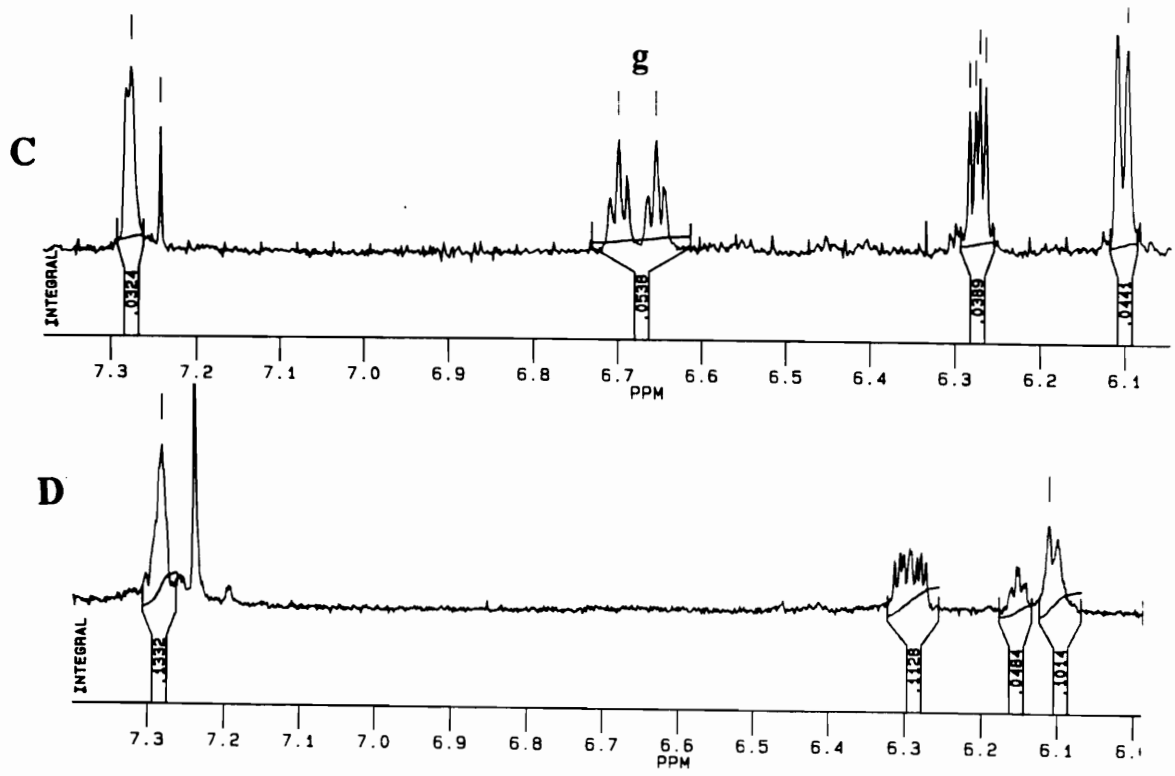

Figure 5.4 (270 MHz) ^{1}H NMR of the vinyl region of (**XIV**) of experiments (**C**) vs (**D**).

Attempts to capture the square pyramid complex failed. When (**IV**) was allowed to react with Tl[PF_6] in either methylene chloride or tetrahydrofuran a number of new products were formed as indicated by multiple hydride resonance signals in the ^{1}H NMR. In either case, t-butylacetylene was added to these reaction, but the metallo-vinyl complex (**XIV**) never formed. The results from both solvents were fairly similar suggesting that the complex may have irreversibly rearranged or decomposed. Nevertheless, complex (**XIV**) should reductively eliminate the organic fragment quite readily if not spontaneously. Previous work by Milstein[95] suggest that reductive elimination can only occur if an octahedral complex is able to lose a ligand by dissociation and reach a five

coordinate geometry. It would seem that the sixth coordintion site filled by a weak agostic interaction could induce reductive elimination, being free to dissociate rather easily. One possibility for the complex to remain stable at room temperature is the inherent geometry and rigidity of the t-butyl-vinyl group. Reductive elimination can be induced by raising the temperature of the metallo-vinyl complex to 80° C in toluene for 24 hrs. Upon work-up and purification by column chromatography, a light brown oil was produced. The ^{1}H NMR spectrum of trans-1-(2-furyl)-3,3-dimethyl-1-butene diplayed a pair of doublets at δ=6.16 & 6.57 ppm (J_{H-H}=16.45 Hz) for the vinylic protons. Three protons of the furyl group were found at δ=6.25 ppm (J_{H-H}=3.08 Hz), & δ=7.42 ppm (J_{H-H}=4.12 Hz) as doublets and the third at δ=6.32 ppm (J_{H-H}=2.95 Hz) as a triplet. The t-butyl group was found as a singlet at δ=1.23 ppm. As for the fate of the metal center, the stucture is unknown. However, there are visible signs of possibly two hydrido-iridium complexes that may have formed with toluene. The ^{1}H NMR spectrum of this crude material displayed a quartet at δ= -12.5 and -13.0 ppm. Hexafluorophosphate, a poor coordinating ligand, was the counter anion and thus the complex most likely decomposed. Although the reaction is not a continous catalytic cyclic, it is a step closer in the right direction toward developing a functionalized catalyst (see Scheme 5.2).

Reaction between (**IV**) and phenylacetylene failed to produce a clean product. The crude material gave a very complicated ^{1}H NMR spectrum in the aromatic and phosphine region.

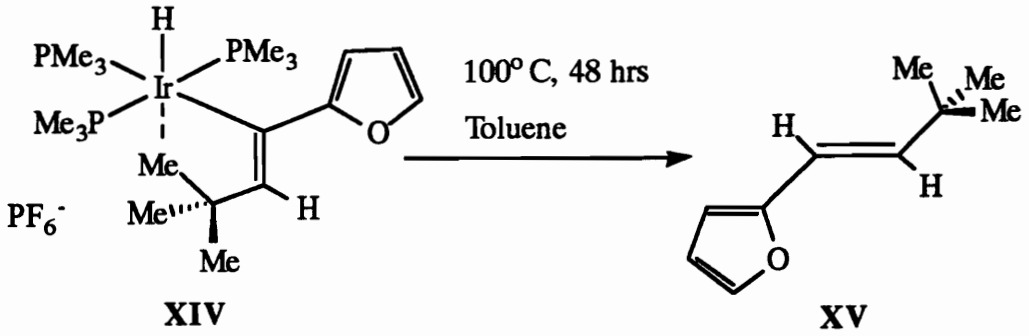

XIV XV

Scheme 5.2

When trimethylsilylacetylene was allowed to react with (**IV**), the ^{1}H NMR spectrum of the crude material revealed two, possibly three products. After purification, the predominant product appears to have a facial arrangement for the phosphine ligands at δ=1.9, 1.6, and1.2 ppm, with two similar singlets at δ=0.12, & 0.22 ppm and a third at δ= -.03 ppm for $SiMe_3$ groups. Resonances for the furanyl group and the hydride were no longer observed (Figure 5.5) Trimethylsilylacetylene may have reacted in a similar fashion as t-butyl-acetylene; however, the trimethylsilyl group could not "stabilize" the product and reductive elimination followed. Figure 5.5 suggests at least three molecules of trimethylsilylacetylene may have rearranged in some fashion around the
metal center.

The reactivity of the furanyl complex proved to be quite interesting. The stabilization of the metal center by the oxygen atom in the furanyl ligand provided the necessary means for insertion of an unsaturate into the Ir-C bond. Thus, the formation of the metallo-vinyl complex was possible. As for the reaction between the furyl complex (**IV**) and trimethylsilyl-acetylene, the structure should be identified to see if a similar mechanism was followed.

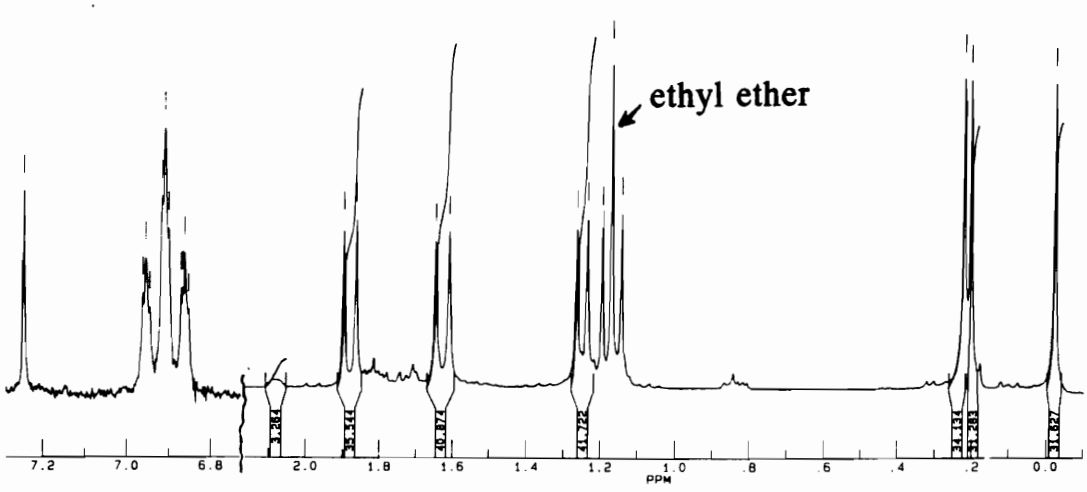

Figure 5.5 (270 MHz) ^{1}H NMR of the reaction between (IV) and trimethylsilylacetylene.

Experimental Section

General Comments can be found in Chapter 2:

Synthesis of the mer-[$(Me_3P)_3Ir(C_{10}H_{13}O)(H)]PF_6$ (HES II 83) (XIV)

A 25 mL flask equipped with a stir bar and a septum was charged with (**IV**) (200 mg, 0.382 mmol) under nitrogen in a dry box. The flask was connected to the nitrogen side of the Schlenk line. Dry methlylene chloride (10 mL) and 3,3-dimethyl-1-butyne (0.47 mL, 4.0mmol, 10 x's) was injected by syringe. Thallium hexafluorophosphate (0.133 g, 0.382 mmol) was added and the mixture was stirred overnight. The thallium chloride was filtered via a cannula fitted with filter paper. Ethyl ether (15 mL) was used to precipitate a snow white product. The product was filtered and rinsed twice with ethyl ether (5 mL) to yield 160 mg (0.224 mmol, 58.6% yield based on (**IV**)) of mer [$(Me_3P)_3Ir(C_{10}H_{13}O)(H)][PF_6]$. C, H elemental analysis calculated for $C_{19}H_{41}F_6IrOP_4$: C-31.5%; H-5.7%. Found: C-31.74%, H-5.71%.

^1H NMR ($CDCl_3$): δ= -29.42 ppm (q, J_{P-H}=16.28 Hz, 1H, Ir-H), δ=0.64 ppm (s, 9H, agostic t-butyl), 1.56 ppm (t, J_{P-H}=3.40 Hz, 18H, trans PMe_3), δ=1.73 ppm (d, J_{P-H}=8.30.0 Hz, 9H, cis PMe_3), δ=6.11 ppm (d, J_{H-H}=3.14 Hz, 1H, furyl),.δ=6.28 ppm (d d, J_{H-H}=1.88 & 3.18 Hz, 1H, furyl),.δ=6.69 ppm (d t, J_{P-H}=12.0 Hz, trans PMe_3, J_{P-H}=2.58 Hz, cis PMe_3, 1H, vinyl),.δ=7.29 ppm (d, J_{H-H}=1.24 Hz, 1H, furyl).

^{13}C NMR (Unity 400, d_6-acetone): δ=18.30 ppm (t, J_{P-C}=78.8 Hz, trans PMe_3), δ=20.75 ppm (d, J_{P-C}=124.4 Hz, cis PMe_3), δ=24.28 ppm (s,

agostic t-butyl), δ=40.3 ppm (br d, J_{P-C}=21.2 Hz, α-carbon vinyl), δ=109.1 ppm (s, β-carbon vinyl), δ=111.9 &141.7 ppm (s, furyl), δ=142.9 ppm (t, J=16.8 Hz, furyl), δ=163.63 ppm (d, J=24.4 Hz, β-carbon furyl).

^{31}P NMR ($CDCl_3$, external standard): δ= -138.4 ppm (m, J=1,748.2 Hz, PF_6), δ= -40.85 ppm (t, J=46.22 Hz, trans PMe_3), δ= -32.17 ppm (d, J=45.88 Hz, cis PMe_3).
Crystal color; Habit: Pale yellow rectangular prism. Crystal size (mm): 0.3x0.3x0.5. Crystal system: Monoclinic. Space group: $P2_1/c$. Unit Cell Dimensions: a=8.974(2) Å, b=17.610(5) Å, c=19.888(5) Å, $\beta=91.56(2)^0$. Volume: 3141.9(13) $Å^3$, Z=4 Formula weight=715.6. Density (Calc.): 1.513 Mg/m^3. Absorption Coefficient: 4.497 mm^{-1}. Single crystal X-ray diffraction data can be found in the appendix.

A.) Reaction Between (IV) and Labeled 3,3-Dimethyl-1-butyne (HES II 135)

The deuterium derivative of 3,3-dimethyl-1-butyne was prepared by charging a 25mL flask with dry tetrahydrofuran (15 mL), and 3,3-dimethyl-1-butyne (115.4 μL) under nitrogen and chilled by a dry ice/ acetone mixture. Butyllithium (380 μL) was slowly injected by syringe and the mixture was allowed to warm to room temperature. Deuterium oxide(16.1 μL, 1eq) was injected by syringe and allowed to react for 30 minutes. This mixture was distilled by simple distillation and the first fraction was collected (10 mL). A 50 mL flask equipped with stir bar and septum was charged with (**IV**) (88 mg, 0.162 mmol) under nitrogen in a dry box. The flask was connected to the nitrogen side of the Schlenk line.

Dry tetrahydrofuran (10 ml) and the first fraction collected (10 ml) was injected by syringe. Thallium hexafluorophosphate 156.7 mg (0.162 mmol) was added and the mixture was stirred overnight. The thallium chloride was filtered off and the solvent was removed under vacuum to yield the product.

^{1}H NMR ($CDCl_3$): δ= -29.45 ppm (q, J_{P-H}=15.42 Hz, 1H, Ir-H), δ=0.64 ppm (s, 9H, agostic t-butyl), 1.56 ppm (t, J_{P-H}=3.49 Hz, 18H, trans PMe_3), δ=1.73 ppm (d, J_{P-H}=8.25 Hz, 9H, cis PMe_3), δ=6.11 ppm (d, J_{H-H}=3.15 Hz, 1H, furyl),.δ=6.28 ppm (m, 1H, furyl),.δ=6.69 ppm (pair of triplets are no longer observed due to deuterium incorporation),.δ=7.28 ppm (s, 1H, furyl).

B.) Reductive elimination of (XIV) (HES II 133) (XV)

A thick wall reaction tube equipped with a stir bar and septum was charged with (**XIV**) (172 mg, 0.240 mmol) under nitrogen in a dry box. The reaction tube was connected to the nitrogen line by a needle (flowing nitrogen) and dry toluene (15 mL) was injected by syringe. The septum was replaced by a teflon cap fitted with an O-ring. The mixture was shaken and placed in an oil bath at 100° C for 48 hrs. Once cooled, the teflon cap was replaced by a septum containing a needle (flowing nitrogen) and a cannula fitted with filter paper. The solution was filtered, transferred via the cannula to a 50 mL flask, and washed twice with dry methylene chloride (10 mL). The solution was collected and was distilled by simple distillation under vacuum. The first fraction (toluene) was collected by a immersed in a dry ice/acetone mixture. The crude product was found to be in the distillation flask. A column made up of neutral

silica gel (50 mL) in ethyl ether was prepared. The dark brown solution was placed on the column and eluted consecutively with 100 mL aliquots of ether, chloro-form, and acetone. The fractions were combined and evaporated yielding a brown product. Another column made up of fluorosil (50 mL) in hexane was prepared. The product was dissolved in methylene chloride (5 mL) and placed on the column. This was eluted with 100 mL aliquots of hexane, ether , chloroform, and acetone. The fractions of chloroform and acetone were found to contain the product. The product was identified as trans-1-(2-furyl)-3,3-dimethyl-1-butene based on ^1H NMR spectral analysis.

^1H NMR. ($CDCl_3$): δ=1.23 ppm (s, 9H, t-butyl), δ=6.16 & 6.57 ppm (pair of doublets, J_{H-H}=16.45 Hz, 1H each, trans vinyl),.δ=6.25 ppm (d, J_{H-H}=3.08 Hz, 1H, furyl), δ=6.32 ppm (t, J_{H-H}=2.95 Hz, 1H, furyl), δ=7.42 ppm (d, J_{H-H}=4.12 Hz, 1H, furyl).

C.) Reaction Between (IV) and Trimethylsilylacetylene (HES II 161)

A 25 mL flask equipped with a stir bar and septum was charged with (**Iv**) (100 mg, 0.191 mmol) under nitrogen in a dry box. The flask was connected to the nitrogen side of the Schlenk Line. Dry methylene chloride (10 mL) and 3,3-dimethyl-1-butyne (0.27 mL, 1.91 mmol, 10 x's) were injected by syringe. Thallium hexafluorophosphate (66.67 mg, 0.191 mmol) was added as a solid and the reaction mixture was stirred overnight. The thallium chloride was filtered out via a cannula fitted with filter paper. Ethyl ether (15 mL) was used to precipitate a black oily product. The product was redissolved in methylene chloride and the slow addition of

ethyl ether precipitated an off white product. The product was filtered and rinse twice using ethyl ether (5mL). The ^{1}H NMR (CD_2Cl_2) displayed: δ= -.03, 0.12, & 0.22 ppm (s, 9H each, Me_3Si), δ=1.24, 1.62, & 1.88 ppm (d, J_{P-H}=7.79, 10.12, & 9.28 Hz, 9H each, cis PMe_3), δ=2.09 ppm (m, 1H),.δ=6.90 ppm (br t, J=12.40 Hz, 1H, vinyl).
^{13}C NMR ($CDCl_3$): δ= -0.35, 0.73, &1.20 ppm (s, Me_3Si), δ=15.99, 19.18, & 21.60 ppm (d, J_{P-C}=117.58, 163.88, & 138.88 Hz, cis PMe_3), δ=25.52, 67.90, 99.56 ppm (s), δ=41.32, 56.49, 84.74, & 149.36 ppm (d, J_{P-C}=27.28, 137.22, 143.36, & 19.6 Hz), δ=157.58 & 155.81 ppm (t, J_{P-C}=476.28 Hz, trans PMe_3, J_{P-C}=28.2 Hz, cis PMe_3).

Chapter 6: Conclusion

The work that was performed in this dissertation was to develop aromatic C-H addition products of hydrido-iridium complexes and investigate the reactivity of these products via insertion of unsaturates for the possibility of developing an active catalyst. Since, only a few reports have shown the functionalization of aryl hydrido metal complexes with unsaturates. In this dissertation the C-H oxidative of several aromatic compounds by $[Ir(COD)(PMe_3)_3]Cl$ were synthesized as well as the C-S bond cleavage of thiophene and benzothiophene, the first step in hydrodesulfurization. Monosubstituted aromatic compounds react with the $[Ir(COD)\text{-}(PMe_3)_3]Cl$ complex rather poorly due to steric crowding about the metal center. Therefore, heterocyclic aromatics such as pyridine, furan, and thiophene were investigated and they were found to react with the $[Ir(COD)(PMe_3)_3]Cl$ complex in fair yields.

Aromatic compounds were found to add across the metal center in two particular orientations. The most common orientation that was found to occur had the hydride on the axis, trans to the chloride ligand. The second orientation had the hydride in the plane with the meridional phosphine ligands. This second arrangement is believed to occur by the initial coordination of the heteroatom followed by addition which provided the regiostereo selective control.

The functionalization of the hydrido-iridium complexes **(I)**, **(III)**, and **(IV)** are non reactive towards unsaturates even in polar solvents. However, these complexes can be made to react with unsaturates upon the removal of the chloride ligand with the aid of thallium hexafluoro-phosphate through an open coordination site. Attempts were made to

replace the chloride ligand via dimerization of (**I**) or direct replacement using pyridine had limited success. The chloro-bridged dimer (**X**) was too unstable and was contaminated with residual Tl[PF_6]. Several ^{1}H NMR experiments were carried out to induce the dissociation of the chloride ligand by using polar protic and aprotic solvents and elevated temperatures. The phenyl (**I**) and furanyl (**IV**) complex were used in the presence of 3,3-dimethyl-1-butyne; however, both complexes decompose before alkyne insertion could be observed.

Complex (**I**) was found to react with 2 equivalence of 3,3-dimethyl-1-butyne to afford the dienyl complex (**VIII**). The mechanism involved the coordination of the alkyne after chloride removal by Tl^+, followed by the hydride migration to form a reactive vinyl complex. Coordination of a second alkyne that rearranged into a vinylidene was followed by a migratory insertion of the vinyl group to form (**VIII**). Instead of a double insertion product, (**III**) was found to react with 2 equivalence of 3,3-dimethyl-1-butyne to form a diacetylide complex (**XIII**). In the case of (**IV**), one equivalent of 3,3-dimethyl-1-butyne was found to insert into the furyl group forming (**XIV**). The mechanism was found to involve the stabilization of the intermediate through the furanyl group allowing the alkyne to coordinate and rearrange into a vinylidene, due to the geometric constraints a migratory-insertion of the furanyl group was found to occur forming (**XIV**). Figure 6.1 shows the different results of the three complexes (**I**), (**III**), and (**IV**) that combine with 3,3-dimethyl-1-butyne. However, both (**I**) and (**III**) were found to react in a similar fashion with 2-butyne to form methyl allyl complexes (**VII**) and reaction (**D**) in Chapter 4. It was also shown that the non-productive elimination of

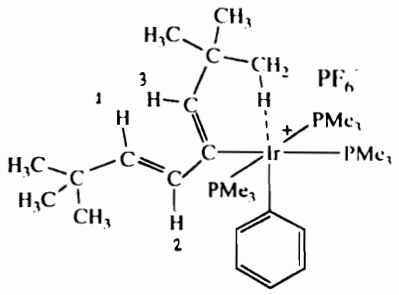

VIII

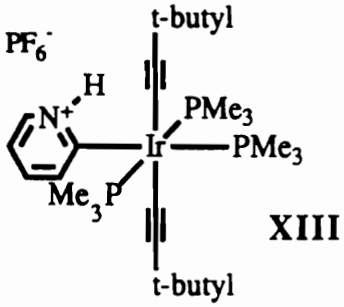

XIII

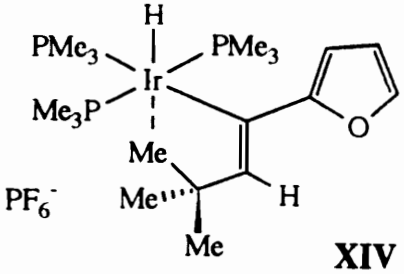

XIV

Figure 6.1 Complexes of **(VIII)**, **(XIII)**, & **(XIV)**.

benzene occurs when (**I**) was found to react with 2-ethynylpyridine to form (**IX**). From this a few conclusions could be drawn. First, the phenyl complex (**I**) appears to be dependent on the alkyne; where, (**III**) was able to alter the course of the reaction by the removal of acidic protons via the nitrogen lone pair. As for the furanyl complex (**IV**), the oxygen lone pair of the furanyl ligand provided the means for alkyne insertion between the Ir-C bond of the furan group.

As for future work in this area, other heavy metal salts which contain better coordinating counter ions than Tl[PF_6] should be investigated to "capture" the iridium complex, such as silver benzoate. However, the resonance structure found in (**IV**) is the most important feature of this work and it should be thoroughly investigated to reproduce a structure that would be capable of a similar resonance structure. While most insertions occur between the M-H bond, the resonance structure found in (**IV**) provides the necessary means for insertion of unsaturates to occur between the M-C bond, leaving the M-H bond intact. A possible complex would be the C-H addition of anisole (ortho or para position) unto a metal center and it in turn may react in a similar fashion like (**IV**). However, the "resonance stability" would be limited to these complexes. If a tripodal ligand containing a heteroatom that is capable of reacting in a similar fashion like that of (**IV**), it may provide the necessary means of selective insertion of unsaturates between the M-C bond of either aryl or alkyl-metal complexes. An example of this ligand would be p-methoxy-terpyridine. Aromatic C-H addition to the iridium(I) complex containing this ligand would be the first step. The addition product can then be made to react with unsaturated hydrocarbons to produce a complex similar to (**XIV**) or

eliminate the organic fragment altogether. If these two steps could be accomplished it would provide a new tool for synthetic chemists.

The mechanism of the reaction between (**III**) and halogen solvents should also be studied in greater detail, especially the affect of the nitrogen lone pair as well as a number of unsaturated hydrocarbons that could be investigated. Allylacetylene and 4,4-dimethyl-1-pentyne are two alkynes that should be studied for possible reactivity with (**I**) and (**IV**) for possible oligomerization. Finally, analagous rhodium complexes should also be investigated which may even avoid some of the difficulties found with the sluggish iridium compounds.

References

(1) Gilman, H. *Organic Chemistry An Advanced Treatise* ; Wiley & Sons, Inc.: London, England, 2nd ed, *vol.I*, 1943, pp. 495.

(2) Gilman, H. *Organic Chemistry An Advanced, Treatise* ; Wiley & Sons, Inc.: London, England, 2nd ed, *vol.I*, 1943, pp. 553.

(3) Vaska, L.; *Acc. Chem. Res.* **1968**, 1, 335.

(4) Dieck, H. A.; Heck, R. F. *J. Organomet. Chem.* **1975**, 93, 259.

(5) Sonogashira, K.; Tohda, Y.; Hagihara, N. *Tetrahedron Lett.* **1975**, 4467.

(6) Farkas, A.; Farkas, L. *Trans, Faraday Soc.* **1937**, 33, 827.

(7) Kliman, J. P.; Dubeck, M. *J. Am. Chem. Soc.* **1963**, 85, 1544.

(8) Chatt, J.; Davidson, J. M. *J. Chem. Soc.* **1965**, 843.

(9) Bennett, M. A.; Milner, D. L. *J. Am. Chem. Soc.* **1969**, 91, 163.

(10) Parshall, G. W. *Acc. Chem. Res.* **1970**, 3, 139.

(11) (a) Cheney, A. J. and Shaw, B. L. *J. Chem. Soc., Dalton Trans* **1972**, 754. (b) Ibid; **1972**, 860. (c) Gill, D. F.; Mann, B. E., and Shaw, B. L. *J. Chem. Soc., Dalton Trans.* **1973**, 270. (d) Gill, D. F.; Shaw, B. L. *J. Chem. Soc., Chem. Commun.* **1972**, 65. (e) Shaw, B. L.; Stainbank, R. E. *J. Chem. Soc., Dalton Trans.* **1973**, 2394.

(12) (a) Gill, D. F.; Mann, B. E; Shaw, B. L. *J. Chem. Soc., Dalton Trans.* **1973**, 270. (b) Gill, D. G.; Shaw, B. L. *J. Chem. Soc. Chem. Commun.* **1972**, 65.

(13) Page, M. I. *Chem. Soc. Rev.* **1973**, 2, 295.

(14) Kirby, A. L. *J. Adv. Phys. Org. Chem.* **1980**, 17, 183.

(15) Castelhano, A. L.; Griller, D. J. *J. Am. Chem. Soc.* **1982**, 104, 3655.

(16) Jones, W. D.; Feher, J. F. *Acc. Chem. Res.* **1989**, 22, 91.

(17) Janowicz, A. H; Bergman, R. G. *J. Am. Chem. Soc.* **1982**, 104, 4240.

(18) Seiwell, L. P. *J. Am. Chem. Soc.* **1974**, 96, 7134.

(19) Crabtree, R.H. *Chem. Rev.*, **1985**,84(4), 245.

(20) Halpem, J. J. *Inorg. Chim. Acta.* **1985**, 100, 41.

(21) Hodges, R. J.; Garnett, J. L. *J. Phys. Chem.* **1969**, 72, 1968.

(22) Parshall, G. W. *Catalysis (London)* **1977**, 1, 335.

(23) Brookhart, M.; Green M. L. H. *J. Organomet. Chem.* **1983**, 250, 395.

(24) Muetterties, E. L. *Chem. Soc. Rev.* **1983**, 12, 283.

(25) (a) Crabtree, R. H.; Lavin, M. E.; Holt, E. M. *Inorg. Chem.* **1985**, 24, 1986. (b) Crabtree, R. H.; Lavin, M. E. *J. Chem. Soc. Chem. Commun.* **1985**, 794.

(26) Latesky, S. L.; McMullen, A.K.; Rothwell, J.P.; Huffman, J. C. *J. Am. Chem. Soc.* **1985**, 107, 5981.

(27) Jordan, R. F.; Guram, A. S. *Organometallics* **1990**, 378(2), 199.

(28) Gibson, V. C.; Kee T. P.; Carter, S. T.; Sanner, R. P.; Clegs, W. J. *Organomet. Chem.* **1991**, 418(2), 197.

(29) Bruno, J. W.; Smith, G. M.; Marks, T. J.; Fair, C. K.; Schult, A. J. *J. Am. Chem. Soc.* **1986**, 108, 46.

(30) Davies, J. A.; Dutremez, S.; Pinkerton, A. A.; Vihner, M. *Organometallics* **1991**, 10(8), 2956.

(31) Broderick, W. E.; Kanamori, K.; WilleH, R. D.; Legg, J. I. *Inorg. Chem.* **1991**, 30(20), 3875.

(32) Jun, C. H.; Kang, J.B.; Lim, Y. G. *Bull. Korean Chem. Soc.* **1991**, 12(3), 251.

(33) Fou, T.; Bergman, R. G. *Organometallics* **1992**, 11(5), 1801.

(34) Bodensieck, U.; Stoeck-Evans, H.; Suess-Fink, G. *J. Chem. Soc., Chem. Commun.* **1990**, 3, 267.

(35) Suess-Fink, G.; Langenbahn, M.; Stoeckl-Evans, H.; Naumann, D. *J. Chem. Soc., Chem. Commun.* **1991**, 6, 447.

(36) Peng, T. S.; Gladyzs, J. A. *J. Organometallics* **1990**, 9(11) 2584.

(37) Ryabov, A. D. *Chem. Rev.* **1990**, 90, 403.

(38) (a) Latesky, S. L.; McMullen, A. K.; Rothwell, I. P.; Huffman, J.C. *J. Am. Chem. Soc.* **1985**, 107, 5981. (b) Smith, L.R.; Blake, D. M. *J. Am. Chem. Soc.* **1977**, 99, 3302.

(39) (a) Chamberlain, L. R.; rothwell, I. P.; Huffman, J. C. *J. Am. Chem. Soc.* **1986**, 108, 1502. (b) Chamberlain, L. R.; Rothwell, I. P. *J. Chem. Soc., Dalton Trans.* **1986**, 163.

(40) Watson, P. L. *J. Am. Chem. Soc.* **1983**, 105, 6491.

(41) (a) Cope, A. C.; SieKmann, R. W. *J. Am. Chem. Soc.* **1965**, 87, 3272. (b) Cope, A. C.; Friedrich, E. C. *J. Am. Chem. Soc.* **1968**, 90, 909.

(42) Takahashi, H.; Tsuji, J. *J. Organomet. Chem.* **1967**, 10, 511.

(43) (a) Bruce, M. I.; Goodall, B. L.; Stone, F. G. A. *J. Chem. Soc., Chem. Commun.* **1973**, 558. (b) Bruce, M. I.; Goodall, B. C.; Stone, F. G. A. *J. Chem. Soc., Dalton Trans.* **1978**, 687.

(44) Hiraki, K.; Fuchita, Y.; Kage, Y. *J. Chem. Soc., Dalton Trans.* **1984**, 99.

(45) Skapski, A. C.; Smart, M. L. *J. Chem. Soc., Chem. Commun.* **1970**, 658.

(46) Yatsimirsky, A. K.; Ryabov, V. P.; Sakodinskaya, I. K.; Kavetskaya, O. I.; Bererzin, I. V. *Inorg. Chim. Acta.* **1981**, 48, 163.

(47) Ryabov, A. D.; Sakodinskaya, I. K.; Yatsimirsky, A. K. *J. Chem. Soc.Dalton Trans.* **1985**, 2629.

(48) Fujiwara, Y.; Ryuzo, A.; Ichiro, M.; Shiichiro, T. *J. Org. Chem. Soc.* **1976**, 41(10) 1681.

(49) Swann, S.; Yanthakos, T. S. *J. Am. Chem. Soc.* **1931**, 53, 40.

(50) (a) Jones, S. R.; Mello, J. M. *J. Chem. Soc. Perkin Trans.* **1977**, 511. (b) Sheldon, R. A.; Kochi, J. K. *Adv. Catal.* **1976**, 25, 272.

(51) Kanamori, K.; Broderick, W. E.; Jordan, R. F.; Willett, R. D.; Legg, J. I. *J. Am. Chem. Soc.* **1986**, 108, 7122.

(52) (a) Whitesides, G. M.; Gaasch, J. F.; Stedronsky, E. R. *J. Am. Chem. Soc.* **1972**, 94, 5258. (b) Reamey, R. H.; Whitesides, G. M. *J. Am. Chem. Soc.* **1984**, 106, 81. (c) Foley, P.; Whitesides, G. M. *J. Am. Chem. Soc.* **1979**, 101, 2732. (d) Foley, P.; Dicosimo, R.; Whitesides, G. M. *J. Am. Chem. Soc.* **1980**, 102, 6713. (e) Dicosimo, R.; Moore, S. S.; Sowinsky, A. F.; Whitesides, G. M. *J. Am. Chem. Soc.* **1982**, 104, 124.

(53) Janowicz, A. H.; Periana, R. A.; Buchanan, J. M.; Kovac, C. A.; Stryker, J. M.; Wax, M. J.; Bergman, R. H. *Pure Appl. Chem.* **1984**, 56(1), 13.

(54) Lavin, M.; Holt, E. M.; Crabtree, R. H. *Organometallics* **1989**, 8, 99.

(55) (a) Jones, W. D.; Feher, J. F. *Acc. Chem. Res.* **1989**, 22, 91. (b) Jones, W. D.; Feher, J. F. *J. Am. Chem. Soc.* **1986**, 108, 4814.

(56) Belt, S. T.; Dong, L.; Duckett, S. B.; Jones, W. D.; Partridge, M. G.; Perutz, R. N. *J. Chem. Soc., Chem. Commun.* **1991**, 4, 266.

(57) Ryabov, A. D. *Synthesis* **1985**, 233.

(58) (a) Sakakura, T.; Sodeyama, T.; Sasaki, K.; Wada, K.; Tanaka, M.

J. Am. Chem. Soc. **1990**, 112, 7221. (b) Sakakura, T.; Tanaka, M. *Chem. Lett.* **1987**, 249. (c) Sakaura, T.; Tanaka, M. *Chem. Lett.* **1987**, 1113. (d) Sakakura, T.; Tanaka, M. *J. Chem. Soc., Chem. Commun.* **1987**, 758. (e) Sakakura, T.; Susaki, K.; Tokunaga, Y.; Wada, K.; Tanaka, M. *Chem. Lett.* **1988**, 155. (f) Eisenberg, R. *J. Am. Chem. Soc.* **1986**, 108, 535.

(59) (a) Jones, W. D.; Hessell, E. T. *Organometallics*. **1990**, 9(3), 718. (b) Jones, W. D.; Feher, F. *J. Organometallics*. **1983**, 2, 686. (c) Jones, W. D.; Feher, F. J.; Putinas, J. M. *Inorg. Chem.* **1987**, 26, 2120. (d) Jones, W. D.; Feher, F. J.; Putinas, J. M. *J. Am. Chem. Soc.* **1987**, 109, 5047. (e) Tanaka, M.; Sakakura, T.; Tokunaga, Y.; Sodeyama, T. *Chem. Lett.* **1987**, 2373.

(60) Diamond, S. E.; Szalkiewicz, A.; Mares, R. *J. Am. Chem. Soc.* **1979**, 101, 490.

(61) Sievert, A. C.; Muetterties, E. C. *Inorg. Chem.* **1981**, 20, 489.

(62) Yamazaki, H.; Hong, P. *J. Mol. Catal.* **1983**, 21, 133.

(63) Hong, P.; Yamazaki, H.; Sonogashira, K.; Hagihara, N. *Chem. Lett.* **1978**, 535.

(64) Hong, P.; Cho, B- R.; Yamazaki, H. *Chem. Lett.* **1979**, 339.

(65) Yamazaki, H.; Hong, P. *Chem. Lett.* **1979**, 1335.

(66) Yamazaki, H.; Cho, B-R.; Hong, P. *Chem. Lett.* **1980**, 507.

(67) Jones, W. D.; Kosar, W. P. *J. Am. Chem. Soc.* **1986**, 108, 5641.

(68) Lin, Y.; Ma, D.; Lu, X. *Tetra Lett.* **1987**, 28(28), 3249.

(69) Jordan, R. F.; Taylor, D. F. *J. Am. Chem. Soc.* **1989**, 111, 778.

(70) Jordan, R. F.; Guram, A. S. *Organometallics* **1990**, 9(8), 2191.

(71) Tokunaga, Y.; Sakakura, T.; Tanaka, M. *J. Mol. Catal.* **1989**, 56, 305.

(72) Boese, W. T.; Goldman, A. S. *Organometallics* **1991**, 10, 782.

(73) Foo, T.; Bergman, R. G. *Organometallics* **1992**, 11, 1811.

(74) Merola, J. S. *Organometallics* **1989**, 8, 2975.

(75) Bleeke, J. R.; Haile, T.; Chiang, M. Y. *Organometallics* **1991**, 10, 19.

(76) (a) Milstein, D. *Acc. Chem. Res.* **1984**, 17, 221. (b) Milstein, D. *Organometallics* **1982**, 1, 1549.

(77) (a) Wink, D. A.; Ford, P. C. *J. Am. Chem. Soc.* **1985**, 107, 5566. (b) Basato, M.; Morandini, F.; Longato, B.; Bresadola, S. *Inorg. Chem.* **1984**, 23, 649. (c) Suggs, J. W. and Workulich, M. J.; Cox, S. D. *Organometallics* **1985**, 4, 1101.

(78) Price, R. T.; Anderson, R. A.; Muetterties, E. L. *J. Organomet. Chem.* **1989**, 376, 407.

(79) Jordan, R. F.; Guran, A. S. *Organometallics* **1990**, 9(7), 2116.

(80) Neve, F.; Ghedini, M.; Munno, G. D.; Crispini, A. *Organometallics* **1991**, 10, 1143.

(81) (a) Goldman, A. S.; Boese, W. T. *Organometallics* **1991**, 10, 782. (b) Vinogradov, M. G.; Kovalev, I. P.; Yerdakov, K. V.; Strelenko, Y. A.; Nikishin, G. I. *J. Organomet. Chem.* **1990**, 386, 139.

(82) (a) Lesch, D. A.; Richardsen, J. W. Jr.; Jacobson, R. A.; Angelici, R. J. *J. Am. Chem. Soc.* **1984**, 106, 2901. (b) Spies, G. H.; Angelici, R. *J. Organometallics* **1987**, 6, 1897. (c) Hachgenei, J. W.; Angelici, R. *J. Angew. Chem. Int. Ed. Engl.* **1987**, 26(9), 909. (d) Latos-Grazynski, L.; Lisowski, J.; Olmstead, M. M.; Balch, A. L.; Angelici, R. *J. Inorg. Chem.* **1989**, 28, 1183. (e) Chen, J.; Angelici, R. *J. Organometallics* **1989**, 8, 2277.

(83) Chen, J.; Daniels, L. M.; Angelici, R. J. *J. Am. Chem. Soc.* **1990**, 112, 199.

(84) Chen, J.; Daniels, L. M.; Angelici, R. J. *J. Am Chem. Soc.* **1992**, 113(7), 2544.

(85) Dong, L.; Duckett, S. B.; Ohman, K. F.; Jones, W. D.

J. Am. Chem. Soc. **1992**, 114(1), 151.

(86) Crabtree, R. H.; Morris, G. E. *J. Organomet. Chem.* **1971**, 135, 395.

(87) Selnau, H. E.; Merola, J. S. *J. Am. Chem. Soc.* **1991**, 113, 4008.

(88) (a) Blackwore, T.; Bruce, M. I.; Stone, F. G. A. *J. Chem. Soc., Dalton Trans.* **1974**, 106. (b) Bruce, M. I.; Gardner, R. C. F.; Howard, J. A. K.; Stone, F. G. A.; Welling, M.; Woodward, P. J. *J. Chem. Soc., Dalton Trans.* **1977**, 621. (c) Eshtiagh-Hossein, H.; Nixon, J. F.; Poland, J. S. *J. Organomet. Chem.* **1979**, 164, 107.

(89) (a) Kern, R. J. *J. Chem. Soc. Chem. Commun.* **1968**, 706. (b) Yoshikana, S.; Kiji, J.; Furukawa, J. *Makromol. Chem.* **1977**, 178, 1077.

(90) (a) O'Conner, J. M.; Pu, L. *J. Am. Chem. Soc.* **1990**, 112(25), 9013.

(91) Levason, W.et al., *J. Am. Soc. Dalton Trans.*, **1987**, 1901.

(92) Mura, P.; *J. Am. Chem. Soc.* **1986**, 108, 351.

(93) Van Beek, Van Koten, G.; Smeets, W. G. J.; Spek, A. L. *J. Amer. Chem. Soc.* **1986**, 108, 5010.

(94) Crabtree, R. H.; Faller, J. W.; Mellea, M. F.; Quirk, J. M. *Organometallics* **1982**, 1, 1361.

(95) Milstein, D. *J. Am. Chem. Soc.* **1982**, 104, 5227.

Appendix

X-ray Crystallographic Data

STRUCTURE DETERMINATION SUMMARY

Crystal Data

Empirical Formula	C_{16} H_{33} Cl Ir O P_3
Color; Habit	Clear prism
Crystal Size (mm)	0.2 x 0.2 x 0.3
Crystal System	Orthorhombic
Space Group	Pbcm
Unit Cell Dimensions	a = 12.687(4) Å
	b = 12.857(3) Å
	c = 13.832(4) Å
Volume	2256.2(11) $Å^3$
Z	4
Formula weight	562.0
Density(calc.)	1.654 Mg/m^3
Absorption Coefficient	6.225 mm^{-1}
F(000)	1104

Data Collection

Diffractometer Used	Siemens R3m/V
Radiation	MoK_α (λ = 0.71073 Å)
Temperature (K)	298
Monochromator	Highly oriented graphite crystal
2θ Range	3.5 to 55.0°
Scan Type	Wyckoff
Scan Speed	Variable; 3.00 to 18.03°/min. in ω
Scan Range (ω)	0.60°
Background MeasurementS	tationary crystal and stationary counter at beginning and end of scan, each for 25.0% of total scan time
Standard Reflections	2 measured every 300 reflections
Index Ranges	0 < h < 16, -16 < k < 0, -17 < l < 0
Reflections Collected	2943
Independent Reflections	2701 (R_{int} = 0.00%)
Observed Reflections	2320 (F > 4.0σ(F))
Absorption Correction	Semi-empirical
Min./Max. Transmission	0.4171 / 0.9390

Solution and Refinement

System Used	Siemens SHELXTL PLUS (VMS)
Solution	Direct Methods
Refinement Method	Full-Matrix Least-Squares
Quantity Minimized	$\Sigma w(F_o-F_c)^2$
Absolute Structure	N/A
Extinction Correction	χ = 0.00118(8), where $F^* = F [1 + 0.002\chi F^2/\sin(2\theta)]^{-1/4}$
Hydrogen Atoms	Riding model, fixed isotropic U
Weighting Scheme	$w-1 = \sigma^2(F) + 0.0005F^2$
Number of Parameters refined	119
Final R indices (obs. data)	R = 3.91 %, wR = 5.25 %
R Indices (all data)	R = 4.96 %, wR = 8.55 %
Goodness-of-Fit	1.69
Largest and Mean Δ/σ	0.089, 0.011
Data-to-Parameter Ratio	19.5:1
Largest Difference Peak	1.77 $eÅ^{-3}$
Largest Difference Hole	-1.12 $eÅ^{-3}$

Table 1. Atomic coordinates ($x10^4$) and equivalent isotropic displacement coefficients ($Å^2x10^3$)

	x	y	z	U(eq)
Ir(1)	2398(1)	180(1)	2500	28(1)
Cl(1)	3791(2)	-1202(2)	2500	87(2)
P(1)	2284(3)	-17(2)	4146(2)	76(1)
C(11)	1594(13)	-1198(10)	4436(8)	165(8)
C(12)	3462(13)	-100(9)	4826(9)	131(7)
C(13)	1522(11)	964(11)	4789(8)	145(7)
P(2)	3668(2)	1548(2)	2500	38(1)
C(21)	5034(8)	1113(11)	2500	75(5)
C(22)	3679(7)	2444(7)	3494(6)	71(3)
C(7)	1233(8)	1227(8)	2500	70(5)
O(1)	1411(7)	2145(7)	2500	194(11)
C(1)	51(7)	964(7)	2500	37(3)
C(2)	-632(8)	1777(7)	2500	47(3)
C(3)	-1740(8)	1587(9)	2500	67(5)
C(4)	-2102(8)	605(10)	2500	52(4)
C(5)	-1399(9)	-223(9)	2500	65(5)
C(6)	-358(10)	-51(9)	2500	81(6)

* Equivalent isotropic U defined as one third of the trace of the orthogonalized U_{ij} tensor

Table 2. Bond lengths (Å)

Ir(1)-Cl(1)	2.506 (3)	P(2)-C(22A)	1.794 (9)
Ir(1)-P(1)	2.295 (3)	C(7)-O(1)	1.202 (13)
Ir(1)-P(2)	2.384 (3)	C(7)-C(1)	1.537 (13)
Ir(1)-C(7)	1.999 (10)	C(1)-C(2)	1.358 (13)
Ir(1)-P(1A)	2.295 (3)	C(1)-C(6)	1.405 (15)
P(1)-C(11)	1.798 (14)	C(2)-C(3)	1.427 (15)
P(1)-C(12)	1.769 (15)	C(3)-C(4)	1.344 (17)
P(1)-C(13)	1.822 (13)	C(4)-C(5)	1.388 (17)
P(2)-C(21)	1.822 (11)	C(5)-C(6)	1.339 (17)
P(2)-C(22)	1.794 (9)		

Table 3. Bond angles (°)

Cl(1)-Ir(1)-P(1)	88.1(1)	Ir(1)-P(2)-C(22)	118.6(3)
Cl(1)-Ir(1)-P(2)	92.7(1)	C(21)-P(2)-C(22)	100.9(4)
P(1)-Ir(1)-P(2)	97.1(1)	Ir(1)-P(2)-C(22A)	118.6(3)
Cl(1)-Ir(1)-C(7)	177.1(3)	C(21)-P(2)-C(22A)	100.9(4)
P(1)-Ir(1)-C(7)	91.6(1)	C(22)-P(2)-C(22A)	100.1(6)
P(2)-Ir(1)-C(7)	90.2(3)	Ir(1)-C(7)-O(1)	121.5(8)
Cl(1)-Ir(1)-P(1A)	88.1(1)	Ir(1)-C(7)-C(1)	125.0(7)
P(1)-Ir(1)-P(1A)	165.4(2)	O(1)-C(7)-C(1)	113.5(9)
P(2)-Ir(1)-P(1A)	97.1(1)	C(7)-C(1)-C(2)	117.0(8)
C(7)-Ir(1)-P(1A)	91.6(1)	C(7)-C(1)-C(6)	124.4(9)
Ir(1)-P(1)-C(11)	110.2(4)	C(2)-C(1)-C(6)	118.6(9)
Ir(1)-P(1)-C(12)	118.7(5)	C(1)-C(2)-C(3)	119.8(9)
C(11)-P(1)-C(12)	104.0(6)	C(2)-C(3)-C(4)	119.8(10)
Ir(1)-P(1)-C(13)	116.2(4)	C(3)-C(4)-C(5)	120.0(10)
C(11)-P(1)-C(13)	102.6(6)	C(4)-C(5)-C(6)	120.5(11)
C(12)-P(1)-C(13)	103.3(6)	C(1)-C(6)-C(5)	121.2(10)
Ir(1)-P(2)-C(21)	114.6(4)		

Table 4. Anisotropic displacement coefficients ($Å^2x10^3$)

	U_{11}	U_{22}	U_{33}	U_{12}	U_{13}	U_{23}
Ir(1)	22(1)	27(1)	35(1)	2(1)	0	0
Cl(1)	36(1)	40(2)	185(4)	15(1)	0	0
P(1)	93(2)	98(2)	38(1)	-53(2)	-3(1)	6(1)
C(11)	249(18)	187(14)	59(7)	-148(14)	-18(9)	39(8)
C(12)	155(14)	171(13)	69(8)	-65(10)	-58(9)	35(7)
C(13)	146(12)	213(15)	77(8)	-90(11)	66(8)	-70(9)
P(2)	30(1)	38(1)	46(1)	-4(1)	0	0
C(21)	22(5)	76(9)	126(11)	-12(5)	0	0
C(22)	75(5)	71(5)	68(5)	-31(5)	17(5)	-27(5)
C(7)	21(5)	35(6)	152(13)	2(4)	0	0
O(1)	33(5)	28(5)	521(32)	0(4)	0	0
C(1)	31(4)	31(4)	51(5)	2(3)	0	0
C(2)	44(6)	34(5)	65(7)	11(4)	0	0
C(3)	34(5)	62(8)	104(10)	20(5)	0	0
C(4)	30(5)	69(7)	58(6)	1(5)	0	0
C(5)	40(6)	51(7)	104(10)	-12(5)	0	0
C(6)	32(6)	44(7)	168(16)	5(4)	0	0

The anisotropic displacement exponent takes the form:
$-2\pi^2(h^2a^{*2}U_{11} + ... + 2hka^*b^*U_{12})$

Table 5. H-Atom coordinates ($x10^4$) and isotropic displacement coefficients ($Å^2x10^3$)

	x	y	z	U
H(11A)	1541	-1281	5124	80
H(11B)	900	-1167	4160	80
H(11C)	1970	-1778	4166	80
H(12A)	3351	-176	5509	80
H(12B)	3830	-698	4584	80
H(12C)	3874	514	4707	80
H(13A)	1487	861	5476	80
H(13B)	1844	1625	4655	80
H(13C)	823	952	4524	80
H(21A)	5480	1717	2500	80
H(21B)	5174	704	3067	80
H(22A)	4224	2953	3404	80
H(22B)	3009	2787	3540	80
H(22C)	3810	2063	4078	80
H(2A)	-358	2473	2500	80
H(3A)	-2222	2163	2500	80
H(4A)	-2849	483	2500	80
H(5A)	-1656	-925	2500	80
H(6A)	128	-623	2500	80

STRUCTURE DETERMINATION SUMMARY

Crystal Data

Empirical Formula	C_{14} H_{31} Cl Ir N P_3
Color; Habit	clear rectangular plate
Crystal Size (mm)	0.4 x 0.5 x 0.1
Crystal System	Orthorhombic
Space Group	Cmca
Unit Cell Dimensions	a = 13.340(4) Å b = 11.999(3) Å c = 26.315(9) Å
Volume	4212(2) $Å^3$
Z	8
Formula weight	534.0
Density(calc.)	1.684 Mg/m^3
Absorption Coefficient	6.662 mm^{-1}
F(000)	2088

Data Collection

Diffractometer Used	Siemens R3m/V
Radiation	MoK_α (λ = 0.71073 Å)
Temperature (K)	298
Monochromator	Highly oriented graphite crystal
2θ Range	3.5.0 to 55.0°
Scan Type	Wyckoff
Scan Speed	Variable; 3.00 to 19.53°/min. in ω
Scan Range (ω)	0.60°
Background Measurement	Stationary crystal and stationary counter at beginning and end of scan, each for 25.0% of total scan time
Standard Reflections	3 measured every 300 reflections
Index Ranges	-3 < h < 14, 0 < k < 15, -28 < l < 14
Reflections Collected	1952
Independent Reflections	1522 (R_{int} = 3.52%)
Observed Reflections	1267 (F > 3.0s(F))
Absorption Correction	Semi-empirical
Min./Max. Transmission	0.6209 / 0.9949

Solution and Refinement

System Used	Siemens SHELXTL PLUS (VMS)
Solution	Direct Methods
Refinement Method	Full-Matrix Least-Squares
Quantity Minimized	$\Sigma w(F_o-F_c)^2$
Absolute Structure	N/A
Extinction Correction	χ = 0.000050(7), where $F^* = F [1 + 0.002\chi F^2/\sin(2\theta)]^{-1/4}$
Hydrogen Atoms	Riding model, fixed isotropic U
Weighting Scheme	$w^{-1} = \sigma^2(F) + 0.0008F^2$
Number of Parameters refined	107
Final R indices (obs. data)	R = 2.19 %, wR = 3.26 %
R Indices (all data)	R = 2.93 %, wR = 3.55 %
Goodness-of-Fit	0.93
Largest and Mean Δ/σ	0.002, 0.000
Data-to-Parameter Ratio	11.8:1
Largest Difference Peak	0.43 $eÅ^{-3}$
Largest Difference Hole	-0.39 $eÅ^{-3}$

Table 1. Atomic coordinates ($x10^4$) and equivalent isotropic displacement coefficients ($Å^2x10^3$)

	x	y	z	U(eq)
Ir(1)	0	-60(1)	1235(1)	34(1)
P(1)	1710(1)	-240(1)	1150(1)	45(1)
C(11)	2456(5)	997(5)	1031(3)	74(3)
C(12)	2373(5)	-911(5)	1666(2)	69(2)
C(13)	2037(4)	-1125(5)	617(2)	65(2)
P(2)	0	659(2)	2073(1)	42(1)
C(21)	-1051(4)	1528(4)	2266(2)	59(2)
C(22)	0	-405(6)	2576(3)	71(3)
Cl(1)	0	-2070(2)	1504(1)	60(1)
N(1)	0	2405(5)	1224(2)	48(3)
C(1)	0	1488(6)	921(3)	37(2)
C(2)	0	1669(7)	398(3)	52(3)
C(3)	0	2707(8)	186(3)	64(3)
C(4)	0	3614(7)	504(3)	64(3)
C(5)	0	3431(6)	1016(3)	56(3)

* Equivalent isotropic U defined as one third of the trace of the orthogonalized U_{ij} tensor

Table 2. Bond lengths (Å)

Ir(1)-H(1)	1.691	P(2)-C(21)	1.820 (5)
Ir(1)-P(1)	2.303 (2)	P(2)-C(22)	1.840 (8)
Ir(1)-P(2)	2.368 (2)	P(2)-C(21A)	1.820 (5)
Ir(1)-Cl(1)	2.514 (2)	N(1)-C(1)	1.358 (9)
Ir(1)-C(1)	2.032 (7)	N(1)-C(5)	1.347 (10)
Ir(1)-P(1A)	2.303 (2)	C(1)-C(2)	1.395 (10)
P(1)-C(11)	1.814 (6)	C(2)-C(3)	1.364 (12)
P(1)-C(12)	1.810 (6)	C(3)-C(4)	1.373 (13)
P(1)-C(13)	1.812 (6)	C(4)-C(5)	1.365 (13)

Table 3. Bond angles (°)

H(1)-Ir(1)-P(1)	83.4(1)	Ir(1)-P(1)-C(13)	111.6(2)
H(1)-Ir(1)-P(2)	171.6(1)	C(11)-P(1)-C(13)	102.3(3)
P(1)-Ir(1)-P(2)	97.2(1)	C(12)-P(1)-C(13)	101.8(3)
H(1)-Ir(1)-Cl(1)	93.4(1)	Ir(1)-P(2)-C(21)	118.0(2)
P(1)-Ir(1)-Cl(1)	86.4(1)	Ir(1)-P(2)-C(22)	114.7(3)
P(2)-Ir(1)-Cl(1)	95.0(1)	C(21)-P(2)-C(22)	101.3(2)
H(1)-Ir(1)-C(1)	79.0(2)	Ir(1)-P(2)-C(21A)	118.0(2)
P(1)-Ir(1)-C(1)	92.7(1)	C(21)-P(2)-C(21A)	100.7(3)
P(2)-Ir(1)-C(1)	92.6(2)	C(22)-P(2)-C(21A)	101.3(2)
Cl(1)-Ir(1)-C(1)	172.4(2)	C(1)-N(1)-C(5)	120.2(6)
H(1)-Ir(1)-P(1A)	83.4(1)	Ir(1)-C(1)-N(1)	120.2(5)
P(1)-Ir(1)-P(1A)	164.5(1)	Ir(1)-C(1)-C(2)	122.9(5)
P(2)-Ir(1)-P(1A)	97.2(1)	N(1)-C(1)-C(2)	116.9(6)
Cl(1)-Ir(1)-P(1A)	86.4(1)	C(1)-C(2)-C(3)	123.0(7)
C(1)-Ir(1)-P(1A)	92.7(1)	C(2)-C(3)-C(4)	118.5(8)
Ir(1)-P(1)-C(11)	118.9(2)	C(3)-C(4)-C(5)	118.3(8)
Ir(1)-P(1)-C(12)	116.9(2)	N(1)-C(5)-C(4)	123.2(7)
C(11)-P(1)-C(12)	103.0(3)		

Table 4. Anisotropic displacement coefficients ($Å^2 x 10^3$)

	U_{11}	U_{22}	U_{33}	U_{12}	U_{13}	U_{23}
Ir(1)	40(1)	31(1)	32(1)	0	0	1(1)
P(1)	43(1)	45(1)	48(1)	5(1)	1(1)	-1(1)
C(11)	48(4)	73(4)	101(5)	-12(4)	0(4)	5(4)
C(12)	61(4)	81(4)	66(4)	21(4)	-7(3)	-2(3)
C(13)	59(4)	73(4)	63(4)	16(3)	2(3)	-8(3)
P(2)	54(1)	39(1)	32(1)	0	0	0(1)
C(21)	61(4)	62(3)	53(3)	3(3)	10(3)	-11(3)
C(22)	117(8)	57(5)	40(5)	0	0	13(5)
Cl(1)	82(2)	37(1)	59(1)	0	0	7(1)
N(1)	58(5)	43(4)	42(5)	0	0	-2(3)
C(1)	46(5)	40(4)	25(4)	0	0	4(3)
C(2)	64(5)	53(5)	38(5)	0	0	7(4)
C(3)	67(6)	78(6)	47(5)	0	0	27(6)
C(4)	73(6)	46(5)	72(7)	0	0	28(5)
C(5)	64(6)	34(4)	68(6)	0	0	10(4)

The anisotropic displacement exponent takes the form:
$-2\pi^2(h^2a^{*2}U_{11} + ... + 2hka^*b^*U_{12})$

Table 5. H-Atom coordinates ($x10^4$) and isotropic displacement coefficients ($Å^2 x 10^3$)

	x	y	z	U
H(1)	0	-376	608	50
H(11A)	3153	804	1005	80
H(11B)	2235	1317	716	80
H(11C)	2367	1527	1300	80
H(12A)	3078	-946	1593	80
H(12B)	2268	-487	1971	80
H(12C)	2117	-1652	1712	80
H(13A)	2752	-1185	591	80
H(13B)	1753	-1851	667	80
H(13C)	1774	-807	310	80
H(21A)	-953	1761	2611	80
H(21B)	-1094	2173	2051	80
H(21C)	-1660	1106	2241	80
H(22A)	0	-48	2902	80
H(22B)	-588	-861	2544	80
H(2A)	0	1035	175	80
H(3A)	0	2804	-176	80
H(4A)	0	4356	367	80
H(5A)	0	4067	1238	80

STRUCTURE DETERMINATION SUMMARY

Crystal Data

Empirical Formula	C_{13} H_{31} Cl Ir O P_3
Color; Habit	Clear colorless rectangular prism
Crystal Size (mm)	0.5 x 0.6 x 0.8
Crystal System	Monoclinic
Space Group	$P2_1/n$
Unit Cell Dimensions	a = 9.723(2) Å b = 11.583(3) Å c = 17.790(5) Å β = 94.68(2)°
Volume	1996.7(9) $Å^3$
Z	4
Formula weight	523.9
Density(calc.)	1.743 Mg/m^3
Absorption Coefficient	7.027 mm^{-1}
F(000)	1024

Data Collection

Diffractometer Used	Siemens R3m/V
Radiation	MoK_α (λ = 0.71073 Å)
Temperature (K)	298
Monochromator	Highly oriented graphite crystal
2θ Range	3.5 to 50.0°
Scan Type	Wyckoff
Scan Speed	Variable; 3.97 to 19.53°/min. in ω
Scan Range (ω)	0.60°
Background Measurement	Stationary crystal and stationary counter at beginning and end of scan, each for 25.0% of total scan time
Standard Reflections	3 measured every 400 reflections
Index Ranges	$0 < h < 11$, $-13 < k < 13$, $-21 < l < 21$
Reflections Collected	7467
Independent Reflections	3512 (R_{int} = 2.17%)
Observed Reflections	3194 ($F > 3.0\sigma(F)$)
Absorption Correction	Semi-empirical
Min./Max. Transmission	0.2788 / 0.5956

Solution and Refinement

System UsedSiemens	SHELXTL PLUS (VMS)
Solution	Direct Methods
Refinement Method	Full-Matrix Least-Squares
Quantity Minimized	$\Sigma w(F_o-F_c)^2$
Absolute Structure	N/A
Extinction Correction	χ = 0.00022(3), where $F^* = F [1 + 0.002\chi F^2/\sin(2\theta)]^{-1/4}$
Hydrogen Atoms	Riding model, fixed isotropic U
Weighting Scheme	$w^{-1} = \sigma^2(F) + 0.0008F^2$
Number of Parameters refined	176
Final R indices (obs. data)	R = 2.88 %, wR = 3.90 %
R Indices (all data)	R = 3.21 %, wR = 4.05 %
Goodness-of-Fit	1.09
Largest and Mean Δ/σ	0.004, 0.001
Data-to-Parameter Ratio	18.1:1
Largest Difference Peak	1.15 $eÅ^{-3}$
Largest Difference Hole	-0.96 $eÅ^{-3}$

Table 1. Atomic coordinates ($x10^4$) and equivalent isotropic displacement coefficients ($Å^2x10^3$)

	x	y	z	U(eq)
Ir(1)	257(1)	3174(1)	3775(1)	36(1)
Cl(1)	187(2)	1310(1)	3067(1)	67(1)
P(1)	-823(1)	2440(1)	4786(1)	45(1)
P(2)	-1809(1)	3676(1)	3100(1)	49(1)
P(3)	1627(2)	4115(1)	2963(1)	54(1)
C(1)	2083(5)	2670(4)	4356(3)	44(2)
C(2)	2884(6)	1712(5)	4348(4)	60(2)
C(3)	4047(7)	1864(6)	4880(4)	76(3)
C(4)	3920(6)	2899(7)	5201(4)	72(2)
O(1)	2722(4)	3417(3)	4889(2)	59(1)
C(11)	299(6)	2268(7)	5642(3)	70(2)
C(12)	-2182(7)	3302(5)	5134(4)	65(2)
C(13)	-1602(7)	1011(5)	4681(4)	76(2)
C(21)	-3230(6)	2667(6)	3134(4)	71(2)
C(22)	-1821(8)	3780(8)	2076(3)	91(3)
C(23)	-2569(6)	5048(5)	3348(4)	73(2)
C(31)	3390(6)	4331(7)	3332(5)	99(3)
C(32)	1853(10)	3476(7)	2050(5)	104(4)
C(33)	1157(7)	5588(5)	2715(3)	66(2)

* Equivalent isotropic U defined as one third of the trace of the orthogonalized U_{ij} tensor

Table 2. Bond lengths (Å)

Ir(1)-Cl(1)	2.497 (2)	P(2)-C(23)	1.822 (6)
Ir(1)-P(1)	2.317 (1)	P(3)-C(31)	1.802 (6)
Ir(1)-P(2)	2.328 (1)	P(3)-C(32)	1.815 (8)
Ir(1)-P(3)	2.315 (2)	P(3)-C(33)	1.812 (6)
Ir(1)-C(1)	2.065 (5)	C(1)-C(2)	1.357 (8)
P(1)-C(11)	1.811 (6)	C(1)-O(1)	1.392 (6)
P(1)-C(12)	1.806 (7)	C(2)-C(3)	1.425 (9)
P(1)-C(13)	1.824 (6)	C(3)-C(4)	1.338 (11)
P(2)-C(21)	1.815 (7)	C(4)-O(1)	1.386 (7)
P(2)-C(22)	1.825 (6)		

Table 3. Bond angles (°)

Cl(1)-Ir(1)-P(1)	94.5(1)	C(21)-P(2)-C(22)	97.6(4)
Cl(1)-Ir(1)-P(2)	88.3(1)	Ir(1)-P(2)-C(23)	116.3(2)
P(1)-Ir(1)-P(2)	93.8(1)	C(21)-P(2)-C(23)	103.2(3)
Cl(1)-Ir(1)-P(3)	94.9(1)	C(22)-P(2)-C(23)	102.4(4)
P(1)-Ir(1)-P(3)	167.7(1)	Ir(1)-P(3)-C(31)	114.6(3)
P(2)-Ir(1)-P(3)	94.4(1)	Ir(1)-P(3)-C(32)	118.9(3)
Cl(1)-Ir(1)-C(1)	89.7(1)	C(31)-P(3)-C(32)	101.6(4)
P(1)-Ir(1)-C(1)	86.2(1)	Ir(1)-P(3)-C(33)	116.7(2)
P(2)-Ir(1)-C(1)	178.0(1)	C(31)-P(3)-C(33)	99.9(3)
P(3)-Ir(1)-C(1)	86.0(1)	C(32)-P(3)-C(33)	102.3(3)
Ir(1)-P(1)-C(11)	114.5(2)	Ir(1)-C(1)-C(2)	134.2(4)
Ir(1)-P(1)-C(12)	117.0(2)	Ir(1)-C(1)-O(1)	118.9(3)
C(11)-P(1)-C(12)	100.4(3)	C(2)-C(1)-O(1)	106.9(4)
Ir(1)-P(1)-C(13)	117.7(2)	C(1)-C(2)-C(3)	108.5(5)
C(11)-P(1)-C(13)	101.7(3)	C(2)-C(3)-C(4)	107.3(6)
C(12)-P(1)-C(13)	103.1(3)	C(3)-C(4)-O(1)	108.8(6)
Ir(1)-P(2)-C(21)	116.7(2)	C(1)-O(1)-C(4)	108.5(5)
Ir(1)-P(2)-C(22)	117.8(3)		

Table 4. Anisotropic displacement coefficients ($Å^2 x 10^3$)

	U_{11}	U_{22}	U_{33}	U_{12}	U_{13}	U_{23}
Ir(1)	30(1)	45(1)	33(1)	1(1)	5(1)	-3(1)
Cl(1)	65(1)	66(1)	71(1)	4(1)	6(1)	-30(1)
P(1)	36(1)	55(1)	44(1)	-3(1)	9(1)	3(1)
P(2)	41(1)	65(1)	40(1)	5(1)	-5(1)	-7(1)
P(3)	51(1)	62(1)	53(1)	10(1)	25(1)	11(1)
C(1)	34(3)	56(3)	42(3)	-1(2)	7(2)	6(2)
C(2)	48(3)	69(4)	64(4)	10(3)	9(3)	7(3)
C(3)	45(4)	103(6)	78(5)	17(3)	-5(3)	19(4)
C(4)	40(3)	103(5)	72(4)	6(3)	-6(3)	0(4)
O(1)	36(2)	76(2)	63(2)	2(2)	-3(2)	-8(2)
C(11)	56(4)	105(5)	50(3)	0(4)	9(3)	13(3)
C(12)	50(4)	84(4)	63(4)	-3(3)	22(3)	-1(3)
C(13)	77(4)	64(3)	89(5)	-7(3)	14(4)	14(3)
C(21)	48(3)	80(4)	82(4)	-3(3)	-13(3)	-13(3)
C(22)	90(5)	137(7)	43(3)	-6(5)	-11(3)	-8(4)
C(23)	57(4)	66(3)	91(5)	16(3)	-22(3)	-1(3)
C(31)	38(3)	122(6)	141(7)	0(4)	26(4)	65(6)
C(32)	141(8)	96(5)	83(5)	35(5)	68(6)	9(4)
C(33)	74(4)	60(3)	66(4)	6(3)	19(3)	4(3)

The anisotropic displacement exponent takes the form:
$-2\pi^2(h^2a^{*2}U_{11} + ... + 2hka^*b^*U_{12})$

Table 5. H-Atom coordinates ($x10^4$) and isotropic displacement coefficients ($Å^2x10^3$)

	x	y	z	U
H(1)	270(50)	4384(39)	4235(28)	50
H(2A)	2719	1066	3942	50
H(3A)	4793	1363	5093	50
H(4A)	4501	3370	5580	50
H(11A)	-224	1959	6031	80
H(11B)	1045	1754	5558	80
H(11C)	663	3009	5796	80
H(12A)	-2562	2923	5550	80
H(12B)	-1802	4034	5297	80
H(12C)	-2896	3422	4736	80
H(13A)	-2011	808	5136	80
H(13B)	-2302	1022	4268	80
H(13C)	-910	452	4583	80
H(21A)	-4028	2957	2840	80
H(21B)	-2963	1940	2932	80
H(21C)	-3445	2564	3647	80
H(22A)	-2727	3989	1865	80
H(22B)	-1175	4367	1960	80
H(22C)	-1557	3058	1866	80
H(23A)	-3414	5179	3042	80
H(23B)	-2754	5033	3870	80
H(23C)	-1930	5658	3267	80
H(31A)	3886	4723	2963	80
H(31B)	3392	4796	3779	80
H(31C)	3825	3603	3454	80
H(32A)	2445	3951	1774	80
H(32B)	2248	2719	2114	80
H(32C)	963	3420	1777	80
H(33A)	1793	5890	2379	80
H(33B)	241	5597	2469	80
H(33C)	1185	6055	3162	80

STRUCTURE DETERMINATION SUMMARY

Crystal Data

Empirical Formula	C_{17} H_{33} Cl Ir P_3 S
Color; Habit	Pale orange irregular prism
Crystal Size (mm)	0.4 x 0.4 x 0.5
Crystal System	Orthorhombic
Space Group	$P2_12_12_1$
Unit Cell Dimensions	a = 11.550(3) Å
	b = 13.598(2) Å
	c = 14.362(4) Å
Volume	2255.7(9) $Å^3$
Z	4
Formula weight	590.1
Density(calc.)	1.737 Mg/m^3
Absorption Coefficient	6.314 mm^{-1}
F(000)	1160

Data Collection

Diffractometer Used	Siemens R3m/V
Radiation	MoK_α (λ = 0.71073 Å)
Temperature (K)	298
Monochromator	Highly oriented graphite crystal
2θ Range	3.5 to 55.0°
Scan Type	Wyckoff
Scan Speed	Variable; 3.97 to 19.53°/min. in ω
Scan Range (ω)	0.60°
Background Measurement	Stationary crystal and stationary counter at beginning and end of scan, each for 25.0% of total scan time
Standard Reflections	3 measured every 300 reflections
Index Ranges	-14 < h < 0, 0 < h < 17, -18 < l < 0
Reflections Collected	2940
Independent Reflections	2916 (R_{int} = 0.00%)
Observed Reflections	2681 ($F > 3.0\sigma(F)$)
Absorption Correction	Semi-empirical
Min./Max. Transmission	0.5527 / 0.9008

Solution and Refinement

System Used	Siemens SHELXTL PLUS (VMS)
SolutionD	irect Methods
Refinement Method	Full-Matrix Least-Squares
Quantity Minimized	$\Sigma w(F_o-F_c)^2$
Absolute Structure	N/A
Extinction Correction	χ = 0.00024(2), where $F^* = F [1 + 0.002xF^2/\sin(2\theta)]^{-1/4}$
Hydrogen Atoms	Riding model, fixed isotropic U
Weighting Scheme	$w^{-1} = \sigma^2(F) + 0.0002F^2$
Number of Parameters refined	209
Final R indices (obs. data)	R = 2.70 %, wR = 2.74 %
R Indices (all data)	R = 3.17 %, wR = 2.80 %
Goodness-of-Fit	1.05
Largest and Mean Δ/σ	0.002, 0.000
Data-to-Parameter Ratio	12.8:1
Largest Difference Peak	1.24 $eÅ^{-3}$
Largest Difference Hole	-0.62 $eÅ^{-3}$

Table 1. Atomic coordinates ($x10^4$) and equivalent isotropic displacement coefficients ($Å^2x10^3$)

	x	y	z	U(eq)
Ir(1)	2669(1)	3373(1)	7302(1)	32(1)
P(1)	2188(2)	4510(1)	6143(1)	46(1)
P(2)	4113(2)	2659(2)	6421(2)	45(1)
P(3)	2797(2)	2209(1)	8517(1)	41(1)
Cl(1)	4271(2)	4392(1)	7958(1)	49(1)
S(1)	1464(2)	4317(1)	8300(1)	45(1)
C(1)	1347(6)	2550(5)	6835(5)	42(2)
C(2)	227(6)	2579(6)	7023(5)	47(3)
C(3)	-441(6)	3208(6)	7649(6)	47(2)
C(4)	-1654(7)	3049(6)	7670(7)	61(3)
C(5)	-2348(8)	3619(8)	8219(7)	80(4)
C(6)	-1909(8)	4357(7)	8752(7)	71(4)
C(7)	-760(7)	4542(6)	8738(6)	53(3)
C(8)	-3(6)	3974(6)	8203(5)	41(2)
C(11)	3100(9)	5595(6)	6045(6)	72(4)
C(12)	737(8)	5063(7)	6215(6)	73(4)
C(13)	2115(8)	4002(7)	4972(5)	70(3)
C(21)	5277(7)	2091(7)	7049(6)	63(3)
C(22)	4997(7)	3503(6)	5733(6)	66(3)
C(23)	3695(8)	1711(6)	5577(6)	71(3)
C(31)	2922(9)	926(5)	8183(7)	71(4)
C(32)	3955(7)	2409(7)	9356(6)	63(3)
C(33)	1534(7)	2129(6)	9252(5)	56(3)

* Equivalent isotropic U defined as one third of the trace of the orthogonalized U_{ij} tensor

Table 2. Bond lengths (Å)

Ir(1)-P(1)	2.340 (2)	P(3)-C(31)	1.815 (8)
Ir(1)-P(2)	2.308 (2)	P(3)-C(32)	1.821 (8)
Ir(1)-P(3)	2.360 (2)	P(3)-C(33)	1.804 (8)
Ir(1)-Cl(1)	2.496 (2)	S(1)-C(8)	1.763 (7)
Ir(1)-S(1)	2.374 (2)	C(1)-C(2)	1.323 (10)
Ir(1)-C(1)	2.009 (7)	C(2)-C(3)	1.461 (11)
P(1)-C(11)	1.818 (9)	C(3)-C(4)	1.418 (10)
P(1)-C(12)	1.840 (9)	C(3)-C(8)	1.404 (11)
P(1)-C(13)	1.819 (8)	C(4)-C(5)	1.366 (13)
P(2)-C(21)	1.793 (9)	C(5)-C(6)	1.361 (14)
P(2)-C(22)	1.827 (9)	C(6)-C(7)	1.350 (13)
P(2)-C(23)	1.834 (9)	C(7)-C(8)	1.398 (11)

Table 3. Bond angles (°)

P(1)-Ir(1)-P(2)	93.4(1)	C(21)-P(2)-C(22)	97.1(4)
P(1)-Ir(1)-P(3)	169.8(1)	Ir(1)-P(2)-C(23)	117.9(3)
P(2)-Ir(1)-P(3)	94.4(1)	C(21)-P(2)-C(23)	103.1(4)
P(1)-Ir(1)-Cl(1)	94.5(1)	C(22)-P(2)-C(23)	103.4(4)
P(2)-Ir(1)-Cl(1)	84.5(1)	Ir(1)-P(3)-C(31)	117.1(3)
P(3)-Ir(1)-Cl(1)	92.7(1)	Ir(1)-P(3)-C(32)	115.8(3)
P(1)-Ir(1)-S(1)	86.2(1)	C(31)-P(3)-C(32)	105.0(4)
P(2)-Ir(1)-S(1)	169.1(1)	Ir(1)-P(3)-C(33)	115.0(3)
P(3)-Ir(1)-S(1)	87.3(1)	C(31)-P(3)-C(33)	99.3(4)
Cl(1)-Ir(1)-S(1)	84.6(1)	C(32)-P(3)-C(33)	102.4(4)
P(1)-Ir(1)-C(1)	87.1(2)	Ir(1)-S(1)-C(8)	111.8(3)
P(2)-Ir(1)-C(1)	97.5(2)	Ir(1)-C(1)-C(2)	131.2(6)
P(3)-Ir(1)-C(1)	85.4(2)	C(1)-C(2)-C(3)	131.3(7)
Cl(1)-Ir(1)-C(1)	177.3(2)	C(2)-C(3)-C(4)	116.5(7)
S(1)-Ir(1)-C(1)	93.3(2)	C(2)-C(3)-C(8)	126.3(6)
Ir(1)-P(1)-C(11)	116.9(3)	C(4)-C(3)-C(8)	117.2(7)
Ir(1)-P(1)-C(12)	116.5(3)	C(3)-C(4)-C(5)	120.4(8)
C(11)-P(1)-C(12)	101.5(4)	C(4)-C(5)-C(6)	121.7(8)
Ir(1)-P(1)-C(13)	114.7(3)	C(5)-C(6)-C(7)	119.7(9)
C(11)-P(1)-C(13)	105.3(4)	C(6)-C(7)-C(8)	121.4(8)
C(12)-P(1)-C(13)	99.5(4)	S(1)-C(8)-C(3)	126.0(5)
Ir(1)-P(2)-C(21)	116.6(3)	S(1)-C(8)-C(7)	114.3(6)
Ir(1)-P(2)-C(22)	115.9(3)	C(3)-C(8)-C(7)	119.7(6)

Table 4. Anisotropic displacement coefficients ($Å^2 x 10^3$)

	U_{11}	U_{22}	U_{33}	U_{12}	U_{13}	U_{23}
Ir(1)	34(1)	28(1)	33(1)	-3(1)	-1(1)	-2(1)
P(1)	53(1)	41(1)	44(1)	-5(1)	-7(1)	7(1)
P(2)	46(1)	40(1)	49(1)	-2(1)	8(1)	-10(1)
P(3)	47(1)	37(1)	39(1)	-2(1)	-4(1)	2(1)
Cl(1)	46(1)	43(1)	56(1)	-9(1)	-7(1)	-7(1)
S(1)	43(1)	44(1)	49(1)	0(1)	-1(1)	-13(1)
C(1)	50(4)	40(4)	36(4)	-10(3)	-3(3)	-8(3)
C(2)	37(4)	57(5)	47(4)	-16(4)	-7(3)	-2(4)
C(3)	39(3)	51(4)	49(4)	-2(3)	-6(3)	12(4)
C(4)	40(4)	66(5)	77(5)	-6(4)	0(4)	10(5)
C(5)	40(4)	102(8)	96(7)	-5(6)	-4(5)	22(6)
C(6)	64(6)	67(6)	82(7)	27(5)	27(5)	21(5)
C(7)	54(5)	43(4)	62(5)	8(4)	10(4)	3(4)
C(8)	36(4)	44(4)	44(4)	3(3)	-1(3)	10(4)
C(11)	93(7)	49(5)	73(6)	-22(5)	-18(5)	15(5)
C(12)	72(6)	76(7)	70(6)	20(6)	-9(5)	32(6)
C(13)	80(6)	86(6)	46(5)	-18(6)	-15(4)	12(4)
C(21)	44(5)	73(6)	71(6)	15(4)	2(4)	-6(5)
C(22)	51(5)	64(6)	83(6)	-1(5)	29(4)	4(5)
C(23)	71(6)	64(6)	79(6)	-19(6)	22(5)	-42(5)
C(31)	104(8)	37(4)	73(6)	-5(5)	5(6)	6(4)
C(32)	55(5)	80(6)	53(5)	-13(5)	-16(4)	18(5)
C(33)	52(5)	64(5)	51(5)	-12(4)	7(4)	15(4)

The anisotropic displacement exponent takes the form:
$-2\pi^2(h^2a^{*2}U_{11} + \ldots + 2hka^*b^*U_{12})$

Table 5. H-Atom coordinates ($x10^4$) and isotropic displacement coefficients ($Å^2x10^3$)

	x	y	z	U
H(1A)	1579	2038	6414	80
H(2A)	-220	2110	6676	80
H(4A)	-1990	2520	7321	80
H(5A)	-3169	3514	8183	80
H(6A)	-2419	4739	9137	80
H(7A)	-459	5086	9089	80
H(11A)	2829	6011	5551	80
H(11B)	3079	5950	6623	80
H(11C)	3880	5392	5918	80
H(12A)	631	5512	5706	80
H(12B)	152	4563	6190	80
H(12C)	677	5414	6793	80
H(13A)	1914	4505	4532	80
H(13B)	2847	3719	4804	80
H(13C)	1530	3501	4969	80
H(21A)	5825	1818	6618	80
H(21B)	5649	2586	7420	80
H(21C)	4987	1580	7446	80
H(22A)	5581	3158	5387	80
H(22B)	4489	3838	5309	80
H(22C)	5359	3973	6138	80
H(23A)	4389	1491	5275	80
H(23B)	3327	1164	5880	80
H(23C)	3178	1986	5123	80
H(31A)	2964	524	8732	80
H(31B)	2279	719	7808	80
H(31C)	3626	859	7833	80
H(32A)	3946	1903	9821	80
H(32B)	4690	2407	9043	80
H(32C)	3834	3037	9646	80
H(33A)	1656	1642	9726	80
H(33B)	1391	2756	9539	80
H(33C)	880	1947	8878	80

STRUCTURE DETERMINATION SUMMARY

Crystal Data	
Empirical Formula	$C_{27}\ H_{53}\ F_6\ P_4\ Ir$
Color; Habit	Yellow rectangular plate
Crystal size (mm)	0.1 x 0.3 x 0.4
Crystal System	Orthorhombic
Space Group	Pbac
Unit Cell Dimensions	a = 11.658(4) Å
	b = 18.041(4) Å
	c = 33.731(8) Å
Volume	7094(4) $Å^3$
Z	8
Formula weight	807.8
Density(calc.)	1.513 Mg/m^3
Absorption Coefficient	3.973 mm^{-1}
F(000)	3248
Data Collection	
Diffractometer Used	Nicolet R3m/V
Radiation	MoK_α (λ = 0.71073 Å)
Temperature (K)	298
Monochromator	Highly oriented graphite crystal
2θ Range	3.5 to 55.0°
Scan Type	ω
Scan Speed	Variable; 3.00 to 15.00°/min. in ω
Scan Range (ω)	0.60°
Background Measurement	Stationary crystal and stationary counter at beginning and end of scan, each for 25.0% of total scan time
Standard Reflections	3 measured every 200 reflections
Index Ranges	0 < h < 15, 0 < k < 23, 0 < l < 43
Reflections Collected	8212
Independent reflections	7449 (R_{int} = 0.00%)
Observed Reflections	4878 ($F > 3.0\sigma(F)$)
Absorption Correction	Semi-empirical
Min./Max. Transmission	0.2177 / 0.7076
Solution and Refinement	
System Used	Nicolet SHELXTL PLUS (MicroVAX II)
Solution	Heavy Atom Methods
Refinement Method	Full-Matrix Least-Squares
Quantity Minimized	$\Sigma w(F_o-F_c)^2$
Absolute Configuration	N/A
Extinction Correction	χ = 0.000030(9), where $F^* = F\ [\ 1 + 0.002\chi F^2/\sin(2\theta)\ ]^{-1/4}$
Hydrogen Atoms	Riding model, fixed isotropic U
Weighting Scheme	$w^{-1} = \sigma^2(F) + 0.0004F^2$
Final R indices (obs. data)	R = 6.20 %, wR = 6.28 %
R Indicies (all data)	R = 10.33 %, wR = 6.80 %
Goodness-of-Fit	1.77
Largest and Mean Δ/σ	0.019, 0.000
Data-to-Parameter Ratio	14.2:1
Largest Difference Peak	2.21 $eÅ^{-3}$
Largest Difference Hole	-1.87 $eÅ^{-3}$

Table 1. Atomic coordinates ($x10^4$) and equivalent isotropic displacement coefficients ($Å^2 x10^3$)

	x	y	z	U(eq)
Ir(1)	1776(1)	2222(1)	1119(1)	39(1)
P(1)	281(3)	3031(1)	928(1)	47(1)
C(1A)	-375(11)	3591(6)	1305(3)	71(5)
C(1B)	591(11)	3744(5)	560(3)	65(5)
C(1C)	-991(11)	2579(6)	727(4)	78(5)
P(2)	3321(3)	1516(1)	1373(1)	57(1)
C(2A)	3499(11)	1533(7)	1914(4)	80(5)
C(2B)	4750(10)	1778(6)	1218(4)	74(5)
C(2C)	3334(12)	520(5)	1287(4)	85(6)
P(3)	2023(3)	1703(1)	470(1)	51(1)
C(3A)	1455(12)	2129(6)	18(3)	80(6)
C(3B)	3439(10)	1485(6)	300(3)	65(5)
C(3C)	1286(12)	819(5)	439(4)	78(5)
C(61)	2951(8)	3050(5)	1025(3)	39(3)
C(62)	3218(10)	3310(5)	642(3)	52(4)
C(63)	4052(10)	3834(5)	573(3)	54(4)
C(64)	4701(10)	4097(5)	882(4)	61(4)
C(65)	4451(10)	3864(5)	1265(3)	56(4)
C(66)	3594(9)	3354(5)	1331(3)	53(4)
C(1)	-101(10)	1336(5)	1771(3)	50(4)
C(2)	532(8)	2031(4)	1905(3)	42(3)
C(3)	1293(9)	2462(5)	1708(3)	45(3)
C(4)	1660(9)	3122(4)	1938(3)	45(3)
C(5)	2038(8)	3118(5)	2305(3)	46(4)
C(6)	2412(10)	3773(5)	2547(3)	51(4)
C(7)	-1392(14)	1453(6)	1800(4)	106(7)
C(8)	220(14)	704(5)	2046(4)	96(7)
C(9)	230(11)	1130(5)	1350(3)	64(4)
C(10)	1930(10)	3726(7)	2966(3)	75(5)
C(11)	3732(13)	3754(7)	2589(4)	96(6)
C(12)	2082(10)	4510(5)	2365(4)	70(5)
P(4)	7139(3)	443(2)	591(1)	71(1)
F(1)	7494(19)	524(13)	994(5)	287(13)
F(2)	5933(9)	327(5)	747(5)	184(7)
F(3)	6830(14)	365(8)	155(4)	223(9)
F(4)	8416(9)	520(6)	488(5)	187(8)
F(5)	6960(11)	1271(4)	566(6)	228(10)
F(6)	7276(9)	-412(4)	573(3)	129(5)

* Equivalent isotropic U defined as one third of the trace of the orthogonalized U_{ij} tensor

Table 2. Bond lengths (Å)

Ir(1)-P(1)	2.363	(3)	C(65)-C(66)	1.377	(15)
Ir(1)-P(2)	2.366	(3)	C(1)-C(2)	1.523	(13)
Ir(1)-P(3)	2.398	(3)	C(1)-C(7)	1.523	(20)
Ir(1)-C(61)	2.053	(9)	C(1)-C(8)	1.515	(14)
Ir(1)-C(3)	2.109	(10)	C(1)-C(9)	1.516	(15)
P(1)-C(1A)	1.796	(12)	C(2)-C(3)	1.352	(13)
P(1)-C(1B)	1.822	(10)	C(3)-C(4)	1.485	(12)
P(1)-C(1C)	1.824	(13)	C(4)-C(5)	1.314	(13)
P(2)-C(2A)	1.838	(13)	C(5)-C(6)	1.503	(13)
P(2)-C(2B)	1.809	(12)	C(6)-C(10)	1.521	(16)
P(2)-C(2C)	1.820	(10)	C(6)-C(11)	1.546	(20)
P(3)-C(3A)	1.831	(12)	C(6)-C(12)	1.513	(14)
P(3)-C(3B)	1.790	(12)	P(4)-F(1)	1.429	(16)
P(3)-C(3C)	1.816	(11)	P(4)-F(2)	1.514	(12)
C(61)-C(62)	1.409	(14)	P(4)-F(3)	1.523	(15)
C(61)-C(66)	1.390	(14)	P(4)-F(4)	1.534	(12)
C(62)-C(63)	1.378	(14)	P(4)-F(5)	1.511	(9)
C(63)-C(64)	1.374	(17)	P(4)-F(6)	1.551	(8)
C(64)-C(65)	1.389	(17)			

Table 3. Bond angles (°)

P(1)-Ir(1)-P(2)	173.1(1)	C(64)-C(65)-C(66)	120.2(10)
P(1)-Ir(1)-P(3)	94.4(1)	C(61)-C(66)-C(65)	122.5(10)
P(2)-Ir(1)-P(3)	91.8(1)	C(2)-C(1)-C(7)	110.4(8)
P(1)-Ir(1)-C(61)	90.0(3)	C(2)-C(1)-C(8)	108.6(9)
P(2)-Ir(1)-C(61)	86.5(3)	C(7)-C(1)-C(8)	108.0(10)
P(3)-Ir(1)-C(61)	93.6(3)	C(2)-C(1)-C(9)	110.8(8)
P(1)-Ir(1)-C(3)	86.4(3)	C(7)-C(1)-C(9)	110.0(10)
P(2)-Ir(1)-C(3)	88.3(3)	C(8)-C(1)-C(9)	109.0(8)
P(3)-Ir(1)-C(3)	166.3(3)	C(1)-C(2)-C(3)	130.3(9)
C(61)-Ir(1)-C(3)	100.1(4)	Ir(1)-C(3)-C(2)	121.1(7)
Ir(1)-P(1)-C(1A)	117.7(4)	Ir(1)-C(3)-C(4)	125.3(7)
Ir(1)-P(1)-C(1B)	118.4(4)	C(2)-C(3)-C(4)	113.4(8)
C(1A)-P(1)-C(1B)	99.7(5)	C(3)-C(4)-C(5)	125.7(8)
Ir(1)-P(1)-C(1C)	115.2(4)	C(4)-C(5)-C(6)	127.4(8)
C(1A)-P(1)-C(1C)	99.8(6)	C(5)-C(6)-C(10)	110.8(9)
C(1B)-P(1)-C(1C)	103.0(6)	C(5)-C(6)-C(11)	108.8(9)
Ir(1)-P(2)-C(2A)	116.0(4)	C(10)-C(6)-C(11)	106.3(9)
Ir(1)-P(2)-C(2B)	117.1(4)	C(5)-C(6)-C(12)	113.3(9)
C(2A)-P(2)-C(2B)	100.2(6)	C(10)-C(6)-C(12)	109.4(9)
Ir(1)-P(2)-C(2C)	118.6(4)	C(11)-C(6)-C(12)	108.0(9)
C(2A)-P(2)-C(2C)	99.9(6)	F(1)-P(4)-F(2)	87.4(11)
C(2B)-P(2)-C(2C)	101.9(6)	F(1)-P(4)-F(3)	176.8(11)
Ir(1)-P(3)-C(3A)	123.6(4)	F(2)-P(4)-F(3)	95.8(8)
Ir(1)-P(3)-C(3B)	119.1(4)	F(1)-P(4)-F(4)	85.6(11)
C(3A)-P(3)-C(3B)	99.2(6)	F(2)-P(4)-F(4)	172.3(8)
Ir(1)-P(3)-C(3C)	109.8(4)	F(3)-P(4)-F(4)	91.2(9)
C(3A)-P(3)-C(3C)	98.6(5)	F(1)-P(4)-F(5)	89.7(12)
C(3B)-P(3)-C(3C)	103.1(5)	F(2)-P(4)-F(5)	91.6(6)
Ir(1)-C(61)-C(62)	122.1(7)	F(3)-P(4)-F(5)	90.1(9)
Ir(1)-C(61)-C(66)	122.2(7)	F(4)-P(4)-F(5)	91.7(7)
C(62)-C(61)-C(66)	115.6(9)	F(1)-P(4)-F(6)	96.3(11)
C(61)-C(62)-C(63)	122.5(10)	F(2)-P(4)-F(6)	88.3(5)
C(62)-C(63)-C(64)	120.0(10)	F(3)-P(4)-F(6)	84.0(7)
C(63)-C(64)-C(65)	119.1(10)	F(4)-P(4)-F(6)	89.1(6)
		F(5)-P(4)-F(6)	174.1(9)

Table 4. Anisotropic displacement coefficients ($Å^2 x 10^3$)

	U_{11}	U_{22}	U_{33}	U_{23}	U_{13}	U_{12}
Ir(1)	50(1)	31(1)	37(1)	0(1)	6(1)	1(1)
P(1)	54(2)	44(1)	42(1)	2(1)	0(1)	3(1)
C(1A)	70(10)	84(7)	59(7)	-6(6)	2(7)	38(6)
C(1B)	81(10)	49(5)	64(8)	17(5)	4(7)	7(5)
C(1C)	70(11)	78(7)	87(10)	10(7)	-9(8)	-17(7)
P(2)	67(2)	49(1)	56(2)	3(1)	8(2)	18(1)
C(2A)	79(11)	97(8)	65(8)	8(7)	-6(7)	46(7)
C(2B)	30(7)	92(8)	101(11)	-7(7)	-8(7)	16(6)
C(2C)	104(12)	45(5)	106(10)	13(6)	21(9)	29(6)
P(3)	64(2)	45(1)	45(2)	-8(1)	13(1)	-12(1)
C(3A)	100(13)	85(8)	55(7)	-8(6)	16(7)	-5(7)
C(3B)	61(10)	79(7)	54(7)	-15(5)	9(6)	-10(6)
C(3C)	110(12)	52(6)	71(8)	-20(5)	30(8)	-21(6)
C(61)	18(6)	46(4)	51(6)	4(4)	7(4)	2(3)
C(62)	70(8)	39(4)	49(6)	1(4)	1(6)	2(5)
C(63)	46(8)	50(5)	66(7)	6(5)	16(6)	0(5)
C(64)	46(8)	49(5)	87(9)	-1(6)	11(7)	-10(5)
C(65)	39(7)	62(6)	67(7)	-10(5)	-6(6)	-8(5)
C(66)	48(8)	57(6)	54(7)	1(5)	-4(6)	-4(5)
C(1)	56(8)	43(5)	50(6)	2(4)	22(6)	-9(4)
C(2)	34(6)	50(5)	43(5)	-5(4)	-7(5)	7(4)
C(3)	59(7)	35(4)	40(5)	-7(4)	8(5)	1(4)
C(4)	63(8)	38(4)	34(5)	-5(4)	4(5)	7(4)
C(5)	47(8)	49(5)	42(6)	1(4)	-2(5)	8(4)
C(6)	43(8)	59(5)	51(6)	-9(5)	-3(6)	4(5)
C(7)	164(18)	74(8)	79(10)	-20(7)	36(11)	-35(9)
C(8)	152(16)	53(6)	83(10)	18(6)	36(10)	-10(8)
C(9)	85(10)	54(5)	53(7)	-5(5)	11(7)	-18(6)
C(10)	59(10)	105(9)	60(8)	-20(7)	1(7)	3(7)
C(11)	107(13)	111(10)	69(10)	-18(8)	-12(9)	14(9)
C(12)	56(9)	68(6)	85(9)	-16(6)	-3(7)	-8(5)
P(4)	64(3)	61(2)	89(3)	-8(2)	5(2)	-5(1)
F(1)	227(20)	509(30)	126(11)	-82(16)	-52(14)	-60(22)
F(2)	109(10)	107(6)	335(18)	-64(8)	112(11)	-24(6)
F(3)	266(21)	263(16)	142(11)	20(10)	-104(12)	55(12)
F(4)	85(10)	163(10)	313(19)	-4(10)	62(11)	-26(6)
F(5)	168(13)	55(5)	460(27)	16(8)	59(14)	2(6)
F(6)	143(9)	81(5)	163(10)	-22(5)	0(8)	19(5)

The anisotropic displacement exponent takes the form:
$-2\pi^2(h^2a^{*2}U_{11} + \ldots + 2hka^*b^*U_{12})$

Table 5. H-Atom coordinates ($x10^4$) and isotropic displacement coefficients ($Å^2x10^3$)

	x	y	z	U
H(1AA)	-965	3893	1190	80
H(1AB)	-706	3274	1504	80
H(1AC)	193	3903	1425	80
H(1BA)	-79	4036	507	80
H(1BB)	1189	4058	660	80
H(1BC)	845	3509	321	80
H(1CA)	-1539	2955	660	80
H(1CB)	-789	2303	494	80
H(1CC)	-1319	2250	920	80
H(2AA)	4145	1230	1984	80
H(2AB)	3628	2032	2002	80
H(2AC)	2821	1341	2039	80
H(2BA)	5300	1454	1339	80
H(2BB)	4806	1737	935	80
H(2BC)	4902	2281	1296	80
H(2CA)	4012	320	1407	80
H(2CB)	2668	300	1406	80
H(2CC)	3341	414	1008	80
H(3AA)	1652	1828	-206	80
H(3AB)	635	2171	37	80
H(3AC)	1783	2613	-12	80
H(3BA)	3395	1284	37	80
H(3BB)	3898	1927	296	80
H(3BC)	3783	1127	473	80
H(3CA)	1387	614	179	80
H(3CB)	1588	481	633	80
H(3CC)	483	897	489	80
H(62A)	2808	3105	420	80
H(63A)	4175	4021	310	80
H(64A)	5327	4431	834	80
H(65A)	4874	4063	1484	80
H(66A)	3432	3200	1597	80
H(2A)	357	2189	2170	80
H(4A)	1602	3595	1808	80
H(5A)	2105	2641	2428	80
H(7A)	-1609	1848	1625	80
H(7B)	-1783	1007	1724	80
H(7C)	-1598	1580	2067	80
H(8A)	-166	261	1963	80
H(8B)	1034	623	2042	80
H(8C)	-20	832	2310	80
H(9A)	36	1531	1176	80
H(9B)	1040	1038	1337	80
H(9C)	-178	692	1271	80
H(10A)	1109	3742	2951	80
H(10B)	2166	3270	3088	80
H(10C)	2197	4137	3122	80
H(11A)	4070	3783	2329	80
H(11B)	3989	4164	2746	80
H(11C)	3958	3297	2712	80
H(12A)	2403	4539	2104	80
H(12B)	1262	4546	2350	80
H(12C)	2373	4910	2524	80

STRUCTURE DETERMINATION SUMMARY

Crystal Data	
Empirical Formula	C_{33} H_{48} F_6 Ir N_3 O P_4
Color; Habit	purple irregular prism
Crystal Size (mm)	0.2 x 0.2 x 0.2
Crystal System	Triclinic
Space Group	P-1
Unit Cell Dimensions	a = 12.060(3) Å
	b = 12.512(3) Å
	c = 14.833(3) Å
	α = 87.25(2)°
	β = 73.21(2)°
	γ = 69.93(2)°
Volume	2009.4(9) $Å^3$
Z	2
Formula weight	932.8
Density(calc.)	1.542 Mg/m^3
Absorption Coefficient	3.521 mm^{-1}
F(000)	932
Data Collection	
Diffractometer Used	Siemens R3m/V
Radiation	MoKα (λ = 0.71073 Å)
Temperature (K)	298
Monochromator	Highly oriented graphite crystal
2θ Range	3.5 to 45.0°
Scan Type	Wyckoff
Scan Speed	Variable; 3.00 to 14.65°/min. in ω
Scan Range (ω)	0.60°
Background Measurement	Stationary crystal and stationary counter at beginning and end of scan each for 25.0% of total scan time
Standard Reflections	2 measured every 300 reflections
Index Ranges	$0 < h < 12$, $-12 < k < 13$, $-15 < l <$
Reflections Collected	5554
Independent Reflections	5251 (R_{int} = 2.38%)
Observed Reflections	4376 ($F > 3.0\sigma(F)$)
Absorption Correction	Semi-empirical
Min./Max. Transmission	0.7940 / 1.0000
Solution and Refinement	
System UsedSiemens	SHELXTL PLUS (VMS)
Solution	Direct Methods
Refinement Method	Full-Matrix Least-Squares
Quantity Minimized	$\Sigma w(Fo-Fc)^2$
Absolute Structure	N/A
Extinction Correction	χ = -0.00016(5), where $F^* = F [1 + 0.002\chi F^2/\sin(2\theta)]^{-1/4}$
Hydrogen Atoms	Riding model, fixed isotropic U
Weighting Scheme	$w-1 = \sigma^2(F) + 0.0008F^2$
Number of Parameters refined	434
Final R indices (obs. data)	R = 4.69 %, wR = 5.12 %
R Indices (all data)	R = 5.95 %, wR = 5.34 %
Goodness-of-Fit 1.16	
Largest and Mean Δ/σ	3.309, 0.024
Data-to-Parameter Ratio	10.1:1
Largest Difference Peak	1.11 eÅ-3
Largest Difference Hole	-1.31 eÅ-3

Table 1. Atomic coordinates ($x10^4$) and equivalent isotropic displacement coefficients ($Å^2x10^3$)

	x	y	z	U(eq)
Ir(1)	2092(1)	1455(1)	2895(1)	38(1)
P(1)	2002(2)	1625(3)	4475(2)	53(1)
C(1A)	3362(12)	1439(17)	4773(10)	137(11)
C(1B)	1032(20)	2908(15)	5081(10)	198(15)
C(1C)	1381(16)	679(16)	5243(9)	145(13)
P(2)	3211(3)	-519(2)	2776(2)	59(1)
C(2A)	4168(16)	-1212(13)	1628(12)	141(11)
C(2B)	2350(13)	-1426(11)	3223(14)	142(11)
C(2C)	4474(13)	-1047(11)	3289(13)	125(9)
P(3)	1895(3)	1450(2)	1371(2)	53(1)
C(3A)	1149(13)	499(13)	1143(9)	100(8)
C(3B)	889(14)	2775(12)	1079(9)	119(9)
C(3C)	3239(10)	1184(12)	377(8)	82(6)
C(1)	312(8)	1392(8)	3360(7)	51(4)
C(2)	-615(8)	2442(8)	3551(7)	50(4)
C(3)	-193(8)	3413(9)	3372(7)	52(4)
C(4)	1054(9)	3138(8)	3035(6)	46(4)
C(5)	3503(9)	2164(8)	2398(7)	51(5)
C(6)	4692(8)	1660(9)	1863(7)	52(4)
C(7)	-1931(9)	2605(9)	3913(8)	54(5)
C(8)	-2474(10)	1970(11)	3570(9)	73(6)
C(9)	-3728(13)	2198(14)	3942(12)	102(9)
C(10)	-4405(12)	3029(14)	4629(12)	102(8)
C(11)	-3786(12)	3618(12)	4916(11)	95(7)
C(12)	1728(9)	3909(8)	2824(6)	48(4)
C(13)	1203(10)	5100(9)	2888(9)	72(6)
C(14)	1941(11)	5747(10)	2780(10)	90(7)
C(15)	3175(12)	5209(10)	2656(10)	89(7)
C(16)	3698(10)	4060(10)	2538(7)	63(5)
C(17)	5567(9)	2124(9)	1203(7)	52(5)
C(18)	6813(9)	1648(10)	1076(8)	69(5)
C(19)	7615(12)	2050(14)	410(10)	90(7)
C(20)	7132(16)	2923(14)	-107(11)	99(9)
C(21)	5887(15)	3359(12)	34(9)	94(8)
N(1)	-2607(8)	3455(8)	4576(7)	73(5)
N(2)	2980(7)	3403(6)	2569(6)	50(4)
N(3)	5095(9)	2990(9)	685(7)	76(5)
P(4)	1233(4)	1767(3)	-1953(2)	83(2)
F(1)	387(12)	2829(10)	-1303(8)	191(8)
F(2)	867(11)	1016(11)	-1141(7)	168(8)
F(3)	2100(11)	732(10)	-2626(8)	182(7)
F(4)	1559(12)	2525(11)	-2774(7)	174(8)
F(5)	165(10)	1757(12)	-2331(8)	184(8)
F(6)	2293(9)	1750(11)	-1574(7)	165(7)
C(1S)	7297(24)	5017(27)	2384(21)	403(38)
C(2S)	6660(18)	5495(16)	1792(19)	150(13)
C(3S)	7409(24)	5624(20)	837(20)	253(27)
O(1S)	5612(14)	5891(15)	2007(15)	223(13)

* Equivalent isotropic U defined as one third of the trace of the orthogonalized U_{ij} tensor

Table 2. Bond lengths (Å)

Ir(1)-P(1)	2.332	(3)
Ir(1)-P(2)	2.360	(3)
Ir(1)-P(3)	2.341	(3)
Ir(1)-C(1)	2.085	(10)
Ir(1)-C(4)	2.032	(8)
Ir(1)-C(5)	2.115	(12)
P(1)-C(1A)	1.757	(17)
P(1)-C(1B)	1.731	(15)
P(1)-C(1C)	1.801	(20)
P(2)-C(2A)	1.818	(15)
P(2)-C(2B)	1.773	(17)
P(2)-C(2C)	1.806	(18)
P(3)-C(3A)	1.813	(19)
P(3)-C(3B)	1.806	(14)
P(3)-C(3C)	1.791	(10)
C(1)-C(2)	1.378	(12)
C(2)-C(3)	1.456	(17)
C(2)-C(7)	1.465	(14)
C(3)-C(4)	1.364	(13)
C(4)-C(12)	1.431	(16)
C(5)-C(6)	1.362	(12)
C(5)-N(2)	1.463	(12)
C(6)-C(17)	1.477	(15)
C(7)-C(8)	1.381	(21)
C(7)-N(1)	1.343	(13)
C(8)-C(9)	1.382	(18)
C(9)-C(10)	1.351	(22)
C(10)-C(11)	1.369	(27)
C(11)-N(1)	1.309	(17)
C(12)-C(13)	1.401	(13)
C(12)-N(2)	1.363	(12)
C(13)-C(14)	1.368	(20)
C(14)-C(15)	1.366	(18)
C(15)-C(16)	1.354	(16)
C(16)-N(2)	1.375	(17)
C(17)-C(18)	1.371	(14)
C(17)-N(3)	1.355	(14)
C(18)-C(19)	1.378	(19)
C(19)-C(20)	1.364	(22)
C(20)-C(21)	1.365	(25)
C(21)-N(3)	1.336	(19)
P(4)-F(1)	1.537	(11)
P(4)-F(2)	1.549	(12)
P(4)-F(3)	1.535	(11)
P(4)-F(4)	1.551	(12)
P(4)-F(5)	1.550	(15)
P(4)-F(6)	1.532	(14)
C(1S)-C(2S)	1.321	(42)
C(2S)-C(3S)	1.480	(36)
C(2S)-O(1S)	1.139	(24)

Table 3. Bond angles (°)

P(1)-Ir(1)-P(2)	92.6(1)	C(2)-C(7)-C(8)	122.8(9)
P(1)-Ir(1)-P(3)	172.0(1)	C(2)-C(7)-N(1)	116.0(11)
P(2)-Ir(1)-P(3)	93.2(1)	C(8)-C(7)-N(1)	121.1(10)
P(1)-Ir(1)-C(1)	87.6(3)	C(7)-C(8)-C(9)	118.8(12)
P(2)-Ir(1)-C(1)	98.7(3)	C(8)-C(9)-C(10)	120.3(18)
P(3)-Ir(1)-C(1)	86.2(3)	C(9)-C(10)-C(11)	116.6(13)
P(1)-Ir(1)-C(4)	86.5(3)	C(10)-C(11)-N(1)	125.8(13)
P(2)-Ir(1)-C(4)	177.2(3)	C(4)-C(12)-C(13)	125.4(9)
P(3)-Ir(1)-C(4)	87.3(3)	C(4)-C(12)-N(2)	115.0(8)
C(1)-Ir(1)-C(4)	78.6(4)	C(13)-C(12)-N(2)	119.6(10)
P(1)-Ir(1)-C(5)	94.3(3)	C(12)-C(13)-C(14)	119.8(10)
P(2)-Ir(1)-C(5)	102.6(2)	C(13)-C(14)-C(15)	118.7(11)
P(3)-Ir(1)-C(5)	89.7(3)	C(14)-C(15)-C(16)	121.6(14)
C(1)-Ir(1)-C(5)	158.5(4)	C(15)-C(16)-N(2)	120.1(11)
C(4)-Ir(1)-C(5)	80.1(4)	C(6)-C(17)-C(18)	121.1(9)
Ir(1)-P(1)-C(1A)	119.4(5)	C(6)-C(17)-N(3)	117.2(9)
Ir(1)-P(1)-C(1B)	116.5(6)	C(18)-C(17)-N(3)	121.6(10)
C(1A)-P(1)-C(1B)	101.3(10)	C(17)-C(18)-C(19)	120.0(11)
Ir(1)-P(1)-C(1C)	115.7(6)	C(18)-C(19)-C(20)	118.1(13)
C(1A)-P(1)-C(1C)	101.9(9)	C(19)-C(20)-C(21)	119.9(15)
C(1B)-P(1)-C(1C)	98.9(8)	C(20)-C(21)-N(3)	122.8(13)
Ir(1)-P(2)-C(2A)	119.4(5)	C(7)-N(1)-C(11)	117.4(13)
Ir(1)-P(2)-C(2B)	116.7(4)	C(5)-N(2)-C(12)	118.3(9)
C(2A)-P(2)-C(2B)	102.3(8)	C(5)-N(2)-C(16)	122.4(8)
Ir(1)-P(2)-C(2C)	119.4(5)	C(12)-N(2)-C(16)	119.2(8)
C(2A)-P(2)-C(2C)	92.7(8)	C(17)-N(3)-C(21)	117.7(11)
C(2B)-P(2)-C(2C)	102.4(8)	F(1)-P(4)-F(2)	88.9(6)
Ir(1)-P(3)-C(3A)	115.4(4)	F(1)-P(4)-F(3)	177.9(7)
Ir(1)-P(3)-C(3B)	114.7(5)	F(2)-P(4)-F(3)	93.1(6)
C(3A)-P(3)-C(3B)	99.2(8)	F(1)-P(4)-F(4)	90.8(6)
Ir(1)-P(3)-C(3C)	119.3(5)	F(2)-P(4)-F(4)	178.1(8)
C(3A)-P(3)-C(3C)	104.4(6)	F(3)-P(4)-F(4)	87.3(6)
C(3B)-P(3)-C(3C)	101.0(6)	F(1)-P(4)-F(5)	91.4(8)
Ir(1)-C(1)-C(2)	114.7(8)	F(2)-P(4)-F(5)	90.7(8)
C(1)-C(2)-C(3)	114.8(9)	F(3)-P(4)-F(5)	89.2(7)
C(1)-C(2)-C(7)	124.2(10)	F(4)-P(4)-F(5)	87.5(8)
C(3)-C(2)-C(7)	121.0(8)	F(1)-P(4)-F(6)	89.4(7)
C(2)-C(3)-C(4)	114.8(8)	F(2)-P(4)-F(6)	88.3(7)
Ir(1)-C(4)-C(3)	117.0(8)	F(3)-P(4)-F(6)	90.1(7)
Ir(1)-C(4)-C(12)	115.7(6)	F(4)-P(4)-F(6)	93.5(8)
C(3)-C(4)-C(12)	127.1(8)	F(5)-P(4)-F(6)	178.8(8)
Ir(1)-C(5)-C(6)	129.3(8)	C(1S)-C(2S)-C(3S)	115.1(21)
Ir(1)-C(5)-N(2)	109.7(6)	C(1S)-C(2S)-O(1S)	123.8(26)
C(6)-C(5)-N(2)	120.2(10)	C(3S)-C(2S)-O(1S)	120.7(26)
C(5)-C(6)-C(17)	131.9(9)		

Table 4. Anisotropic displacement coefficients ($Å^2 x 10^3$)

	U_{11}	U_{22}	U_{33}	U_{12}	U_{13}	U_{23}
Ir(1)	35(1)	40(1)	36(1)	-15(1)	-5(1)	2(1)
P(1)	48(2)	65(2)	44(2)	-23(1)	-9(1)	5(1)
C(1A)	65(9)	260(23)	88(11)	-50(12)	-27(8)	-20(12)
C(1B)	318(29)	144(17)	65(10)	32(17)	-87(14)	-29(10)
C(1C)	185(17)	269(24)	56(9)	-168(18)	-43(10)	49(11)
P(2)	60(2)	43(2)	67(2)	-15(1)	-12(1)	8(1)
C(2A)	158(16)	77(11)	144(16)	3(11)	-26(13)	-23(10)
C(2B)	84(11)	56(9)	260(23)	-23(8)	-14(12)	35(11)
C(2C)	91(11)	62(9)	208(19)	2(8)	-62(12)	26(10)
P(3)	53(2)	60(2)	42(2)	-19(1)	-10(1)	1(1)
C(3A)	115(11)	142(13)	65(8)	-64(10)	-32(8)	-16(8)
C(3B)	150(14)	100(11)	68(9)	23(10)	-51(9)	0(8)
C(3C)	68(8)	117(11)	55(7)	-38(8)	-3(6)	5(7)
C(1)	39(6)	49(6)	62(7)	-17(5)	-8(5)	3(5)
C(2)	38(6)	55(7)	54(6)	-20(5)	-8(5)	5(5)
C(3)	36(6)	55(6)	58(6)	-13(5)	-8(5)	6(5)
C(4)	47(6)	43(6)	46(6)	-21(5)	-5(5)	3(5)
C(5)	54(7)	48(6)	53(6)	-23(5)	-13(5)	8(5)
C(6)	37(6)	55(6)	59(6)	-16(5)	-5(5)	5(5)
C(7)	43(6)	56(7)	65(7)	-16(5)	-24(5)	16(6)
C(8)	55(7)	85(9)	90(9)	-34(7)	-27(6)	19(7)
C(9)	68(10)	123(13)	143(14)	-60(9)	-45(10)	32(11)
C(10)	40(8)	115(13)	126(13)	-17(8)	-2(8)	27(10)
C(11)	59(9)	86(10)	118(12)	-18(8)	2(8)	4(8)
C(12)	45(6)	47(6)	41(6)	-14(5)	3(5)	-4(4)
C(13)	56(7)	37(6)	106(10)	-9(6)	-8(6)	3(6)
C(14)	64(9)	35(6)	146(13)	-15(6)	3(8)	3(7)
C(15)	73(9)	61(8)	128(12)	-47(7)	10(8)	-21(8)
C(16)	53(7)	66(8)	70(7)	-33(6)	1(5)	-5(6)
C(17)	49(7)	51(6)	56(6)	-26(5)	-1(5)	-5(5)
C(18)	40(6)	87(9)	70(8)	-23(6)	0(6)	-5(6)
C(19)	50(7)	117(12)	95(10)	-46(8)	14(7)	-21(9)
C(20)	113(13)	94(11)	89(11)	-66(10)	13(10)	-3(9)
C(21)	113(12)	79(10)	77(9)	-42(9)	0(9)	16(7)
N(1)	37(5)	80(7)	85(7)	-15(5)	4(5)	2(6)
N(2)	50(5)	46(5)	55(5)	-27(4)	-1(4)	-7(4)
N(3)	76(7)	77(7)	67(6)	-35(6)	-1(5)	13(5)
P(4)	96(3)	104(3)	50(2)	-29(2)	-30(2)	9(2)
F(1)	207(12)	156(10)	143(9)	5(9)	-25(8)	-45(8)
F(2)	190(11)	215(12)	122(8)	-101(9)	-51(7)	75(8)
F(3)	191(11)	172(10)	136(9)	15(8)	-60(8)	-47(8)
F(4)	249(13)	209(12)	107(7)	-126(11)	-70(8)	77(8)
F(5)	148(9)	287(15)	168(10)	-98(10)	-102(8)	45(10)
F(6)	127(8)	278(14)	126(8)	-80(9)	-73(7)	8(8)
C(1S)	199(32)	526(67)	460(59)	-93(35)	-153(36)	379(55)
C(2S)	78(12)	111(14)	280(28)	-59(11)	-61(16)	88(16)
C(3S)	252(34)	162(24)	404(52)	-139(25)	-105(33)	45(26)
O(1S)	94(10)	217(17)	377(26)	-75(11)	-87(13)	116(16)

The anisotropic displacement exponent takes the form:
$-2\pi^2(h^2a^*2U_{11} + \ldots + 2hka^*b^*U_{12})$

Table 5. H-Atom coordinates ($x10^4$) and isotropic displacement coefficients ($Å^2x10^3$)

	x	y	z	U
H(1AA)	3177	1533	5445	80
H(1AB)	3946	691	4558	80
H(1AC)	3705	2000	4476	80
H(1BA)	1061	2897	5722	80
H(1BB)	1258	3532	4783	80
H(1BC)	211	3000	5074	80
H(1CA)	1378	809	5876	80
H(1CB)	553	806	5231	80
H(1CC)	1889	-92	5024	80
H(2AA)	4569	-2010	1685	80
H(2AB)	3649	-1118	1224	80
H(2AC)	4778	-865	1361	80
H(2BA)	2898	-2203	3139	80
H(2BB)	1927	-1237	3881	80
H(2BC)	1759	-1330	2882	80
H(2CA)	4848	-1860	3190	80
H(2CB)	5079	-699	3008	80
H(2CC)	4155	-846	3954	80
H(3AA)	1106	552	505	80
H(3AB)	1625	-266	1235	80
H(3AC)	331	698	1569	80
H(3BA)	862	2704	445	80
H(3BB)	78	2931	1508	80
H(3BC)	1177	3388	1135	80
H(3CA)	3008	1213	-193	80
H(3CB)	3614	1748	381	80
H(3CC)	3817	441	409	80
H(1A)	149	689	3438	80
H(3A)	-748	4188	3476	80
H(6A)	5013	852	1925	80
H(8A)	-1979	1388	3077	80
H(9A)	-4114	1763	3707	80
H(10A)	-5275	3186	4896	80
H(11A)	-4252	4204	5410	80
H(13A)	331	5457	2988	80
H(14A)	1594	6563	2809	80
H(15A)	3684	5657	2642	80
H(16A)	4569	3698	2443	80
H(18A)	7117	1025	1445	80
H(19A)	8490	1727	310	80
H(20A)	7673	3231	-561	80
H(21A)	5563	3954	-351	80
H(1SA)	6729	4996	2985	80
H(1SB)	7849	4258	2166	80
H(1SC)	7762	5482	2447	80
H(3SA)	6843	5950	474	80
H(3SB)	7875	6110	842	80
H(3SC)	7961	4886	560	80

STRUCTURE DETERMINATION SUMMARY

Crystal Data

Empirical Formula	C_{30} H_{66} Cl F_6 Ir_2 P_7
Color; Habit	Clear rectangular prism
Crystal Size (mm)	0.2 x 0.2 x 0.3
Crystal System	Monoclinic
Space Group	$P2_1$
Unit Cell Dimensions	a = 10.323(2) Å b = 19.337(5) Å c = 12.204(2) Å β = 110.090(10)°
Volume	2288.0(8) $Å^3$
Z	2
Formula weight	1177.5
Density(calc.)	1.709 Mg/m^3
Absorption Coefficient	6.133 mm^{-1}
F(000)	1152

Data Collection

Diffractometer Used	Siemens R3m/V
Radiation	MoK_α (λ = 0.71073 Å)
Temperature (K)	298
Monochromator	Highly oriented graphite crystal
2θ Range	3.5 to 50.0°
Scan Type	2θ-θ
Scan Speed	Variable; 3.00 to 14.65°/min. in ω
Scan Range (ω)	0.60° plus K_α-separation
Background Measurement	Stationary crystal and stationary counter at beginning and end of scan, each for 25.0% of total scan time
Standard Reflections	3 measured every 300 reflections
Index Ranges	$-12 < h < 0$, $0 < k < 22$, $-13 < l < 14$
Reflections Collected	4429
Independent Reflections	4176 (R_{int} = 1.86%)
Observed Reflections	3537 ($F > 3.0\sigma(F)$)
Absorption Correction	Semi-empirical
Min./Max. Transmission	0.6693 / 0.9924

Solution and Refinement

System UsedSiemens	SHELXTL PLUS (VMS)
Solution	Direct Methods
Refinement Method	Full-Matrix Least-Squares
Quantity Minimized	$\Sigma w(F_o-F_c)^2$
Absolute Structure	η = 0.11(6)
Extinction Correction	χ = 0.00020(2), where $F^* = F\ [\ 1 + 0.002\chi F^2/\sin(2\theta)\ ]^{-1/4}$
Hydrogen Atoms	Riding model, fixed isotropic U
Weighting Scheme	$w^{-1} = \sigma^2(F) + 0.0004F^2$
Number of Parameters refined	416
Final R indices (obs. data)	R = 4.06 %, wR = 3.81 %
R Indices (all data)	R = 5.39 %, wR = 4.07 %
Goodness-of-Fit	1.07
Largest and Mean Δ/σ	0.030, 0.005
Data-to-Parameter Ratio	8.5:1
Largest Difference Peak	1.27 $eÅ^{-3}$
Largest Difference Hole	-0.59 $eÅ^{-3}$

Table 1. Atomic coordinates ($x10^4$) and equivalent isotropic displacement coefficients ($Å^2 x10^3$)

	x	y	z	U(eq)
Ir(1)	206(1)	31	-1358(1)	43(1)
P(1)	-1564(6)	-791(3)	-1992(4)	62(2)
C(11)	-1315(20)	-1655(9)	-1352(17)	79(9)
C(12)	-3203(16)	-559(10)	-1809(18)	89(9)
C(13)	-2150(27)	-964(12)	-3547(15)	121(13)
P(2)	2006(6)	-723(4)	-1222(6)	89(3)
C(21)	3432(25)	-790(21)	177(26)	265(31)
C(22)	1827(33)	-1610(16)	-1311(38)	239(33)
C(23)	2955(30)	-535(15)	-2121(26)	196(25)
P(3)	1558(5)	1020(3)	-1005(4)	56(2)
C(31)	1314(23)	1514(11)	-2326(16)	102(10)
C(32)	1157(19)	1657(10)	-44(16)	83(9)
C(33)	3441(19)	1035(12)	-381(20)	106(11)
Cl(1)	542(4)	-134(3)	882(3)	66(2)
Ir(2)	575(1)	-353(1)	3039(1)	49(1)
P(4)	-981(5)	541(3)	2904(4)	64(2)
C(41)	-1202(25)	733(12)	4265(15)	111(12)
C(42)	-704(22)	1380(9)	2387(17)	88(10)
C(43)	-2716(18)	362(9)	1992(18)	88(9)
P(5)	2602(5)	296(3)	3833(4)	74(2)
C(51)	3831(20)	269(14)	3057(18)	111(12)
C(52)	3578(21)	38(14)	5280(15)	132(11)
C(53)	2582(24)	1203(12)	4095(22)	122(13)
P(6)	1698(5)	-1417(3)	3199(4)	62(2)
C(61)	1358(24)	-1988(11)	4251(17)	107(11)
C(62)	1121(23)	-1922(11)	1852(16)	104(10)
C(63)	3509(19)	-1509(12)	3521(22)	113(12)
C(1)	-1454(16)	721(9)	-1707(13)	45(6)
C(2)	-2196(16)	964(9)	-2872(14)	61(7)
C(3)	-3347(20)	1393(10)	-3147(19)	81(9)
C(4)	-3860(21)	1567(11)	-2304(20)	87(10)
C(5)	-3181(19)	1369(10)	-1140(19)	80(9)
C(6)	-2026(17)	923(10)	-890(14)	64(7)
C(1A)	-1188(16)	-990(9)	2578(13)	49(6)
C(2A)	-1874(18)	-1186(10)	1429(15)	70(8)
C(3A)	-3073(19)	-1587(10)	1133(16)	73(8)
C(4A)	-3637(22)	-1826(13)	1946(25)	102(12)
C(5A)	-2902(23)	-1641(12)	3084(23)	94(11)
C(6A)	-1769(18)	-1251(11)	3362(15)	67(8)
P(7)	5345(5)	2383(3)	2804(4)	66(2)
F(1)	5773(16)	1974(10)	3963(13)	165(9)
F(2)	6887(13)	2471(10)	3056(14)	152(8)
F(3)	4897(17)	2852(10)	1697(11)	147(8)
F(4)	3842(15)	2255(13)	2599(20)	227(14)
F(5)	5331(23)	3033(11)	3462(14)	220(13)
F(6)	5399(25)	1739(11)	2178(19)	271(16)

* Equivalent isotropic U defined as one third of the trace of the orthogonalized U_{ij} tensor

Table 2. Bond lengths (Å)

Ir(1)-P(1)	2.344 (6)
Ir(1)-P(2)	2.323 (7)
Ir(1)-P(3)	2.319 (5)
Ir(1)-Cl(1)	2.654 (4)
Ir(1)-C(1)	2.097 (17)
P(1)-C(11)	1.825 (18)
P(1)-C(12)	1.837 (20)
P(1)-C(13)	1.815 (18)
P(2)-C(21)	1.836 (25)
P(2)-C(22)	1.725 (32)
P(2)-C(23)	1.742 (37)
P(3)-C(31)	1.815 (21)
P(3)-C(32)	1.841 (21)
P(3)-C(33)	1.828 (18)
Cl(1)-Ir(2)	2.655 (4)
Ir(2)-P(4)	2.327 (6)
Ir(2)-P(5)	2.345 (5)
Ir(2)-P(6)	2.337 (6)
Ir(2)-C(1A)	2.109 (16)
P(4)-C(41)	1.792 (22)
P(4)-C(42)	1.798 (20)
P(4)-C(43)	1.788 (17)
P(5)-C(51)	1.826 (26)
P(5)-C(52)	1.777 (18)
P(5)-C(53)	1.784 (23)
P(6)-C(61)	1.817 (24)
P(6)-C(62)	1.828 (20)
P(6)-C(63)	1.782 (20)
C(1)-C(2)	1.442 (21)
C(1)-C(6)	1.379 (27)
C(2)-C(3)	1.392 (25)
C(3)-C(4)	1.352 (36)
C(4)-C(5)	1.404 (29)
C(5)-C(6)	1.417 (26)
C(1A)-C(2A)	1.388 (22)
C(1A)-C(6A)	1.387 (28)
C(2A)-C(3A)	1.400 (26)
C(3A)-C(4A)	1.389 (38)
C(4A)-C(5A)	1.381 (35)
C(5A)-C(6A)	1.334 (30)
P(7)-F(1)	1.547 (17)
P(7)-F(2)	1.524 (14)
P(7)-F(3)	1.560 (16)
P(7)-F(4)	1.505 (17)
P(7)-F(5)	1.495 (21)
P(7)-F(6)	1.472 (23)

Table 3. Bond angles (°)

P(1)-Ir(1)-P(2)	96.4(2)	C(42)-P(4)-C(43)	101.7(9)
P(1)-Ir(1)-P(3)	166.4(2)	Ir(2)-P(5)-C(51)	116.8(7)
P(2)-Ir(1)-P(3)	95.1(2)	Ir(2)-P(5)-C(52)	112.4(9)
P(1)-Ir(1)-Cl(1)	94.0(2)	C(51)-P(5)-C(52)	104.5(10)
P(2)-Ir(1)-Cl(1)	91.8(2)	Ir(2)-P(5)-C(53)	122.4(8)
P(3)-Ir(1)-Cl(1)	92.9(2)	C(51)-P(5)-C(53)	100.0(13)
P(1)-Ir(1)-C(1)	82.8(5)	C(52)-P(5)-C(53)	97.8(12)
P(2)-Ir(1)-C(1)	172.7(5)	Ir(2)-P(6)-C(61)	112.6(8)
P(3)-Ir(1)-C(1)	84.9(5)	Ir(2)-P(6)-C(62)	113.3(7)
Cl(1)-Ir(1)-C(1)	95.4(5)	C(61)-P(6)-C(62)	103.2(10)
Ir(1)-P(1)-C(11)	120.1(6)	Ir(2)-P(6)-C(63)	124.0(8)
Ir(1)-P(1)-C(12)	116.1(7)	C(61)-P(6)-C(63)	103.1(11)
C(11)-P(1)-C(12)	99.9(10)	C(62)-P(6)-C(63)	97.9(12)
Ir(1)-P(1)-C(13)	114.3(9)	Ir(1)-C(1)-C(2)	121.8(13)
C(11)-P(1)-C(13)	103.1(10)	Ir(1)-C(1)-C(6)	123.8(11)
C(12)-P(1)-C(13)	100.5(11)	C(2)-C(1)-C(6)	114.0(15)
Ir(1)-P(2)-C(21)	118.5(12)	C(1)-C(2)-C(3)	123.5(18)
Ir(1)-P(2)-C(22)	123.7(12)	C(2)-C(3)-C(4)	119.4(18)
C(21)-P(2)-C(22)	91.3(17)	C(3)-C(4)-C(5)	120.8(19)
Ir(1)-P(2)-C(23)	115.6(10)	C(4)-C(5)-C(6)	118.4(21)
C(21)-P(2)-C(23)	98.9(14)	C(1)-C(6)-C(5)	123.6(16)
C(22)-P(2)-C(23)	103.8(19)	Ir(2)-C(1A)-C(2A)	121.5(14)
Ir(1)-P(3)-C(31)	112.1(7)	Ir(2)-C(1A)-C(6A)	124.5(11)
Ir(1)-P(3)-C(32)	114.6(7)	C(2A)-C(1A)-C(6A)	114.0(15)
C(31)-P(3)-C(32)	102.8(10)	C(1A)-C(2A)-C(3A)	120.7(19)
Ir(1)-P(3)-C(33)	125.2(8)	C(2A)-C(3A)-C(4A)	123.4(18)
C(31)-P(3)-C(33)	99.5(11)	C(3A)-C(4A)-C(5A)	114.3(21)
C(32)-P(3)-C(33)	99.5(10)	C(4A)-C(5A)-C(6A)	122.2(26)
Ir(1)-Cl(1)-Ir(2)	173.3(2)	C(1A)-C(6A)-C(5A)	125.3(18)
Cl(1)-Ir(2)-P(4)	92.2(2)	F(1)-P(7)-F(2)	85.5(9)
Cl(1)-Ir(2)-P(5)	91.7(2)	F(1)-P(7)-F(3)	174.9(10)
P(4)-Ir(2)-P(5)	97.3(2)	F(2)-P(7)-F(3)	95.1(10)
Cl(1)-Ir(2)-P(6)	93.5(2)	F(1)-P(7)-F(4)	91.3(11)
P(4)-Ir(2)-P(6)	166.1(2)	F(2)-P(7)-F(4)	176.5(12)
P(5)-Ir(2)-P(6)	95.2(2)	F(3)-P(7)-F(4)	88.3(11)
Cl(1)-Ir(2)-C(1A)	96.5(5)	F(1)-P(7)-F(5)	89.5(10)
P(4)-Ir(2)-C(1A)	84.5(5)	F(2)-P(7)-F(5)	89.9(12)
P(5)-Ir(2)-C(1A)	171.5(5)	F(3)-P(7)-F(5)	85.5(10)
P(6)-Ir(2)-C(1A)	82.3(5)	F(4)-P(7)-F(5)	91.6(13)
Ir(2)-P(4)-C(41)	113.1(7)	F(1)-P(7)-F(6)	89.6(11)
Ir(2)-P(4)-C(42)	120.4(8)	F(2)-P(7)-F(6)	88.7(12)
C(41)-P(4)-C(42)	103.0(11)	F(3)-P(7)-F(6)	95.5(11)
Ir(2)-P(4)-C(43)	114.8(7)	F(4)-P(7)-F(6)	89.8(14)
C(41)-P(4)-C(43)	101.4(11)	F(5)-P(7)-F(6)	178.4(9)

Table 4. Anisotropic displacement coefficients ($Å^2 x 10^3$)

	U_{11}	U_{22}	U_{33}	U_{12}	U_{13}	U_{23}
Ir(1)	44(1)	45(1)	44(1)	-3(1)	21(1)	-4(1)
P(1)	76(3)	59(3)	47(2)	-16(3)	14(2)	-2(2)
C(11)	82(13)	50(10)	106(14)	-6(10)	36(12)	5(10)
C(12)	54(11)	82(15)	128(16)	-18(10)	30(11)	4(12)
C(13)	211(28)	88(16)	66(12)	-65(18)	48(15)	-24(11)
P(2)	79(4)	71(3)	143(5)	18(3)	72(4)	8(4)
C(21)	111(23)	461(74)	258(39)	189(37)	110(26)	182(46)
C(22)	140(29)	157(32)	490(71)	22(24)	197(40)	-44(40)
C(23)	275(38)	141(28)	297(40)	51(27)	258(36)	37(27)
P(3)	56(3)	57(3)	58(2)	-13(2)	22(2)	-7(2)
C(31)	120(18)	86(15)	78(13)	-30(14)	6(12)	12(11)
C(32)	79(13)	78(13)	101(14)	-13(11)	44(11)	-13(11)
C(33)	78(15)	99(16)	130(18)	-28(13)	24(13)	-49(15)
Cl(1)	70(2)	83(3)	49(2)	4(2)	24(2)	13(2)
Ir(2)	46(1)	61(1)	38(1)	-1(1)	14(1)	3(1)
P(4)	73(3)	70(3)	56(3)	14(3)	31(2)	-2(2)
C(41)	168(22)	105(17)	72(12)	35(17)	60(14)	14(12)
C(42)	127(18)	54(11)	92(13)	28(12)	48(13)	18(10)
C(43)	72(13)	47(10)	140(17)	17(10)	30(12)	8(11)
P(5)	66(3)	86(4)	63(3)	-16(3)	14(2)	4(2)
C(51)	69(12)	152(25)	128(17)	-21(14)	52(12)	21(16)
C(52)	117(17)	140(19)	94(14)	-51(18)	-21(12)	30(16)
C(53)	99(18)	104(18)	144(21)	-35(15)	18(16)	-36(16)
P(6)	50(3)	67(3)	62(3)	6(2)	9(2)	14(2)
C(61)	124(19)	83(15)	105(16)	25(15)	27(14)	44(13)
C(62)	126(18)	109(17)	74(12)	55(15)	32(12)	9(12)
C(63)	58(13)	118(19)	171(23)	28(13)	49(14)	20(17)
C(1)	34(9)	59(11)	44(8)	-4(8)	18(7)	4(8)
C(2)	54(10)	61(11)	61(10)	-5(9)	11(8)	6(8)
C(3)	66(13)	60(12)	93(14)	27(10)	-3(11)	17(11)
C(4)	62(13)	78(14)	104(16)	22(11)	5(12)	14(13)
C(5)	62(12)	72(13)	117(16)	15(11)	45(12)	-3(12)
C(6)	57(10)	81(13)	56(9)	10(10)	20(8)	-2(9)
C(1A)	43(9)	52(11)	49(9)	1(8)	11(7)	15(8)
C(2A)	64(12)	82(13)	68(11)	-18(10)	28(9)	-2(10)
C(3A)	67(12)	69(12)	82(12)	1(10)	27(10)	-13(10)
C(4A)	53(13)	106(18)	160(23)	8(12)	53(15)	45(18)
C(5A)	71(15)	99(18)	115(18)	7(14)	37(14)	17(15)
C(6A)	53(11)	89(14)	63(10)	-7(11)	25(9)	11(10)
P(7)	58(3)	59(3)	67(3)	-4(2)	6(2)	8(2)
F(1)	136(12)	187(17)	150(12)	-17(12)	19(10)	96(13)
F(2)	81(9)	210(17)	172(13)	-5(10)	54(9)	55(12)
F(3)	167(13)	180(16)	92(9)	11(12)	42(9)	49(10)
F(4)	69(10)	285(26)	291(24)	5(13)	14(13)	167(22)
F(5)	300(27)	189(20)	117(11)	124(19)	2(14)	-41(12)
F(6)	260(25)	183(19)	249(26)	111(19)	-69(19)	-128(19)

The anisotropic displacement exponent takes the form:
$-2\pi^2(h^2a^{*2}U_{11} + \ldots + 2hka^*b^*U_{12})$

Table 5. H-Atom coordinates ($x10^4$) and isotropic displacement coefficients ($Å^2x10^3$)

	x	y	z	U
H(11A)	-2133	-1926	-1700	80
H(11B)	-552	-1873	-1496	80
H(11C)	-1122	-1623	-526	80
H(12A)	-3833	-936	-2100	80
H(12B)	-3091	-476	-1005	80
H(12C)	-3563	-151	-2258	80
H(13A)	-2880	-1299	-3734	80
H(13B)	-2479	-549	-3987	80
H(13C)	-1391	-1147	-3739	80
H(21A)	4129	-1112	154	80
H(21B)	3818	-333	316	80
H(21C)	3097	-916	792	80
H(22A)	2703	-1799	-1269	80
H(22B)	1634	-1735	-622	80
H(22C)	1119	-1792	-1986	80
H(23A)	3672	-874	-1990	80
H(23B)	2339	-564	-2914	80
H(23C)	3357	-82	-1977	80
H(31A)	1872	1924	-2168	80
H(31B)	1579	1220	-2848	80
H(31C)	361	1639	-2679	80
H(32A)	1754	2050	52	80
H(32B)	214	1803	-380	80
H(32C)	1302	1447	701	80
H(33A)	3729	1509	-332	80
H(33B)	3742	835	386	80
H(33C)	3839	784	-866	80
H(41A)	-1851	1106	4145	80
H(41B)	-1528	340	4575	80
H(41C)	-324	876	4805	80
H(42A)	-1441	1684	2382	80
H(42B)	153	1556	2913	80
H(42C)	-661	1351	1615	80
H(43A)	-3283	757	1986	80
H(43B)	-2710	281	1217	80
H(43C)	-3080	-37	2255	80
H(51A)	4616	554	3447	80
H(51B)	4128	-198	3018	80
H(51C)	3377	441	2281	80
H(52A)	4386	323	5559	80
H(52B)	3038	94	5776	80
H(52C)	3848	-438	5287	80
H(53A)	3521	1358	4419	80
H(53B)	2128	1442	3376	80
H(53C)	2114	1298	4636	80
H(61A)	1845	-2416	4288	80
H(61B)	1663	-1774	5007	80
H(61C)	386	-2079	4013	80
H(62A)	1640	-2345	1998	80
H(62B)	160	-2024	1673	80
H(62C)	1247	-1686	1204	80

H(63A)	3773	-1987	3559	80
H(63B)	3725	-1286	2903	80
H(63C)	4001	-1288	4249	80
H(2A)	-1828	833	-3465	80
H(3A)	-3803	1520	-3948	80
H(4A)	-4676	1848	-2496	80
H(5A)	-3506	1537	-540	80
H(6A)	-1618	762	-101	80
H(2AA)	-1531	-1028	834	80
H(3AA)	-3490	-1727	334	80
H(4AA)	-4465	-2097	1731	80
H(5AA)	-3218	-1795	3696	80
H(6AA)	-1326	-1112	4159	80

STRUCTURE DETERMINATION SUMMARY

Crystal Data

Empirical Formula	C_{14} H_{32} Cl F_6 Ir N P_4
Color; Habit	Clear flat plate
Crystal Size (mm)	0.4 x 0.4 x 0.2
Crystal System	Monoclinic
Space Group	C2/c
Unit Cell Dimensions	a = 22.943(6) Å b = 19.457(5) Å c = 13.292(3) Å β = 121.35(2)°
Volume	5068(2) $Å^3$
Z	8
Formula weight	679.9
Density(calc.)	1.782 Mg/m^3
Absorption Coefficient	5.649 mm^{-1}
F(000)	2648

Data Collection

Diffractometer Used	Siemens R3m/V
Radiation	MoK_α (λ = 0.71073 Å)
Temperature (K)	298
Monochromator	Highly oriented graphite crystal
2θ Range	3.5 to 45.0°
Scan Type	Wyckoff
Scan Speed	Variable; 3.97 to 19.53°/min. in ω
Scan Range (ω)	0.60°
Background Measurement	Stationary crystal and stationary counter at beginning and end of scan, each for 25.0% of total scan time
Standard Reflections	3 measured every 300 reflections
Index Ranges	0 < h < 24, 0 < k < 20, -14 < l < 12
Reflections Collected	3547
Independent Reflections	3326 (R_{int} = 1.99%)
Observed Reflections	2798 (F > 3.0σ(F))
Absorption Correction	Semi-empirical
Min./Max. Transmission	0.6679 / 1.0000

Solution and Refinement

System Used	Siemens SHELXTL PLUS (VMS)
Solution	Direct Methods
Refinement Method	Full-Matrix Least-Squares
Quantity Minimized	$\Sigma w(F_o-F_c)^2$
Absolute Structure	N/A
Extinction Correction	χ = -0.000014(6), where $F^* = F [1 + 0.002\chi F^2/\sin(2\theta)]^{-1/4}$
Hydrogen Atoms	Riding model, fixed isotropic U
Weighting Scheme	$w^{-1} = \sigma^2(F) + 0.0010F^2$
Number of Parameters refined	257
Final R indices (obs. data)	R = 4.21 %, wR = 5.38 %
R Indices (all data)	R = 5.18 %, wR = 5.72 %
Goodness-of-Fit	1.32
Largest and Mean Δ/σ	2.258, 0.015
Data-to-Parameter Ratio	10.9:1
Largest Difference Peak	1.54 $eÅ^{-3}$
Largest Difference Hole	-0.79 $eÅ^{-3}$

Table 1. Atomic coordinates ($x10^4$) and equivalent isotropic displacement coefficients ($Å^2x10^3$)

	x	y	z	U(eq)
Ir(1)	2178(1)	6494(1)	2516(1)	50(1)
P(1)	1230(1)	5836(2)	2091(3)	67(1)
P(2)	2901(2)	5535(2)	3118(3)	69(2)
P(3)	3028(2)	7231(2)	2683(3)	76(2)
Cl(1)	2494(2)	6624(1)	4602(2)	66(2)
C(1)	1544(5)	7336(5)	1966(9)	58(5)
C(2)	1140(5)	7565(5)	798(9)	70(5)
C(3)	736(6)	8121(7)	477(12)	92(7)
C(4)	712(7)	8502(6)	1329(16)	108(10)
C(5)	1111(7)	8310(7)	2512(13)	93(8)
N(1)	1498(4)	7743(4)	2746(8)	75(5)
C(11)	403(5)	6248(7)	1240(11)	95(7)
C(12)	1081(6)	5070(6)	1188(11)	95(7)
C(13)	1184(6)	5523(7)	3326(11)	104(8)
C(21)	2764(7)	4882(6)	3929(12)	101(8)
C(22)	3796(5)	5678(7)	4164(11)	100(7)
C(23)	2934(7)	5064(8)	1983(12)	111(9)
C(31)	2748(7)	8063(7)	2067(16)	134(11)
C(32)	3494(8)	6981(8)	1989(15)	134(13)
C(33)	3722(7)	7471(9)	4144(12)	139(10)
P(4)	0	10317(2)	2500	76(2)
F(41)	0	11055(7)	2500	294(21)
F(42)	0	9579(7)	2500	282(29)
F(43)	-756(5)	10322(10)	1722(10)	256(11)
F(44)	55(5)	10285(6)	1386(8)	168(7)
P(5)	0	3618(2)	2500	76(2)
F(51)	-15(9)	3073(9)	1747(12)	311(14)
F(52)	777(6)	3617(6)	3260(15)	242(12)
F(53)	-38(8)	4202(8)	1754(11)	266(12)
Cl(1A)	1985(10)	6278(10)	575(18)	61(10)

* Equivalent isotropic U defined as one third of the trace of the orthogonalized U_{ij} tensor

Table 2. Bond lengths (Å)

Ir(1)-P(1)	2.328	(3)	C(1)-N(1)	1.352	(16)
Ir(1)-P(2)	2.342	(3)	C(2)-C(3)	1.342	(17)
Ir(1)-P(3)	2.335	(4)	C(3)-C(4)	1.380	(26)
Ir(1)-Cl(1)	2.488	(3)	C(4)-C(5)	1.397	(22)
Ir(1)-C(1)	2.055	(9)	C(5)-N(1)	1.348	(16)
Ir(1)-Cl(1A)	2.415	(25)	P(4)-F(41)	1.435	(15)
P(1)-C(11)	1.814	(11)	P(4)-F(42)	1.437	(15)
P(1)-C(12)	1.830	(13)	P(4)-F(43)	1.487	(9)
P(1)-C(13)	1.804	(16)	P(4)-F(44)	1.551	(13)
P(2)-C(21)	1.796	(16)	P(4)-F(43A)	1.487	(9)
P(2)-C(22)	1.805	(10)	P(4)-F(44A)	1.551	(13)
P(2)-C(23)	1.801	(18)	P(5)-F(51)	1.446	(18)
P(3)-C(31)	1.777	(15)	P(5)-F(52)	1.525	(11)
P(3)-C(32)	1.806	(23)	P(5)-F(53)	1.481	(17)
P(3)-C(33)	1.818	(12)	P(5)-F(51A)	1.446	(18)
C(1)-C(2)	1.404	(13)	P(5)-F(52A)	1.525	(11)
			P(5)-F(53A)	1.481	(17)

Table 3. Bond angles (°)

P(1)-Ir(1)-P(2)	92.9(1)	C(2)-C(1)-N(1)	113.1(9)
P(1)-Ir(1)-P(3)	171.8(1)	C(1)-C(2)-C(3)	123.9(12)
P(2)-Ir(1)-P(3)	92.8(1)	C(2)-C(3)-C(4)	119.3(12)
P(1)-Ir(1)-Cl(1)	91.1(1)	C(3)-C(4)-C(5)	119.8(12)
P(2)-Ir(1)-Cl(1)	87.5(1)	C(4)-C(5)-N(1)	116.6(15)
P(3)-Ir(1)-Cl(1)	95.0(1)	C(1)-N(1)-C(5)	127.4(10)
P(1)-Ir(1)-C(1)	87.3(3)	F(41)-P(4)-F(42)	180.0(1)
P(2)-Ir(1)-C(1)	179.2(4)	F(41)-P(4)-F(43)	89.7(8)
P(3)-Ir(1)-C(1)	86.9(3)	F(42)-P(4)-F(43)	90.3(8)
Cl(1)-Ir(1)-C(1)	93.2(3)	F(41)-P(4)-F(44)	92.3(5)
P(1)-Ir(1)-Cl(1A)	90.9(5)	F(42)-P(4)-F(44)	87.7(5)
P(2)-Ir(1)-Cl(1A)	86.0(5)	F(43)-P(4)-F(44)	88.9(7)
P(3)-Ir(1)-Cl(1A)	83.6(5)	F(41)-P(4)-F(43A)	89.7(8)
Cl(1)-Ir(1)-Cl(1A)	173.3(5)	F(42)-P(4)-F(43A)	90.3(8)
C(1)-Ir(1)-Cl(1A)	93.2(6)	F(43)-P(4)-F(43A)	179.3(4)
Ir(1)-P(1)-C(11)	116.7(5)	F(44)-P(4)-F(43A)	91.2(7)
Ir(1)-P(1)-C(12)	116.0(5)	F(41)-P(4)-F(44A)	92.3(5)
C(11)-P(1)-C(12)	100.0(6)	F(42)-P(4)-F(44A)	87.7(5)
Ir(1)-P(1)-C(13)	117.1(4)	F(43)-P(4)-F(44A)	91.2(7)
C(11)-P(1)-C(13)	100.3(7)	F(44)-P(4)-F(44A)	175.4(10)
C(12)-P(1)-C(13)	104.0(7)	F(43A)-P(4)-F(44A)	88.9(7)
Ir(1)-P(2)-C(21)	117.1(5)	F(51)-P(5)-F(52)	93.2(9)
Ir(1)-P(2)-C(22)	117.4(5)	F(51)-P(5)-F(53)	97.3(10)
C(21)-P(2)-C(22)	97.5(6)	F(52)-P(5)-F(53)	94.9(9)
Ir(1)-P(2)-C(23)	116.8(4)	F(51)-P(5)-F(51A)	85.7(14)
C(21)-P(2)-C(23)	103.8(7)	F(52)-P(5)-F(51A)	86.7(9)
C(22)-P(2)-C(23)	101.3(7)	F(53)-P(5)-F(51A)	176.5(11)
Ir(1)-P(3)-C(31)	115.6(5)	F(51)-P(5)-F(52A)	86.6(9)
Ir(1)-P(3)-C(32)	118.2(5)	F(52)-P(5)-F(52A)	180.0(11)
C(31)-P(3)-C(32)	100.2(9)	F(53)-P(5)-F(52A)	85.2(9)
Ir(1)-P(3)-C(33)	118.9(6)	F(51A)-P(5)-F(52A)	93.2(9)
C(31)-P(3)-C(33)	99.4(7)	F(51)-P(5)-F(53A)	176.5(11)
C(32)-P(3)-C(33)	101.1(8)	F(52)-P(5)-F(53A)	85.2(9)
Ir(1)-C(1)-C(2)	125.7(9)	F(53)-P(5)-F(53A)	79.8(13)
Ir(1)-C(1)-N(1)	121.2(7)	F(51A)-P(5)-F(53A)	97.3(10)
		F(52A)-P(5)-F(53A)	94.9(9)

Table 4. Anisotropic displacement coefficients ($Å^2x10^3$)

	U_{11}	U_{22}	U_{33}	U_{12}	U_{13}	U_{23}
Ir(1)	47(1)	52(1)	53(1)	-2(1)	26(1)	-5(1)
P(1)	60(2)	77(2)	67(2)	-19(1)	36(1)	-13(1)
P(2)	79(2)	64(2)	72(2)	16(1)	45(2)	4(1)
P(3)	60(2)	72(2)	102(2)	-9(1)	46(2)	-2(2)
Cl(1)	73(2)	67(2)	54(2)	-3(1)	29(1)	-15(1)
C(1)	46(5)	56(6)	69(7)	-3(4)	28(5)	-16(5)
C(2)	67(6)	64(7)	62(7)	13(6)	22(5)	8(5)
C(3)	81(8)	82(9)	80(8)	10(7)	18(7)	9(7)
C(4)	80(9)	61(8)	157(15)	14(6)	44(10)	2(9)
C(5)	95(10)	83(9)	87(9)	17(8)	37(8)	-5(7)
N(1)	64(5)	69(6)	75(6)	5(5)	25(5)	-12(5)
C(11)	53(7)	118(10)	99(9)	-14(7)	29(6)	-2(8)
C(12)	93(9)	100(9)	89(9)	-34(7)	46(7)	-27(7)
C(13)	90(9)	150(13)	93(9)	-32(9)	60(8)	3(9)
C(21)	119(11)	78(8)	113(10)	29(8)	66(9)	30(7)
C(22)	67(7)	112(10)	105(10)	28(7)	34(7)	32(8)
C(23)	115(11)	129(12)	111(11)	38(9)	73(9)	8(9)
C(31)	92(10)	92(11)	209(18)	-3(8)	71(11)	27(11)
C(32)	171(15)	118(12)	172(16)	-45(11)	130(14)	-19(11)
C(33)	101(11)	165(15)	127(13)	-55(11)	44(10)	-27(11)
P(4)	62(3)	82(3)	95(3)	0	48(2)	0
F(41)	419(33)	87(12)	234(22)	0	69(21)	0
F(42)	572(45)	71(9)	373(29)	0	365(33)	0
F(43)	77(6)	516(28)	158(10)	-8(10)	49(7)	-87(13)
F(44)	148(8)	269(13)	133(7)	-35(8)	107(7)	-18(8)
P(5)	92(3)	64(3)	80(3)	0	49(3)	0
F(51)	289(18)	273(18)	212(14)	118(16)	20(14)	-126(13)
F(52)	92(7)	190(12)	358(22)	10(7)	56(10)	-35(11)
F(53)	287(17)	251(14)	209(13)	-127(13)	93(13)	75(11)
Cl(1A)	51(11)	60(12)	69(13)	8(9)	29(10)	3(9)

The anisotropic displacement exponent takes the form:
$-2\pi^2(h^2a^{*2}U_{11} + ... + 2hka^*b^*U_{12})$

Table 5. H-Atom coordinates ($x10^4$) and isotropic displacement coefficients ($Å^2x10^3$)

	x	y	z	U
H(2A)	1146	7295	198	80
H(3A)	472	8258	-334	80
H(4A)	432	8907	1124	80
H(5A)	1108	8572	3121	80
H(1A)	1741	7611	3505	80
H(11A)	44	5939	1109	80
H(11B)	391	6647	1655	80
H(11C)	340	6386	496	80
H(12A)	682	4834	1065	80
H(12B)	1013	5211	443	80
H(12C)	1467	4768	1573	80
H(13A)	777	5257	3067	80
H(13B)	1577	5241	3802	80
H(13C)	1187	5908	3781	80
H(21A)	3090	4519	4129	80
H(21B)	2814	5072	4637	80
H(21C)	2311	4704	3442	80
H(22A)	4045	5254	4351	80
H(22B)	3976	5996	3840	80
H(22C)	3840	5870	4866	80
H(23A)	3239	4678	2292	80
H(23B)	2479	4904	1444	80
H(23C)	3075	5365	1577	80
H(31A)	3123	8339	2172	80
H(31B)	2431	7994	1241	80
H(31C)	2523	8294	2410	80
H(32A)	3834	7314	2112	80
H(32B)	3706	6540	2264	80
H(32C)	3157	6954	1163	80
H(33A)	4041	7771	4103	80
H(33B)	3512	7707	4508	80
H(33C)	3957	7072	4601	80

STRUCTURE DETERMINATION SUMMARY

Crystal Data	
Empirical Formula	$C_{14}\ H_{32}\ Cl\ F_6\ Ir\ N\ P_4$
Color; Habit	Clear amber rectangular prism
Crystal Size (mm)	0.4 x 0.4 x 0.5
Crystal System	Monoclinic
Space Group	$P2_1/c$
Unit Cell Dimensions	a = 9.876(2) Å b = 15.327(3) Å c = 16.427(3) Å β = 97.58(2)°
Volume	2464.8(8) $Å^3$
Z	4
Formula weight	679.9
Density(calc.)	1.832 Mg/m^3
Absorption Coefficient	5.807 mm^{-1}
F(000)	1324
Data Collection	
Diffractometer Used	Siemens R3m/V
Radiation	MoK_α (λ = 0.71073 Å)
Temperature (K)	298
Monochromator	Highly oriented graphite crystal
2θ Range	3.5 to 55.0°
Scan Type	Wyckoff
Scan Speed	Variable; 3.97 to 19.53°/min. in ω
Scan Range (ω)	0.60°
Background Measurement	Stationary crystal and stationary counter at beginning and end of scan, each for 25.0% of total scan time
Standard Reflections	3 measured every 300 reflections
Index Ranges	$0 < h < 12,\ 0 < k < 19,\ -21 < l < 21$
Reflections Collected	6217
Independent Reflections	5664 (R_{int} = 1.00%)
Observed Reflections	4795 ($F > 3.0\sigma(F)$)
Absorption Correction	Semi-empirical
Min./Max. Transmission	0.5865 / 0.8719
Solution and Refinement	
System Used	Siemens SHELXTL PLUS (VMS)
Solution	Direct Methods
Refinement Method	Full-Matrix Least-Squares
Quantity Minimized	$\Sigma w(F_o-F_c)^2$
Absolute Structure	N/A
Extinction Correction	χ = 0.00022(3), where $F^* = F\ [\ 1 + 0.002\chi F^2/\sin(2\theta)\ ]^{-1/4}$
Hydrogen Atoms	Riding model, fixed isotropic U
Weighting Scheme	$w^{-1} = \sigma^2(F) + 0.0008F^2$
Number of Parameters refined	245
Final R indices (obs. data)	R = 3.95 %, wR = 4.84 %
R Indices (all data)	R = 4.80 %, wR = 5.26 %
Goodness-of-Fit	1.26
Largest and Mean Δ/σ	0.036, 0.004
Data-to-Parameter Ratio	19.6:1
Largest Difference Peak	1.56 $eÅ^{-3}$
Largest Difference Hole	-1.23 $eÅ^{-3}$

Table 1. Atomic coordinates ($x10^4$) and equivalent isotropic displacement coefficients ($Å^2 x10^3$)

	x	y	z	U(eq)
Ir(1)	9149(1)	9386(1)	2255(1)	36(1)
P(1)	10979(2)	9269(1)	3298(1)	51(1)
P(2)	9909(2)	8216(1)	1460(1)	50(1)
P(3)	7263(2)	9819(1)	1351(1)	51(1)
Cl(1)	10495(2)	10447(1)	1573(1)	61(1)
C(1)	7953(5)	8658(4)	2894(3)	41(2)
C(2)	7667(7)	7766(4)	2839(4)	57(2)
C(3)	6818(7)	7349(5)	3315(5)	66(3)
C(4)	6202(7)	7835(5)	3881(4)	66(3)
C(5)	6461(6)	8686(5)	3944(4)	58(2)
N(1)	7319(5)	9063(3)	3467(3)	48(2)
C(11)	11174(10)	10227(6)	3944(5)	91(4)
C(12)	12677(7)	9152(6)	3000(6)	89(4)
C(13)	10854(9)	8396(6)	4037(5)	86(3)
C(21)	11149(9)	8513(5)	794(5)	86(3)
C(22)	8683(9)	7633(5)	734(5)	79(3)
C(23)	10778(7)	7301(4)	2031(5)	67(3)
C(31)	6968(10)	10982(6)	1384(6)	94(4)
C(32)	5623(7)	9381(6)	1525(6)	92(4)
C(33)	7241(10)	9660(6)	266(4)	86(3)
P(4)	4362(2)	6414(1)	1054(1)	63(1)
F(1)	4605(9)	5768(5)	388(6)	180(5)
F(2)	3909(9)	7076(5)	375(5)	169(4)
F(3)	4056(7)	7079(4)	1737(4)	132(3)
F(4)	4718(9)	5722(5)	1746(5)	164(4)
F(5)	5851(5)	6736(5)	1123(5)	157(4)
F(6)	2840(5)	6057(5)	991(4)	118(3)

* Equivalent isotropic U defined as one third of the trace of the orthogonalized U_{ij} tensor

Table 2. Bond lengths (Å)

Ir(1)-P(1)	2.328 (2)	P(3)-C(33)	1.795 (8)
Ir(1)-P(2)	2.396 (2)	C(1)-C(2)	1.397 (8)
Ir(1)-P(3)	2.321 (2)	C(1)-N(1)	1.350 (7)
Ir(1)-Cl(1)	2.461 (2)	C(2)-C(3)	1.377 (10)
Ir(1)-C(1)	2.017 (6)	C(3)-C(4)	1.392 (11)
P(1)-C(11)	1.806 (9)	C(4)-C(5)	1.331 (10)
P(1)-C(12)	1.817 (8)	C(5)-N(1)	1.356 (8)
P(1)-C(13)	1.821 (9)	P(4)-F(1)	1.519 (9)
P(2)-C(21)	1.805 (9)	P(4)-F(2)	1.530 (8)
P(2)-C(22)	1.819 (8)	P(4)-F(3)	1.574 (7)
P(2)-C(23)	1.836 (7)	P(4)-F(4)	1.560 (8)
P(3)-C(31)	1.809 (9)	P(4)-F(5)	1.541 (6)
P(3)-C(32)	1.810 (8)	P(4)-F(6)	1.590 (6)

Table 3. Bond angles (°)

P(1)-Ir(1)-P(2)	94.3(1)	C(31)-P(3)-C(33)	100.5(4)
P(1)-Ir(1)-P(3)	166.6(1)	C(32)-P(3)-C(33)	102.3(4)
P(2)-Ir(1)-P(3)	98.5(1)	Ir(1)-C(1)-C(2)	129.4(5)
P(1)-Ir(1)-Cl(1)	88.4(1)	Ir(1)-C(1)-N(1)	117.8(4)
P(2)-Ir(1)-Cl(1)	91.1(1)	C(2)-C(1)-N(1)	112.8(5)
P(3)-Ir(1)-Cl(1)	87.5(1)	C(1)-C(2)-C(3)	123.4(6)
P(1)-Ir(1)-C(1)	91.5(1)	C(2)-C(3)-C(4)	119.0(7)
P(2)-Ir(1)-C(1)	96.7(2)	C(3)-C(4)-C(5)	118.6(7)
P(3)-Ir(1)-C(1)	90.9(1)	C(4)-C(5)-N(1)	120.1(6)
Cl(1)-Ir(1)-C(1)	172.2(2)	C(1)-N(1)-C(5)	126.1(6)
Ir(1)-P(1)-C(11)	112.5(3)	F(1)-P(4)-F(2)	88.0(4)
Ir(1)-P(1)-C(12)	117.6(3)	F(1)-P(4)-F(3)	178.0(4)
C(11)-P(1)-C(12)	102.0(4)	F(2)-P(4)-F(3)	91.4(4)
Ir(1)-P(1)-C(13)	115.6(3)	F(1)-P(4)-F(4)	92.3(4)
C(11)-P(1)-C(13)	102.6(4)	F(2)-P(4)-F(4)	176.0(5)
C(12)-P(1)-C(13)	104.7(4)	F(3)-P(4)-F(4)	88.1(4)
Ir(1)-P(2)-C(21)	115.3(3)	F(1)-P(4)-F(5)	91.2(5)
Ir(1)-P(2)-C(22)	119.7(3)	F(2)-P(4)-F(5)	91.5(4)
C(21)-P(2)-C(22)	99.9(4)	F(3)-P(4)-F(5)	90.7(4)
Ir(1)-P(2)-C(23)	116.9(2)	F(4)-P(4)-F(5)	92.5(4)
C(21)-P(2)-C(23)	101.2(4)	F(1)-P(4)-F(6)	88.0(4)
C(22)-P(2)-C(23)	100.7(3)	F(2)-P(4)-F(6)	89.8(4)
Ir(1)-P(3)-C(31)	112.5(3)	F(3)-P(4)-F(6)	90.1(3)
Ir(1)-P(3)-C(32)	116.9(3)	F(4)-P(4)-F(6)	86.2(4)
C(31)-P(3)-C(32)	102.1(4)	F(5)-P(4)-F(6)	178.5(4)
Ir(1)-P(3)-C(33)	120.0(3)		

Table 4. Anisotropic displacement coefficients ($Å^2x10^3$)

	U_{11}	U_{22}	U_{33}	U_{12}	U_{13}	U_{23}
Ir(1)	39(1)	33(1)	36(1)	0(1)	8(1)	2(1)
P(1)	49(1)	48(1)	54(1)	-2(1)	-3(1)	4(1)
P(2)	60(1)	42(1)	51(1)	1(1)	22(1)	-2(1)
P(3)	52(1)	53(1)	46(1)	4(1)	0(1)	11(1)
Cl(1)	71(1)	47(1)	71(1)	-11(1)	26(1)	9(1)
C(1)	39(3)	48(3)	37(3)	1(2)	4(2)	6(2)
C(2)	66(4)	45(3)	62(4)	-6(3)	24(3)	-4(3)
C(3)	69(4)	54(4)	81(5)	-12(3)	26(4)	6(4)
C(4)	66(4)	71(5)	64(4)	-10(4)	27(3)	11(4)
C(5)	54(3)	73(5)	51(4)	1(3)	20(3)	6(3)
N(1)	49(3)	49(3)	48(3)	3(2)	14(2)	4(2)
C(11)	95(6)	85(6)	83(6)	-11(5)	-28(5)	-23(5)
C(12)	48(4)	97(6)	118(8)	-6(4)	1(4)	11(6)
C(13)	92(5)	98(6)	62(5)	-7(5)	-14(4)	32(4)
C(21)	111(6)	71(5)	90(6)	1(5)	65(5)	-2(4)
C(22)	107(6)	57(4)	70(5)	-4(4)	5(4)	-16(4)
C(23)	72(4)	45(4)	87(5)	16(3)	24(4)	1(3)
C(31)	104(7)	66(5)	104(7)	30(5)	-13(5)	8(5)
C(32)	41(4)	130(9)	101(7)	0(4)	-10(4)	38(5)
C(33)	105(6)	99(6)	50(4)	22(5)	-6(4)	16(4)
P(4)	58(1)	66(1)	69(1)	-1(1)	24(1)	-3(1)
F(1)	218(9)	150(6)	203(8)	-39(6)	145(7)	-95(6)
F(2)	211(8)	154(7)	136(6)	3(6)	-3(5)	71(5)
F(3)	145(5)	129(5)	131(5)	-9(4)	49(4)	-49(4)
F(4)	176(7)	154(7)	163(7)	37(5)	28(6)	73(5)
F(5)	59(3)	188(7)	226(8)	-28(4)	33(4)	-17(6)
F(6)	80(3)	151(5)	128(5)	-36(3)	31(3)	-34(4)

The anisotropic displacement exponent takes the form:
$-2\pi^2(h^2a^{*2}U_{11} + ... + 2hka^*b^*U_{12})$

Table 5. H-Atom coordinates ($x10^4$) and isotropic displacement coefficients ($Å^2x10^3$)

	x	y	z	U
H(2A)	8091	7422	2455	80
H(3A)	6655	6733	3262	80
H(4A)	5602	7553	4214	80
H(5A)	6036	9032	4326	80
H(1A)	7488	9637	3538	80
H(11A)	11937	10154	4365	80
H(11B)	11318	10733	3621	80
H(11C)	10354	10301	4191	80
H(12A)	13341	9111	3481	80
H(12B)	12711	8635	2674	80
H(12C)	12874	9652	2684	80
H(13A)	11650	8401	4441	80
H(13B)	10054	8485	4302	80
H(13C)	10788	7844	3758	80
H(21A)	11407	8013	498	80
H(21B)	10765	8949	413	80
H(21C)	11941	8746	1125	80
H(22A)	9140	7186	464	80
H(22B)	8012	7371	1029	80
H(22C)	8242	8031	332	80
H(23A)	11035	6876	1650	80
H(23B)	11580	7509	2369	80
H(23C)	10172	7038	2371	80
H(31A)	6182	11137	1003	80
H(31B)	6818	11145	1929	80
H(31C)	7756	11284	1240	80
H(32A)	4919	9605	1120	80
H(32B)	5668	8758	1475	80
H(32C)	5421	9531	2063	80
H(33A)	6399	9871	-26	80
H(33B)	7992	9974	90	80
H(33C)	7336	9049	156	80

STRUCTURE DETERMINATION SUMMARY

Crystal Data

Empirical Formula	$C_{26}\ H_{50}\ F_6\ Ir\ N\ P_4$
Color; Habit	Clear irregular prism
Crystal Size (mm)	0.3 x 0.3 x 0.4
Crystal System	Monoclinic
Space Group	$P2_1/c$
Unit Cell Dimensions	a = 9.847(3) Å b = 18.284(8) Å c = 19.849(6) Å β = 92.96(3)°
Volume	3569(2) $Å^3$
Z	4
Formula weight	806.8
Density(calc.)	1.501 Mg/m^3
Absorption Coefficient	3.949 mm^{-1}
F(000)	1616

Data Collection

Diffractometer Used	Siemens R3m/V
Radiation	MoK_α (λ = 0.71073 Å)
Temperature (K)	298
Monochromator	Highly oriented graphite crystal
2θ Range	3.5 to 35.0°
Scan Type	Wyckoff
Scan Speed	Variable; 3.97 to 19.53°/min. in ω
Scan Range (ω)	0.60°
Background Measurement	Stationary crystal and stationary counter at beginning and end of scan, each for 25.0% of total scan time
Standard Reflections	3 measured every 400 reflections
Index Ranges	$0 < h < 11,\ 0 < k < 21,\ -23 < l < 23$
Reflections Collected	6910
Independent Reflections	6281 (R_{int} = 1.86%)
Observed Reflections	3634 ($F > 4.0\sigma(F)$)
Absorption Correction	Semi-empirical
Min./Max. Transmission	0.5481 / 1.0000

Solution and Refinement

System Used	Siemens SHELXTL PLUS (VMS)
Solution	Direct Methods
Refinement Method	Full-Matrix Least-Squares
Quantity Minimized	$\Sigma w(F_o-F_c)^2$
Absolute Structure	N/A
Extinction Correction	χ = 0.000023(13), where $F^* = F\ [\ 1 + 0.002xF2/\sin(2\theta)\ ]^{-1/4}$
Hydrogen Atoms	Riding model, fixed isotropic U
Weighting Scheme	$w^{-1} = \sigma^2(F) + 0.0005F^2$
Number of Parameters refined	344
Final R indices (obs. data)	R = 4.09 %, wR = 4.44 %
R Indices (all data)	R = 8.20 %, wR = 5.22 %
Goodness-of-Fit	1.24
Largest and Mean Δ/σ	0.079, 0.008
Data-to-Parameter Ratio	10.6:1
Largest Difference Peak	0.74 $eÅ^{-3}$
Largest Difference Hole	-0.51 $eÅ^{-3}$

Table 1. Atomic coordinates ($x10^4$) and equivalent isotropic displacement coefficients ($Å^2x10^3$)

	x	y	z	U(eq)
Ir(1)	3438(1)	7471(1)	585(1)	47(1)
P(1)	4184(3)	6726(2)	-280(1)	63(1)
C(1A)	2935(13)	6128(8)	-664(7)	168(8)
C(1B)	4682(16)	7173(7)	-1025(5)	129(7)
C(1C)	5500(12)	6074(6)	-84(6)	100(5)
P(2)	5374(3)	8212(2)	585(1)	75(1)
C(2A)	5952(13)	8604(7)	1385(6)	129(7)
C(2B)	6957(12)	7768(7)	423(8)	145(8)
C(2C)	5378(13)	8964(6)	16(6)	123(6)
P(3)	2369(3)	8186(2)	1372(1)	79(1)
C(3A)	2379(14)	9161(6)	1223(6)	122(7)
C(3B)	2911(13)	8092(7)	2241(5)	105(5)
C(3C)	582(11)	8056(10)	1365(7)	171(9)
C(1)	1794(9)	6770(5)	623(4)	54(3)
N(1)	1785(10)	6206(5)	1093(5)	93(4)
C(3)	660(19)	5727(8)	1107(8)	138(9)
C(4)	-365(17)	5795(10)	654(10)	150(10)
C(5)	-342(13)	6336(8)	194(7)	104(7)
C(2)	662(9)	6803(5)	197(5)	55(3)
C(6)	2407(8)	8081(5)	-136(4)	51(3)
C(7)	1771(9)	8443(5)	-541(4)	56(3)
C(8)	961(11)	8903(5)	-1035(5)	68(4)
C(8A)	-489(11)	8927(8)	-855(7)	124(7)
C(8B)	1537(14)	9662(6)	-1010(7)	132(7)
C(8C)	1127(14)	8600(7)	-1747(5)	125(7)
C(9)	4476(9)	6861(5)	1301(4)	53(3)
C(10)	5084(11)	6491(5)	1715(4)	65(4)
C(11)	5801(13)	6017(6)	2215(5)	76(4)
C(11A)	7235(18)	6031(14)	2116(10)	318(21)
C(11B)	5476(24)	5276(9)	2117(9)	310(18)
C(11C)	5616(21)	6194(10)	2878(7)	275(15)
P(4)	1557(5)	3627(2)	1804(2)	104(2)
F(1)	1272(15)	3068(7)	2324(5)	239(8)
F(2)	3105(12)	3547(9)	2041(5)	244(8)
F(3)	2103(13)	4173(5)	1304(6)	202(7)
F(4)	195(10)	3769(10)	1529(6)	290(10)
F(5)	1822(11)	3033(5)	1257(4)	174(5)
F(6)	1403(13)	4242(6)	2329(5)	214(7)

* Equivalent isotropic U defined as one third of the trace of the orthogonalized U_{ij} tensor

Table 2. Bond lengths (Å)

Ir(1)-P(1)	2.339 (3)
Ir(1)-P(2)	2.339 (3)
Ir(1)-P(3)	2.330 (3)
Ir(1)-C(1)	2.070 (9)
Ir(1)-C(6)	2.042 (8)
Ir(1)-C(9)	2.040 (8)
P(1)-C(1A)	1.786 (14)
P(1)-C(1B)	1.781 (12)
P(1)-C(1C)	1.789 (12)
P(2)-C(2A)	1.807 (13)
P(2)-C(2B)	1.802 (12)
P(2)-C(2C)	1.779 (12)
P(3)-C(3A)	1.807 (11)
P(3)-C(3B)	1.787 (9)
P(3)-C(3C)	1.775 (12)
C(1)-N(1)	1.391 (13)
C(1)-C(2)	1.364 (12)
N(1)-C(3)	1.414 (20)
C(3)-C(4)	1.323 (25)
C(4)-C(5)	1.346 (24)
C(5)-C(2)	1.307 (16)
C(6)-C(7)	1.193 (11)
C(7)-C(8)	1.492 (13)
C(8)-C(8A)	1.491 (15)
C(8)-C(8B)	1.499 (15)
C(8)-C(8C)	1.536 (15)
C(9)-C(10)	1.201 (12)
C(10)-C(11)	1.470 (14)
C(11)-C(11A)	1.436 (22)
C(11)-C(11B)	1.404 (20)
C(11)-C(11C)	1.378 (17)
P(4)-F(1)	1.490 (12)
P(4)-F(2)	1.579 (13)
P(4)-F(3)	1.524 (12)
P(4)-F(4)	1.445 (11)
P(4)-F(5)	1.567 (10)
P(4)-F(6)	1.546 (11)

Table 3. Bond angles (°)

P(1)-Ir(1)-P(2)	92.9(1)	C(1)-N(1)-C(3)	120.3(10)
P(1)-Ir(1)-P(3)	171.4(1)	N(1)-C(3)-C(4)	120.0(14)
P(2)-Ir(1)-P(3)	94.1(1)	C(3)-C(4)-C(5)	119.4(15)
P(1)-Ir(1)-C(1)	86.6(3)	C(4)-C(5)-C(2)	121.1(13)
P(2)-Ir(1)-C(1)	176.4(2)	C(1)-C(2)-C(5)	124.6(10)
P(3)-Ir(1)-C(1)	86.6(3)	Ir(1)-C(6)-C(7)	177.6(7)
P(1)-Ir(1)-C(6)	88.1(2)	C(6)-C(7)-C(8)	178.8(9)
P(2)-Ir(1)-C(6)	93.4(2)	C(7)-C(8)-C(8A)	110.2(9)
P(3)-Ir(1)-C(6)	86.5(2)	C(7)-C(8)-C(8B)	108.2(8)
C(1)-Ir(1)-C(6)	90.1(3)	C(8A)-C(8)-C(8B)	109.3(10)
P(1)-Ir(1)-C(9)	91.6(2)	C(7)-C(8)-C(8C)	108.9(8)
P(2)-Ir(1)-C(9)	86.4(3)	C(8A)-C(8)-C(8C)	112.3(9)
P(3)-Ir(1)-C(9)	93.8(3)	C(8B)-C(8)-C(8C)	107.8(9)
C(1)-Ir(1)-C(9)	90.0(3)	Ir(1)-C(9)-C(10)	178.9(7)
C(6)-Ir(1)-C(9)	179.7(3)	C(9)-C(10)-C(11)	178.0(10)
Ir(1)-P(1)-C(1A)	115.8(5)	C(10)-C(11)-C(11A)	109.7(12)
Ir(1)-P(1)-C(1B)	116.9(4)	C(10)-C(11)-C(11B)	112.2(11)
C(1A)-P(1)-C(1B)	98.0(6)	C(11A)-C(11)-C(11B)	102.5(16)
Ir(1)-P(1)-C(1C)	118.7(4)	C(10)-C(11)-C(11C)	115.1(12)
C(1A)-P(1)-C(1C)	99.2(6)	C(11A)-C(11)-C(11C)	107.8(14)
C(1B)-P(1)-C(1C)	105.0(6)	C(11B)-C(11)-C(11C)	108.6(13)
Ir(1)-P(2)-C(2A)	116.7(4)	F(1)-P(4)-F(2)	86.7(8)
Ir(1)-P(2)-C(2B)	116.8(4)	F(1)-P(4)-F(3)	170.2(8)
C(2A)-P(2)-C(2B)	95.7(6)	F(2)-P(4)-F(3)	83.5(7)
Ir(1)-P(2)-C(2C)	118.4(4)	F(1)-P(4)-F(4)	100.4(9)
C(2A)-P(2)-C(2C)	104.0(6)	F(2)-P(4)-F(4)	172.9(8)
C(2B)-P(2)-C(2C)	101.8(6)	F(3)-P(4)-F(4)	89.4(8)
Ir(1)-P(3)-C(3A)	115.9(4)	F(1)-P(4)-F(5)	92.8(6)
Ir(1)-P(3)-C(3B)	118.1(4)	F(2)-P(4)-F(5)	87.1(7)
C(3A)-P(3)-C(3B)	104.4(6)	F(3)-P(4)-F(5)	85.8(6)
Ir(1)-P(3)-C(3C)	113.7(5)	F(4)-P(4)-F(5)	92.7(7)
C(3A)-P(3)-C(3C)	98.3(7)	F(1)-P(4)-F(6)	90.1(6)
C(3B)-P(3)-C(3C)	104.0(6)	F(2)-P(4)-F(6)	89.6(7)
Ir(1)-C(1)-N(1)	121.0(7)	F(3)-P(4)-F(6)	90.8(6)
Ir(1)-C(1)-C(2)	124.4(7)	F(4)-P(4)-F(6)	90.2(8)
N(1)-C(1)-C(2)	114.6(8)	F(5)-P(4)-F(6)	175.5(7)

Table 4. Anisotropic displacement coefficients ($Å^2 x 10^3$)

	U_{11}	U_{22}	U_{33}	U_{12}	U_{13}	U_{23}
Ir(1)	50(1)	44(1)	45(1)	3(1)	-13(1)	3(1)
P(1)	55(2)	71(2)	62(2)	7(1)	-1(1)	-9(1)
C(1A)	105(11)	213(17)	188(15)	-30(12)	35(11)	-155(14)
C(1B)	170(15)	160(13)	59(7)	59(11)	19(8)	3(8)
C(1C)	108(10)	93(9)	100(9)	46(8)	17(8)	-3(7)
P(2)	73(2)	67(2)	80(2)	-19(2)	-23(1)	15(2)
C(2A)	108(11)	131(12)	143(12)	-48(9)	-46(9)	-9(10)
C(2B)	65(8)	129(12)	235(17)	-25(8)	-37(10)	57(12)
C(2C)	124(11)	101(10)	138(11)	-32(9)	-54(9)	56(9)
P(3)	96(2)	77(2)	62(2)	26(2)	-15(1)	-19(1)
C(3A)	172(14)	95(10)	95(9)	60(10)	-42(9)	-22(7)
C(3B)	139(11)	116(10)	59(6)	41(9)	-13(7)	-19(7)
C(3C)	73(9)	270(21)	171(14)	33(12)	14(9)	-127(15)
C(1)	60(6)	47(5)	55(5)	4(5)	0(5)	1(4)
N(1)	100(8)	83(7)	93(7)	6(6)	-7(6)	18(6)
C(3)	190(19)	90(10)	137(14)	-66(13)	49(13)	29(9)
C(4)	81(11)	152(17)	220(23)	-64(13)	37(13)	-73(16)
C(5)	60(8)	140(14)	112(11)	-6(9)	-9(7)	-19(9)
C(2)	36(5)	60(6)	69(6)	-2(5)	-4(4)	-2(5)
C(6)	46(5)	50(5)	55(5)	5(4)	-10(4)	-5(4)
C(7)	51(6)	57(5)	58(5)	5(5)	-10(5)	10(5)
C(8)	71(7)	60(6)	69(6)	3(6)	-23(5)	13(5)
C(8A)	67(9)	147(13)	156(13)	19(9)	-18(8)	20(11)
C(8B)	158(14)	68(8)	161(13)	-8(9)	-74(10)	40(8)
C(8C)	153(13)	144(13)	74(8)	17(11)	-34(8)	12(8)
C(9)	61(6)	48(5)	50(5)	7(5)	-9(4)	2(4)
C(10)	81(7)	64(6)	48(5)	21(6)	-16(5)	-3(5)
C(11)	90(9)	71(7)	64(7)	28(6)	-23(6)	10(5)
C(11A)	182(24)	527(52)	237(26)	79(28)	-63(21)	229(31)
C(11B)	539(48)	105(15)	255(24)	75(22)	-278(28)	-1(16)
C(11C)	438(36)	302(27)	80(11)	294(27)	-26(16)	17(14)
P(4)	121(3)	116(3)	74(2)	7(3)	5(2)	2(2)
F(1)	344(19)	202(12)	180(10)	-31(12)	106(11)	55(9)
F(2)	192(12)	375(19)	162(10)	72(13)	-26(9)	-63(11)
F(3)	287(15)	155(9)	172(10)	-6(9)	80(10)	21(7)
F(4)	93(7)	518(25)	250(13)	90(12)	-67(8)	-100(16)
F(5)	228(11)	147(8)	146(7)	3(8)	11(7)	-61(6)
F(6)	293(14)	215(12)	134(8)	46(10)	9(8)	-82(8)

The anisotropic displacement exponent takes the form:
$-2\pi^2(h^2a^{*2}U_{11} + \ldots + 2hka^*b^*U_{12})$

Table 5. H-Atom coordinates ($x10^4$) and isotropic displacement coefficients ($Å^2x10^3$)

	x	y	z	U
H(1AA)	3316	5841	-1012	80
H(1AB)	2598	5810	-326	80
H(1AC)	2202	6420	-856	80
H(1BA)	4967	6820	-1347	80
H(1BB)	3930	7449	-1219	80
H(1BC)	5422	7498	-907	80
H(1CA)	5712	5801	-479	80
H(1CB)	6293	6335	83	80
H(1CC)	5213	5744	257	80
H(2AA)	6748	8897	1329	80
H(2AB)	5244	8905	1552	80
H(2AC)	6165	8218	1701	80
H(2BA)	7671	8126	437	80
H(2BB)	7164	7397	754	80
H(2BC)	6881	7549	-17	80
H(2CA)	6224	9223	65	80
H(2CB)	5255	8781	-437	80
H(2CC)	4644	9288	107	80
H(3AA)	1917	9409	1571	80
H(3AB)	3306	9324	1227	80
H(3AC)	1935	9268	793	80
H(3BA)	2393	8412	2512	80
H(3BB)	2790	7596	2384	80
H(3BC)	3856	8219	2291	80
H(3CA)	222	8368	1701	80
H(3CB)	175	8180	930	80
H(3CC)	383	7555	1466	80
H(2A)	2568	6153	1398	80
H(3A)	687	5374	1466	80
H(4A)	-1075	5438	681	80
H(5A)	-1104	6349	-128	80
H(1A)	590	7168	-107	80
H(8AA)	-581	9126	-412	80
H(8AB)	-988	9223	-1181	80
H(8AC)	-842	8437	-871	80
H(8BA)	1449	9864	-568	80
H(8BB)	2480	9645	-1109	80
H(8BC)	1052	9964	-1338	80
H(8CA)	2069	8593	-1849	80
H(8CB)	774	8110	-1763	80
H(8CC)	627	8897	-2073	80
H(11A)	7678	6498	2157	80
H(11B)	7689	5687	2415	80
H(11C)	7267	5860	1659	80
H(11D)	4535	5241	2217	80
H(11E)	5584	5132	1657	80
H(11F)	6006	4959	2413	80
H(11G)	5916	6690	2947	80
H(11H)	4674	6156	2977	80
H(11I)	6147	5875	3172	80

STRUCTURE DETERMINATION SUMMARY

Crystal Data	
Empirical Formula	$C_{19}\ H_{41}\ F_6\ Ir\ O\ P_4$
Color; Habit	Pale yellow rectangular prism
Crystal Size (mm)	0.3 x 0.3 x 0.5
Crystal System	Monoclinic
Space Group	$P2_1/c$
Unit Cell Dimensions	a = 8.974(2) Å b = 17.610(5) Å c = 19.888(5) Å β = 91.56(2)°
Volume	3141.9(13) $Å^3$
Z	4
Formula Weight	715.6
Density(calc.)	1.513 Mg/m^3
Absorption Coefficient	4.497 mm^{-1}
F(000)	1416
Data Collection	
Diffractometer Used	Siemens R3m/V
Radiation	MoK_α (λ = 0.71073 Å)
Temperature (K)	298
Monochromator	Highly oriented graphite crystal
2θ Range	3.5 to 45.0°
Scan Type	Wyckoff
Scan Speed	Variable; 3.97 to 19.53°/min. in ω
Scan Range (ω)	0.60°
Background Measurement	Stationary crystal and stationary counter at beginning and end of scan, each for 25.0% of total scan time
Standard Reflections	3 measured every 300 reflections
Index Ranges	$-9 < h < 0,\ 0 < k < 18,\ -21 < l < 21$
Reflections Collected	4607
Independent Reflections	4119 (R_{int} = 3.37%)
Observed Reflections	3230 ($F > 3.0\sigma(F)$)
Absorption Correction	Semi-empirical
Min./Max. Transmission	0.6994 / 0.8154
Solution and Refinement	
System Used	Siemens SHELXTL PLUS (VMS)
Solution	Direct Methods
Refinement Method	Full-Matrix Least-Squares
Quantity Minimized	$\Sigma w(F_o-F_c)^2$
Absolute Structure	N/A
Extinction Correction	χ = 0.00005(2), where $F^* = F\ [\ 1 + 0.002\chi F^2/\sin(2\theta)\ ]^{-1/4}$
Hydrogen Atoms	Riding model, fixed isotropic U
Weighting Scheme	$w^{-1} = \sigma^2(F) + 0.0000F^2$
Number of Parameters Refined	281
Final R Indices (obs. data)	R = 4.99 %, wR = 5.01 %
R Indices (all data)	R = 6.63 %, wR = 5.23 %
Goodness-of-Fit	1.01
Largest and Mean Δ/σ	0.315, 0.012
Data-to-Parameter Ratio	11.5:1
Largest Difference Peak	3.74 $eÅ^{-3}$
Largest Difference Hole	-0.69 $eÅ^{-3}$

Table 1. Atomic coordinates ($x10^4$) and equivalent isotropic displacement coefficients ($Å^2 x10^3$)

	x	y	z	U(eq)
Ir(1)	-177(1)	1965(1)	1584(1)	45(1)
P(1)	-2153(4)	2703(2)	1966(2)	63(1)
P(2)	675(4)	1660(3)	2680(2)	74(1)
P(3)	1363(4)	1070(2)	1074(2)	67(1)
C(1)	-849(12)	2273(7)	605(6)	51(4)
C(2)	-183(16)	2897(8)	313(7)	71(5)
C(3)	1032(17)	3390(9)	581(8)	81(6)
C(4)	2315(25)	3405(17)	129(10)	173(13)
C(5)	512(27)	4197(10)	646(12)	140(10)
C(6)	1583(17)	3148(9)	1268(7)	84(6)
C(7)	-2026(14)	1884(7)	252(6)	57(4)
C(8)	-2859(14)	1265(8)	388(7)	67(5)
C(9)	-3854(16)	1145(11)	-182(8)	85(6)
C(10)	-3610(18)	1683(12)	-604(9)	98(7)
O(1)	-2481(12)	2157(6)	-376(4)	89(4)
C(11)	-3492(20)	3040(13)	1330(10)	120(8)
C(12)	-1762(22)	3572(12)	2397(13)	137(10)
C(13)	-3337(18)	2200(10)	2532(11)	109(8)
C(21)	2457(31)	1421(32)	2837(12)	431(64)
C(22)	627(36)	2419(16)	3305(12)	189(16)
C(23)	-219(27)	958(17)	3130(11)	174(13)
C(31)	3371(16)	1169(13)	1159(10)	114(8)
C(32)	1040(23)	109(10)	1350(11)	126(9)
C(33)	1170(20)	983(12)	171(8)	106(7)
P(4)	3618(4)	4470(2)	2912(2)	78(1)
F(1)	1974(13)	4291(9)	2756(9)	176(8)
F(2)	3291(26)	4445(16)	3644(7)	254(13)
F(3)	5276(14)	4564(9)	3099(11)	203(9)
F(4)	3958(25)	4413(16)	2181(8)	247(13)
F(5)	3392(19)	5331(7)	2927(11)	206(10)
F(6)	3902(17)	3616(7)	2905(12)	212(11)

* Equivalent isotropic U defined as one third of the trace of the orthogonalized U_{ij} tensor

Table 2. Bond lengths (Å)

Ir(1)-P(1)	2.341 (4)	C(2)-C(3)	1.482 (21)
Ir(1)-P(2)	2.352 (4)	C(3)-C(4)	1.480 (26)
Ir(1)-P(3)	2.346 (4)	C(3)-C(5)	1.503 (24)
Ir(1)-C(1)	2.096 (11)	C(3)-C(6)	1.502 (21)
P(1)-C(11)	1.821 (20)	C(7)-C(8)	1.353 (18)
P(1)-C(12)	1.784 (22)	C(7)-O(1)	1.389 (14)
P(1)-C(13)	1.802 (19)	C(8)-C(9)	1.439 (20)
P(2)-C(21)	1.675 (31)	C(9)-C(10)	1.289 (26)
P(2)-C(22)	1.827 (27)	C(10)-O(1)	1.380 (21)
P(2)-C(23)	1.735 (27)	P(4)-F(1)	1.533 (12)
P(3)-C(31)	1.814 (15)	P(4)-F(2)	1.493 (16)
P(3)-C(32)	1.805 (19)	P(4)-F(3)	1.533 (13)
P(3)-C(33)	1.806 (16)	P(4)-F(4)	1.497 (17)
C(1)-C(2)	1.385 (18)	P(4)-F(5)	1.530 (13)
C(1)-C(7)	1.427 (16)	P(4)-F(6)	1.525 (13)

Table 3. Bond angles (°)

P(1)-Ir(1)-P(2)	93.2(1)	C(2)-C(3)-C(4)	111.7(15)
P(1)-Ir(1)-P(3)	166.8(1)	C(2)-C(3)-C(5)	111.0(14)
P(2)-Ir(1)-P(3)	93.8(1)	C(4)-C(3)-C(5)	106.4(18)
P(1)-Ir(1)-C(1)	87.5(3)	C(2)-C(3)-C(6)	112.4(13)
P(2)-Ir(1)-C(1)	177.3(3)	C(4)-C(3)-C(6)	108.4(14)
P(3)-Ir(1)-C(1)	85.9(3)	C(5)-C(3)-C(6)	106.6(14)
Ir(1)-P(1)-C(11)	116.5(7)	C(1)-C(7)-C(8)	133.9(11)
Ir(1)-P(1)-C(12)	119.4(7)	C(1)-C(7)-O(1)	118.1(11)
C(11)-P(1)-C(12)	99.9(10)	C(8)-C(7)-O(1)	108.0(11)
Ir(1)-P(1)-C(13)	113.2(6)	C(7)-C(8)-C(9)	107.2(12)
C(11)-P(1)-C(13)	101.8(8)	C(8)-C(9)-C(10)	107.0(15)
C(12)-P(1)-C(13)	103.5(10)	C(9)-C(10)-O(1)	111.5(14)
Ir(1)-P(2)-C(21)	121.0(9)	C(7)-O(1)-C(10)	106.4(11)
Ir(1)-P(2)-C(22)	116.8(9)	F(1)-P(4)-F(2)	88.7(11)
C(21)-P(2)-C(22)	95.5(18)	F(1)-P(4)-F(3)	174.0(9)
Ir(1)-P(2)-C(23)	119.8(8)	F(2)-P(4)-F(3)	89.0(12)
C(21)-P(2)-C(23)	100.2(18)	F(1)-P(4)-F(4)	90.5(11)
C(22)-P(2)-C(23)	98.7(12)	F(2)-P(4)-F(4)	174.5(15)
Ir(1)-P(3)-C(31)	119.4(7)	F(3)-P(4)-F(4)	91.2(12)
Ir(1)-P(3)-C(32)	113.4(7)	F(1)-P(4)-F(5)	94.6(9)
C(31)-P(3)-C(32)	103.2(10)	F(2)-P(4)-F(5)	88.9(13)
Ir(1)-P(3)-C(33)	116.5(6)	F(3)-P(4)-F(5)	91.0(9)
C(31)-P(3)-C(33)	99.7(9)	F(4)-P(4)-F(5)	96.7(13)
C(32)-P(3)-C(33)	102.2(10)	F(1)-P(4)-F(6)	87.4(9)
Ir(1)-C(1)-C(2)	118.5(8)	F(2)-P(4)-F(6)	91.0(14)
Ir(1)-C(1)-C(7)	121.6(8)	F(3)-P(4)-F(6)	87.0(9)
C(2)-C(1)-C(7)	119.8(11)	F(4)-P(4)-F(6)	83.5(14)
C(1)-C(2)-C(3)	129.5(12)	F(5)-P(4)-F(6)	178.0(9)

Table 4. Anisotropic displacement coefficients ($Å^2 x 10^3$)

	U_{11}	U_{22}	U_{33}	U_{12}	U_{13}	U_{23}
Ir(1)	45(1)	48(1)	43(1)	-4(1)	2(1)	0(1)
P(1)	58(2)	60(2)	73(2)	1(2)	10(2)	-17(2)
P(2)	71(2)	98(3)	53(2)	-17(2)	-8(2)	16(2)
P(3)	56(2)	63(2)	81(2)	7(2)	12(2)	0(2)
C(1)	47(6)	58(7)	47(6)	-14(5)	1(5)	-10(5)
C(2)	82(9)	79(10)	52(7)	-20(8)	-8(6)	4(7)
C(3)	90(10)	70(9)	82(10)	-29(8)	-6(8)	20(8)
C(4)	169(20)	268(32)	85(12)	-138(22)	42(13)	-44(16)
C(5)	194(22)	69(12)	153(19)	-43(14)	-56(16)	11(12)
C(6)	92(10)	82(11)	78(9)	-45(9)	-23(8)	4(9)
C(7)	70(7)	56(8)	45(6)	-10(7)	0(5)	-1(6)
C(8)	63(8)	68(9)	69(8)	-8(7)	5(6)	-5(7)
C(9)	64(9)	120(14)	72(9)	-31(9)	-4(7)	-23(10)
C(10)	81(11)	140(16)	71(10)	-36(10)	-24(8)	2(10)
O(1)	109(7)	106(8)	52(5)	-36(6)	-18(5)	15(5)
C(11)	95(12)	128(15)	136(15)	57(13)	2(10)	-9(14)
C(12)	103(14)	120(16)	191(22)	-14(12)	49(14)	-73(16)
C(13)	73(9)	102(14)	154(16)	0(9)	49(10)	-12(11)
C(21)	151(28)	1073(188	68(15)	151(62)	-2(16)	108(41)
C(22)	251(34)	180(26)	130(20)	-26(25)	-95(22)	0(19)
C(23)	150(19)	251(31)	119(16)	-98(21)	-53(15)	86(19)
C(31)	66(10)	139(17)	136(16)	15(10)	12(10)	-10(13)
C(32)	137(16)	80(12)	166(19)	27(11)	79(14)	18(12)
C(33)	107(13)	123(14)	89(11)	14(11)	11(9)	-51(11)
P(4)	71(2)	74(3)	86(3)	13(2)	-10(2)	-20(2)
F(1)	84(7)	191(14)	253(17)	2(8)	-10(9)	-43(12)
F(2)	286(22)	380(32)	97(10)	49(21)	23(11)	21(14)
F(3)	93(8)	182(14)	331(23)	-9(9)	-56(11)	-62(14)
F(4)	278(22)	352(31)	112(11)	-70(20)	40(12)	-32(14)
F(5)	205(15)	84(8)	325(23)	37(9)	-79(15)	-22(11)
F(6)	160(12)	81(8)	396(29)	22(8)	0(14)	-17(12)

The anisotropic displacement factor exponent takes the form:
$-2\pi^2(h^2a^{*2}U_{11} + ... + 2hka^*b^*U_{12})$

Table 5. H-Atom coordinates ($x10^4$) and isotropic displacement coefficients ($Å^2 x10^3$)

	x	y	z	U
H(2A)	-549	3018	-132	80
H(4A)	2681	2895	92	80
H(4B)	1996	3586	-307	80
H(4C)	3095	3727	307	80
H(5A)	-316	4216	941	80
H(5B)	1300	4515	821	80
H(5C)	202	4374	207	80
H(6A)	1924	2632	1248	80
H(6B)	2390	3470	1415	80
H(6C)	787	3184	1579	80
H(8A)	-2796	963	790	80
H(9A)	-4572	744	-235	80
H(10A)	-4152	1761	-1021	80
H(11A)	-4257	3335	1535	80
H(11B)	-2986	3347	1009	80
H(11C)	-3935	2609	1106	80
H(12A)	-2686	3801	2520	80
H(12B)	-1158	3480	2795	80
H(12C)	-1243	3906	2103	80
H(13A)	-4127	2526	2673	80
H(13B)	-3753	1762	2309	80
H(13C)	-2752	2041	2918	80
H(21A)	2626	1304	3305	80
H(21B)	2776	1003	2568	80
H(21C)	3014	1867	2725	80
H(22A)	995	2238	3734	80
H(22B)	1231	2835	3162	80
H(22C)	-386	2585	3344	80
H(23A)	255	901	3566	80
H(23B)	-1249	1087	3181	80
H(23C)	-149	490	2886	80
H(31A)	3831	759	923	80
H(31B)	3668	1644	968	80
H(31C)	3678	1152	1625	80
H(32A)	1692	-235	1126	80
H(32B)	1230	83	1827	80
H(32C)	23	-29	1251	80
H(33A)	1835	605	3	80
H(33B)	161	851	48	80
H(33C)	1407	1468	-21	80
H(1)	-1159	1264	1608	50

VITA

The author was born in Langley Air Force Base, Hampton, Virginia, on February 11, 1964, to Henry and Lillian Selnau. He graduated from Kecoughtan High School in Hampton, in the spring of 1982. In August of that year, he entered the traditional Rat Line at Virginia Military Institute in Lexingtion, Virginia and majored in chemistry. On March 16, 1983 he became one of the members of the Class of '86. He then received his B. S. Degree in chemistry at Virginia Military Institute in May 14, 1986. He worked for a small chemical company as an analytical-formulation chemist. In the summer of 1988, he entered graduate school at Virginia Tech under the direction of Dr. Wolfe. Dr. Wolfe was then promoted to Vice Provost of Virginia Tech in the fall of 1989. Due to Dr. Wolfe's promotion at Virginia Tech he then joined a new group under the supervision of Dr Merola.

Henry E Selnau, Jr.